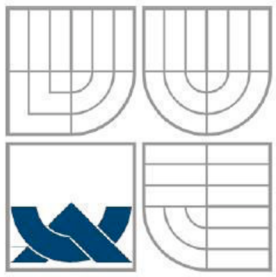

VYSOKÉ UČENÍ TECHNICKÉ V BRNĚ
BRNO UNIVERSITY OF TECHNOLOGY

FAKULTA STROJNÍHO INŽENÝRSTVÍ
ÚSTAV MECHANIKY TĚLES, MECHANOTRONIKY A BIOMECHANIKY

FACULTY OF MECHANICAL ENGINEERING
INSTITUTE OF SOLID MECHANICS, MECHANOTRONICS AND BIOMECHANICS

STOCHASTIC CRACK PROPAGATION MODELLING USING THE EXTENDED FINITE ELEMENT METHOD

STOCHASTICKÉ MODELOVÁNÍ ŠÍŘENÍ TRHLIN S VYUŽITÍM ROZŠÍŘENÉ METODY KONEČNÝCH PRVKŮ

DISERTAČNÍ PRÁCE
DISERTATION

AUTOR PRÁCE
AUTHOR

ING. LUKÁŠ NEŠPŮREK

VEDOUCÍ PRÁCE
SUPERVISOR

Prof. RNDr. ZDENĚK KNÉSL, CSc.
Prof. MAURICE LEMAIRE

BRNO 2009

Université Blaise Pascal – Clermont II

ECOLE DOCTORALE
SCIENCES POUR L'INGENIEUR DE CLERMONT-FERRAND

Thèse

présentée par

Lukáš Nešpůrek
Ingénieur en Génie Civile

pour obtenir le grade de
DOCTEUR D'UNIVERSITE

Modélisation stochastique de propagation de fissure utilisant la méthode des éléments finis étendue

Stochastic Crack Propagation Modelling using the Extended Finite Element Method

---

Abstract

The PhD. thesis is based on the research conducted by the author under a joint guidance and advice within a French-Czech doctoral research project. The French part of the research was carried out at the Institut Français de Mécanique Avancée in Clermont-Ferrand and was directed by Maurice Lemaire and Jean-Marc Bourinet. The Czech part of the work, guided by Zdeněk Knésl, was elaborated at the Institute of Physics of Materials of the Academy of Sciences of the Czech Republic in Brno.

This thesis is organised such as to provide the reader a balanced presentation of fracture, fatigue, computational mechanics and reliability analysis methods. Together with original developments in direct differentiation of the fatigue life equation, this constitutes the set of tools that was leveraged in a novel architecture to develop a stochastic fatigue crack propagation analysis procedure meeting the requirements of robustness, speed and accuracy.

The Czech part of the research was in the field of computational fracture mechanics. It is given a detailed exposure in an appendix not to break the continuity of the main text. It consisted in a continuum mechanics based study of the stress field around the crack front of a through-thickness crack in two and three dimensions. The main question to be answered was whether the special type of singularity at the intersection of the crack front with the free surface can be one of the sources of abnormalities in the behaviour of cracks in very thin foils. The theoretical bases of the concepts commonly used in fracture mechanics were reviewed to understand their applicability to problems with special geometries, such as the one of thin foils. A detailed numerical investigation of the stress conditions along and around the crack front was carried out. The carefully elaborated 3D finite element models of through cracks in thin foils exposed certain distinct trends in the contours of the stress field as the sheet metal becomes thinner. But these findings could not offer an explanation for the abnormal behaviour observed in fatigue tests on cracked thin foils.

Despite the fact that the above hypothesis appeared ungrounded, this research helped to fully appreciate the assumptions behind two-dimensional fracture mechanics models as well as behind two-dimensional crack propagation models.

The larger part of the thesis, which also brings an original contribution, deals with numerical modelling and stochastic analysis of complex-geometry crack propagation problems. The use of numerical mechanical models for such analysis has so far been scarce because of prohibitively high computational effort. This thesis shows that through application of advanced com-

putational mechanics and suitable reliability analysis techniques, the task is tractable even on a personal computer.

The basic choice when solving a stochastic problem is a choice of the reliability analysis method. In this thesis, the First Order Reliability Method (FORM) was employed. From previous analyses of similar problems, it appeared that the problem in hand showed no important non-linearity. FORM also directly provides information on sensitivities. Further, FORM proved to be very advantageous in that it does not require the mechanical model to compute responses with very low-probability realisations of the random variables. It may be quite difficult to ensure that the underlying computational model can deal with all low-probability configurations of the problem. Moreover, such configurations may result in a different type of failure than the one of interest in the analysis.

An essential step in the FORM analysis is to transform the reliability problem in the physical space to a space of standard normal uncorrelated variables. An intermediate step of the Nataf transformation employed here for this purpose is to solve an integral equation in order to calculate a correlation coefficient of a bi-variate normal distribution. While the usual approach is to use approximate solution formulæ, it was solved in this thesis by an optimisation procedure to achieve a higher accuracy.

It was assumed that the crack propagation velocity obeys the Paris-Erdogan crack growth equation. Its parameters were obtained from actual fatigue test results (the well-known Virkler data). The fatigue life in simulations using statistic models based on these data was extremely sensitive to the correlation of the two parameters of the fatigue equation. Considerable attention was paid to choice of an appropriate statistic model. A bi-variate model of normal multiplier and log-normal exponent of the equation gave satisfactory results.

For problems involving crack-crack and crack-structure interactions, a solution of the underlying fracture mechanics problem by a numerical method becomes necessary. Classical finite element formulation requires updating the finite element mesh as the crack is growing. Remeshing introduces numerical noise which can hamper the convergence of the FORM reliability algorithm. The accuracy achievable with the finite elements that is quite satisfactory for deterministic purposes may be insufficient for FORM.

On the other hand, the Extended Finite Element Method (XFEM) avoids remeshing and offers a good numerical stability. XFEM was used in this thesis as a numerical solution method that is very well suited for reliability analysis of crack propagation problems. The method approximates the displacement field in the vicinity of the crack through a sum of several dis-

continuous shape functions, which add up to unity at all points. The nodal coefficients for these functions are found by invoking the minimum energy principle.

FORM requires the computation of the derivatives of the response function, which is in the present case the fatigue life integral. Numerical differentiation is time consuming and introduces numerical errors. Several useful direct differentiation formulæ were therefore derived and used. They speed up the computation dramatically. In test examples, the numerical differentiation results appeared to approach the direct differentiation results as the differentiation step was refined. However, the response derivatives with respect to certain variables could only be obtained by employing numerical differentiation by means of the finite difference method.

An important challenge is to treat variable-amplitude loading. This is mainly due to the effect of crack growth retardation after overload. From among the various approaches available, the choice was made to apply the so called PREFFAS method, well accepted in the French aerospace industry. In PREFFAS, it is assumed that the loading consists of a repeated sequence of peaks and troughs, such as a standard design load sequence, and that the geometrical factor to the stress intensity equation changes only negligibly through a single application of the load sequence. The method is therefore applicable also to problems with multiple and interacting cracks, since the changing geometry interactions do not enter into the load transformation. PREFFAS transforms the variable-amplitude load sequence into a constant-amplitude load sequence, operating on the load sequence only, without any consideration to the structure itself.

The author also had the opportunity to use a cluster of personal computers running Linux operating system with the OpenPBS distributed computing utility, which appeared to be perfectly suited and easy-to-use for reliability analysis purposes. The distribution of the computations of the structural response brought a further acceleration of the reliability analysis procedure.

The computational implementation leveraged available software. The reliability analysis tools of the FERUM code written in Matlab were employed. The crack propagation procedures were also scripted in Matlab, ensuring seamless integration with FERUM. The XFEM code developed by the LAMCOS institute in Lyon was exploited to carry out fracture mechanics analysis. While the Matlab code can be run under an arbitrary operating system, distributed computing and the XFEM code need to be run on a Linux machine, which can be accessed through a network connection. Communication between the codes is enabled by launching executable

scripts from Matlab, data exchange takes place via text files and several custom scripts in Perl are used to manage the computational jobs.

Two application examples are presented in the text. In the first, PREFFAS load transformation was carried out separately prior to the analysis itself, in which the transformed constant-amplitude load was applied in a deterministic manner. A limited study of randomness in the PRFEFAS model was conducted within the first example. In the second example, the load transformation was an integral part of the overall stochastic analysis procedure and a material parameter of PREFFAS was considered random. Both of the example problems had very low probabilities of failure.

The implemented procedure appeared capable to analyse stochastic crack propagation problems, with a complexity at the level of industrial applications, with robustness, accuracy and reasonable requirements on computational hardware and time. The procedure is ready to be applied on a wide range of complex-geometry two-dimensional crack propagation problems.

As the approach is based on the stress intensity factor and the Paris crack growth law, extension to three dimensions would require substantial changes in the methods used, despite the fact that XFEM has been developed for 3D problems as well.

Abstrakt

Tato disertace je výsledkem práce, která vznikla v rámci doktorského studijního programu autora pod společným francouzsko-českým vedením. Francouzským partnerem byl Institut Français de Mécanique Avancée v Clermont-Ferrand, kde autorovu práci vedli prof. Maurice Lemaire a Dr. Jean-Marc Bourinet. V České republice se na projektu podílel Ústav fyziky materiálů AV ČR Brno, kde autora vedl prof. RNDr. Zdeněk Knésl, CSc.

Text disertace je strukturován tak, aby čtenáři poskytl vyvážený přehled teoretických východisek v oblasti lomové mechaniky, únavy, numerických metod mechaniky těles a metod analýzy spolehlivosti. Spolu s původním odvozením přímé derivace vztahu pro únavovou životnost jsou popsané metody souborem nástrojů, na nichž je vystavěn nový přístup stochastické analýzy šíření únavových trhlin, který splňuje požadavky na robustnost, rychlost a přesnost výpočtové metody.

Na českém pracovišti ÚFM AV ČR se autor zabýval především výpočtovými metodami lomové mechaniky. Výsledky této práce jsou podrobněji rozvedeny v příloze s ohledem na plynulost hlavního textu. Jejím cílem bylo zkoumat z hlediska mechaniky těles v trojrozměrném prostoru pole napětí v okolí čela trhliny procházející materiálem. Zejména měla být zodpovězena otázka, zda specifický typ singularity v průsečíku čela trhliny s volným povrchem nemůže být jednou z příčin anomálního chování trhlin ve velmi tenkých kovových foliích. Teoretické základy metod běžně používaných v lomové mechanice byly prostudovány z hlediska správnosti jejich aplikace na problémy se specifickými geometrickými aspekty, zejména na problém tenkých folií. Byla provedena podrobná numerická analýza prostorového pole napětí v okolí čela trhliny. Pečlivě modelování trhliny procházející tenkou kovovou folií pomocí metody konečných prvků ukázalo na určité charakteristické jevy v prostorovém poli napětí v závislosti na tloušťce folie. Tyto jevy se však zřejmě nejsou vysvětlením pro anomální chování, které bylo u tenkých kovových folií pozorováno.

Přestože se výše uvedená hypotéza této části výzkumu nepotvrdila, autorovi tato práce velmi přispěla k dobrému porozumění předpokladům, které stojí za běžně používanými rovinnými řešeními v lomové mechanice, a předpokladům rovinných modelů šíření únavových trhlin.

Větší část disertace, v níž jsou rovněž prezentovány původní příspěvky k řešené problematice, se zabývá numerickým modelováním a stochastickou analýzou rovinných problémů šíření únavových trhlin se složitější geometrií. Využití numerického modelování příslušného problému mechaniky těles pro takovou stochastickou analýzu bylo dosud řídké z důvodu nepřiměřeně vysoké

výpočtové náročnosti. Tato disertace ukazuje, že díky aplikaci pokročilých numerických metod mechaniky těles a vhodných technik ve spolehlivostní analýze lze takovou úlohu řešit i na osobním počítači.

Zásadním metodickým rozhodnutím je při řešení stochastického problému volba spolehlivostní metody. V této disertaci je využita aproximační metoda FORM. To bylo možné díky zkušenosti z předchozích analýz obdobných problémů, v nichž funkce poruchy nevykazovala žádnou výraznou nelinearitu. V metodě FORM rovněž přímo získáváme cenné informace o citlivosti spolehlivostního indexu na jednotlivé proměnné a parametry. Výraznou výhodou se ukázalo být také to, že není třeba, aby byl numerický mechanický model schopen spočítat odezvu také pro všechny velmi málo pravděpodobné realizace náhodných proměnných. Zajistit takovou robustnost numerického modelu může být nebývale obtížné. Zmíněné nepravděpodobné konfigurace navíc mohou vést na jiný způsob poruchy, než který je předmětem našeho zájmu.

Základním prvkem metody FORM je transformace spolehlivostního problému z fyzikálního prostoru proměnných do prostoru standardně normálně rozložených nekorelovaných proměnných. K tomu se v disertaci využívá Natafova transformace. Jedním z jejích kroků je vyřešení integrální rovnice, jejímž řešením je korelační koeficient dvojrozměrného normálního rozložení. Zatímco běžným přístupem je aplikace přibližných vzorců, v této disertaci byla řešení nalezeno s vysokou přesností aplikací optimalizačních metod.

U rychlosti šíření vychází práce z předpokladu platnosti Parisova-Erdoganova vztahu. Parametry jeho proměnných byly stanoveny z výsledků reálných únavových zkoušek (ze známých Virklerových dat). Únavová životnost ve výpočtech využívajících statistické modely založené na těchto datech byla extrémně citlivá na korelaci obou parametrů Parisova vztahu. K volbě vhodného statistického modelu se proto přistupovalo s náležitou péčí. Dvourozměrný model s normálním násobitelem a log-normálním exponentem Parisova vztahu umožnil reprodukovat realitu únavových testů s uspokojivou přesností.

Problémy šíření trhlin, kde dochází ke vzájemné interakci více trhlin nebo k interakci trhlin s prvky konstrukce, kterou se trhliny šíří, vyžadují řešit příslušný problém lomové mechaniky numericky. V klasické metodě konečných prvků je třeba neustále aktualizovat síť konečných prvků s tím, jak se trhliny šíří. Změny sítě jsou zdrojem numerického šumu, který může i znemožnit konvergenci spolehlivostní metody FORM. Přesnost metody konečných prvků, která je zcela postačující pro deterministické problémy, může být pro stochastické problémy řešené metodou FORM nedostatečná.

Nutnosti aktualizace sítě se lze vyhnout a numerické stability dosáhnout

nasazením rozšířené metody konečných prvků (XFEM). Pro výhody této metody při řešení spolehlivostních problémů šíření trhlin byla XFEM aplikována v této disertaci. V metodě se pole deformací v okolí trhliny aproximuje součtem několika nespojitých tvarových funkcí, jejichž součet je v každém bodě jednotkový. Uzlové hodnoty každé z těchto funkcí se naleznou aplikací principu minimální energie.

Metoda FORM je v podstatě optimalizační metodou a vyžaduje proto výpočet derivací funkce odezvy, tj. v našem případě diferenciaci integrálního vztahu pro únavovou životnost. Numerická derivace klade vysoké nároky na výpočtový čas a je zatížena chybou. V rámci této doktorské práce proto bylo přímou derivací integrální rovnice odvozeno několik velmi užitečných vztahů. Jejich aplikace vede k dramatickému snížení výpočetní náročnosti. Správnost odvozených vztahů byla ověřena srovnáním s numerickou derivací. Ukázalo se, že výsledky numerické diferenciace měly tendenci se blížit výsledkům odvozených vztahů s tím, jak se zjemňoval krok numerické diferenciace. Pro některé proměnné však nebylo možné derivaci funkce odezvy získat jinak než numerickou derivací metodou konečných rozdílů.

Důležitým prvkem řešení problému šíření trhlin je uvážit proměnlivost zatížení. Ta se projevuje zejména zpomalením rychlosti růstu trhliny po přetížení. Z různých dostupných přístupů byla zvolena metoda PREFFAS, která je široce akceptována ve francouzském leteckém průmyslu. Metoda vychází z předpokladu, že zatížení sestává z opakovaných sekvencí maxim a minim (například ze standardních zatěžovacích profilů), a z předpokladu, že vliv změny geometrie trhliny, k níž dojde během jediné aplikace zatěžovací sekvence, na součinitel intenzity napětí je zanedbatelný. PREFFAS lze proto využít i pro řešení problémů s více vzájemně se ovlivňujícími trhlinami, protože měnící se geometrické poměry nemají vliv na transformaci zatížení. Metoda PREFFAS transformuje zatěžovací sekvenci s proměnlivými amplitudami zatížení na sekvenci s konstantní amplitudou zatížení, a to bez potřeby jakékoliv informace o zatěžované konstrukci.

Autor měl také možnost využívat cluster osobních počítačů s operačním systémem Linux a se systémem OpenPBD pro distribuci výpočetních úkolů, který se ukázal být výborným a snadno použitelným systémem pro spolehlivostní analýzy. Distribuce výpočtů odezvy konstrukce přinesla další zrychlení celé spolehlivostní analýzy.

Při počítačové implementaci navržené metody se využilo dostupného softwaru. Pro spolehlivostní analýzu se uplatnily algoritmy systému FERUM napsaného v jazyce Matlab. Procedury simulace šíření trhlin byly rovněž napsány v Matlabu, což zajistilo snadnou integraci s kódem FERUM. Analýza problému lomové mechaniky byla provedena metodou XFEM napro-

gramovanou ústavem LAMCOS univerzity INSA v Lyonu. Skripty v Matlabu lze spustit na počítači s libovolným operačním systémem. Distribuce výpočtů a program XFEM běží pouze na počítači se systémem Linux, k němuž může být i vzdálený přístup po síti. Komunikace mezi oběma Matlabem a XFEM je zprostředkována spustitelnými skripty volanými z Matlabu. Výměna dat probíhá prostřednictvím textových souborů a výpočetní úkoly jsou spravovány několika skripty v jazyce Perl.

V disertaci jsou prezentovány dva příklady aplikace navržené výpočetní metody. V prvním příkladu je transformace zatížení metodou PREFFAS provedena zvlášť před spuštěním vlastní analýzy, v níž pak bylo transformované zatížení o konstantní amplitudě aplikováno už jen deterministicky. V rámci prvního příkladu tak byla okrajově provedena i analýza náhodnosti v modelu PREFFAS. V druhém příkladu byla transformace zatížení nedílnou součástí celkového postupu stochastické analýzy a materiálový parametr vstupující do algoritmu PREFFAS byl modelován jako náhodná proměnná. Pravděpodobnost poruchy v obou příkladech byla velmi nízká.

Implementovaný postup se ukázal být dobrou metodou analýzy stochastických problémů šíření trhlin, jejichž geometrie dosahuje složitosti aplikací v průmyslu, přičemž vykazoval robustnost, přesnost a přiměřenou náročnost na výpočetní prostředky a čas. Postup lze snadno uplatnit na širokou řadu rovinných problémů šíření trhlin se složitou geometrií.

Vzhledem k tomu, že je vyvinutý postup založen na použití součinitele intenzity napětí a Parisova vztahu pro rychlost šíření trhlin, by rozšíření na prostorové úlohy vyžadovalo značné změny v používaných přístupech, a to i přesto, že numerická metoda XFEM byla vyvinuta i pro prostorové problémy.

Résumé

Cette thèse se basse sur la recherche réalisée par l'auteur sous direction conjointe de deux tuteurs dans le cadre d'un doctorat en cotutelle franco-tchèque. La partie française de cette recherche a été réalisée à l'Institut Français de Mécanique Avancée à Clermont-Ferrand sous la direction de Maurice Lemaire et Jean-Marc Bourinet. La partie tchèque du travail, guidée par Zdeněk Knésl, a été menée à l'Institut de physique de matériaux de l'Académie des Sciences de la République Tchèque.

La thèse est organisée d'une manière à donner au lecteur une présentation équilibrée des méthodes de la mécanique de rupture, de fatigue, de mécanique numérique et de l'analyse fiabiliste. Ces méthodes, ainsi que des développements originaux en différentiation directe de l'équation de la tenue en fatigue, représentent la boîte à outils qui a été exploitée dans une architecture originelle pour développer une procédure d'analyse stochastique de la propagation de fissure, qui répond aux exigences de robustesse, vitesse et précision du calcul.

La partie tchèque da la recherche se situe dans le domaine de le mécanique numérique de rupture. Ce travail est présenté en détail dans l'annexe afin de ne pas interrompre la continuité du texte principal. Il consistait en une étude, fondée sur la mécanique de milieux continus, du champ tridimensionnel de contraintes dans le voisinage du front d'une fissure passante à travers d'une plaque. La question principale à répondre était si le type particulier de singularité du champ à l'intersection du front de la fissure avec la surface libre pourrait-t-il être une des sources de comportement anormal de fissures dans des feuilles métalliques très minces. Les bases théoriques des approches couramment utilisées dans la mécanique de la rupture ont été révisées afin de bien apprécier leur applicabilité aux problèmes présentent des caractéristiques géométriques particulières, par exemple au problème d'une plaque très mince. Une étude numérique détaillée du champ de contrainte le long du front de la fissure était menée. Une modélisation tridimensionnelle par éléments finis soigneusement élaborée de fissure traversant une feuille mince a fait ressortir à certaines tendances des contours du champ de contraintes en fonction de l'épaisseur diminuant de la feuille. Or, ces constatations ne constituent pas une explantation pour le comportement anormal observé dans des essaies en fatigue de feuilles minces fissurées.

Malgré le fait que l'hypothèse ci-dessus n'était pas confirmée, cette recherche a aidé à apprécier pleinement les hypothèses derrière les modèles à deux dimensions de la mécanique de rupture, ainsi que derrière les modèles à deux dimensions de propagation de fissures par fatigue.

La partie plus étendue de la thèse, qui apporte également une contribution originale, traite de la modélisation numérique et de l'analyse stochastique des problèmes de propagation de fissures présentant une géométrie complexe. L'utilisation de modèles mécaniques numériques pour une telle analyse a jusqu'ici été limitée par un effort de calcul trop élevé. Cette thèse démontre que, par application des méthodes de mécanique numérique avancées et des techniques d'analyse fiabiliste convenables, la tâche est tractable même sur un ordinateur personnel.

Le choix fondamental lors de la résolution d'un problème stochastique est le choix de la méthode d'analyse de fiabilité. Dans cette thèse, l'approximation de fiabilité de premier ordre (FORM) a été employée. D'après analyses précédentes des problèmes similaires, il est apparu que le problème en main n'a montré aucune non-linéarité importante. Aussi, la méthode FORM fournit-elle directement les sensibilités de l'index de fiabilité à des différents paramètres. En outre, FORM s'est avérée très avantageuse en ce qu'elle n'exige pas que le modèle mécanique soit capable de calculer la réponse mécanique pour toutes réalisations des variables aléatoires de très faible probabilité. Il se peut avérer très difficile d'assurer que le modèle mécanique numérique puisse traiter toutes les configurations de faible probabilité du problème. D'autre part, ces configurations de faible probabilité peuvent entraîner un autre type de défaillance que celui auquel on s'intéresse dans l'analyse.

Une étape essentielle dans l'analyse FORM consiste à transformer le problème de fiabilité de l'espace physique à un espace de variables normales standards non-corrélées. Une étape intermédiaire de la transformation Nataf employée ici pour cet objectif est de résoudre une équation intégrale afin de calculer un coefficient de corrélation d'une distribution normale bi-variée. Alors que l'approche habituelle consiste à se servir de formules approximatives, l'équation intégrale a été résolue dans cette thèse par une procédure d'optimisation pour atteindre une précision plus élevé.

Il était supposé que la vitesse de propagation de fissure obéissait l'équation de Paris-Erdogan. Ses paramètres ont été obtenus à partir des résultats des essaies réelles en fatigue (les données bien connues des Virkler). La tenue en fatigue dans les simulations utilisant les modèles statistiques basées sur ces données a été extrêmement sensible à la corrélation des deux paramètres de l'équation de Paris-Erdogan. On a prêté une attention soigneuse au choix d'un modèle statistique approprié. Un modèle bi-varié de multiplicateur normal et exposant log-normale de l'équation a donné des résultats satisfaisants.

Pour des problèmes présentant des interactions entre des fissures ou

des interactions d'une fissure avec la structure, une solution du problème de mécanique de rupture sous-jacent par une méthode numérique devient indispensable. La formulation classique de la méthode des éléments finis nécessite la mise à jour du maillage des éléments finis chaque fois que la fissure s'accroît. Le remaillage introduit un bruit numérique qui peut nuire à la convergence de l'algorithme d'optimisation de calcul de fiabilité. La précision réalisable avec les éléments finis, qui est tout à fait satisfaisant à des fins déterministes, peut être insuffisante pour FORM.

Or, la méthode des éléments finis étendue (XFEM) évite le remaillage et offre une bonne stabilité numérique. XFEM était utilisée dans cette thèse en tant qu'une méthode de solution numérique très bien adaptée pour l'analyse fiabiliste des problèmes de propagation de fissure. La méthode construit une approximation du champ de déplacement en proximité de la fissure par une somme de plusieurs fonctions de forme discontinues, dont la somme et l'unité à tous points. Les coefficients nodaux de ces fonctions sont trouvés en invoquant le principe d'énergie minimale.

FORM nécessite le calcul des dérivés de la fonction de réponse, qui est, dans le cas présent, l'intégral de la tenue en fatigue. La différenciation numérique prend trop de temps et introduit des erreurs numériques. Plusieurs formules très utiles ont donc été dérivées par différenciation directe de l'équation intégrale. Elles accélèrent le calcul considérablement. Dans des exemples d'essaie, les résultats de différenciation numérique semblaient approcher les résultats de différenciation directe avec le raffinement du pas de différenciation. Toutefois, les dérivés de la réponse par rapport à certaines variables ne pouvaient être obtenus que en employant la différenciation numérique au moyen de la méthode de différences finies.

Un défi important consiste à traiter le chargement d'amplitude variable. Il s'agit principalement de l'effet de retard de croissance de la fissure après une surcharge. Parmi les diverses approches disponibles, le choix a été fait d'appliquer la méthode PREFFAS, bien acceptée dans l'industrie aéronautique française. Dans PREFFAS, il est supposé que le chargement consiste en une séquence répétée de pics et vallées, comme par exemple les séquences de chargement de conception standards, et que le facteur géométrique de l'équation d'intensité de contrainte soit perturbé d'une façon négligeable lors d'une seule application de la séquence de chargement. Cette méthode est donc applicable également à des problèmes de multiples fissures en interaction, car les interactions géométriques changeantes n'entrent pas dans la transformation de chargement. PREFFAS transforme la séquence de chargement d'amplitude variable en une séquence de chargement d'amplitude constante, opérant seulement sur la séquence de chargement, sans

aucune considération à la structure elle-même.

L'auteur avait aussi l'occasion d'utiliser un cluster de PC exécutant le système d'exploitation Linux avec l'outil de calcul distribué OpenPBS, qui semblait être parfaitement adapté et facile à utiliser pour des fins de l'analyse fiabiliste. La distribution des calculs de la réponse mécanique a apporté une accélération supplémentaire de la procédure d'analyse de fiabilité. Dans la mise en œuvre informatique, on exploitait les logiciels disponibles. Les outils d'analyse fiabiliste du code FERUM écrits dans MATLAB étaient employés. Les procédures de propagation de fissure ont été également écrites au format de scripts de MATLAB, assurant une intégration avec FERUM sans interfacer. Le code XFEM développé par le laboratoire LAMCOS de INSA de Lyon a été exploité pour mener les analyses de mécanique de rupture. Alors que le code MATLAB peut être exécuté sous un système d'exploitation arbitraire, le calcul distribué et le code XFEM doit être exécuté sur un ordinateur sous Linux, auquel on peut accéder également par le biais d'une connexion réseau. La communication entre les codes est réalisée en lançant des scripts exécutables à partir de MATLAB. L'échange de données s'effectue par des fichiers texte et plusieurs scripts écrits en Perl sont utilisés pour gérer les tâches de calcul.

Deux exemples d'application sont présentés dans le texte. Dans le premier, la transformation de chargement PREFFAS a été effectuée séparément avant l'analyse elle-même, dans laquelle l'amplitude constante du chargement transformé a été appliquée dans une manière déterministe. Une étude limitée du caractère aléatoire du modèle de PREFFAS a été menée au sein du premier exemple. Dans le deuxième exemple, la transformation du chargement faisait une partie intégrale de la procédure d'analyse stochastique et le paramètre de matériau de PREFFAS était considéré aléatoire. Tous les deux problèmes d'exemple présentaient une probabilité de défaillance très faible.

La procédure proposée semblait capable d'analyser des problèmes stochastiques de propagation de fissure d'une complexité au niveau des applications industrielles, avec robustesse et précision, en ne posant que des exigences raisonnables sur le matériel informatique et le temps de calcul. La procédure est prête à être appliquée sur un large éventail de problèmes de propagation de fissure à deux dimensions de géométrie complexe.

L'approche est fondée sur l'utilisation du facteur d'intensité de contrainte et la loi de Paris de propagation de fissure. Pour cela, une extension à trois dimensions nécessiterait des changements substantiels dans les méthodes utilisés, malgré le fait que le code XFEM a été développé ainsi pour les problèmes 3D.

Keywords

fatigue, crack propagation, reliability analysis, extended finite element method, XFEM, variable amplitude loading, computational fracture mechanics

Klíčová slova

únava, šíření trhlin, spolehlivostní analýza, rozšířená metoda konečných prvků, XFEM, zatížení s proměnlivou amplitudou, výpočtová lomová mechanika

Bibliographic reference of this thesis / Bibliografická citace disertační práce:

Nešpůrek, L. Stochastic crack propagation modelling using the extended finite element method. 2009. 208s. Disertační práce na Fakultě strojního inženýrství Vysokého učení technického v Brně. Vedoucí práce Zdeněk Knésl a Maruce Lemaire.

Prohlášení autora o původnosti práce / Author's declaration of originality of work

Čestně prohlašuji, že jsem disertační práci vypracoval samostatně, na základě uvedené literatury a za podpory školitelů.

I declare on my word of honour that I have developed this thesis independently, using the cited literature and with the support of my tutors.

Brno, ... Lukáš Nešpůrek.....

Acknowledhements

I wish to thank my toturs Maurice Lemaire, Jean-Marc Bourinet and Zdeněk Knésl, without whose advice, patience and support this thesis would have never come to existence.

My thanks belong also to Anthony Gravouil and the LAMCOS institure in Lyon for making their XFEM code available for the purposes of this research.

I express my gratitude to the French government for the financial support I have enjoyed through the program of doctoral studies under joint tutorship.

Contents

Chapter 1

Introduction

This PhD. thesis is based on the research conducted by the author under a joint guidance and advice within a French-Czech doctoral research project. The French part of the research was carried out at the Institut Français de Mécanique Avancée in Clermont-Ferrand and was directed by Maurice Lemaire and Jean-Marc Bourinet. The Czech part of the work, guided by Zdeněk Knésl, was elaborated at the Institute of Physics of Materials of the Academy of Sciences of the Czech Republic in Brno.

Accordingly, the presentation in this thesis evolves along two major axes. The Czech contribution consists in a continuum mechanics based study of the stress field around the crack front of a through-thickness crack in two and three dimensions. The main question to be answered was whether the special type of singularity at the intersection of the crack front with the free surface can be one of the sources of abnormalities in the behaviour of cracks in very thin foils. This part of the research was motivated by the efforts to identify the possible causes of the mentioned abnormal behaviour observed in experiments [37].

The theoretical background established by the above research helps to understand some of the issues involved in the fracture mechanics based modelling of crack propagation, which is the subject of the French part of the research.

It is also this latter part of the work where a majority of the original contributions of this thesis are put forward. The most significant result is a proposal, implementation and demonstration of an efficient approach for a reliability analysis of complex fatigue crack propagation problems. The complexity here involves both complex 2D structural configurations requiring a finite element analysis and complex loading conditions. The inevitable con-

sequence of including of these comprehensive considerations in the analysis results in the formulation of a computational task with formidable demands on computer resources. This barrier of excessive computer time has so far discouraged researchers and engineers from embarking onto a reliability analysis of crack propagation with finite element modelling. The contribution of this research is then the proposed efficient approach rendering this comprehensive analysis computationally tractable.

1.1 The Crack Propagation Problem

This section briefly outlines the general background for the engineering problem of interest in this thesis. The development of cracks is an important phenomenon in many engineering materials subjected to fatigue loading. The fatigue problem entered the field of engineering vigorously together with the expansion of railway transportation. Broek [15] reports how incredibly frequently serious fatigue failures occurred on the British railway in mid 19^{th} century. In 1850's, Whöler pioneered fatigue testing on rail vehicle axles. He developed the concept of stress level – fatigue life curves, which has ever since been the design principle widely used by the engineers.

In 1920's, Griffith [36] studied the material fracture itself. Three decades later, the description of the crack tip stress field [42], [97] laid the basis for a study of the current velocity of propagation of an actual crack. Paris [73] was the first to propose that the propagation velocity may be related to the general elastic state of stress at the crack tip. As a matter of fact, Paris thereby laid down the fundamentals for an engineering discipline concerned with the prediction of propagation of existing cracks, which is the field of interest of this thesis.

1.1.1 Domains of Application

Modelling of crack propagation is needed in industrial problems where we are interested in the remaining life under propagation of actually existing cracks. Explicitely said, we admit that the structure in operation does contain cracks, but we continue operating it despite this knowledge. Such daring decision is only admissible for structures that are subject to periodic inspections. Often, this is not the case and modelling of crack propagation than makes no sense. However, in some sectors, namely in air and naval traffic, inspections are obligatory and modelling of crack propagation becomes an important tool in inspection scheduling and in verification of repair designs.

1.1.2 Objectives

The objectives of this thesis can be formulated as follows:

- review various crack propagation approaches;
- propose an efficient approach allowing for stochastic crack propagation analysis with a finite element mechanical model;
- develop and implement a full crack propagation procedure based on the proposed approach;
- demonstrate the feasibility and utility of the developed procedure on a reliability problem of a complexity relevant to industrial applications.

1.2 Organisation of the Thesis

The significant contribution of this thesis consists in proposing a comprehensive approach to perform an efficient reliability analysis of fatigue crack propagation using finite element stress analysis. Rather than developing completely new methods, the approach is based on putting together pieces of available methods in efficient ways and in performing certain numerical operations in a more thoughtful manner than what would be an initial-choice engineering approach.

In line with this, the thesis is organised in two parts. Part I presents the theory fundamentals as a basis for choosing the most appropriate method for the problem of interest. The presentation is developed to a greater detail when it comes to the analysis of stresses around the crack front, which was the area of concern of the Czech part of the research of the author, as mentioned above. Technical details of the presentation have mostly been moved to the appendices to keep the text concise.

Readers familiar with the theory of fracture mechanics and fatigue (Chapter 2), crack front stress field analysis (Chapter 2.3), finite element, meshless and extended finite element methods (Chapter 3) or with reliability analysis (Chapter 4) may only quickly skim through the respective chapters of this part of the thesis.

Based on the theory review presented in Part I, the second part of the thesis identifies the challenges of proper and efficient crack propagation modelling. Then, the proposed crack propagation reliability analysis approach is developed. This includes statistical modelling and reliability analysis methods (Chapter 6), the actual crack growth simulation and integration algorithm (Chapter 7) and distributed computing techniques used to further

accelerate the computations (Chapter 8). The validity of some of the proposed techniques is then verified by a comparison with a purely numerical approach. Finally, an application of the developed approach is demonstrated on a full-scope crack propagation reliability analysis example.

Part I

Deterministic and Stochastic Crack Propagation Theory and Methods

Chapter 2

Fracture Mechanics and Fatigue

2.1 Introduction

Practical modelling of fatigue crack propagation relies on engineering approaches that have been successfully used for decades, but that involve a number of simplifications. To put these models in contrast with the physical reality, the physical mechanisms of crack propagation and fracture are described first in Section 2.2.1. The crack propagation and fracture models that are still in use today were established in times when electron microscopy was not available and the developments were driven by a need for easily deployable crack propagation models. As a matter of fact, tractable engineering models of crack growth based on *ab initio* principles do not seem to be available.

Section 2.3 reviews the theory of lienar elastic fracture mechanics as a prerequisite for comprehension of the crack propagation models.

The crack propagation models that have proven efficient in use relate the propagation velocity or the fatigue life to the (general) level of stress. The objective is to present these practical crack propagation modelling methods. In Sections 2.5, 2.6 and 2.7, we review the deterministic models. Then, we will study in Section 2.8 the approaches allowing to take into account the inherent randomness in crack propagation.

2.2 The Physics of Cracking and Fracture

Before one starts discussing the modelling of crack propagation and fracture, it is useful to describe, albeit very briefly, the physical mechanisms behind crack nucleation, crack growth and fracture. The discussion here is limited to mechanisms relevant to metals. Moreover, certain processes that are not the subject of this thesis, such as thermal fatigue or stress corrosion fatigue, are left aside in the discussion.

2.2.1 Mechanisms of Crack Nucleation and Propagation by Fatigue

Of a particular relevance to this thesis is the physics of fatigue damage, which occurs under cyclic loading of a magnitude a single application of which would not be sufficient to cause failure. Wood [99] proposed the following concept. An application of a tensile stress results in a slip along the shear plane in a material grain whose crystallographic orientation with respect to the applied stress is favourable for a slip. The slip occurs first in those favourably oriented grains that are subject to increased stresses, or micro-defects and surface roughness, which act as local stress concentrators.

Hardening on the slip planes results on the one hand in a slight shift of the plane along which the next slip upon stress reversal is going to take place, and on the other hand, it locks the movement of dislocations. This in turns gives rise to a formation of the so called slip bands oriented in the direction of the slip, through which the dislocations can move easily. In addition, reversing slips along parallel planes form intrusions and extrusion on the material surface. These two features mark the onset of crack initiation. Damaged grains contained within the material are not critical in terms of crack initiation, with fatigue being essentially a surface effect [15].

In the first phase, the cracking takes place in Mode II along the slip bands direction, which is inclined about 45° from the surface. Due to hardening in the surface grains, the slipping may cross the grain boundary to spread into the neighbouring grains. As the size of the crack increases, its tendency to follow the shear plane direction weakens and the crack turns towards the direction perpendicular to the applied stress. Cracks experiencing relatively higher stresses propagate faster and become what is often termed the leading crack.

A mechanism of propagation in the second phase, when the crack tends to grow perpendicularly to the maximum tensile stress, was suggested by Forsyth [31]. The tip of the existing crack causes large stress concentrations.

A slip may then occur, starting from the crack front, along a slip plane inclined from the crack face and more or less matching the shear stress direction. Activation of other parallel and perpendicular slip planes results in an extention of the crack as well as in blunting of the crack tip. Stress reversal, or alone the compressive stresses persisting due to an action of the surrounding elastic material on the plastified region around the crack tip, will close the crack again and re-sharpen the crack tip.

Over the load history, the successive crack tips and blunted crack faces create a pattern of the so called striation. These are well apparent on crack surfaces of materials exhibiting a manifold of possible slip planes to accommodate yielding along the usually curved crack front. In other crystallographic structures, cleavage may come into play and the yielding-induced striation is less apparent. Nevertheless, the essential mechanism of crack propagation is linked to local yielding at the crack tip, i.e. to a slip. However, slip can occur only along the slip planes of the grains. Depending on the local grain orientation and size, the crack advances on many and variably oriented mini-crack-fronts through the thickness of the specimen. Locally, the crack extension direction may deviate considerably from the overall crack growth direction.

Fatigue crack evolution also depends largely on the residual compressive stresses existing around the crack tip due to overloads or due to the roughness of the crack surface, which also makes the crack faces come into contact. Once the crack lips are separated, their surfaces will never match again perfectly, as the fractal theory explains. This effect is more pronounced in coarser grained materials.

Other local effects may also intervene to alter the crack propagation direction. Inclusions from material phases contained in the material that cannot easily deform plastically as well as microcracks represent local stress concentrators, acting as crack attractors. Some second-phase particles cannot be traversed by the crack, which is forced to bypass them. This results in crack defection and Mode II propagation, and effectively into slowing down of the growth rate. Macroscopic geometrical boundaries, such as openings, corners and nearby cracks, also act as stress concentrators and crack attractors.

It is also known that commonly used engineering materials, including aluminium alloy sheets finding wide application in the aerospace industry, are anisotropic with respect to their strength, fatigue and fracture properties. Specimens of these materials exhibit different crack propagation speeds in fatigue tests, depending on whether the crack propagates in parallel or perpendicular to the rolling or extrusion direction of their manufacturing

process.

The above notes suggest that the actual direction of crack propagation is on the one hand prevalently governed by the surrounding stress field, but on the other hand, it has also a random component, depending on a random distribution of inclusions and second phase particles, on random crystallographic orientation within the grains, and on the size of the grains.

2.2.2 Fracture Mechanisms

Under extreme stresses occurring due to extreme loads or in structures where cracks have largely propagated by fatigue, fracture failure occurs. It is recognised that there are two major mechanisms of fracture, namely ductile and brittle fracture, depending on the crystalline properties of the material of concern and on the temperature [32], [15].

In certain materials, like austenitic steel or aluminium alloys, many material grains are oriented such that their crystallographic planes are aligned with the direction of the shearing stresses, allowing for easy plastic deformation by sliding along the dense atomic planes. Fracture is in such cases preceeded by apparent plastic deformation and one speaks of a ductile fracture. In highly pure materials, sliding on conjugate slip planes gradually leads to necking down of the specimen to just a few percent of its initial section size. However, engineering materials contain inclusions that are incapable of much plastic deformation. In presence of high stresses due to deformations of the neighbouring alloy crystals, the inclusions tend to yield by cleaving apart, forming thus a large cavity in the material, which increases the stresses locally. Meanwhile, smaller particles cannot take the same plastic deformation as the surrounding matrix and de-bond from the alloy. The material between the voids necks down by slip until the voids ultimately coalesce to to form a macroscopic crack.

The crystallographic nature of certain other materials, including ferritic steel, makes them susceptible to cleavage of the material grains, rather than sliding along the dense atomic planes. In many other materials, low temperature favours the occurrence of this brittle type of facture. Fracture than occurs by separation of crystallographic planes by breaking of atomic bonds. As the effective section of the material is weakened by the ruptured grains, the remaining grains are subject to an increased stress. The microcracks in grains whose cleavage plane is favourably oriented (perpendicular) with respect to the applied tension may then propagate to the neighbouring grains, ultimately provoking a brittle fracture failure. This mechanism is termed transgranular fracture. The grain boundary phase of some materials, such

as cementite in iron, is particularly weak and brittle. In such situation, it is easier for the crack to travel along the grain boundary than through the grain. The so called inter-granular fracture occurs.

It remains to note that from the engineering point of view, ductile and brittle fracture are distinguished based not on the microscopic fracture mechanism, but rather on the amount of plastic deformation occurring before fracture, which accompanies the above described ductile fracture mechanism. However, the plasticity may be confined to a small volume and the overall plastic deformation remains relatively small. Then, the fracture is considered brittle in the engineering sense.

2.3 Crack Tip Stress Field

2.3.1 Introduction

The parameters used in crack propagation theory largely derive from the theory of linear elastic fracture mechanics (LEFM). In this Chapter, we show how the energy based description of fracture relates to the description building on the knowledge of the stress field around the crack tip. We will formally introduce the stress intensity factor (SIF) K that appears in the empirical crack growth laws reviewed in Section 2.5. It is of course not the aim of the presentation herein to give a complete review of these theoretical concepts. The scope will be limited to aspects relevant to this thesis.

In Section 2.3.5, we will also study the behaviour of the stresses as they change along the crack front in three dimensions (3D). A numerical investigation relating to this topic is presented in Appendix A.3. The conclusions of this study have a direct bearing on the extensibility of the crack propagation modelling approaches to 3D problems.

This chapter has been compiled based on the theoretical studies and numerical simulations carried out by the author as that part of his doctoral thesis research, which was conducted in Brno, Czech Republic.

2.3.2 Griffith's Energy-Based Approach

The fundamentals of brittle fracture theory were laid down by Griffith in his 1921 paper [36]. His reasoning was that in a plate stretched by a fixed displacement, the energy needed to fracture the material and thus extend the crack comes from a release of elastic energy in the material.

Considering also the work of external forces, the energy balance of an extension of the crack by ∂a in the elastic body reads (neglecting the kinetic

energy):

$$\frac{\partial}{\partial a}\left(W_{ext} - W_{el}\right) = \frac{\partial W_{sep}}{\partial a}\,, \tag{2.1}$$

where W_{ext} is the work done by the external forces, W_{el} is the elastic energy contained in the plate, and W_{sep} is the energy needed to separate the crack faces over a length ∂a (assuming a unit thickness of the plate traversed by the crack). In words, the work delivered by the external forces is consumed by 1) augmenting of the elastic energy of the material, and in 2) separating of the crack faces. Griffith defined γ to be bonding energy per unit surface. Then, for two crack lips in a plate of a unit thickness, $W_{sep} = 2\gamma\,\partial a$. This separation energy per unit crack extension defines the *energy release rate* G:

$$G = \partial W_{sep} = -\frac{\partial}{\partial a}\left(W_{ext} - W_{el}\right)\,. \tag{2.2}$$

The criterion for crack growth is then $G \geq 2\gamma$.

Consider now a plate (domain Ω) with traction T_i^d prescribed over a part $\partial\Omega_T$ of its boundary $\partial\Omega$ and displacements u_i^d prescribed over $\partial\Omega_u$, such that $\partial\Omega_T \bigcap \partial\Omega_u = \partial\Omega$ and $\partial\Omega_T \bigcup \partial\Omega_u = \emptyset$. $\partial\Omega_T$ includes also the crack faces Γ, which are however considered traction free. The change in the elastic energy is:

$$\frac{d}{\partial a}\int_\Omega \frac{1}{2}\sigma_{ij}\varepsilon_{ij}\,d\omega = \frac{d}{\partial a}\int_{\partial\Omega}\frac{1}{2}T_i u_i\,ds = \frac{1}{2}\int_{\partial\Omega}\left(T_i\frac{\partial u_i}{\partial a} + u_i\frac{\partial T_i}{\partial a}\right)\,ds\,, \tag{2.3}$$

and the change in the work of the external forces is:

$$\frac{\partial W_{ext}}{\partial a} = \int_{\partial\Omega_T} T_i^d\frac{\partial u_i}{\partial a}\,ds\,. \tag{2.4}$$

Note that $\partial u_i^d/\partial a = 0$ on $\partial\Omega_u$ and $\partial T_i^d/\partial a = 0$ on $\partial\Omega_T$. Equation 2.2 then reads:

$$G = \frac{1}{2}\int_{\partial\Omega}\left(T_i\frac{\partial u_i}{\partial a} - \frac{\partial T_i}{\partial a}u_i\right)\,ds\,. \tag{2.5}$$

2.3.3 Irwin's Relation between G and K

The energy release rate G defined in Section 2.3.2 and the stress intensity factor K to be introduced in Section 2.3.6 were related to each other by Irwin [42].

Irwin's approach to relate the two quantities was based on the idea that the work expended in separating the crack lips over a length Δa is equal to the work done by a crack-face traction necessary to close the separated

crack faces over the length Δa. In fact, the atomic bond forces in the non-separated material are equated with the crack face traction on the separated crack faces and work is done by the bond forces on the displacements of closing or opening of the crack.

A derivation of Irwin's relation using the stress and displacement formulæ deduced by Williams (see Appendix A) was shown in [48] or [16]. If you are interested, read the detailed derivation in Appendix A, Section A.1. The important result is:

$$G = -\frac{1}{2\partial a}\int_{\Gamma_{\Delta a}} {}^{1}T_i\,{}^{2}u_i\,ds = \frac{1-\nu^2}{E}(K_I^2 + K_{II}^2) + \frac{1+\nu}{E}K_{III}^2\,, \qquad (2.6)$$

where 1 and 2 denote a state before and after the crack has extended by Δa, respectively. T stands for traction, u are displacements, and K_I, K_{II} and K_{III} are the stress intensity factors for the respective fracture modes. The interesting aspect of Eq. 2.6 is that G depends only on the intensity of the crack-tip stress field (see Appendix A, Section A.2).

2.3.4 The Elastostatic Problem

For purposes of crack propagation modelling, the essential result of the fracture mechanics theory is the knowledge of the crack tip stress field. The two-dimensional (2D) linear elastic solution includes a magnitude factor termed the stress intensity factor (SIF) and denoted K. K is the parameter most extensively used as the crack propagation driver in the empirical crack growth laws, see Section 2.5.

The understanding of the crack tip stress field solution is useful for several reasons. Firstly, it is simply good to understand where the SIF one uses in crack propagation modelling comes from and what it means. Secondly, it is always advisable to be aware of the specific assumptions implicitly made in crack propagation modelling. Also, the definition of the SIF will shed light on the question of possible extension of the procedures developed in 2D to three dimensional (3D) problems.

The front of a crack is considered ideally sharp, which gives rise to stresses exceeding the elastic limit. However, as long as the crack-front plastic zone is contained within a small volume, an assumption of linear elasticity may be valid. In addition, the elasto-plastic fracture mechanics theories have been developed as an extension of the linear elastic fracture mechanics (LEFM). Static LEFM is discussed in this section.

The problem we will seek to solve is to find the displacement field and stress field in an elastic body containing a notch or a crack. The body

is subject to a remotely applied static loading and all other surfaces are stress-free, including the faces of the notch or crack.

In general, the solution to such three dimensional problem can be sought by representing it in terms of harmonic potentials. This leads to three partial differential equations for the three displacement components. However, such approach is very difficult and can provide a solution for a single specific geometry only.

A more tractable approach is to apply variational calculus. A variational method using a special numerical discretisation was applied to solve the problem by Bažant & Estenssoro [7] – see Section 2.3.5.

The 3D problem can of course also be solved numerically by the finite element method (FEM) or the boundary element method. FEM was used in this thesis to study the shape of the stress field in the vicinity of the crack front in 3D.

Finally, for certain problems, such as through cracks in relatively thin plates, we can simplify the problem by reducing it to two dimensions. Then, solutions by means of complex potentials or Airy's stress function become available. The latter solution is presented in Appendix A.2. Important results are summarised in Section 2.3.6.

2.3.5 3D Elastic Crack Front Field

The assumption made in the stress analysis of cracks is that the crack front in 3D or crack tip in 2D are perfectly sharp. In elasticity, this results in a singularity in terms of infinite stresses at the crack front or crack tip. Stress singularity exists also at the tip or front of a V-notch, but it is of a different order than in the case of a crack. Note that a notch is a dent manufactured into the plate, not showing any fatigue damage. But from a mathematical point of view, a crack may be regarded as a special case of a notch, having a notch opening angle $\alpha = 0$.

The above distinction between two- and three-dimensional analysis and between crack tip and crack front is not an end in self. For most problems of plate fracture with through cracks, 2D modelling is a valid assumption. However, for surface cracks and in a rigorous 3D continuum analysis of through cracks, the effect of the intersection of the crack front and the body surface, which is termed the crack corner or crack vertex, needs to be considered.

Dauge ([19],[20]) considers both the edge singularity and the corner singularity. In [20], it is shown how a combined edge-and-corner expansion of the stress field can be derived mathematically. The expansion consists of

both the edge singularity related stress intensity factor together with the respective shape functions (see Appendix A), and the analogous coefficient of the corner expansion with a remainder of the respective shape functions. The cylindrical coordinate system of the edge expansion and the spherical coordinate system of the corner expansion are shown in Fig. 2.1.

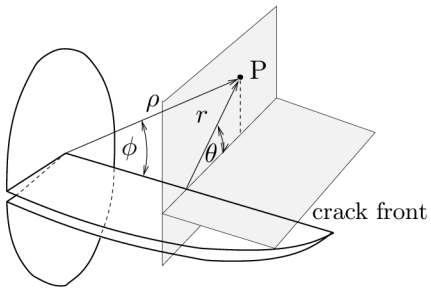

Figure 2.1: *Spherical and cylindrical coordinates*

A number of researchers have been looking at the problem of the corner of a through crack, attempting to find an analytical solution for the stress field. Some authors ([29],[17]) accounted in their developments for the effect of the free surface, but did not explicitly include the corner singularity in their considerations. Their results disagree with the works, in which the corner singularity was explicitely considered ([10],[7]).

It appears that a purely analytical solution to the crack vertex-edge problem is yet to be devised. Pook [75] even makes a remark that *"the derivation of exact analytical solution does not appear to be possible"*.

Of a particular interest is the paper of Bažant & Estenssoro [7]. The authors represented the stress field around the crack as follows:

$$u = \rho^{\lambda}\, r^{1/2}\, f(\phi,\theta)\,,\ v = \rho^{\lambda}\, r^{1/2}\, g(\phi,\theta)\,,\ w = \rho^{\lambda}\, r^{1/2}\, h(\phi,\theta)\,, \tag{2.7}$$

where u, v and w were the displacements in the directions ρ, ϕ and θ, respectively, of a spherical coordinate system with origin at the corner point and $\phi = 0$ being the direction of the crack front (cf. Fig. 2.1). However, only the (θ,ϕ)-space was discretised by the finite element method. Then, the minium energy principle was invoked. The relevant solution in the (θ,ϕ)-space depends on the exponent λ on the third coordinate ρ, and λ was obtained as an eigensolution of the finite element problem.

The results obtained in [7] show that value of λ depends on the Poisson ratio ν and the local geometry, defined by the crack front termination angle β (measured from the edge formed by the intersection of the crack face and

the free surface) and the crack plane inclination angle γ to the free surface. For $\nu = 0.3$ and $\gamma = \pi/2$, the authors obtained values of λ (characterising the behaviour of the displacements) decreasing with β becoming smaller. For $\beta = \pi/2$ (crack front perpendicular to the free surface), λ can be read from the plot in [7] to be about 0.547, i.e. $\lambda > 1/2$. The value $\lambda = 1/2$ corresponds in the cited results to an angle β of about 101°. This is in agreement with the results actually observed in fatigue tests on thicker specimens: the crack corners tend to trail beyond the mid-thickness region of the crack front.

Behaviour of the Stress Field along the Crack Front

The author has carried out a linear elastic finite element study of the stress field behaviour along the crack front. Since this level of investigation would be a little disruptive for the coherence of this concise theoretical background, the study is presented in Appendix A.3. The important result that can be learnt from this study is an evidence that the stresses around the crack front show a truly three-dimensional behaviour, see Fig. 2.2.

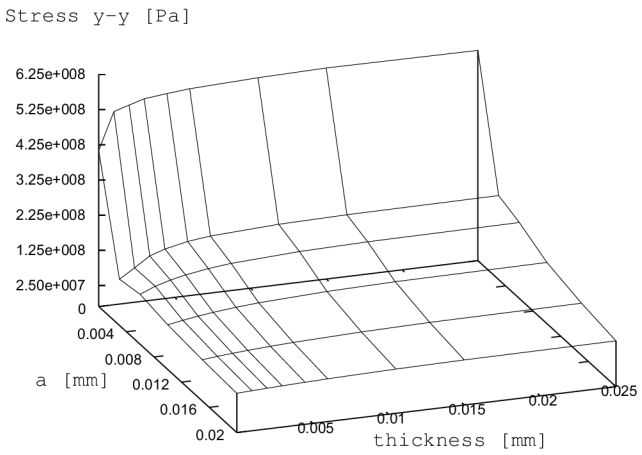

Figure 2.2: *Variation of stresses perpendicular to the crack face in the vicinity of the crack front*

Consequences can be drawn for thick plate-like specimens and cracked bodies of a pronounced 3D nature, and to some extent also for very thin foils. In both cases, the stress distribution is influenced by the presence of the corner point singularity discussed above. However, in the latter case, it is a question whether a continuous mechanics investigation can give answers

to real-world phenomena, since in very thin foils, the microstructure effects may become prevalent.

2.3.6 2D Elastic Crack Tip Field

The classical fracture mechanics and crack propagation theory has been developed around a solution of the stress field in the vicinity of the crack that was made possible by a reduction of the problem to a two-dimensional domain. Once the problem is postulated in a plane, effective mathematical tools become available for its solution. Among them are the theory of complex potentials [62] and Airy's stress function.

A rather complete derivation of the 2D solution using Airy's stress function is exposed in Appendix A.2. In this theoretical background overview, it will be sufficient to just outline the solution method and present the resulting solution.

In 1957, Williams published a paper [97] in which he showed that the stress field has a singularity of the type $1/\sqrt{r}$ at the crack tip, where r is the distance from the crack tip. He proposed a solution for the governing biharmonic equation

$$\nabla^2\nabla^2\Phi = 0 \tag{2.8}$$

with Φ being Airy's stress function:

$$\sigma_{xx} = \frac{\partial^2\Phi}{\partial y^2}\,, \quad \sigma_{xy} = -\frac{\partial^2\Phi}{\partial x\partial y}\,, \quad \sigma_{yy} = \frac{\partial^2\Phi}{\partial x^2}\,, \tag{2.9}$$

in a factorised form with the polar coordinates r and θ constituting multiplicative terms in the solution, together with a proportionality factor K_Φ:

$$\Phi = K_\Phi\, r^{2-s} f(\theta)\,. \tag{2.10}$$

Note that s will determine the order of singularity of the solution. Using the power $2 - s$ ensures that r can be factored out from Eq. (2.8) when we substitute Eq. (2.10) in it. What results is a homogeneous ordinary differential equation with θ being the only variable. Symmetric loading conditions (Mode I, Mode II and Mode III) are then considered and the solution function $f(\theta)$ is sought in the space of trigonometric functions.

To determine the value of s, boundary conditions (stress-free crack faces) are applied. This leads to an eigenvalue problem and the complete solution is an eigenexpansion. The first eigenvalue determines the order of the singularity, which depends on the initial notch opening angle α.

For a crack, where $\alpha = 0$, there exists also an eigenvalue equal to zero. This results in a constant stress term, called the T-stress. It has been shown [45] that accounting for the T-stress improves the prediction of crack propagation, especially for certain geometries of the problem.

When the eigenexpansion is truncated after the first term (the remainder will thus include also the T-stress), the stress components in the polar coordinate system for the crack opening fracture Mode I are:

$$\begin{aligned} \sigma_{rr} &= \frac{K_I}{\sqrt{2\pi r}} \left(\frac{5}{4} \cos\frac{\theta}{2} - \frac{1}{4} \cos\frac{3\theta}{2} \right) \\ \sigma_{\theta\theta} &= \frac{K_I}{\sqrt{2\pi r}} \left(\frac{2}{4} \cos\frac{\theta}{2} + \frac{1}{4} \cos\frac{3\theta}{2} \right) \\ \sigma_{r\theta} &= \frac{K_I}{\sqrt{2\pi r}} \left(\frac{1}{4} \sin\frac{\theta}{2} + \frac{1}{4} \sin\frac{3\theta}{2} \right) . \end{aligned} \tag{2.11}$$

2.3.7 Conclusions

Next to shedding light onto the meaning of the stress intensity factor and the assumptions under which it is defined, the discussion above brings forward the three dimensional character of the crack front stress field.

Notwithstanding the above, two dimensional modelling of fracture and fatigue is appropriate in most problems of a prevalently two dimensional nature. After all, experience has shown that 2D modelling can provide very useful results. Stress intensity factor (SIF) based crack propagation laws have turned out to be effective tools to predict crack growth. They appear to be a good operative means of relating the crack growth rate to the state of stress in the structure. And we have seen in Section 2.3.6 that it is indeed the stress intensity factor K which characterises the magnitude of stresses at the crack tip.

However, care must be taken when using K. It has been defined as the proportionality factor in a solution for a 2D problem. We have also established a relation between K and the energy release rate G. Sure, G does have a sense as the energy to separate the crack faces over a certain area, which is a three dimensional description. But when its equivalence with the two-dimensional K is established, we implicitly assume that the area reduces to a distance of crack extension. A self-similar extension takes place everywhere along the crack front.

The stress intensity factor has a sense as a global variable that can govern the advance of the crack front as a whole. When we use some analogy to calculate SIF at various points along the crack length, we are actually using a

theory developed under 2D assumptions for another problem. (Admittedly, this is exactly what is done in the numerical simulations in Appendix A.3).

Various methods have been developed to calculate SIF varying along the crack front – their brief overview can be found in Section 3.7. These methods have been applied in crack propagation simulations. But perhaps due to the ill assumption on the direct extensibility of SIF to three dimensions, the validity of such methods is disputable.

This has a direct bearing also on the extensibility of the stochastic crack propagation procedure developed in this thesis to three dimensions. It is based on SIF driven crack growth. Although the numerical method used has been successfully applied to 3D problems, the same cannot be said about the prediction of crack growth.

2.4 Fatigue Life Phases

The lifetime of structures subjected to fatigue loading consists of three distinct phases, in which different physical processes are taking place and which can therefore be analysed separately. These three phases are crack initiation, crack propagation and residual fracture strength.

2.4.1 Crack Initiation

Under high-cycle fatigue conditions, a vast majority of the fatigue life of structures is spent in the crack initiation phase. This fact permits to carry out an engineering assessment of the entire fatigue life until failure of the structure without modelling the crack propagation and fracture failure phases explicitely. Such engineering approaches have proven quite efficient in characterising the fatigue strength of structures. As a matter of fact, the actual physical mechanisms involved in crack initiation, as discussed in Chapter 2.2, are difficult to model and a simpler engineering approach is thus desirable.

Around 1850's, Wöhler [98] pioneered fatigue testing in his investigations why railway axles fail. Wöhler conceived ingenious machines using which he subjected specimens to cyclic loading with partial or full load relaxation. He showed that the fatigue life of the specimens depended on the level of maximal stress and on the minimal to maximal stress ratio. The plot of stress S against the number of cycles N known as the Wöhler curve or the $S-N$ curve conveniently describes the high-cycle fatigue data and remains in use in engineering fatigue practice until today.

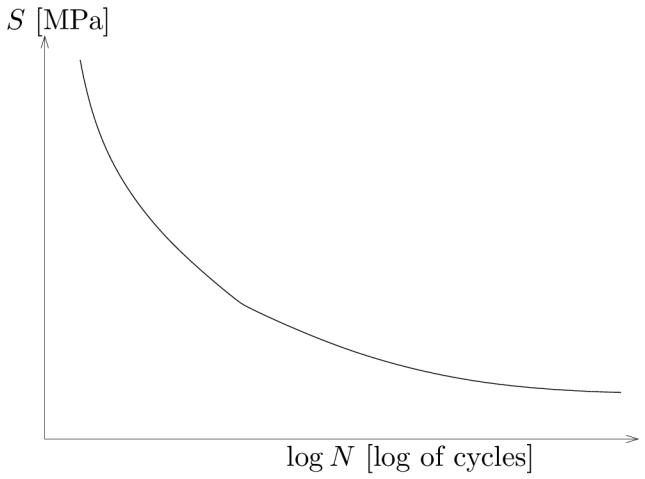

Figure 2.3: *A illustration of an S-N curve.*

Figure 2.3 shows an illustration of a stress-life curve. The so called runout lives, at which the tested specimens fail, are often plotted in log scale since lives in the order of magnitude of 10^7 cycles are often needed to break engineering test specimens. Obtaining a useful $S-N$ curve thus also requires a considerable number of very long fatigue tests.

The $S-N$ curves are constructed for sinusoidal loading varying with a constant amplitude. In general, the loading is a time history with varying amplitudes. In such case, one usually employs a convenient counting method. The Rainflow counting [57] is the most widely used one. The counting procedure transforms the complex loading history into k blocks of monotonous loading of n_i cycles each. If N_i is the fatigue life given for the amplitude of the block considered, the damage of the structure can be accumulated using Miner's [60] *linear damage accumulation* hypothesis:

$$D = \sum_{i=1}^{k} \frac{n_i}{N_i} \,. \tag{2.12}$$

The structure is considered failed if $D \geq 1$.

The important issues in this methodology are test result censoring and including the test statistics (scatter) in the design for fatigue. Rich literature exists on these topics, but is not reviewed here since the $S-N$ approach, although important, is not the subject of interest for the purposes of this thesis.

2.4.2 Crack Propagation

The crack propagation phase of the total fatigue life is the very focus of this thesis. While the physical mechanism of crack propagation was briefly described in Chapter 2.2, deterministic crack propagation models are presented in Sections 2.5 and 2.6, and stochastic crack propagation modelling is the subject of Section 2.8.

2.4.3 Residual Strength

In a situation of high cycle fatigue, where a very large number of fatigue load cycles is necessary before a failure occurs, the growth of the crack starts to accelerate after a certain time spent in the propagation phase. This growth rate acceleration is a sign of a different crack advance mechanism staring to gain ground, in particular the mechanism of fracture. In physical terms, it has been described in Section 2.2.2. For the purposes of the reliability analysis carried out in this thesis, the onset of fracture will be considered as the event of failure. It will be assumed that this event occurs when the stress intensity factor attains the value of the fracture toughness K_c.

Strictly speaking, fracture failure does not automatically happen when K_c is reached. Especially under plane stress conditions and with ductile materials, the fracture resistance, defined as the energy release rate required to extend the crack, increases after an initial advance of the crack. Depending on how much additional load is supplied, the crack, propagating now already by fracture, may stop growing, progress in a stable manner or depart for a final unstable fracture. The fracture resistance is characterised by the so called "R-curves". For their discussion, the reader is referred to any standard fracture mechanics textbook, e.g. [15] or [2].

2.5 Empirical Crack Growth Laws

In 1961, Paris *et al.* [74] were the first to propose that the velocity of crack growth was controlled by the stress intensity factor K. At that time, the response to this assertion was rejective. In his historical reflection, Paris [72] notes:

> Well, that paper was very promptly rejected by three of the world's leading journals. All of the reviewers simply stated that 'no elastic parameter, e.g. K, could possibly correlate fatigue cracking rates because plasticity was a dominant feature'. They

> proceeded to somehow totally disregard the facts clearly demonstrated by the data!

Indeed, using the stress intensity factor K characterising the stress field in the vicinity of the crack appears to be a suitable way of linking the crack propagation velocity to the stresses in the body, which are easy to determine. It is by fitting the crack growth equation parameters to actual crack growth data that one obtains a plausible model for engineering prediction of crack propagation in components and structures. In this way, one can abstract from the actual physical mechanisms of cracking. The determination of the crack growth law parameters is the subject of Section 6.2.

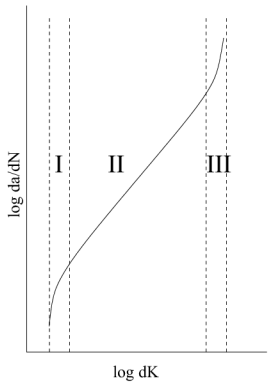

Figure 2.4: *The range of validity of the Paris-Erdogan law*

While the model of Paris & Erdogan is a well-performing engineering tool, it should be noted that:

- it is not based on the actual fatigue crack extension mechanism, which is a plastic slip,
- the exponential form of the law allows for a good fit to the actual crack propagation data (see Fig. 6.1). But the parameters of the law are merely fitting coefficients without a clear physical meaning. Moreover, due to the exponential form of the law, their physical dimensions for the given specimen change with the optimum fit.

Nevertheless, the so called Paris-Erdogan law [73] (called in the following just the "Paris law" for brevity) remains the most widely accepted crack propagation model. It is necessary to note that it is suitable for describing the medium range of the crack growth history (Phase II), while it fails to

capture the phases of crack initiation and short crack growth (Phase I) as well as the near-critical crack propagation phase, as K approaches its critical value, where the crack growth happens by fracture (Phase III), see Fig. 2.4. It is also recognised that the crack growth rate changes with the minimal to maximal stress ratio. Various modifications of the Paris law have been proposed to include the above effects, among which the Forman equation.

It is also important to accentuate that we consider so far only a monotonous cyclic loading with a constant amplitude and constant maximum, such as a sinusoidal load history.

The Paris law has a very simple form:

$$\frac{\mathrm{d}a}{\mathrm{d}N} = C\,(\Delta K)^m\ , \tag{2.13}$$

where the growth rate $\mathrm{d}a/\mathrm{d}N$ is expressed in terms of the increment of crack length $\mathrm{d}a$ per an increment in the number of load cycles $\mathrm{d}N$. ΔK is the stress intensity factor range and C and m are coefficients to be fitted from experimental data.

Forman *et al.* [30] modified the Paris law to account for the acceleration of crack growth as K approaches the value of the fracture toughness K_c and for the effect of the stress ratio $R = \sigma_{\min}/\sigma_{\max}$:

$$\frac{\mathrm{d}a}{\mathrm{d}N} = \frac{C\,(\Delta K)^m}{(1-R)K_c - \Delta K} = \frac{C\,(\Delta K)^m}{(1-R)\,(K_c - K_{\max})}\,, \tag{2.14}$$

where $K_{\max}$ is the stress intensity value at the load peak. Equation (2.14) can be further extended ([82], [77]) to give a zero crack growth when the stress intensity factor range ΔK is below its threshold value ΔK_0:

$$\frac{\mathrm{d}a}{\mathrm{d}N} = \frac{C\,(\Delta K - \Delta K_0)^m}{(1-R)\,(K_c - K_{\max})}\,. \tag{2.15}$$

For steels and aluminium alloys, equation (2.15) gives satisfactory results.

The widely used crack growth software NASGRO utilises the equation developed by Newman [67], [68]:

$$\frac{da}{dN} = C\,(\Delta K_{\mathrm{eff}})^m\,\frac{\left(1-\frac{\Delta K_0}{\Delta K_{\mathrm{eff}}}\right)^p}{\left(1-\frac{K_{\max}}{K_c}\right)^q}\,, \tag{2.16}$$

where ΔK_{eff} is the effective stress intensity factor range between the crack opening stress σ_0 (see Eq. 2.23) and the maximal applied stress $\sigma_{\max}$. p

and q are material constants that characterise the crack growth behaviour near the threshold ΔK_0 and the fracture toughness K_c, respectively. The model extends the validity of the crack growth equation to these regions, but requires more material parameters to be determined.

2.6 Propagation under Variable Amplitude Loading

In Section 2.5, we have assumed that the structure in which the crack propagates experiences a loading that oscillates periodically between some fixed minimum and maximum values. This may be the reality for structures subject to periodic loading due to machines and mechanisms attached to them or applied in a controlled fatigue test.

However, a second important class of structures is one that experiences fatigue loading with peaks and troughs of varying amplitudes. This type of loading covers both a realisation of a random loading process as well as any deterministic complex loading spectra, such as typical loading sequences applied in the analysis of aircraft structures.

The pitfall in variable amplitude stressing is that the rate of crack propagation depends not only on the current elastic stresses in the body, but also on the loading history and the related history of plastic stresses in the vicinity of the crack tip.

In 1970's Elber [24], [25], introduced an important concept of *plasticity induced crack closure*. This concept served as the basis for the development of several different models and procedures to take into account namely the retardation in crack growth occurring after an overload in the stressing sequence. These approaches are described below.

The consequences of variable amplitude or "complex" loading are twofold. On the one hand, neglecting overloads may lead to an excessive overdesign of structures for fatigue. On the other hand, a structure that experiences during its actual service life loading less severe in overloads than has been predicted may fail prematurely.

In this Section, we review the various models that have been proposed to take account of variable amplitude loading. We briefly sketch the approaches based on the plastic zone size, which appeared in 1960's. Next, we introduce the concept of plasticity induced crack closure developed by Elber and discuss the methods based on the concept. Special attention is paid to the so called PREFFAS model, which is the one that was actually chosen as the method to address variable amplitude loading within the crack

propagation reliability analysis framework proposed in this thesis.

2.6.1 Models Based on Plastic Zone Size

The first analytical approaches proposed to deal with the issue of crack growth retardation after overloads recognise the role of the plastic zone developed at the crack tip.

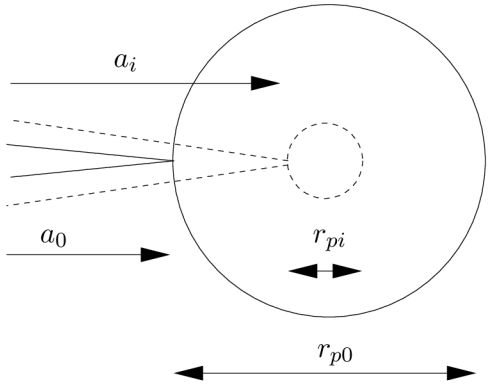

Figure 2.5: *Wheeler crack growth retardation model*

Specifically, Wheeler [94] considers the size of the plastic zone due to an overload of K_o occurring at length a_0:

$$r_{p0} = c_p \frac{K_o^2}{\sigma_{ys}^2} \tag{2.17}$$

and the theoretical plastic zone size at a length a_i to which the crack has propagated after the overload:

$$r_{pi} = c_p \frac{K_i^2}{\sigma_{ys}^2} \,. \tag{2.18}$$

In the above equations, σ_{ys} is the yield stress, K is the elastic stress intensity factor and c_p is a factor applied to obtain a plastic zone size, which can be based on a simplified analytical model. The retarded crack growth rate is then obtained by multiplying the pure K-based crack growth rate by a correction factor corresponding to the ratio of r_{pi} to the distance from a_i up to the limit of the plastic zone ahead of the crack tip created by the preceeding overload:

$$\frac{\mathrm{d}a}{\mathrm{d}N}_{\text{retarded}} = \left(\frac{r_{pi}}{a_0 + r_{p0} - a_i} \right)^q \frac{\mathrm{d}a}{\mathrm{d}N}_{\text{linear}} \,. \tag{2.19}$$

The power q is to be determined experimentally.

Willenborg *et al.* [96] looked at the same situation of the overload and the current plastic zones from a somewhat different angle and sought the K_i that would make r_{pi} extend to the limit of the overload plastic zone ahead of the crack tip. Thus, they first determined $K_{i,\text{req}}$, which is the K_i that would hypothetically be necessary to produce the same propagation velocity as before the overload. $K_{i,\text{req}}$ can be obtained from

$$c_p \frac{K_{i,\text{req}}}{\sigma_{ys}^2} = a_0 + r_{p0} - a_i \,. \tag{2.20}$$

Looking for the way to use the information provided by $K_{i,\text{req}}$, Willenborg *et al.* chose to use in the crack advance calculation a stress intensity factor range ΔK_{eff}, which is the current stress intensity factor range ΔK_i reduced by an amount of $K_{\text{red}} = K_{i,\text{req}} - K_{\max,i}$. Using the Paris law (Eq. (2.13)), the retarded crack propagation rate is then given by:

$$\frac{\mathrm{d}a}{\mathrm{d}N}_{\text{retard}} = C(1 - R_{\text{eff}})K_{\text{eff}}^m \,, \tag{2.21}$$

in which

$$R_{\text{eff}} = \frac{K_{\min,i} - K_{\text{red}}}{K_{\max,i} - K_{\text{red}}} \,. \tag{2.22}$$

2.6.2 Elber's Crack Closure Concept

A far more popular concept in determining the retarded propagation rate is the one proposed by Elber [24], [25]. As a matter of fact, Elber observed in his crack propagation tests that the crack lips get separated only starting from a certain tensile load stress, denoted σ_0 and termed the crack opening stress. Similarly as Wheeler and Willenborg *et al.*, Elber considered that the plastic zone created by the previous stress peak closes the crack by an action on the still elastic material surrounding the plastic zone.

The opening stress level $\sigma_{0,i}$ of a load cycle i can be calculated from the peak $\sigma_{\max,i}$ and the valley $\sigma_{\min,i}$ of the given cycle as follows:

$$\sigma_{0,i} = \sigma_{\max,i} - U_{R,i}\,(\sigma_{\max,i} - \sigma_{\min,i}) \;, \quad U_{R,i} = a_U R + b_U \tag{2.23}$$

with $a_U + b_U = 1$, in which b_U is a material dependent parameter determined by specific fatigue tests.

Elber's crack closure concept is the basis of the PREFFAS model, see Section 2.6.3 below.

2.6.3 The PREFFAS Model

In his 1985 PhD. thesis [21], Davy proposed an approach to deal with variable amplitude fatigue loading in crack propagation, which gained a wide acceptance in the French aerospace industry. It is known under the acronym PREFFAS, which stands for "Prévision de la fissuration en fatigue aérospatiale". This method relies on a transformation of the variable amplitude time history of applied stress into a constant amplitude, sinusoidally varying stresses, making use of Elber's crack closure concept.

The increment Δa of the crack length over an applied load sequence with N cycles can be calculated using the Paris law as follows:

$$\Delta a = \sum_{i=1}^{N} C \left(\Delta K_i\right)^m \ , \tag{2.24}$$

where K_i is the stress intensity factor occurring in the given load cycle and C and m are material parameters entering the Paris law, considered constant throughout the structure.

In general, K depends on the current crack length through some geometry function $F(a)$:

$$K_i = F(a_i)\sigma_i \tag{2.25}$$

In addition, PREFFAS is based on Elber's concept of opening stress (see Section 2.6.2), whereby only a part of ΔK is effective in making the crack tip advance. Pulling together the above, we can rewrite Eq. (2.24) as:

$$\Delta a = \sum_{i=1}^{N} C F^m(a_i) \left(\sigma_{\max,i} - \sigma_{0,i}\right)^m \ , \tag{2.26}$$

PREFFAS makes two major assumptions:

1. the load sequence results in a crack growth that is small enough to consider that the relation between the crack length and the stress intensity factor remains unchanged;

2. the crack opening stress is determined by the previous loading history and does not disappear with time.

Note that when the first of the assumptions in satisfied, the use of the method *can be extended to high-cycle fatigue problems with multiple and interfering cracks.*

Indeed, crack interference results in a change of the *geometry factor* relating the the crack tip stresses to the *remotely applied stress.*

PREFFAS operates at the level of the remotely applied stress. It transforms the variable-amplitude load sequence into a constant-amplitude load sequence to be applied on the structure a single time. The assumption taken in PREFFAS is that this single application of the load sequence brings about only a negligible change in the geometry of the problem.

The geometry factor accounts for crack interaction with all discontinuities. It needs to be updated every time that a significant change in the geometry of the problem takes place. But when the first assumption is satisfied, this cannot happen during a single application of the load sequence. Therefore, crack interaction considerations do not enter into the stress transformation by PREFFAS.

As the geometry factor $F(a)$ does not change throughout the load sequence, it can be separated out of the sum in Eq (2.26):

$$\Delta a = CF^m(a) \sum_{i=1}^{N} \left(\sigma_{\max,i} - \sigma_{0,i}\right)^m \ , \tag{2.27}$$

We see that the sum

$$E_s = \sum_{i=1}^{N} \left(\sigma_{\max,i} - \sigma_{0,i}\right)^m \tag{2.28}$$

in Eq. (2.27) does not depend on a. Thus, under the above assumptions, we can calculate a stress sequence effect E_s without any regard to the cracked structure itself.

The PREFFAS algorithm processes the remote applied stress history. It calculates the stress sequence effect on the basis of Elber's crack opening stress and on some significant history values of cycle peaks and valleys. The details are given in Appendix A.4.

The PREFFAS method can be used to obtain for a chosen number of equivalent load cycles N_{eq} an equivalent load level σ_{eq} that will cause the same damage as the actual load sequence.

The remarkable point about PREFFAS is that a computer simulation of crack propagation using PREFFAS can reproduce surprisingly well actual variable-amplitude fatigue tests.

2.6.4 Randomness in PREFFAS

Eq. (2.23) involves a material parameter b_U. Davy [21] suggests to determine its value from two fatigue tests, one with a monotonous loading and one with an overload every 1000 cycles. For a value of crack length retardation rate T_R observed and known m, one can read b_U from a graphical chart.

We will follow this approach, setting up a two dimensional grid of discrete values of b_U and m. For each pair of values, we will calculate the crack length retardation rate as $T_R = E_{s\,\text{no overload}}/E_{s\,\text{overload}}$ using Eq. (2.28), applying the correct opening stresses calculated from Eq. (2.23).

The numerical map thus constructed can be inverted to obtain b_U for any pair of values T_R and m. Then, assuming that the statistics of T_R and m are known from experiments, Monte Carlo simulation (MCS) can be used to produce a sample of b_U and estimate its statistics.

Note that the simulated scatter in b_U captures only the randomness due to considering only the material properties T_R and m as random, while the uncertainty about the PREFFAS model itself is completely disregarded.

2.6.5 Strip Yield Model

In Section 2.6.3 above, we noted that the transformation of the loading history to a constant amplitude loading by the PREFFAS method takes place under the explicit assumption that the geometry factor to the stress intensity range does not change. It is thus applicable only to load sequences that are quite short with respect to the total fatigue crack propagation life of the structure.

On the other hand, in the so called Strip Yield method [87], it is in principle possible to take the structural geometry explicitely into account.

Similarly as PREFFAS, the Strip Yield model relies on Elber's crack closure concept and the related crack opening stress. The essential difference is in the way the opening stress magnitude is calculated. Instead of using a very simple analytical formula as in PREFFAS, Strip Yield takes advantage of a mechanical model.

In this model, the material around the crack tip is idealised as narrow plastic-rigid bars. The unbroken bars in front of the crack tip carry load both in tension, when they can undergo permanent plastic deformation, and in compression, under which they are considered rigid. The bars in the wake of the crack act only in compression and retain their permanent plastic deformation from the time they were still in front of the crack. This bar model is employed to calculate the crack opening stresses.

From the computational point of view, the advantage of the Strip Yield model is that the stresses and deformations in the hypothetic bars can be found from an elastic continuum model by superposing the elastic solutions of two problems. In each of them appears a crack with a length increased by the size of the plastic zone. The first problem has loading by the remote applied stress. In the second case, the part of the crack face corresponding

to the plastic zone is loaded in compression by the yield stress. In general, the solution method can also be a numerical one to account for complex geometrical configurations.

2.6.6 Note on Full Numerical Calculation

A further step towards realistic modelling of crack propagation is to employ a finite element model including plastic and contact capabilities to solve the mechanical problem at each increment of the crack length. Such full numerical calculation requires advanced solution techniques. Elguedj *et al.* [26] have presented developments aiming at the implementation of such crack propagation simulation using the Extended Finite Element Method with plasticity and contact. Alizadeh *et al.* [1] have proposed a method to calculate crack growth rates based on crack closure analysis in the context of cassical finite elements, relying on releasing of nodes as the crack propagates.

2.7 Propagation Direction

An important part of modelling of crack propagation is to determine the direction in which the crack will next propagate. It this thesis, we are interested in two-dimensional problems. The direction of propagation depends on the stress field surrounding the crack tip. In terms of the fracture mechanics theory, it depends on the mutual proportion of the stress intensity factors for Modes I, II and III of crack propagation.

The three most widely used criteria to determine the current crack growth propagation direction are the following:

- the maximum hoop stress criterion [27];
- the maximum potential energy release rate criterion [40];
- the minimum strain energy density criterion [80].

It was shown in [11] that the three criteria provide practically the same results. We will thus detail only the first of the above criteria, which is also practical for application in that it provides a closed-form solution.

The maximum hoop stress criterion assumes that the crack extension will occur in the direction that maximises the circumferential stress in the region close to the crack tip. In polar coordinate system r, θ, the circumferential

stress σ_θ and the shear stress $\sigma_{r\theta}$ are given by

$$\sigma_\theta = \frac{1}{\sqrt{2\pi r}} \cos\frac{\theta}{2}\left[K_I \cos^2\frac{\theta}{2} - \frac{3}{2}K_{II}\sin\theta\right],$$
$$\sigma_{r\theta} = \frac{1}{2\sqrt{2\pi r}} \cos\frac{\theta}{2}\left[K_I \sin\theta + K_{II}(3\cos\theta - 1)\right]. \tag{2.29}$$

The stress σ_θ will be a principal stress if $\sigma_{r\theta} = 0$. This leads to the condition

$$K_I \sin\theta + K_{II}(3\cos\theta - 1) = 0\,. \tag{2.30}$$

Solving for θ, the crack propagation direction reads:

$$\theta = 2\arctan\left[\frac{1}{4}\left(\frac{K_I}{K_{II}} \pm \sqrt{\left(\frac{K_I}{K_{II}}\right)^2 + 8}\right)\right]. \tag{2.31}$$

Equation (2.31) contains a $\pm$ sign. Of the two values of θ given by the equation, the one resulting in the higher hoop stress σ_θ is taken as the direction of crack propagation.

2.8 Stochastic Nature of Fatigue Crack Propagation

As discussed in Section 2.2, the velocity of fatigue crack propagation depends on a number of local circumstances of a random character, including the crystallographic structure, material impurity, presence of second-phase particles and grain size. In addition, the overload effect (see Section 2.6) comes into play under variable-amplitude loading, and many structures subject to fatigue loading experience random load histories. The modelling of these random aspects of crack propagation is the subject of this Section.

Before a crack extends to a size provoking a failure of the structure by fracture, crack initiation and crack propagation take place. In high-cycle fatigue settings with low levels of the applied stress, the structure of concern may spend a significant part of its lifetime before failure in the crack initiation phase. In general, there are two major modelling approaches. In the $S-N$ curve approach (see Section 2.4.1), crack initiation is included in the total fatigue lifetime. Alternatively, crack initiation is modelled statistically by considering a random life until the initiation of a macro-crack of a given size or a random length of an initial macro-crack at a given time.

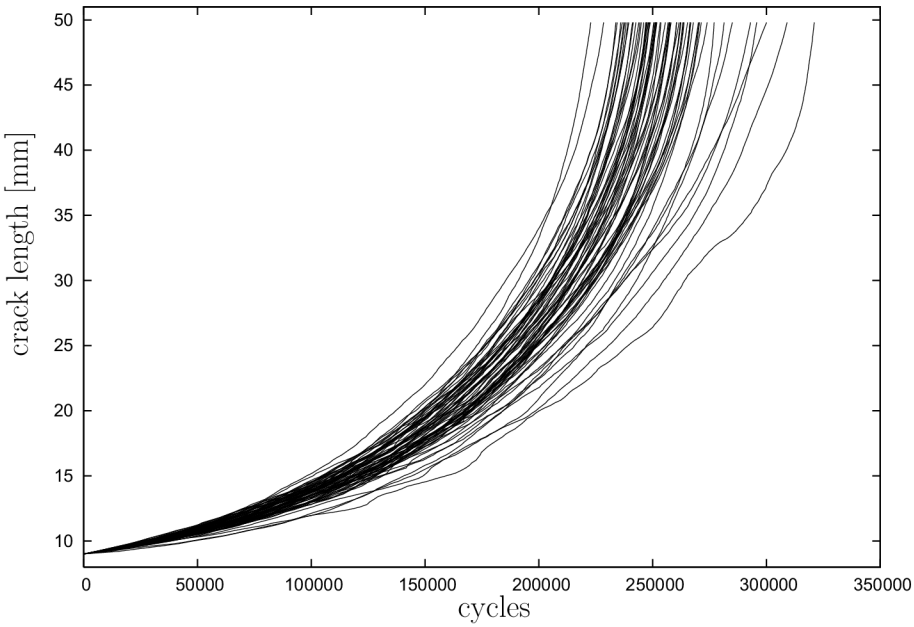

Figure 2.6: *The Virkler crack growth data [89]*

The propagation phase of the initiated crack is then modelled by fracture mechanics techniques (see Section 2.5).

Fatigue tests ([89],[34]) reveal randomness of crack propagation both in terms of differences from specimen to specimen, as well as within a single specimen. In a rigorous analysis, both the inter-specimen and the intra-specimen scatter should be taken into account by the crack propagation model. However, if we are interested in an estimation of the lifetime of a component rather than in the exploration of the variability of crack propagation during the lifetime, considering only the specimen-to-specimen dispersion should generally suffice.

For completeness of presentation, we shall formally include also the intra-specimen variability in the following discussion. In general, the stochastic crack growth equation can be written as follows:

$$\frac{\partial a}{\partial t} = Q\left(t, \Delta K\right) , \tag{2.32}$$

where we consider that the crack growth rate depends not only on the stress intensity factor range, but it is a stochastic process in time. Some authors,

e.g. [82], write down the equation (2.32) in a factored form:

$$\frac{\partial a}{\partial t} = X(t)\, Q\left(\Delta K\right) , \tag{2.33}$$

where $X(t)$ is a positive-valued random process and Q is a (deterministic) crack growth law. In addition to the stress intensity factor range ΔK, Q may involve also other factors. An example of Q is the Paris law (2.13). Assuming that Q is a known deterministic function and that $X(t)$ is a constant mean value plus a Gaussian white noise, Sobczyk & Spencer [82] have derived a distribution of the crack size at a given time and the fatigue propagation life distribution.

It was noted in [51] that the correlation structure of the process $X(t)$ determines the statistical dispersion of the time at which a given crack length a is reached. In two extreme cases, $X(t)$ can be considered as totally uncorrelated, leading to the smallest dispersion, and as totally correlated at all times, resulting in the highest scatter. The latter extreme correlation case is equivalent to replacing the stochastic process $X(t)$ by a random variable X.

The following sections present various approaches that have been applied in stochastic modelling of the fatigue crack propagation process.

2.8.1 Stochastic Differential Equations

A natural way to include uncertainties in the crack propagation analysis is to randomise the crack growth law used as the model for the crack advance. Considering the Paris law (2.13), its parameters C and m are taken as random variables. The stress intensity factor range ΔK is considered to be determined by the given deterministic loading history and structural configuration in time. The integration limits may also be random. The Paris law thus turns into a stochastic differential equation.

It is in general very difficult to find an explicit solution to such nonlinear stochastic differential equation. To circumvent this difficulty, one usually postulates a reliability problem by taking a certain limit in terms of maximal allowable crack length or minimal required service life. In terms of solution methods, one usually resorts to Monte Carlo integration or reliability approximation techniques. This approach is discussed below.

Random Variable Approach

The number of cycles to failure can be expressed using the randomised Paris law as follows:

$$N_R(\omega) = \int_{a_0(\omega)}^{a_f(\omega)} C(\omega)\,(\Delta K(a))^{m(\omega)}\,\mathrm{d}a\,, \tag{2.34}$$

where $x(\omega)$ indicates a variable in the probability space and $x(a)$ indicates a variable that is a function of the crack length.

Given the uncertainty in crack detection and uncertainty about the accuracy of the measurement of the initial crack length a_0, it is natural that a_0 is considered random.

The random or deterministic nature of the final crack length a_f depends on its definition. We may fix a certain deterministic crack length limit that we do not allow to be exceeded. Alternatively, we may define a_f for example as the crack length attained at the instant when the leading crack reaches a certain critical size. The critical size may be the crack length at which the stress intensity factor (SIF) reaches the fracture toughness. Fracture toughness tests show some scatter and the value of SIF may depend not only on the current crack size, but also on a random initial geometry and the resulting interaction of propagating cracks. Thus, a_f is in general also random.

Special care needs to be taken to estimate the statistics of the parameters C and m from crack propagation test data. A correlation between C and m is an important issue, see Section 6.2.

If we require the structure to survive N_S load cycles without failure, the reliability problem can be formulated with the following limit state function:

$$G = N_R - N_S\,. \tag{2.35}$$

The problem is then to determine the probability of failure or the reliability index. It is amenable to solution through Monte Carlo simulation or reliability approximation methods, see Chapter 4.

Note that once the realisations of the random variables including the random initial geometry are known, the crack propagation is completely deterministic. Thus, the random variable approach is capable of taking into account only the specimen-to-specimen scatter, but not the intra-specimen scatter.

2.8.2 Stochastic Process Approach

The stochastic nature of fatigue crack propagation has lead researchers to renounce on empirical crack growth equations and regard the crack propagation as a stochastic process. Two essential types of stochastic process approaches to random crack growth are briefly outlined below.

Markov Chain Models

Markov processes constitute a special class of stochastic processes. A process is said to be Markovian if its future evolution is determined only by its present state and independent of how the process arrived to the present state. Here, we describe the discrete-time and discrete-state Markov chain modelling approach as put forward by Bogdanoff *et al.* [12]. The discrete time points are the ends of *duty cycles*, which are repetitive periods of loading histories. It is assumed that the damage can attain discrete states $1 \dots n$.

The initial state of damage is described by the initial probability density $\mathbf{P}_0 = [\pi_1, \pi_2, \dots, \pi_n]$, where π_i is the probability that the damage is initially in state i. The elements $\{P_{ij}\}$ of the transition matrix $\tilde{\mathbf{P}}$ are the probabilities that the damage will be in state j after the duty cycle given that in was in state i before the duty cycle.

The state of damage at time t is described by the probability density $\mathbf{P}_t = [P_t(1), P_t(2), \dots, P_t(n)]$, where $P_t(i)$ is the probability that the damage is in state i at time t. $\mathbf{P}_t$ can be calculated as follows

$$\mathbf{P}_t = \mathbf{P}_0 \tilde{\mathbf{P}}_1 \tilde{\mathbf{P}}_2 \dots \tilde{\mathbf{P}}_{t-1} \tilde{\mathbf{P}}_t \,. \tag{2.36}$$

We note that the estimation of $\{P_{ij}\}$ is a difficult and laborious task.

Cumulative Jump Stochastic Processes

The cumulative jump approach, proposed in [83], models fatigue crack propagation by random sums of random crack increments:

$$A(t, \omega) = a_0 + \sum_{i=1}^{N(t)} Y_i(\omega) \,, \tag{2.37}$$

where a_0 is the initial crack length, which may be a random variable, $Y_i(\omega)$ are the random crack increments and $N(t)$ is a stochastic counting process such as the Poisson process or a birth process.

It is shown in [82] how the distributions of the crack size at a given time and that of the fatigue life can be derived.

The parameters of the model (the intensity of the Poisson process and the parameters of $Y_i(\omega)$) need to be estimated from crack propagation test data. In [82], it is suggested to take the Poisson process intensity as the average number of maxima in the load history. In the cited monograph, it is further proposed to relate the parameters of $Y_i(\omega)$ to the Paris law parameters by minimising the mean-square difference between the prediction of the stochastic process model and the prediction of the Paris law.

General Note on Parameter Estimation

We can make a generally valid observation that the estimated parameters of the crack propagation stochastic process account for the material effects, for the crack and structure geometry, and for loading. Thus, they need to be estimated anew every time the crack trajectory, the structural configuration or the loading changes.

On the other hand, the parameters of empirical crack growth equations capture only the material effect. The geometry and loading effects are accounted for through the stress intensity factor range. The latter may be given by an analytical formula or obtained from a numerical solution.

2.9 Conclusions

In this Chapter, we have reviewed the elastic theory of the crack tip stress field and saw the nature of the related assumptions that are inherent to the classical crack propagation models.

We also discussed some of the most common methods in deterministic and stochastic fatigue crack propagation modelling. As a matter of fact, two general classes of stochastic crack propagation modelling approaches can be discerned.

The first class relies on continuum mechanics modelling of the underlying mechanical problem. The random nature of crack growth is accounted for through a randomisation of the material-dependent parameters of the empirical crack growth laws. Loading is represented by a time-domain load history and load interaction effects are modelled by means of simplified mechanical models, such as the PREFFAS method, or the strip yield model.

The other class of approaches is inspired by the fact that fatigue crack propagation is a highly random phenomenon. These approaches therefore renounce on any mechanical modelling and consider the crack growth as a stochastic process. They are able to describe the scatter of crack growth

within the specimen. But next to this, the process has to adequately capture all of the load history, material and geometrical aspects. The somewhat wanting propositions how to model curvilinear crack growth [84] or load interaction effects [82] reveal about the difficulty of stochastic process models to account for these aspects. Certainly, the process parameters can be estimated for particular geometrical configurations and loading processes. But the use of stochastic processes to predict crack growth appears to be troublesome.

In summary, stochastic process based modelling can directly provide mathematically elegant answers as to the distribution of fatigue life or crack length at a given instant. But for predictive purposes, mechanistic models seem to have the edge on stochastic processes precisely in that they dispose of the mechanical model. As we will see in Part II of this thesis, this is at the expense of immense computation effort and precautions that necessarily need to be taken in the implementation.

A final note is made about the ability to capture the scatter in crack growth within a specimen or just the random variability from specimen to specimen. In engineering application, it is often the total life under fatigue crack propagation that is of interest. Therefore, for the purposes of this thesis, the random variable approach, where the parameters of the empirical crack growth laws are random variables with a single realisation applicable to the entire specimen, is considered sufficient and appropriate.

Chapter 3

Solution Methods for Elastic Continuum Problems

3.1 Introduction

In Chapter 2.3, we have investigated the nature of the stress field around the crack front when the problem is analysed in three dimensions. In many practical applications, simplification of the problem to two dimensions has been shown to provide very useful results.

In Section 2.3.6 (and Appendix A.2), the solution for the problem of a single two-dimensional crack in an infinite 2D body has been presented. Analytical solutions can also be derived for various configurations involving multiple cracks. However, practical crack propagation prediction problems give rise to complicated structural geometries that require numerical analysis.

In certain predictive applications, such as the design and assessment of repair and crack arrest interventions or inspection scheduling, a correct calculation of stresses in the vicinity of the crack tip in complex structural configurations is a crucial component of the analysis.

This chapter reviews several numerical methods suitable for the solution of complex-geometry crack problems. The objective is to prepare grounds for choosing a numerical method to use in stochastic crack propagation analysis.

3.2 Variational Methods

In Section 2.3.6, we sought a solution (i.e. the stress and displacement field) to the boundary value problem (BVP) of a crack in an infinite plate. We were looking for solutions satisfying the governing biharmonic equation and the boundary conditions.

An alternative solution approach is based on the minimum energy principle. Instead of seeking a solution to the governing differential equation satisfying the boundary conditions, we look for solutions minimising the potential energy of deformation or the so called complementary energy.

This approach lends itself to various approximations of the sought function. With the approximation, the energy will be somewhat higher than the minimum (that is why finite element models are "stiffer" than the reality), but the minimisation can be used to find the parameters of the approximating functions.

We shall consider a loading varying in time. But at the same time, we will always assume that the rates of change of the loading and the displacements involved are such that inertia forces are negligibly smaller as compared to the applied loads and the elastic forces. We shall therefore limit our attention to solution methods for static problems.

3.2.1 The Minimum Potential Energy Principle

In the process of elastic deformation, the energies involved are the work W done by the external (surface and body) forces and the strain energy. The strain energy U stored in a volume Ω can be quantified as:

$$U = \frac{1}{2}\int_{\Omega} (\sigma_{xx}\epsilon_{xx} + \sigma_{yy}\epsilon_{yy} + 2\sigma_{xy}\epsilon_{xy} + 2\sigma_{yz}\epsilon_{yz} + 2\sigma_{xz}\epsilon_{xz})\, \mathrm{d}\Omega\,, \tag{3.1}$$

or, in tensor notation:

$$U = \frac{1}{2}\int_{\Omega} \boldsymbol{\sigma\epsilon}\, \mathrm{d}\Omega\,. \tag{3.2}$$

Let us suppose that a body Ω is in equilibrium under the action of given surface forces $\boldsymbol{T}$ and body forces $\boldsymbol{X}$. The surface forces $\boldsymbol{T}$ are prescribed over a portion Γ_t of the surface, while on the remaining part of the surface Γ_u, the displacements are known. The displacements of the equilibrium state are denoted $\boldsymbol{u}$. Now, consider arbitrary *virtual displacements* $\boldsymbol{u}+\delta\boldsymbol{u}$ with $\delta\boldsymbol{u}$ vanishing over Γ_u. The work done by the external forces $\boldsymbol{T}$ and $\boldsymbol{X}$ through the virtual displacements $\delta\boldsymbol{u}$ is:

$$\delta W = \int_{\Gamma} \boldsymbol{T}\delta\boldsymbol{u}\mathrm{d}\Gamma + \int_{\Omega} \boldsymbol{X}\delta\boldsymbol{u}\mathrm{d}\Omega\,.$$

The strain energy U is equal to the work done by the external forces in deforming the body. Thus:

$$\delta\Pi = \delta\left(\frac{1}{2}\int_{\Omega}\boldsymbol{\sigma\epsilon}\,\mathrm{d}\Omega - \int_{\Gamma}\boldsymbol{T u}\,\mathrm{d}\Gamma - \int_{\Omega}\boldsymbol{X u}\,\mathrm{d}\Omega\right) = 0\,, \tag{3.3}$$

or, in an abbreviated notation:

$$\delta\Pi = \delta\,(U - W) = 0\,. \tag{3.4}$$

Eq. 3.4 above indicates that the potential energy has an extremum at equilibrium. For a stable equilibrium, it can be shown that for any virtual displacement, the change in the potential energy is positive. Therefore, the state of stable equilibrium corresponds to a minimum. This is formulated in the *Minimum Potential Energy Principle*, stating:

> Of all displacements satisfying the given boundary conditions, the displacements satisfying the equilibrium conditions make the potential energy an absolute minimum.

3.2.2 The Minimum Complementary Energy Principle

When the body and the external forces are at equilibrium, we may vary the stresses instead of varying the displacements. In addition to the equilibrium and the boundary conditions that must be fulfilled, the stresses must also fulfil the compatibility conditions, i.e. for two dimensional problems:

$$\frac{\partial^2\epsilon_{xx}}{\partial y^2} + \frac{\partial^2\epsilon_{yy}}{\partial x^2} = \frac{\partial^2\epsilon_{xy}}{\partial x\partial y}\,. \tag{3.5}$$

The stress variations $\delta\boldsymbol{\sigma}$ satisfy the equilibrium conditions within Ω

$$\frac{\partial\delta\sigma_{xx}}{\partial x} + \frac{\partial\delta\sigma_{xy}}{\partial y} = 0\,, \qquad \frac{\partial\delta\sigma_{yy}}{\partial y} + \frac{\partial\delta\sigma_{xy}}{\partial x} = 0\,, \tag{3.6}$$

as well as the boundary conditions in terms of prescribed stresses on Γ_T

$$n_1\delta\sigma_{xx} + n_2\delta\sigma_{xy} = 0\,, \qquad n_2\delta\sigma_{yy} + n_1\delta\sigma_{xy} = 0\,, \tag{3.7}$$

where n_1, n_2 are the outward normals to Γ_T, but they give rise to variations $\delta\boldsymbol{T}$ in boundary surface forces on Γ_u. Let us not require that the stress variations $\delta\boldsymbol{\sigma}$ satisfy the compatibility conditions (3.5).

If we define the *complementary energy* as

$$\Pi^* = U - \int_{\Gamma_u}\boldsymbol{T u}\,\mathrm{d}\Gamma\,, \tag{3.8}$$

it can be shown (see e.g. [91]) that

$$\delta\Pi^* = \delta\left(U - \int_{\Gamma_u} \boldsymbol{T}\boldsymbol{u}\,\mathrm{d}\Gamma\right) = 0\,. \tag{3.9}$$

Eq. (3.9) proves the *Minimum Complementary Energy Principle*:

> With the stresses satisfying the equilibrium conditions in Ω, the boundary conditions on Γ and the compatibility, the complementary energy functional Π^* attains an absolute minimum.

3.2.3 The Ritz Method

The above minimum energy principles can be used to derive the differential equations for specific problems (see e.g. [85]). More importantly, they can be employed to construct series of functions converging to the solution of the respective differential equation. The latter use of these principles was exploited by Ritz [78] and his method is exposed below.

Recall from Eq. (3.3) that the potential energy of deformation is

$$\Pi = \frac{1}{2}\int_{\Omega} \boldsymbol{\sigma}\boldsymbol{\epsilon}\,\mathrm{d}\Omega - \int_{\Gamma} \boldsymbol{T}\boldsymbol{u}\,\mathrm{d}\Gamma - \int_{\Omega} \boldsymbol{X}\boldsymbol{u}\,\mathrm{d}\Omega\,. \tag{3.10}$$

If one substitutes a certain set of functions, e.g. in two dimensions $\tilde{u}_k(x,y) = \sum_{k=1}^{n} a_k\varphi_k(x,y)$, satisfying the boundary conditions, into Eq. (3.10), the unknown parameters a_k can be determined from a system of k equations

$$\frac{\partial\Pi}{\partial a_k} = 0\,, \quad k = (1,2,\ldots,n)\,. \tag{3.11}$$

With such function $\tilde{u}_k(x,y)$ substituted, the energy functional will yield some value $\tilde{\Pi}(\tilde{u})$ that will be different from the minimal energy value $m_E = \Pi(u)$ corresponding to the exact solution $u(x,y)$. If the set of functions constructed by increasing the number of parameters k is *relatively complete*, then

$$\lim_{k\to\infty} \tilde{\Pi}(\tilde{u}) = \min\Pi \quad \text{and} \quad \lim_{k\to\infty} \tilde{u}_k(x,y) = u(x,y)\,. \tag{3.12}$$

3.2.4 The Galerkin Method

In 1915, Galerkin [33] proposed a solution method, which can be shown to be equivalent to the Ritz method in the case of problems of linear self-adjoint differential equations, but which is more general, since it does not

require to formulate the energy functional. Moreover, it can be shown that the Galerkin method gives the best approximation of the actual solution.

The method is based on the following consideration: If the sought solution u to the differential equation $L(u) = 0$ is represented in terms of a series $u_n = \sum_{i=1}^{n} a_i \varphi_i$ with suitable properties, then the orthogonality conditions:

$$\int_\Omega L(\sum_{i=j}^{n} a_j \varphi_j)\, \varphi_i \, \mathrm{d}\Omega = 0 \quad \text{as } n \to \infty \tag{3.13}$$

are equivalent to $L(u) = 0$. If the series u_n has n terms, Eq. (3.13) provides a set of n simultaneous equations to determine the coefficients a_i.

The equivalence postulated above tells us why in the formulation of finite element equations we multiply the governing differential equations with the *trial functions* to obtain the set of simultaneous equations. Naturally, the trial and test functions must posses certain properties for the orthogonality property to hold. In the finite element and related methods, these properties are enforced by applying the *partition of unity* principle – see Section 3.3.

We will end the discussion here, having presented the principles of the energy methods. Readers who want to dwell into more detail of the theory can continue reading in Appendix B.1, where a simple example is presented that illustrates the application of the minimum energy principle and of the Galerkin method.

3.3 The Finite Element Method

In Section 3.2.4 above, we introduced the Galerkin method, which is the mathematical foundation for the finite element method (FEM) as well as for its generalisations going by the names of the Extended Finite Element Method (XFEM) and meshless methods. In this Section, we briefly outline the formulation and the resulting static equations of the FEM. The FEM theory is well known and a detailed presentation in the main text is thus not considered necessary. For interested readers, there is more detail in Appendix B.2.

From a historical perspective, the rise of the finite element method as a tool to solve a wide variety of engineering problems was triggered by the 1956 paper of Turner *et al.* [88]. An earlier (1943) paper of Courant [18] did not awake that much attention due to the fact that the extensive computational means that make the finite element method convenient were not yet available. However, the paper presented the basis of the modern finite ele-

ment method. Courant used a variational formulation with piecewise linear approximation over the domain decomposed into triangular elements.

Once the potential of the FEM was recognised, huge development efforts were devoted to the method. Among the milestones, let us mention the 1965 paper [102] of Zienkiewicz & Cheung, where FEM was first applied to other than structural problems. In his 1972 book, Oden [71] introduced nonlinear finite element analysis. A comprehensive bibliography on finite element developments up to 1975 can be found in [95].

3.3.1 The Boundary Value Problem

The static equilibrium equation reads:

$$\mathbf{D} \cdot \boldsymbol{\sigma} + \boldsymbol{f} + \boldsymbol{T} = \mathbf{0}\,, \tag{3.14}$$

where $\mathbf{D}$ is the gradient operator matrix, $\boldsymbol{\sigma} = \mathbf{E} \cdot \boldsymbol{\epsilon}$ is the stress tensor, $\boldsymbol{\epsilon} = \mathbf{D} \cdot \mathbf{u}$ is the strain tensor, $\boldsymbol{f}$ are the body forces and $\boldsymbol{T} = \mathbf{n} \cdot \boldsymbol{\sigma}$ are the boundary tractions satisfying the natural boundary conditions.

Equation (3.14) is called the *strong form* equilibrium equation, since it requires that equilibrium be satisfied at each point. We relax this strong requirement by demanding that equilibrium be satisfied in a weaker, integral sense:

$$\int_\Omega \mathbf{D} \cdot \boldsymbol{\sigma} \mathrm{d}\Omega + \int_\Omega \boldsymbol{f} \mathrm{d}\Omega + \int_{\Gamma_t} \boldsymbol{T} \mathrm{d}\Gamma_t = \mathbf{0}\,. \tag{3.15}$$

This is called the *weak form* of the equilibrium equation. Applying the Galerkin method, we approximate the solution by functions $\mathbf{u}$ in the trial functions space, satisfying the essential boundary conditions, and multiply Eq. (3.15) by variations $\mathbf{v}$ from the test function space:

$$\int_\Omega \boldsymbol{\epsilon}(\mathbf{v}) \cdot \mathbf{E}\boldsymbol{\epsilon}(\mathbf{u}) \mathrm{d}\Omega + \int_\Omega \boldsymbol{v} \cdot \boldsymbol{f} \mathrm{d}\Omega + \int_{\Gamma_t} \boldsymbol{v} \cdot \boldsymbol{T} \mathrm{d}\Gamma_t = \mathbf{0}\,. \tag{3.16}$$

3.3.2 Finite Element Approximation

Up to now, the only assumption made about the trial and test functions was that they are of a form fulfilling Galerkin's orthogonality condition, see Eq. (3.13). This condition is assured in finite elements by requiring that the base functions satisfy the *partition of unity* principle. It states that the displacement at a material point ξ is the sum of contributions from the shape functions whose support domain includes the point ξ. The concept can be expressed as follows:

- The domain Ω is covered by overlapping sub-domains Ω_i.
- Each sub-domain Ω_i is the support of a shape function N_i.
- $N_i \neq 0$ only within its support domain: $\xi \in \Omega_i$.
- The shape functions Ω_i verify:

$$\sum_i N_i(\xi) = 1 \quad \forall\, \xi \in \Omega\,.$$

In FEM, the domain Ω is broken up into individual elements, on which the displacement field is approximated by base functions called the *shape functions* with a support domain (i.e. the domain where the shape functions have a non-zero value) consisting of the elements sharing the node to which the shape function belongs. The FEM approximation u^h of the displacements is expressed for any displacement component as:

$$u^h(\mathbf{x}) = \sum_{i=1}^{I} u_i N_i(\mathbf{x})\,, \tag{3.17}$$

where u_i are the nodal values of the displacement component and N_i are the shape functions. Note that the derivative of the displacement w.r.t. to a coordinate direction x_j is then

$$\frac{\partial u^h}{\partial x_j}(\mathbf{x}) = \sum_{i=1}^{I} u_i \frac{\partial N_i}{\partial x_j}(\mathbf{x})\,. \tag{3.18}$$

Expressing the trial and test functions in Eq. (3.16) in terms of the FEM shape functions, we obtain:

$$\mathbf{\Theta}^T \int_\Omega \mathbf{B}^T \mathbf{E}\mathbf{B}\,\mathrm{d}\Omega\,\mathbf{U} + \mathbf{\Theta}^T \int_\Omega \mathbf{N}^T \mathbf{f}\,\mathrm{d}\Omega + \mathbf{\Theta}^T \int_\Gamma \mathbf{N}^T \mathbf{T}\,\mathrm{d}\Gamma = \mathbf{0}\,, \tag{3.19}$$

where $\mathbf{B}$ is the matrix of shape function derivatives and $\mathbf{U}$ is a vector of nodal displacements. Invoking the arbitrariness of the variations, the nodal displacements $\mathbf{\Theta}$ of the test functions disappear from the equations. Introducing the following notation:

$$\begin{aligned}
\text{Stiffsness matrix} \quad &: \quad \mathbf{K} = \int_\Omega \mathbf{B}^T \mathbf{E}\mathbf{B}\,\mathrm{d}\Omega\,,\\
\text{Body force vector} \quad &: \quad \mathbf{F}^s = \int_\Omega \mathbf{N}^T \mathbf{f}\,\mathrm{d}\Omega\,,\\
\text{Traction force vector} \quad &: \quad \mathbf{F}^t = \int_\Gamma \mathbf{N}^T \mathbf{T}\,\mathrm{d}\Gamma\,,
\end{aligned}$$

we arrive at the familiar static finite element equation:

$$\mathbf{KU} = \mathbf{F}^s + \mathbf{F}^t \,. \tag{3.20}$$

Note that due to the support domain of the shape functions being limited to the elements surrounding the given node, the stiffness matrix $\mathbf{K}$ is banded, provided that an appropriate node numbering is used.

3.4 The Extended Finite Element Method

Researchers realised that next to the finite element shape functions, there were other ways to approximate the displacements that conform to the partition of unity concept and that may indeed be more advantageous for certain problems involving evolving discontinuities such as cracks and interfaces.

The earliest numerical method that was not based on element-wise approximation was the so called smooth particle hydrodynamics [35], which is best suited for modelling the interaction of a large number of particles. A field approximation method that has been successfully applied in solid mechanics is the moving least squares (MLS) approximation proposed by Lancaster & Salkauskas [47]. Nayroles *et al.* [65] were the first to employ MLS in a Galerkin method. The approach was popularised under the name of Element Free Galerkin Method (EFGM) or "meshless" method by Belytschko *et al.* [9]. The meshless methods are discussed in Section 3.5.

Of interest here is another approach to approximate the displacement proposed by Möes *et al.* [61]. Basing themselves on the partition of unity finite element method put forward by Melenk & Babuška [4], they enriched the finite element approximation space locally with problem-specific shape functions.

3.4.1 XFEM Equations

XFEM is an extension of the finite element method and as such, it is derived in much the same way by the Galerkin's method, see Section 3.2.4. Thus, we can take also here Eq. (3.16) as the point of departure. The difference is that we substitute for displacements into the equation the displacements approximated by functions corresponding to the known shape of the displacement field. In the case of a crack in a linear-elastic 2D body under plane strain or plane stress, the approximation reads:

$$u^h(\mathbf{x}) = \sum_{i=1}^{n_I} u_i N_i(\mathbf{x}) + \sum_{j=1}^{n_J} b_j N_j(\mathbf{x}) H(\mathbf{x}) + \sum_{k=1}^{n_K} N_k(\mathbf{x}) \left(\sum_{l=1}^{4} c_k^l F_l(\mathbf{x}) \right) \,, \tag{3.21}$$

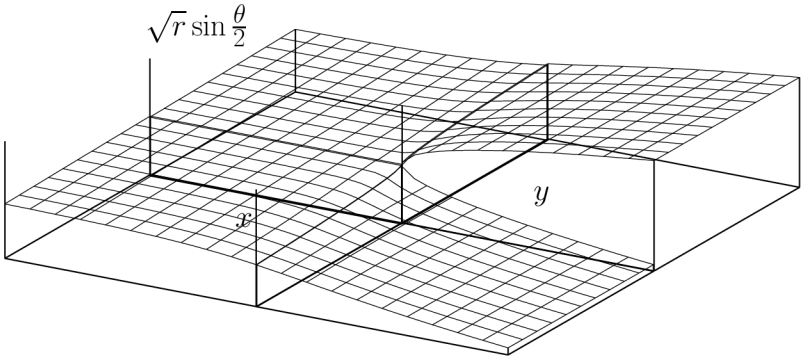

Figure 3.1: *Crack tip enrichment function* $\sqrt{r}\sin\frac{\theta}{2}$

where u_i are the classical finite element nodal displacements, b_j and c_k are additional nodal parameters related to the enriching shape functions, n_J and n_K are the sets of enriched nodes along the crack and around the crack tip, respectively, $H(\mathbf{x})$ is a jump function of the discontinuity enrichment having the value 1 "above" and -1 "below" the crack, and there are four crack tip enrichment functions used, defined as:

$$\{F_l(r,\theta)\} = \left\{ \sqrt{r}\cos\frac{\theta}{2},\ \sqrt{r}\sin\frac{\theta}{2},\ \sqrt{r}\sin\theta\sin\frac{\theta}{2},\ \sqrt{r}\sin\theta\cos\frac{\theta}{2} \right\}, \quad (3.22)$$

where (r,θ) are the local polar coordinates at the crack tip. The functions in Eq. (3.22) span the crack-tip displacement field. Note that by multiplying the enrichment functions $H(\mathbf{x})$ and $F_l(r,\theta)$ with the finite element shape functions in Eq. 3.21, the enrichment is effectively localised to the region around the crack; at the same time, the partition of unity is enforced.

3.4.2 Integration and Solution

Note that the jump function $H(\mathbf{x})$ and the tip-enrichment function $\sqrt{r}\sin\frac{\theta}{2}$ are discontinuous across the crack, while the remaining functions in $F_l(r,\theta)$ are not smooth across the crack. But the Gauss integration routinely used in finite element solutions only performs well with continuous and smooth

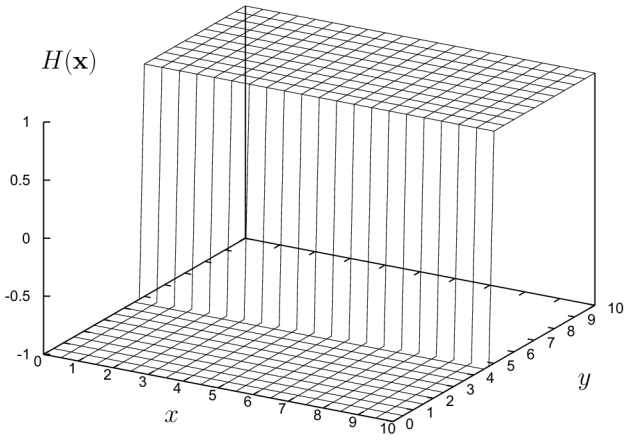

Figure 3.2: *Generalised Heaviside function* $H(\mathbf{x})$ *used for enrichment along the crack*

functions. Therefore, each element intersected by a crack must be subdivided into sub-triangles as shown in Fig. 3.3, except for cases where the area of the parent element cut off by the crack is negligibly small. Note that such partitioning is for integration purposes only and no new nodes or elements are created, as the displacements are still interpolated over the parent elements.

In a static analysis, the variational calculus on weak form yields the familiar finite element equations $\mathbf{Ku} = \mathbf{f}$, in which appear the additional nodal degrees of freedom due to the enrichment. In particular, the enriched element contributions to the stiffness matrix $\mathbf{K}$ and the external force vector $\mathbf{f}$ are:

$$\mathbf{k}_{ij}^{(e)} = \begin{bmatrix} \mathbf{k}_{ij}^{uu} & \mathbf{k}_{ij}^{ub} & \mathbf{k}_{ij}^{uc} \\ \mathbf{k}_{ij}^{ub} & \mathbf{k}_{ij}^{bb} & \mathbf{k}_{ij}^{bc} \\ \mathbf{k}_{ij}^{uc} & \mathbf{k}_{ij}^{bc} & \mathbf{k}_{ij}^{cc} \end{bmatrix}, \tag{3.23}$$

$$\mathbf{f}_{i}^{(e)} = \left\{ \mathbf{f}_{i}^{u} \, \mathbf{f}_{i}^{b} \, \mathbf{f}_{i}^{c1} \, \mathbf{f}_{i}^{c2} \, \mathbf{f}_{i}^{c3} \, \mathbf{f}_{i}^{c4} \right\}, \tag{3.24}$$

where b and c denote the enrichment degrees of freedom, cf. Eq. 3.21, and the sub-matrices k_{ij}^{rs} appearing in Eq. 3.23 are:

$$\mathbf{k}_{ij}^{rs} = \int_{\Omega^{(e)}} (\mathbf{B}_i^r)^T \, \mathbf{E} \mathbf{B}_j^s \mathrm{d}\Omega \quad (r, s = u, b, c) \,. \tag{3.25}$$

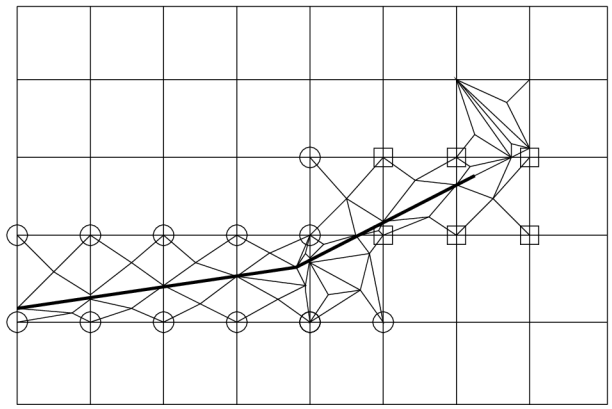

Figure 3.3: *Enriched nodes and element partitioning for integration*

In Eq. 3.25 above, $\mathbf{E}$ is the elasticity matrix and $\mathbf{B}_i^u$, $\mathbf{B}_i^b$, and $\mathbf{B}_i^c$ are the matrices of shape function derivatives given by:

$$\mathbf{B}_i^u = \begin{bmatrix} N_{i,x} & 0 \\ 0 & N_{i,y} \\ N_{i,y} & N_{i,x} \end{bmatrix}, \tag{3.26}$$

$$\mathbf{B}_i^b = \begin{bmatrix} (N_i H)_{,x} & 0 \\ 0 & (N_i H)_{,y} \\ (N_i H)_{,y} & (N_i H)_{,x} \end{bmatrix}, \tag{3.27}$$

$$\mathbf{B}_i^c = \begin{bmatrix} \mathbf{B}_i^{c1} \, \mathbf{B}_i^{c2} \, \mathbf{B}_i^{c3} \, \mathbf{B}_i^{c4} \end{bmatrix}, \tag{3.28}$$

$$\mathbf{B}_i^{cl} = \begin{bmatrix} (N_i F_l)_{,x} & 0 \\ 0 & (N_i F_l)_{,y} \\ (N_i F_l)_{,y} & (N_i F_l)_{,x} \end{bmatrix} \quad (l = 1, 2, 3, 4)\,. \tag{3.29}$$

While the part of the stiffness matrix constructed using Eq. (3.26) remains invariant throughout the crack growth analysis, new enrichment degrees of freedom and/or integration points are added to the remaining parts of $\mathbf{K}$ whenever the crack advances. Therefore, $\mathbf{K}$ has to be re-factorised each time.

3.5 Meshless Methods

Meshless methods were the first among the numerical methods successfully applied to evolving boundary value problems which the finite element

method does not treat very efficiently due to a need for remeshing. The pioneering works on meshless methods were cited in Section 3.4. A rather comprehensive treatise of meshless methods can be found in a monograph by G.-R. Liu [52]. A good review of meshless methods can be found in Belytschko *et al.* [8].

In meshless methods, displacement approximation is constructed from values at discrete nodes. However, a background mesh is still usually used to evaluate the underlying integrals. But the discontinuities can stretch arbitrarily among the nodes.

In this brief presentation of the meshless methods, we will focus on the Element Free Galerkin Method (EFGM) [9] using the moving least squares (MLS) approximation [47].

3.5.1 Moving Least Squares Approximation

Similarly as in the case of the extended finite element method, the main difference in the formulation of the EFGM as compared to FEM is in the method of approximation of the displacement field.

Let us come back to the finite element approximation. The support domain of a finite element shape function is defined as the domain delimited by the elements sharing the node to which the shape function belongs. Thus, each element is covered by a number of overlapping domains equal to the number of the element's nodes.

In MLS, the discretised domain is also covered by overlapping support domains belonging to individual discrete nodes. The value of the displacement field component at any given point is influenced by the values at all nodes whose support domain contains the point. To evaluate the integrals in Eq. (3.16), we are interested in the values of the MLS shape functions and their derivatives at the integration points.

A complete derivation of the MLS approximation is exposed in Appendix B.3. It is shown there that the MLS shape functions can be condensed to the form

$$u^h(\mathbf{x}) = \mathbf{\Phi}_I(\boldsymbol{\xi}, \mathbf{x})\mathbf{u}_I \,, \tag{3.30}$$

much resembling the form finite element approximation and nothing prevents us from using it as the trial and test functions in a Galerkin method. In the above equation, $\boldsymbol{\xi}$ is the integration point for which the approximation is constructed and $\mathbf{u}_I$ is the nodal value.

3.5.2 Treatment of Discontinuities

It has been said above that in EFGM, cracks can pass arbitrarily among the nodes. Let us then briefly look how discontinuities are treated in EFGM. A common approach is the visibility method, illustrated in Figure 3.4. Figure 3.4 depicts a discontinuity line, EFGM nodes, a point, marked with

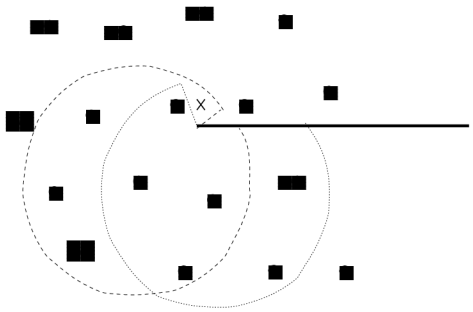

Figure 3.4: *Treatment of discontinuities in EFGM.*

a cross, for which the MLS approximation is constructed, and two support domains of two distinct nodes. We see that the support domains are cut off by the discontinuity by applying the criterion of visibility of the support domain points from the respective node. Thus, while the node whose support domain is delimited by the dashed-line will be taken into consideration in constructing the MLS approximation for the point of interest, the node of the dotted-line support domain will not. The nodes hidden behind the discontinuity have no influence on the field value at the point of interest.

3.5.3 Note on Computational Effort

Equations (B.58) and (B.59) give the formulæ to construct the shape function and its derivative, respectively. Remember that in the MLS approximation, the shape functions need to be constructed anew for each integration point.

This is a key issue for the difference in computational time required for the FEM and XFEM methods on the one hand and the EFGM on the other hand. In FEM and XFEM, the shape functions are known beforehand, in EFGM, they are not and need to be constructed for each of the integration points. It can be seen from Equations (B.58) and (B.59) that a matrix inversion and a number of matrix multiplications are involved in their construction. Notwithstanding the small size of the matrices, this still adds a

significant computational burden.

3.6 The Finite Element Alternating Method

A boundary value problem solution method that is applicable to crack propagation problems is the analytical-numerical finite element alternating method (FEAM), used for the multi-site damage problem by Nishioka & Atluri [70], Wang et al.[92], among others. An example of FEAM application in a stochastic crack propagation problem can be found in [66].

The algorithm of FEAM alternates iteratively between an FE solution for a finite body without cracks, and an analytical solution for stresses in an infinite body due to traction on the faces of cracks contained in this body. The underlying principle of FEAM is the following concept: by subtracting the stresses in the analytical solution from the stresses in the FE solution, one obtains the stress field of the finite body with cracks.

Assuming a linear behaviour:

$$T = A_{FE}\, t_{FE}\,, \quad t_a = A_{AN}\, T\,, \tag{3.31}$$

where T is the crack face traction, t_{FE} is the stress applied on the boundaries of the FE model, t_a are the resulting stresses at the locations of the finite model boundary, obtained in the analytical solution, and A_{FE} and A_{AN} are linear operators. This is illustrated in Fig. 3.5.

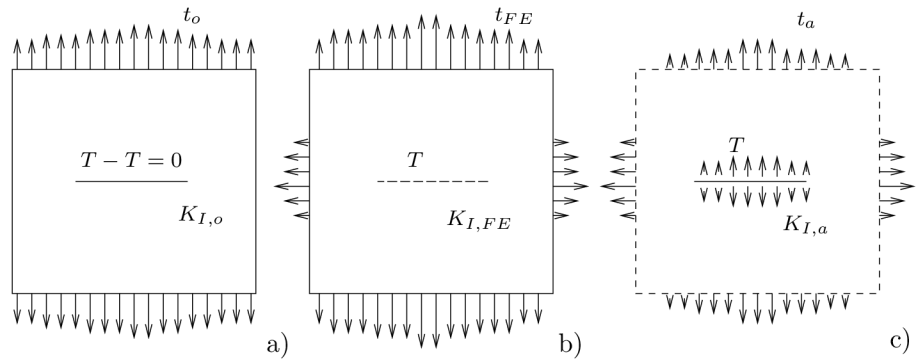

Figure 3.5: *Constructing the solution for a finite body with cracks from solutions for a finite body without cracks, and for stresses in an infinite body due to crack face traction.*

The same tractions T are applied on the crack faces both in the analytical and the FE solution. The stress on the boundary of the body have to be

equal to the applied stresses t_o. The stress t_{FE} for which $t_o = t_{FE} - t_a$ can be calculated by iteration. The iteration step is broken into the FE and the analytical solution:

$$\begin{aligned} T^1 &= K_{FE} t_o \,, \\ t_a^i &= K_{AN} T^i = t_r^i \,, \\ T^{i+1} &= K_{FE} t_{FE}^i = K_{FE} \left(t_o + t_r^i \right) \,, \end{aligned} \tag{3.32}$$

where i denotes the current iteration step and t_r^i the residual stress or the difference between t_o and $t_{FE} - t_a$, which approaches zero with the iteration and which occurs due to the crack face traction: $t_r^i = t_{FE}^i - t_o = t_a^i$. It is seen in Eq. 3.32 that the iteration takes the form of a Neumann series expansion, although other methods, such as relaxation methods, would certainly also apply here. At k iterations, t_r^k will be small enough to be neglected and the stresses on the finite body boundary will be $\sum t_{FE}^i = t_o + \sum t_a^i$.

3.6.1 Analytical Solution for Embedded Straight Cracks

The analytical solution for FEAM used in this paper is based on Muskhelishvili's [62] solution for stresses acting on a straight cut in an elastic plane. A solution for a single crack is used together with superposition of traction to construct the solution for n cracks.

The stresses are obtained from a complex potential function, which involves an improper integral evaluated along the crack path. Wang et al. [92] presented an explicit solution to this integral, approximating the distribution of the crack face traction by a sum of piecewise constant and piecewise linear base functions. This solution was implemented also for the purposes of the the present paper.

The tractions T_j on the face of a particular crack j give rise to stresses also at the locations of an other crack i. The residual stresses $T_{i,r} = A_{AN,j} T_j$ have to be removed. The stress field is determined by linear operators, hence by means of influence coefficients one can find a distribution of stresses X such that on each crack face this stress X and the residual stress due to traction on other crack faces add up to the crack face traction T of the FE solution (see also [92]).

3.7 Stress Intensity Factor Calculation

The stress intensity factor is the magnitude factor of first term of the crack tip stress field expansion, see Section 2.3.6. As such, it characterises much

of the properties of the crack tip stress filed. The stress intensity factor is therefore the variable that is most often used to predict crack growth velocity and direction.

When a numerical mechanical model is used, we need only a few characteristic values to provide the connection between the numerical model of the current crack configuration and the crack propagation simulation model. The stress intensity facor is a suitable characteristic to build this bridge.

It is obvious that a reliable and accurate method of computation of the stress intensity factor is central to any crack propagation approach using a numerical mechanical model. A number of methods to evaluate stress intensity factors and strain energy release rates from numerical results have been proposed in the literature ([63], [81], [41], [69], [79]). We will briefly review a few of them in this section.

3.7.1 Stress and Displacement Fitting

A method that is eminent when looking to find the SIF is fitting the SIF as a parameter of the theoretical stress distribution from the numerical results. The stress data in planes perpendicular to the crack front are compared with William's [97] 2D solution, which is in stresses. One only needs to choose the interval in terms of distance from the crack tip, in which the fitting to the numerical data is performed, such that this region is SIF dominated and that the numerical errors in the vicinity of the crack tip are avoided. Note that the resulting SIF depends to some extent on the choice of such interval.

SIF can also be fitted from the displacements obtained from a numerical solution. In this case, however, one needs to assume either plane strain or plane stress to relate the displacements to the stress solution of [97]. A method employed by the post-processing routines of some FEM packages (e.g. [86]) is based on fitting SIF from the displacements of three points on the crack face. Ingraffea & Manu [41] used the property of quarter-point elements [5] that the displacements on the element behave as $\sqrt{\rho}$. They expressed the crack opening displacement in terms of the quarter-point element shape functions and compared the leading order terms with the theoretical formula for displacements under plane strain or plane stress. The SIF can thus be obtained as a function of the quarter-point element nodal displacements only.

3.7.2 Global Energy Approach

In the well-known global energy approach, the strain energy release rate G (and corresponding SIF) may be obtained by performing two analyses with the original crack length and a crack length grown by a small amount. The strain energy is in such case obtained from the work of the loads acting on the displacements at the corresponding load action points. The strain energy release rate G then represents a global quantity, giving no indication of its variation along the crack front.

3.7.3 Local Energy Approach

One is tempted to adopt an analogy to 2D also here and try to use the J-integral on contours lying in successive planes perpendicular to the crack face. However, when this was attempted and an integration path distant enough from the crack front was used to avoid high solution gradients, the J-integral showed no significant variation along the crack front of energy flow to the crack tip region. This suggests significant 3D effects in the corner region.

More rigorous domain integral formulations for three dimensions were proposed by Nikishkov & Atluri [69] and Wen *et al.* [93].

Another approach to calculate strain energy release rate G is Irwin's crack closure integral. The concept is based on the idea the energy absorbed by fracturing over a small length is equal to the work necessary for closing the crack again by the same length. Rybicki & Kanninen [79] modified the method by considering the stresses in in front of the crack front and the displacements behind the crack front, avoiding thus the need to perform two numerical analyses. It was shown in [79] that the accuracy of this modified crack closure integral (MCCI) method is good. In the FEM formulation, MCCI calculates with nodal forces, obtained from stresses using the element shape functions. Implementations of MCCI for specific element types were then developed, see e.g. Ramamurthy *et al.* [76] and Narayana *et al.* [63]. Singh [81] proposed a MCCI method independent of the numerical method by which the stresses and displacements were obtained.

3.7.4 The Interaction Integral

A method of calculation of SIF that is particularly well adapted for finite element post-processing is the method of the interaction integral [100], which is equivalent to SIF calculation using the independently developed "G-θ" method [59].

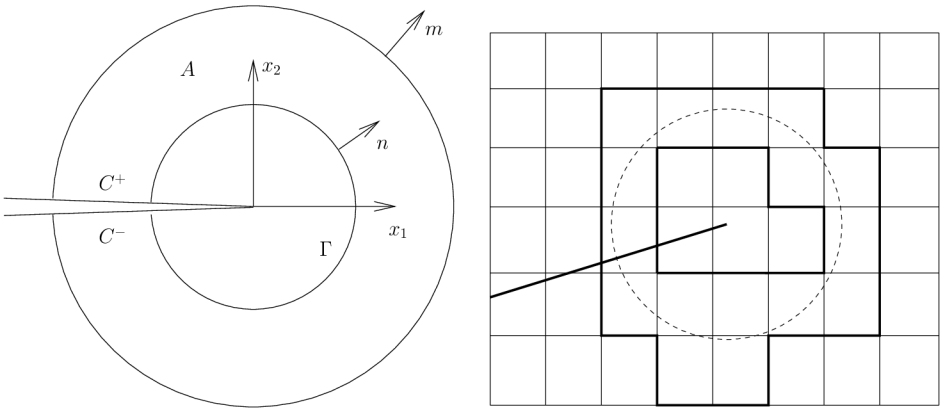

Figure 3.6: *Integration contours and finite element integration area.*

The well known Rice's contour integral is defined as:

$$J = \int_{\Gamma} \left[W n_1 - \sigma_{ij} n_j \frac{\partial u_i}{\partial x} \right] d\Gamma \,. \tag{3.33}$$

Its value is related to the Mode I and Mode II stress intensity factors:

$$J = \frac{K_I^2}{\bar{E}} + \frac{K_{II}^2}{\bar{E}}, \tag{3.34}$$

where

$$\bar{E} = \begin{cases} E & \text{for plane stress} \\ \frac{E}{1-\nu^2} & \text{for plane strain} \end{cases},$$

with E being the Young's modulus and ν the Poisson's ratio.

Two states of the cracked body considered:

– the actual state (1): $\left[\sigma_{ij}^{(1)},\, \varepsilon_{ij}^{(1)},\, u_i^{(1)}\right]$

– an auxiliary state (2): $\left[\sigma_{ij}^{(2)},\, \varepsilon_{ij}^{(2)},\, u_i^{(2)}\right]$

such that $u_i^{(2)}(x,y) = u_i^{(2)}(x,-y)$ and $\sigma_{ij}^{(2)}(x,y) = \sigma_{ij}^{(2)}(x,-y)$, i.e. asymptotic Mode I field is chosen such that $K_I^{(2)} = 1$ and $K_{II}^{(2)} = 0$. The J-integral for the sum of the two states is

$$J^{(1+2)} = J^{(1)} + J^{(2)} + I^{(1+2)} \,, \tag{3.35}$$

where $I^{(1+2)}$ is the interaction integral

$$\begin{aligned} I^{(1,2)} &= \frac{2}{\bar{E}}\left(K_I^{(1)}K_I^{(2)} + K_{II}^{(1)}K_{II}^{(2)}\right) \\ &= \int_\Gamma \left[W^{(1+2)}\delta_{1j} - \sigma_{ij}^{(1)}\frac{\partial u_i^{(2)}}{\partial x_1} - \sigma_{ij}^{(2)}\frac{\partial u_i^{(1)}}{\partial x_1}\right] n_j d\Gamma \end{aligned} \tag{3.36}$$

and $W^{(1+2)}$ is the interaction strain energy

$$W^{(1+2)} = \sigma_{ij}^{(1)}\varepsilon_{ij}^{(2)} = \sigma_{ij}^{(2)}\varepsilon_{ij}^{(1)}\,. \tag{3.37}$$

Multiplying the integrand in Eq. (3.36) by a weighting function q that equals a unity on the inner integration contour and vanishes on the outer integration contour (cf. Fig. 3.6), and by virtue of the divergence theorem, the contour integral is converted to an area integral:

$$I^{(1,2)} = \int_A \left[\sigma_{ij}^{(1)}\frac{\partial u_i^{(2)}}{\partial x_1} + \sigma_{ij}^{(2)}\frac{\partial u_i^{(1)}}{\partial x_1} - W^{(1+2)}\delta_{1j}\right]\frac{\partial q}{\partial x_j} dA\,. \tag{3.38}$$

With the state 2 chosen as the asymptotic field for Mode I, we have:

$$K_I^{(1)} = \frac{2}{E} I^{(1,2)}\,. \tag{3.39}$$

K_{II} may be calculated in an analogical way by choosing the state 2 to be an asymptotic field for Mode II.

By conveniently choosing the function q, the integration area can be made to coincide with a band of elements forming a ring around the crack tip – see Fig. 3.6.

3.7.5 SIF in the Finite Element Alternating Method

In the Finite Element Alternating Method outlined in Section 3.6, the stress intensity factor comes directly from the analytical part of the solution. Thus, no finite element post processing is necessary and the accuracy of the calculated SIF is very good.

3.8 Conclusions

In this Chapter, we have reviewed several numerical methods that have been applied in the analysis of fracture mechanics problems. The discussion

	FEM	XFEM	Meshless	FEAM
geometry update	remeshing, automated algorithms exist	base function enrichment, automated	reconstruction of approximation, automated	through analytical model
general geometry	yes	yes	yes	no
computational effort	high in remeshing	additional DOF	high in reconstruction of approximation	iterations
stability, accuracy	mesh dependent	good	good	good

Table 3.1: *Summary of important features of the finite element (FEM), extended finite element (XFEM), meshless and finite element alternating method (FEAM).*

has revealed some of the advantages and disadvantages of the individual methods. Table 3.1 attempts to summarise the features and the pros and cons of the methods in the view of crack propagation modelling applications.

The important properties for crack propagation modelling of the individual methods follow from the strategy that each method uses to track the geometry of the evolving crack. The finite element method relies on remeshing, while the remaining methods reviewed do not. Remeshing introduces numerical noise, which is the cause of the deficiency of FEM in terms of stability of results. Though highly performing remeshing algorithms are nowadays available, they are available only as a part of expensive software systems and the remeshing process consumes a significant computer time.

On the contrary, the XFEM and meshless methods liberate the analyst from the remeshing work. Geometry update to follow the crack is carried out through enrichment of the base function space in the case of XFEM and through reconstruction of the meshless approximation of the displacement field in the case of the meshless method. In both cases, these procedures are usually integrated in the overall analysis algorithm.

While enrichment increases the number of DOF and thus the size of the matrix to be factorised every time the crack advances, reconstruction of the field approximation is by far more costly in terms of computer time. This represents an advantage of XFEM over the meshless methods.

A significant drawback of the finite element alternating method is that the analytical solution must be known for a crack with an arbitrary shape

and arbitrary crack face loading. This makes an automation of the method difficult, if it should be capable of application to arbitrary geometries.

Chapter 4

Reliability Analysis

4.1 Introduction

Due to uncertainties in the inputs, which include material, geometrical and loading uncertainties, the response of structural models is also uncertain. The scatter in the input variables is conveniently characterised by statistical modelling. The available information on the statistical dispersion is summarised by means of random variables. And where spatial variability is of concern, random fields can be used. In this thesis, the attention is limited to reliability models involving random variables only.

Given the statistical models of the input variables, the objective of probabilistic analysis is to determine the statistics of the response (sensitivity analysis) and/or the probability of failure (reliability analysis). The methods to achieve this, including Monte Carlo simulation, advanced simulation techniques and reliability approximation methods, are described in the sections to follow.

Note that there is also an uncertainty about the accuracy of the models used. However, this concerns the question how well does the model represent the actual physics of the problem. Most often, one can expect a systematic bias or limited applicability of the model rather than a randomness in its performance.

4.2 Probability Transformation

A classical approach in reliability analysis is to transform the problem from the physical domain to the so called *standard normal space*, in which uncorrelated Gaussian variables with zero mean and unit variance U correspond

to the variables X having their actual distributions in the physical space.

The transformation is termed the *probability transformation* because the corresponding pairs of values of the variables $x \leftrightarrow u$ in the transformation have the same probabilities of occurrence.

As we will see in Section 4.3, this transformation is indispensable for the reliability approximation methods. It will also prove useful in sampling from correlated distributions.

4.2.1 Independent Variables

When the variables are independent, each variable X_i can be transformed independently of the remaining variables. We invoke the principle of equal probabilities in the physical and the standard normal space $F_{X_i}(x_i) = \Phi(u_i)$, where F_{X_i} is the cumulative density function of the variable X_i and Φ is the standard normal cumulative density function. The transformation is then:

$$x_i \xrightarrow{T} u_i = \Phi^{-1}\left(F_{X_i}(x_i)\right) . \tag{4.1}$$

When the variable X_i is normal, the transformation is simply:

$$u_i = \frac{x_i - \mu_{X_i}}{\sigma_{X_i}} , \tag{4.2}$$

with μ_{X_i} and σ_{X_i} the mean and the standard deviation of X_i, respectively. For lognormal X_i, the transformation becomes:

$$u_i = \frac{\ln X_i - \lambda}{\zeta} \quad \text{with} \quad \zeta = \sqrt{\ln\left(1 + \left(\frac{\sigma_{X_i}}{\mu_{X_i}}\right)^2\right)} , \lambda = \ln \mu_{X_i} - \frac{1}{2}\zeta^2 . \tag{4.3}$$

If the inverse of F_{X_i} exists, the inverse transformation back to the physical space reads:

$$u_i \xrightarrow{T^{-1}} x_i = F_{X_i}^{-1}\left(\Phi(u_i)\right) . \tag{4.4}$$

From the principle of equal probabilities, it follows that the origin of the normal space corresponds to the joint median of the physical variables, not to their mean.

4.2.2 Nataf Transformation

Various transformations have been proposed and successfully applied for the probability transformation of *correlated* variables. The reader is referred to

[49] for a comprehensive review of the various methods. The presentation here will be limited to the Nataf transformation.

The Nataf transformation, proposed in [23], requires the knowledge of only the means μ_{X_i} and the standard deviations σ_{X_i} of the marginal distributions, and of the correlation matrix ρ_{ij}.

The authors [23] made use a transformation originally developed by Nataf [64]. The joint probability density of two physical-space variables X_i and X_j with a correlation coefficient ρ_{ij} can be expressed in terms of two joint-normally distributed variables $\hat{U}_i$ and $\hat{U}_j$ with a correlation coefficient $\rho_{0,ij}$:

$$f_{X_i,X_j}(x_i,x_j) = \phi_2(\hat{u}_i,\hat{u}_j,\rho_{0,ij})\,\frac{f_{X_i}(x_i)\,f_{X_j}(x_j)}{\phi(\hat{u}_i)\,\phi(\hat{u}_j)}\,, \tag{4.5}$$

where $\phi_2(\hat{u}_i,\hat{u}_j,\rho_{0,ij})$ is a bivariate normal probability density. The correlation coefficient $\rho_{0,ij}$ must be found such that

$$\rho_{ij} = \int_{-\infty}^{\infty}\int_{-\infty}^{\infty}\frac{x_i-\mu_{X_i}}{\sigma_{X_i}}\frac{x_j-\mu_{X_j}}{\sigma_{X_j}}\phi_2(\hat{u}_i,\hat{u}_j,\rho_{0,ij})\,\frac{f_{X_i}(x_i)\,f_{X_j}(x_j)}{\phi(\hat{u}_i)\,\phi(\hat{u}_j)}\,. \tag{4.6}$$

For any couple of variables X_i and X_j, the Nataf-modified correlation coefficient $\rho_{0,ij}$ can be found numerically by a minimisation procedure. ρ_{ij} can be used as the point of departure, for which the integral (4.6) will yield a value $\overline{\rho_{ij}}$. The optimisation then consists in finding the minimum of the absolute value of the error $|\rho_{ij}-\overline{\rho_{ij}}|$.

The components of the full Nataf-modified correlation matrix $\mathbf{R}_0$ are the one-to-one correlation coefficients obtained from Eq. (4.6). The Nataf transformation reads:

$$u_i = \sum_j \mathbf{\Gamma}_{0,ij}\Phi^{-1}\left(F_{X_j}(x_j)\right)\,, \tag{4.7}$$

where $\mathbf{\Gamma}_0$ is the inverse of the lower triangular matrix of Cholesky decomposition $\mathbf{L}_0$ of the Nataf-modified correlation matrix $\mathbf{R}_0$. The cases where the fictive correlation matrix $\mathbf{R}_0$ is not positive definite are rather rare in physical problems [49] and the decomposition can thus usually be performed.

In summary, the transformation of the variables is performed in the following steps:

- compute the modified the correlation matrix $\mathbf{R}_0$ using Eq. (4.6);
- compute Cholesky decomposition of $\mathbf{R}_0$: $\mathbf{R}_0 = \mathbf{L}_0\mathbf{L}_0^T$;

– transform the variables X_i to centred, unit-variance, but correlated variables $\hat{U}_i$ by Eq. (4.1);

– de-correlate the variables by applying the following formula:

$$\mathbf{U} = \mathbf{\Gamma}_0 \hat{\mathbf{U}} \,. \tag{4.8}$$

4.2.3 Sampling from Correlated Distributions

When performing a Monte Carlo Simulation, in which the random variables are correlated, it is necessary to sample from a joint distribution function, or in the Nataf sense, from correlated distributions.

While alternative approaches exist, it is possible to use the Nataf transformation described in Sec. 4.2.2. We sample an *uncorrelated* vector $\mathbf{U}$ in the standard normal space and transform it to a correlated, centred and reduced (unit-variance) vector $\hat{\mathbf{U}}$:

$$\hat{\mathbf{U}} = \mathbf{L}_0 \mathbf{U} \,. \tag{4.9}$$

The variables X_i are obtained using Eq. (4.4):

$$x_i = F_{X_i}^{-1} \left(\Phi(\hat{u}_i) \right) \,.$$

4.3 Approximation Methods

The state of failure of a structure is defined through a deterministic limit state function G. An evaluation of G may involve a possibly computationally demanding numerical analysis. G is a function of a particular realisation of the problem random variables $\mathbf{x}$. By convention, a negative or zero value of G defines the failure domain:

$$G(\mathbf{x}) = G(x_1, x_2, \ldots, x_n) \leq 0 \,. \tag{4.10}$$

Each combination of the random variables, i.e. each point in the n-dimensional space with the coordinates $x_1, x_2, \ldots, x_n$, is assigned a probability density. The probability of failure is then given by the n-dimensional integral

$$p_f = P[\mathbf{X} | G(X) \leq 0] = \int_{G(\mathbf{x}) \leq 0} f_{\mathbf{X}}(\mathbf{x}) \, \mathrm{d}\mathbf{x} \,, \tag{4.11}$$

where $f_{\mathbf{X}}(\mathbf{x})$ is the joint probability density function of the variables $\mathbf{X}$. An example of the joint probability density function with an indication of the failure domain D_f is shown in Figure 4.1.

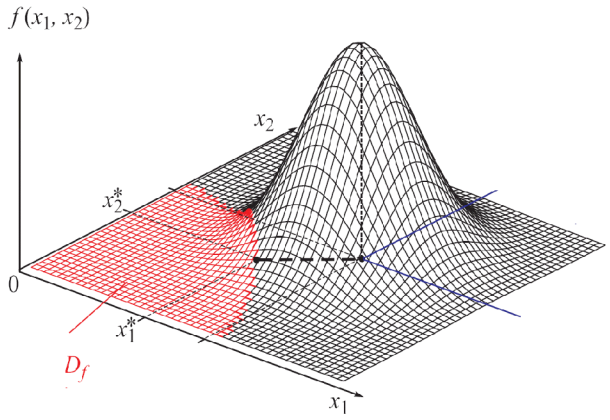

Figure 4.1: *Probability mass in the failure domain*

A closed form integration of Eq. (4.11) is possible only in exceptional cases. In most cases, the integral in Eq. (4.11) has to be resolved by means of numerical methods such as the Monte Carlo Simulation or through the reliability approximation methods, which are the subject of this Section.

In the standard normal space, the First Order Reliability Method (FORM) and Second Order Reliability Method (SORM) approximate the limit state function G by a linear or quadratic function, respectively, at the so called design point and provide an estimation of the integral (4.11). A linearisation (in FORM) of $G(\mathbf{x})$ about the design point will be denoted $\bar{G}(\mathbf{x})$ and is illustrated in Figure 4.2.

If all the variables were normal, the integral would be calculated exactly for a linear limit state function. In other cases, the basic variables $\mathbf{X}$ need to be transformed [38] to the *standard normal space* of uncorrelated Gaussian variables, see Section 4.2.

The design point $\mathbf{x}^*$ is the point on the limit state function having the highest probability density in the standard normal space

$$\mathbf{x}^* : \mathbf{x} \in \tilde{\mathbf{x}} : G(\tilde{\mathbf{x}}) = 0 \wedge f_{\mathbf{X}}(\mathbf{x}^*) = \max\left(f_{\mathbf{X}}(\tilde{\mathbf{x}})\right) . \tag{4.12}$$

As a consequence, in the standard normal space, the transformed coordinates of the design point $\mathbf{u}^*$ give the point on the transformed limit state function $G\left(\mathbf{u}(\mathbf{x})\right) = 0$ that is the closest to the origin of the standard normal space. This distance is a measure of reliability and is termed the Hasofer-Lind reliability index β_{HL} [38].

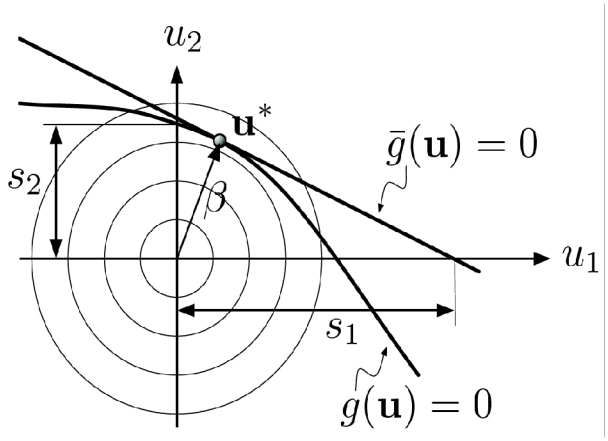

Figure 4.2: *Limit state function linearisation in FORM*

The fact that $\mathbf{u}^*$ is the limit state function point lying closest to the origin means that it can be found through constrained minimisation:

$$\mathbf{u}^* = \arg\min \left\{ \|\mathbf{u}\| \;\middle|\; G\left(\mathbf{u}(\mathbf{x})\right) = 0 \right\} \tag{4.13}$$

Having found $\mathbf{u}^*$, the FORM approximation of the probability of failure is easily determined using the distribution function Φ of standard normal distribution

$$p_f \simeq \Phi\left(-\beta_{HL}\right) . \tag{4.14}$$

A very instructive overview of optimisation algorithms suitable for the present problem can be found in [49]. An essential procedure on which these methods rely is the calculation of the response function derivatives, or sensitivities. The following Section 4.4 briefly discusses the respective computational approaches.

4.4 Sensitivity of the Response Function

In computational reliability analysis by the approximation methods, the calculation of the sensitivities of the response is indeed critical. On the one hand, the sensitivities are required to be computed with high accuracy. And on the other hand, the computational time spent in their calculation may be excessively high. Methods allowing for an accurate and fast computation of sensitivities are therefore of a great value.

This is also one of the concerns of this thesis: to improve the computational efficiency, accuracy and stability in the calculation of the sensitivities of the life under fatigue crack propagation governed by an empirical crack growth law.

In principle, the sensitivity of the response to a certain variable or parameter can be calculated in two ways. The first class of methods are various finite difference methods (FDM), such as the forward finite difference (FFD) method or the central difference method, which differ from each other by their respective level of accuracy and computational performance.

In the direct differentiation method, the response derivatives are not obtained numerically as in FDM, but by differentiating the underlying equations.

4.4.1 Direct Differentiation Method

This section discusses briefly in Subsection 4.4.1 the direct differentiation method. The details would encumber the continuity of the presentation. But the reader is encouraged to read Appendix C or the original reference [39].

When the mechanical response is obtained using a finite element model, many of the response sensitivities can be calculated together with the response itself by implementing in the finite element code the Direct Differentiation Method (DDM).

The bases of DDM were laid down in [3]. Its extension to geometrically nonlinear problems is presented in [53]. A very instructive and complete presentation of DDM and its extension to material nonlinearities can be found in [39]. In Appending C, the techniques of DDM are set out in a rather detailed manner, but still as just a specialisation of the formulæ found e.g. in [39] for the static linear-elastic case. This is, however, considered sufficient for expounding the ideas of the method and the reader is referred for further details to the cited literature.

For purposes of reliability analysis and optimisation of problems involving crack propagation, one is interested in the sensitivity of the fatigue propagation life N_R to the variables involved. The direct differentiation method was developed as a method to calculate sensitivity of finite element results to finite element model loads, geometry and material parameters.

DDM can for example be employed to calculate the sensitivity of the current stress intensity factor at the crack tip to the current crack length. However, the sensitivity of the fatigue propagation life to e.g. a previous crack length can only be determined based on the crack growth law, which

governs the crack propagation and which is completely external to any finite element procedures.

In Sections 7.4.1 through 7.4.4, equations for the sensitivities of the fatigue propagation life to certain variables will be derived. By differentiating the fatigue life integral formula, and sometimes taking certain simplifying assumptions, straightforward sensitivity equations will be derived. In some cases, such as the case of sensitivity to the initial crack length, the assumptions taken that will lead to particularly simple sensitivity formulæ. This may be regarded as a specific contribution of this thesis.

4.5 Sensitivity of the Reliability Index

Within the reliability approximation method, the sensitivities of the reliability index to each of the random variables, to their distribution parameters and to the parameters of the limit state function can be obtained in a rather straightforward way. The presentation here is limited to the sensitivity to the random variables. Sensitivities to the above mentioned parameters are discussed e.g. in [49].

4.5.1 Sensitivity in the Standard Normal Space

The FORM the limit state function is linearised about the design point:

$$\begin{aligned} G(\mathbf{u}) &\approx G(\mathbf{u}^*) + \nabla G(\mathbf{u}^*)^T(\mathbf{u}-\mathbf{u}^*) \\ &= \frac{\nabla G(\mathbf{u}^*)}{\|\nabla G(\mathbf{u}^*)\|}(\mathbf{u}-\mathbf{u}^*) = \boldsymbol{\alpha}^T(\mathbf{u}-\mathbf{u}^*) \\ &= \beta_{HL} + \boldsymbol{\alpha}^T\mathbf{u} = 0\,, \end{aligned} \tag{4.15}$$

where we used the fact that $G(\mathbf{u}^*) = 0$ and scaled the limit state function by the norm of its gradient $\nabla G(\mathbf{u}^*)$, calculated at the design point. Note that $\boldsymbol{\alpha}$ are the direction cosines of the gradient vector ∇G.

From the above Eq. (4.15)

$$\beta_{HL} = -\boldsymbol{\alpha}^T\mathbf{u} \Rightarrow \left.\frac{\partial \beta_{HL}}{\partial \mathbf{u}}\right|_{\mathbf{u}^*} = -\boldsymbol{\alpha}\,. \tag{4.16}$$

This shows that the direction cosines $\boldsymbol{\alpha}$ express the sensitivities of the reliability index β_{HL} to the individual variables $\mathbf{u}$ in the standard-normal space.

4.5.2 Sensitivity to the Physical Variables

When the variables $\mathbf{x}$ are statistically independent, the direction cosines in the standard normal space express correctly the sensitivity of β_{HL} also to the corresponding physical variables. However, when $\mathbf{x}$ are dependent, the importance of the variables in the physical space differs from $\boldsymbol{\alpha}$ due to the (nonlinear) probability transformation between the physical and the standard normal space. The sensitivities to the physical variables can be obtained as follows (based on [22] and [49]).

The probability transformation is linearised at at the design point

$$\mathbf{u} \approx \mathbf{u}^* + \mathbf{J}_{\mathbf{u},\mathbf{x}}(\mathbf{x} - \mathbf{x}^*) \tag{4.17}$$

where $\mathbf{J}_{\mathbf{u},\mathbf{x}}$ is the Jacobian of the probability transformation at the design point

$$\mathbf{J}_{\mathbf{u},\mathbf{x}} = \left.\frac{\partial T_i(\mathbf{x})}{\partial x_j}\right|_{\mathbf{x}^*} . \tag{4.18}$$

Separating out $\mathbf{x}$, Eq. (4.17) can be rewritten as

$$\begin{aligned} \mathbf{x} &\approx \mathbf{J}_{\mathbf{u},\mathbf{x}}^{-1}(\mathbf{u} - \mathbf{u}^*) + \mathbf{x}^* \\ \text{or} \quad \hat{\mathbf{x}} &= \mathbf{J}_{\mathbf{u},\mathbf{x}}^{-1}(\mathbf{u} - \mathbf{u}^*) + \mathbf{x}^* . \end{aligned} \tag{4.19}$$

The variables $\mathbf{x}^*$ for which the equality sign holds in Eq. (4.19) differ somewhat from $\mathbf{x}$. But more importantly, they are given by a linear function of $\mathbf{u}$ and are therefore joint normally distributed, with the mean vector and variance matrix given by

$$\begin{aligned} \boldsymbol{\mu}_{\hat{\mathbf{X}}} &= \mathbf{x}^* - \mathbf{J}_{\mathbf{u},\mathbf{x}}^{-1}\mathbf{u}^* \\ \hat{\boldsymbol{\Sigma}} &= \mathbf{J}_{\mathbf{u},\mathbf{x}}^{-1}\left(\mathbf{J}_{\mathbf{u},\mathbf{x}}^{-1}\right)^T . \end{aligned} \tag{4.20}$$

In terms of these variables $\mathbf{x}^*$, the linearised probability transformation (4.17) reads:

$$\mathbf{u} = \mathbf{u}^* + \mathbf{J}_{\mathbf{u},\mathbf{x}}(\hat{\mathbf{x}} - \mathbf{x}^*) . \tag{4.21}$$

Substituting the latter relation into the linearised limit state function (4.15), we obtain

$$\hat{G}(\mathbf{u}) = \boldsymbol{\alpha}\mathbf{J}_{\mathbf{u},\mathbf{x}}(\hat{\mathbf{x}} - \mathbf{x}^*) . \tag{4.22}$$

The mean and variance of $\hat{G}$ are

$$\begin{aligned} \mu_{\hat{G}} &= -\boldsymbol{\alpha}^T\mathbf{J}_{\mathbf{u},\mathbf{x}}\mathbf{J}_{\mathbf{u},\mathbf{x}}^{-1}\mathbf{u}^* = \beta_{HL} \\ \sigma_{\hat{G}} &= \boldsymbol{\alpha}^T\mathbf{J}_{\mathbf{u},\mathbf{x}}\hat{\boldsymbol{\Sigma}}\mathbf{J}_{\mathbf{u},\mathbf{x}}^T\boldsymbol{\alpha} = 1 . \end{aligned} \tag{4.23}$$

The variance of $\hat{G}$ involves both variances and covariances of $\hat{\mathbf{x}}$. To isolate the contributions from the individual variances, the covariance matrix $\hat{\boldsymbol{\Sigma}}$ is decomposed as follows:

$$\hat{\boldsymbol{\Sigma}} = \boldsymbol{\sigma}_{\hat{\mathbf{X}}} \boldsymbol{\sigma}_{\hat{\mathbf{X}}} + \hat{\boldsymbol{\Sigma}} - \boldsymbol{\sigma}_{\hat{\mathbf{X}}} \boldsymbol{\sigma}_{\hat{\mathbf{X}}} \,, \tag{4.24}$$

where $\boldsymbol{\sigma}_{\hat{\mathbf{X}}}$ is a diagonal matrix of the standard deviations of $\hat{\mathbf{X}}$. Expanding Eq. (4.23) through this decomposition, it comes out that

$$\sigma_{\hat{G}} = \boldsymbol{\alpha}^T \mathbf{J}_{\mathbf{u},\mathbf{x}} \boldsymbol{\sigma}_{\hat{\mathbf{X}}} \boldsymbol{\sigma}_{\hat{\mathbf{X}}} \mathbf{J}_{\mathbf{u},\mathbf{x}}^T \boldsymbol{\alpha} + \boldsymbol{\alpha}^T \mathbf{J}_{\mathbf{u},\mathbf{x}} \left(\hat{\boldsymbol{\Sigma}} - \boldsymbol{\sigma}_{\hat{\mathbf{X}}} \boldsymbol{\sigma}_{\hat{\mathbf{X}}} \right) \mathbf{J}_{\mathbf{u},\mathbf{x}}^T \boldsymbol{\alpha} = 1 \,. \tag{4.25}$$

The first member in the above equation is identified as the contribution of the individual variables $\hat{\mathbf{x}}$. The first member itself is no longer equal to unity. If we consider not the square term but only $\boldsymbol{\alpha}^T \mathbf{J}_{\mathbf{u},\mathbf{x}} \boldsymbol{\sigma}_{\hat{\mathbf{X}}}$ and normalise it, we finally obtain a vector $\boldsymbol{\gamma}$ expressing the sensitivities to $\hat{\mathbf{x}}$:

$$\boldsymbol{\gamma}^T = \frac{\boldsymbol{\alpha}^T \mathbf{J}_{\mathbf{u},\mathbf{x}} \boldsymbol{\sigma}_{\hat{\mathbf{X}}}}{\left\| \boldsymbol{\alpha}^T \mathbf{J}_{\mathbf{u},\mathbf{x}} \boldsymbol{\sigma}_{\hat{\mathbf{X}}} \right\|} \,. \tag{4.26}$$

4.6 Monte Carlo Simulation

An alternative way to evaluate the probability of failure integral in Eq. (4.11) is to use the so called Monte Carlo integration, more often referred to as Monte Carlo simulation (MCS).

Instead of integrating just over the failure domain, in MCS, we integrate Eq. (4.11) over the entire domain, but multiply the integrand by an indicator function $I\left(G(\mathbf{x})\right)$ which returns 0 if the integration point is in the safe domain ($G(\mathbf{x}) > 0$) and returns 1 if it belongs to the failure domain ($G(\mathbf{x}) \leq 0$):

$$p_f = \int_{\mathbf{x}} I\left(G(\mathbf{x})\right) f_{\mathbf{X}}(\mathbf{x}) \, \mathrm{d}\mathbf{x} \,. \tag{4.27}$$

It is clear that (4.27) is the expected value of $I\left(G(\mathbf{x})\right)$. Thus, from statistics,

$$p_f \approx \mathfrak{I}_{MC} = \frac{1}{N} \sum_{i=1}^{N} I\left(G(\mathbf{x})\right) \,. \tag{4.28}$$

where $\mathbf{x}_i$ is the i-th of the total of N realisations of the random vector $\mathbf{x}$ sampled from $f_{\mathbf{X}}(\mathbf{x})$.

Since $G(\mathbf{X})$ is a random variable in $\mathbf{X}$, $I\left(G(\mathbf{X})\right)$ is also a random variable. Considering the sum in Eq. (4.28) and invoking the central limit theorem,

it follows that $\mathfrak{I}_{MC}$ approaches a normal distribution as $N \to \infty$. The mean of $\mathfrak{I}_{MC}$ is thus estimated by

$$\mu_{\mathfrak{I}_{MC}} = \mathrm{E}\left[\mathfrak{I}_{MC}\right] = \sum_{i=1}^{N} \frac{1}{N} \mathrm{E}\left[I\left(G(\mathbf{X})\right)\right] = \mathrm{E}\left[I\left(G(\mathbf{X})\right)\right] , \tag{4.29}$$

which is equal to $\mathfrak{I}_{MC}$. By the same token, the variance of $\mathfrak{I}_{MC}$ is estimated by

$$\sigma^2_{\mathfrak{I}_{MC}} = \mathrm{E}\left[(\mathfrak{I}_{MC} - \mu_{\mathfrak{I}_{MC}})\right] = \sum_{i=1}^{N} \frac{1}{N^2} \mathrm{var}\left[I\left(G(\mathbf{X})\right)\right] = \frac{\sigma^2_{I(G(\mathbf{X}))}}{N} . \tag{4.30}$$

It is seen that the standard deviation of $\mathfrak{I}_{MC}$ is inversely proportional to the square root of the number of simulations $\sigma_{\mathfrak{I}_{MC}} \propto \frac{1}{\sqrt{N}}$ and proportional to the standard deviation of the indicator function $\sigma_{\mathfrak{I}_{MC}} \propto \sigma_{I(G(\mathbf{X}))}$.

It follows that there are two ways to improve the accuracy of the MCS estimate of the integral (4.11): increase the number of simulations, or, more efficiently, reduce the variance of $I\left(G(\mathbf{X})\right)$. One of the variance reduction strategies is the so-called importance sampling technique, discussed briefly below. Other techniques have been developed and are described in reliability monographes, e.g. [49].

4.6.1 Importance Sampling

A way to reduce variance in $I\left(G(\mathbf{X})\right)$ is to limit the simulations to the region of interest, which is essentially the region around the design point [13]. This is achieved by doing the following manipulation on Eq. (4.27):

$$p_f = \int I\left(G(\mathbf{x})\right) \frac{f_{\mathbf{X}}(\mathbf{x})}{h_{\mathbf{S}}(\mathbf{x})} h_{\mathbf{S}}(\mathbf{x}) \mathrm{d}\mathbf{x} , \tag{4.31}$$

where $h_{\mathbf{S}}(\mathbf{x})$ is termed the sampling density function. The integral (4.31) is now an expectation on $I\left(G(\mathbf{x})\right) \frac{f_{\mathbf{X}}(\mathbf{x})}{h_{\mathbf{S}}(\mathbf{x})}$. An estimate of the probability of failure is then

$$p_f \approx \mathfrak{I}_{IS} = \frac{1}{N} \sum_{i=1}^{N} I\left(G(\mathbf{x})\right) \frac{f_{\mathbf{X}}(\mathbf{x})}{h_{\mathbf{S}}(\mathbf{x})} . \tag{4.32}$$

Note that the sampling is now from the sampling density $h_{\mathbf{S}}(\mathbf{x})$. The choice of $h_{\mathbf{S}}(\mathbf{x})$ controls the variance in $\mathfrak{I}_{IS}$. A good choice can significantly reduce the variance, while a poor choice may increase it.

4.6.2 Latin Hypercube Sampling

Latin Hypercube Sampling (LHS) is a simulation method that has proven effective for problems where only a small number of simulations is computationally affordable [58].

The domain of definition of the marginal distribution of each of the n variables is partitioned into N intervals with equal probability content. A representative sample is then chosen from each of the N^n intervals. Simulation is carried out not by sampling from a distribution, but by randomly combining the intervals. The resulting samples will show some correlation, which is different from the correlation between the variables. A method based on simulated annealing has been proposed [90] to introduce the desired correlation.

An additional indicator function w_{ij} is introduced that returns 1 if the interval j of the random variable i belongs to the random sample, and 0 otherwise. The estimator for the failure probability than reeds:

$$p_f \approx \mathfrak{I}_{LHS} = \frac{1}{N} \sum_{i_1=1}^{N} \overset{n-\text{times}}{\cdots} \sum_{n_1=1}^{N} w_{ij} I\left(G(\mathbf{x})\right) , \tag{4.33}$$

where summation is done over all of the intervals.

4.6.3 Estimation of a Variable's Importance

In the approximation methods, the sensitivity of the probability of failure to each of the random variables, or in other words the importance of each variable, was directly related to the coordinates of the design point. In the context of Monte Carlo simulation, such information is in general not available.

However, rough estimates of the variables' importance can be made based on correlation between the sampled realisations of a random variable and the corresponding values of the limit state function.

4.7 Conclusions

In this Chapter, we have reviewed the essentials of basic structural reliability methods, which represent the means to work with the uncertainties inherent to fatigue crack propagation, the problem in the focus of this thesis. Note that there are certain issues that arise in particular in the analysis of crack propagation problems. These include:

- accuracy of calculation of the limit state function value and of its derivatives, which is key to the convergence of the deign point search algotithm,
- low-probability configurations in Monte Carlo Simulation,
- heavy computational effort.

The above issues are discussed in the following Chapter 5, where they are addressed together with other challenges faced when analysing complex fatigue crack growth problems.

Part II

Stochastic Crack Propagation Model

Chapter 5

Challenges and Coping Strategies

5.1 Challenges in Crack Propagation Modelling

The phenomenon of propagation of an existing crack can be viewed and approached from several perspectives, including microstructural, phenomenological or engineering considerations. In a reliability analysis of crack propagation problems, the life until failure is of interest. The purpose of this Chapter is to identify the challenges faced when designing a numerical model to calculate this failure life. Where appropriate, various possible approaches to deal with these challenges are also discussed. In Section 5.2, the strategies to appropriately include the key issues in the modelling will be formulated.

5.1.1 Scatter in Crack Initiation

Point of crack initiation

It was argued in Section 2.2.1 that cracks initiate in material grains favourably oriented for slip and experiencing increased stresses due to notches, indents or surface roughness. Then, cracks finding themselves in regions with generally higher stresses take on the role of the leading cracks. In an *ab initio* approach, the analysis would depart from local effects, the random distribution of which would be discussed more appropriately as a material-related one. However, considering just the leading cracks, it is reasonable to model cracks initiating from known points of major stress concentrations, such as notches, corners and holes, and to alter the respective initiation point by a random distance to account for the presence of randomly located

micro-defects favouring crack initiation.

Initial crack size

Except for controlled laboratory tests, the size of an existing macro-crack at a given instant is uncertain. Therefore, a probability distribution is considered for the crack size at the instant when the propagation simulation starts. An alternative approach is sometimes adopted, which consist in considering a randomly distributed number of load cycles at which a macro-crack of a given size occurs.

5.1.2 Scatter in Crack Propagation

The statistical dispersion in crack propagation can be seen to have two components: the dispersion in the propagation velocity and the uncertain direction of propagation at any given instant.

Crack growth rate

The rate or velocity of crack growth depends on multiple factors, among which the material properties. It was noted in Section 2.5 that empirical crack growth laws constitute a useful model to represent crack propagation, whereby the model coefficients can be fitted to actual fatigue test results. This approach is adopted also here.

A possible way to take into account the scatter inherent to crack propagation velocity is to introduce into the crack growth equation a random process as suggested by equation 2.32, or to simply "randomise" the crack growth law by modelling its parameters as random variables. The crack propagation model adopted in this thesis uses the latter approach.

Let us return to the Paris-Erdogan crack growth law defined in equation (2.13). Both its parameters C and m are considered to be random variables. Their parameters can be estimated from fatigue crack propagation experiments.

In the present approach, the scatter and dependence of C and m was modelled by considering normally distributed correlated random variables $\ln C$ and m, the statistical parameters of which were established from the Virkler data [89]. Taking the exact values of the estimated statistical parameters, Virkler's results were reproduced with certain accuracy. Section 6.2 studies also various other statistical models for C and m. It appears that the extremely high sensitivity of the calculated failure probability to the correlation of $\ln C$ and m is a weak point of the model as it requires

extreme precision in the prescribed correlation coefficient as well as in the sampling from the correlated distribution.

When the fatigue life is so much sensitive to the accuracy of the statistical model, the question of accuracy of the mechanical model also arises. Reference [14] shows how the correct failure probability can be calculated through introducing a random model error with appropriate statistical parameters.

But in particular, it shows how the issue of high sensitivity to correlation can be circumvented by reformulating the statistical model. The modified statistical model had two uncorrelated variables and employed a formula derived from the regression analysis. The stringency of using only a single random variable and having the other functionally dependent was elegantly overcome by considering as the second random variable just the difference $\varepsilon_{\ln C}$ between $\ln C$ and the expectation on $\ln C$ coming from the regresion. $\varepsilon_{\ln C}$ and m appeared to be uncorrelated and the sensitivity to their correlation of was negligible.

A combination of this decorrelation of the random variables and the model error seems to be the best modelling approach. However, for the purposes of this thesis, we will satisfy ourselves with the statistical model considering $\ln C$ and m normally distributed, together with the accurate correlation coefficient. We will also renounce on introducing the random model error.

Direction of Crack Propagation

The direction of crack extension is essentially governed by the surrounding stress field; various criteria to choose the crack extension angle have been described in Section 2.7. However, as fatigue tests reveal, the actual crack path is far from being smooth and the directions of the crack extentions at the individual load cycles are seen to have some random component.

In Section 2.2.1, it was argued that the crack extension direction may change due to the effect of microstructural features, the distribution of which can be considered random. In addition, the randomness in multi-axial loading also leads to random crack paths. It is useful to recall at this point that a crack path in two dimensions is an idealisation and that the actual fatigue crack surface will be knurled over its area. Thus, we seek a model to describe the observed crack deflection from its 2D path rather than to relate the crack path to complicated three-dimensional microstructural features. In [54], the crack extension angle was determined by the governing deterministic criterion combined with a randomly distributed direction vari-

able, which had a joint probability density function with the length of the crack extension. This corresponds to the expected behaviour that the crack deflection over a short distance can be greater.

On the other hand, in [84], the authors considered a random length of crack increment uncorrelated with a random deflection angle at each step of crack growth.

No systematic experimental results are available that would allow for estimation of the random crack deflection characteristics and the predictions of the above cited models cannot be verified in the light of experimental evidence.

In the present approach, the randomness in crack growth direction is neglected and the direction is governed only by fracture mechanics considerations.

Elastic Material Constants

Within the framework of linear elastic fracture mechanics, the stress and strain field that governs the crack propagation velocity and direction depends on the elastic constants of the material, i.e. on Young's modulus E and Poisson's ratio ν. Because of inherent material inhomogeneity, the elastic constants may be considered to vary with the position in the material as a random field, or may be considered as random variables representing a characteristic value applicable to the whole body. However, it can be reasonably assumed that the effect of local stress concentrators is more important than the spatial variability of the elastic constants. And when we did not take account of the local material inhomogeneities, it would not be consistent to consider the less important variability of the elastic constants.

5.1.3 Complexity and Randomness of the Loading

In a number of engineering applications, the cyclic loading experienced by cracked structures is not only complex, but often includes a random component. The complexity is usually accommodated by considering standard time records of loading for the application in question and including the effect of retardation after overloads in the model (see Section 2.6). This approach, which corresponds to the industrial practice, was adopted also within the analysis procedure proposed in this thesis. Randomness of the loading can be conveniently represented by modelling the loading as a stochastic process. In this thesis, this is not done, as measured loading data are not available to the author. It would be interesting to evaluate the importance

of randomness in the loading. The fact that this randomness is neglected in the analysis should be kept in mind when interpreting the calculated probablility of failure. On the other hand, the loads can hardly be controlled and the importance factor for loading can therefore not serve to the operator as a guidance where to direct resorces in orther to improve reliability.

5.1.4 Remeshing

A major difficulty in numerical modelling of crack propagation stems from the necessity to update the crack geometry. Two major axes of development can be identified today. The first one focuses on the remeshing process itself. Very powerful remeshing algorithms have now become commercially available.

It is however necessary to note that removing the burden of remeshing does not mean that all problems have been solved. Keeping in mind that the response of finite element models is mesh dependent, remeshing inevitably leads to noise in the calculated response. This has troublesome connotations in all applications when response sensitivity is of interest, including reliability analysis. Response derivatives need in many cases to be evaluated by finite difference methods. The change in the response is then not only due to a perturbation of the geometry, but also due to remeshing noise.

Numerical noise in the calculation of the life under crack propagation often leads to a failure of the design point search procedure to converge. **Computational accuracies that are quite satisfactory in deterministic analysis may prove insufficient in reliability analysis**.

The competing approach goes to the root cause of the difficulty and seeks to replace classical remeshing by other techniques. The various techniques have been described in Chapter 3. The novelty of the modelling approach adopted in this thesis is to combine the Extended Finite Element Methods with reliability methods to present an efficient approach for stochastic analysis of crack propagation with a numerical mechanical model.

5.1.5 Structural interactions

Engineering crack propagation problems often involve complex geometries or interaction of cracks. Examples include the modelling of wide-spread fatigue damage or of crack propagation in aircraft fuselage. For such problems, analytical expressions for calculation of fracture parameters are inadequate and numerical models of the underlying real structure are required.

The fundamental concept determining the crack propagation modelling

approach adopted in this thesis is that *the evolving crack geometries in the process of crack propagation are important* because the geometries of various cracks may influence the velocity of crack growth as well as the severity of the accumulated damage in terms of the crack length. These two effects have the following consequences:

- the crack propagation velocity,
- the critical crack size, and
- the current direction of crack propagation

all *depend* on the path (geometry) of the respective crack itself as well as on the size and path of any *other cracks*. Consequently, crack propagation models considering only the size of the leading crack, as presented namely in Section 2.8, may be inadequate given the above considerations.

5.1.6 Accuracy in FORM

Mechanical Model Response

As it has been already noted above, an implementation of a crack propagation model relying on a numerical (finite element based) prediction of fracture parameters, namely the stress intensity factors, brings up the issue of numerical accuracy, which is particularly relevant in the context of reliability analysis.

The (in)accuracy of the mechanical model can be assessed at two levels. First, there is the question of how truly does the model represent the actual physics. The other dimension of model accuracy is important when one needs to evaluate the sensitivity of the response. The desirable property of the model is that the calculated response correctly and consistently reflects small changes in the input parameters, including the geometry. Probably the best way to achieve this is to analytically differentiate the equations of the numerical model. This approach has been termed the Direct Differentiation Method and is outlined in Section 4.4.1.

However, such direct differentiation may in some cases be rather difficult and finite difference methods become the most practical solution. It then matters very much that the calculated difference in the response correctly translates nothing but the perturbation in the variable with respect to which the sensitivity is calculated. Where the response difference contains a significant portion of numerical noise, *convergence of the First Order Reliability Method* (i.e. the design point search, see Section 4.3) *can be lost*.

Crack Propagation Life Integration

Another source of inaccuracy, which occurs regardless of whether one uses FORM or Monte Carlo Simulation, is the numerical integration of life under fatigue crack propagation from the initial to the critical crack size. The crack growth law has the form of a differential equation. To calculate the fatigue crack propagation life, the equation is inverted and integrated, with the integration limits being the initial and the final crack length. Two factors come into play as concerns the integration accuracy:

- **Integration step size.** The integrand of the propagation life integral depends on the stress intensity factor (SIF), which is calculated in the present approach by a numerical mechanical model. For practical reasons, SIF is evaluated only at discrete increments of the crack length. Obviously, there is a trade off between the accuracy and the computational effort, which both come hand in hand with a finer integration step size. Not only does a small step size require a higher number of SIF computations, but it usually also necessitates a finer mesh.
- **Integration method.**
  - *A quadrature rule* is the standard numerical integration method. In crack propagation context, a quadrature rule for non-uniform interval lengths must be used. It can be easily developed e.g. based on Lagrange polynomials. As the integrated curve of life spent in propagating the crack over a unit length is highly non-linear, only higher order quadratures can perform successfully.
  - *Analytical integration of a curve fitted to the data* can prove advantageous, in particular when the numerical method used to evaluate SIF is unstable in the prediction of the SIF. Any outlier points on the plot of the SIF versus the crack length can result in gross errors in quadrature based integration. However, fitting a conveniently chosen function to this curve and integrating the function analytically has proven to be a stable and accurate integration method, also in cases of rather smooth SIF curves.

5.1.7 Low-probability Configurations in Monte Carlo Simulation

Notwithstanding that Monte Carlo Simulation is known to be a rather robust probability integration method, it is also known to have some drawbacks.

Variance reduction methods and Latin Hypercube Sampling have done away with the extremely high numbers of simulations needed in reliability analysis of low-probability failure scenarios.

A less often discussed problem of simulation methods is that they require the underlying mechanical model to calculate the response at extremely low-probability realisations of the random variables. Note that with the reliability approximation methods, the response is generally evaluated in the region surrounding the mean and the most probable failure point.

Numerical mechanical models are commonly built with the usual geometrical configurations in mind. With common values of the variables involved, the mechanical models behave as expected and the specific mode of failure that one wants to analyse then also occurs. Such models may however fail to compute the response for low-probability geometries, mainly because a different mode of failure occurs that the one considered in the analysis. The mechanical model may then fail to compute the response for numerical reasons. Examples may include cracks growing in unexpected directions, arriving at cold spots where their propagation is halted, intersecting or merging with other cracks, or growing through the entire ligament without the failure condition (e.g. fracture toughness or overall plastic collapse of the structure) being reached. To be used in Monte Carlo Simulation, the model must be developed such as to provide a correct response in all such geometrical configurations. In some cases, such robust models may be difficult to construct. And what is also important to note is that we then start solving a different reliability problem than the one with which we started.

5.1.8 Heavy computational effort

Computational reliability analysis in general, and Monte Carlo Simulation in particular, require a large number of evaluations of the structural response. With crack propagation simulation, the situation is yet more aggravated: multiple numerical mechanical model responses (SIF calculations) are needed to evaluate a single response in terms of the life under fatigue crack propagation that is of interest. This adds up to an extraordinary computational effort that has so far discouraged many researchers and engineers from pursuing the path of stochastic crack propagation analysis using a numerical mechanical model.

5.2 Coping Strategies and Objectives

In the above, we have discussed the difficulties and challenges of the reliability analysis of crack propagation problems. Some approaches to face these challenges were also outlined. This section highlights the most important strategies used in this thesis to develop an efficient and robust reliability tool for crack propagation problems, being aware of the issues identified above.

The proposed method can be seen as a particular development of the fundamental concept of **integration of mechanical and probabilistic models**, which was put forward already in 1970's, see e.g. [50]. As a matter of fact, extremely high computational effort has been preventing researchers and in particular the engineers in the industry to exploit numerical mechanical models in a stochastic analysis of crack propagation problems. This thesis hopefully shows that by choosing appropriate numerical methods and computational techniques, a feasible procedure can be developed to leverage the benefits of both a numerical mechanical model offering clear physical interpretations, and of the use of the available statistical information, in order to provide a basis for better informed and better grounded decisions on real industrial problems involving propagation.

5.2.1 Reliability Analysis

When analysing crack propagation, one is confronted with an extraordinary amount of dispersion in crack initiation times and crack propagation rates, even under well controlled conditions. At the same time, experimental evidence has show that this scatter is very well described by statistical models.

With increasing level of randomness, it becomes increasingly less justified to use deterministic models, even if these have a relation to the statistics of the random variables involved, e.g. through partial safety factors.

Stochastic analysis makes it possible to rigorously account for the dispersion in the underlying variables and, using the mechanical model, to learn about the actual dispersion of the response, the true probability of failure and the importance of each of the variables. Compared to taking a large safety factor, such richer information allows the engineer to better understand the problem and make better informed decisions.

5.2.2 Equivalent Monotonous Spectrum Loading

The length of life under fatigue crack propagation is heavily influenced by specific features of the time history of the applied load. More than on the

statistical properties of the loading process, the fatigue life depends on the sequence of peaks and valleys in the load history.

Fatigue life evaluation therefore cannot make use of statistical or spectral methods and has to work in the time domain. Simple models have been developed to account for the effects of overloads and underloads. A method that has gained much acceptance in the aeronautical industry is the PREFFAS method, [21] which is remarkable for its ability to reproduce actual fatigue test results. PREFFAS is used also in the developments of this thesis.

5.2.3 Numerical Methods without Remeshing

A computational method that is to accommodate arbitrary geometries involving multiple cracks cannot do without a numerical mechanical model. A vast majority of the computational time in the reliability analysis of crack propagation problems using a numerical mechanical model is spent in the calculation of the structural response upon all updates of the crack geometry. The efficiency of this computation is thus of paramount importance. In addition, the accuracy of the calculated response affects the stability of the fatigue life calculation.

The computation of the static structural response (e.g. of stress intensity factors) comprises the following major operations:

- geometry update,
- assembling of the stiffness matrix,
- matrix factorisation,
- post-processing.

A factorisation of the stiffness matrix invariably needs to be carried out every time a new geometry is analysed, regardless of the features of the particular numerical method used. Post-processing of the numerical analysis results to calculate the response of interest is also similar using any of the numerical methods – none of the methods offers any particular advantages that could expedite the response calculation.

Some improvement in efficiency could be attained by rebuilding just the part of the stiffness matrix that is concerned by the geometry change.

The strength of the meshless and extended finite element (XFEM) approximations comes forth in the update of geometry in the numerical model. In contrast to classical finite elements, which rely on automated or guided

remeshing to ensure that the mesh aligns with the discontinuities, in the meshless and XFEM methods, discontinuities can pass independently of the discretisation. This both avoids remeshing and improves the stability, since numerical noise due to remeshing is also reduced.

These improvements are at the expense of additional computational effort that is necessary to search for the nodes in the neighbourhood of the geometry change (e.g. a crack tip). Depending of the efficiency of the search algorithm, this operation may take a considerable amount of time. On the other hand, it can be and usually is fully automated and reliable.

As compared to XFEM, the shape functions are *a priori* unknown in meshless methods and need to be reconstructed for each integration point. As far as computational effort is concerned, this represents a major drawback of meshless approximations.

In the application part of this thesis, the structural response is calculated and post-processing to evaluate the stress intensity factors is carried out within an XFEM package, developed at the LAMCOS laboratory of INSA de Lyon.

5.2.4 Direct Differentiation Method

In all applications requiring the evaluation of sensitivities of the structural response (optimisation, reliability), the efficiency and accuracy of computation of the partial derivatives of the response is a key issue.

In applications where the response of interest for the reliability or optimisation analysis is directly obtained from a numerical mechanical model, there are in general two methods to calculate the response sensitivity. The better of them, termed the Direct Differentiation Method (DDM) [39], consists in differentiating the equations of the discretised mechanical model with respect to the variable of interest. The advantage of DDM is that that the calculation of sensitivities is much faster and always consistent (the derivatives are found as a solution of the differentiated equations).

DDM can be qualified as an "intrusive" method in that it requires modifying the finite element or other code. When one wishes to use a standard (commercial) finite element software, one needs to put up with a finite difference scheme to calculate the sensitivities. However, in case of the crack propagation problems, sensitivities to the variables entering just the crack propagation life integral and not the numerical mechanical model can be calculated by "non-intrusive methods", see below. This fact is exploited in this thesis and simple sensitivity equations are derived, which improve the accuracy and speed of computation of the sensitivities.

Finite difference methods are known to lack computational speed (multiple evaluations of the response are necessary) and accuracy. The latter depends on the finite difference step size. It may be too small such that the difference in the response is more due to numerical noise than due to the perturbation of the variable of interest. It may also be too large, which leads to inaccuracy resulting from a failure to correctly capture the non-linear character of the response.

Sensitivity of Crack Propagation Life

In the present work, we are interested in the sensitivity of the life under fatigue crack propagation. Numerical mechanical model is used here to calculate the structural response at discrete points of the crack length until the critical crack size at the time of failure, which is the variable of interest in the reliability analysis.

The fatigue life is then calculated using the numerical model responses at the discrete crack length by integrating the inverse crack growth rate over the crack length. Sensitivity to many of the random variables of interest can be calculated by differentiating the integral formula. Sensitivity equations are derived in this way in Sections 7.4.1 through 7.4.4.

This approach is thereby "non-intrusive" to the numerical code, as far as the calculation of the sensitivity of interest does not involve a derivative with respect to the stress intensity factor.

5.2.5 Distributed Computing

Reliability analysis is a typical example of computational task that is suitable for distributed computing. The mechanical models of many reliability problems can today be solved on inexpensive personal computers. What makes reliability analysis computationally non affordable is the necessity to evaluate the response many times. Either, this is due to a large number of simulations needed to analyse the reliability of problems with low probability of failure by Monte Carlo Simulation. Or, the multiple response evaluations come with the need to calculate the response and its derivatives at each step of the design point search in the reliability approximation methods (see Section 4.3).

Distribution of computing in reliability analysis (and for that matter also in optimisation) of problems modelled by numerical mechanical models, a single solution of which is not particularly computationally intensive, is made simpler and cheaper by the fact that the computer architecture can be built

as a cluster of relatively inexpensive personal computers.

5.3 Conclusions

In this chapter, we have reviewed the major challenges faced when developing an efficient procedure for the reliability analysis of crack propagation problems. The strategies to cope with these issues that can be identified as the feasible ones can be summarised in the following points.

- Carry out a stochastic analysis to account for the extraordinary amount of dispersion in crack propagation and provide for better informed engineering decisions.
- Use a numerical structural model to capture the geometrical interactions inherent to complex crack propagation problems.
- Improve the efficiency, ease and accuracy of structural response evaluation by using the Extended Finite Element Method.
- Apply an accurate and stable integration procedure for the calculation of the life under fatigue crack propagation.
- Employ the direct differentiation approach to evaluate the sensitivities of the crack propagation life with respect to most of the variables entering the crack growth law.
- Make use of a cluster of PCs available at IFMA Clermont-Ferrand to enhance the computational speed of the reliability analysis.

The rest of the thesis will be concerned with the development, implementation and application of a computational approach based on the above strategies.

Chapter 6

Statistical Modelling and Reliability Analysis

6.1 Introduction

This Chapter deals with the statistical and reliability modelling used for purposes of the analysis of the stochastic crack propagation problem. The choice of appropriate statistical distributions and the estimation of their parameters is a crucial point. Reliability analysis only makes sense when we have a knowledge about the statistical properties of the underlying variables. Only then can reliability methods be used to provide valuable information about the statistics of the structural response.

Section 6.2 focuses on the estimation of the two material dependent parameters of the Paris law. This issue has attracted considerable attention, in particular as concerns the correlation of the two parameters and the appropriate statistical model to be used.

In the remaining sections of this Chapter, we will define the failure model and make a choice of a reliability method to suit the needs of crack propagation analysis.

6.2 Estimation of the Paris Law Parameters

The most commonly used models to predict the rate of crack propagation are based on the Paris law [73]

$$\frac{\mathrm{d}a}{\mathrm{d}N} = C\,(\Delta K)^m \ , \tag{6.1}$$

which models the crack propagation rate $\frac{\mathrm{d}a}{\mathrm{d}N}$ as a function of the stress intensity factor range ΔK. Its validity is limited to the crack propagation stage from a time when the crack has already been well initiated until the time when the crack growth accelerates before fracture failure occurs.

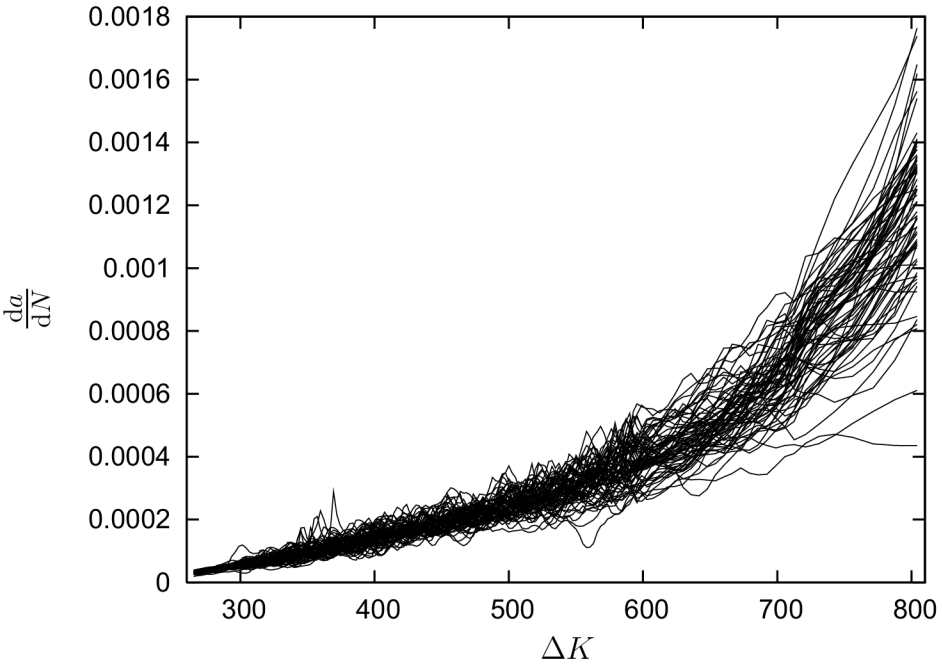

Figure 6.1: $\frac{\mathrm{d}a}{\mathrm{d}N}(\Delta K)$ *plot based on the Virkler data* [89]

It is interesting to examine the general shape or trend of the $\frac{\mathrm{d}a}{\mathrm{d}N}(\Delta K)$ curves. To do this, we need the corresponding data. The well known Virkler [89] fatigue data set was used for this purpose. Virkler performed his tests by measuring the number of load cycles N at predetermined crack lengths a on 68 identical central crack tension (CCT) specimens, for which an analytical expression giving the stress intensity factor is known. Virkel took good care to ensure that the test conditions be identical in all of the tests.

First, the crack propagation velocity or the slope of the $N(a)$ curve is determined at each crack length by numerical differentiation. Rather than finding the slope between two consecutive crack lengths, a straight line is fitted through five consecutive pairs of the $[a, N]$ values observed by Virkler. The stress intensity factor at each of the predetermined lengths is calculated using the analytical formula for CCT. The resulting pairs of ΔK and $\frac{\mathrm{d}a}{\mathrm{d}N}$,

connected into lines, are plotted in Fig. 6.1.

Note that the numerical differentiation and the use of the analytical equation both constitute a part of a model that we chose for processing of the fatigue data. The errors of these modelling approaches will be inherent to any results that we will obtain.

It can be seen in Fig. 6.1 that despite the averaging of the slope over five points, as described above, the curves are quite misbehaved. However, one may observe a general exponential trend of the $\frac{\mathrm{d}a}{\mathrm{d}N}(\Delta K)$ function. This is consistent with Paris and Erdogan's [73] choice to model the dependence of the crack growth rate on the stress intensity factor by the exponential form of their law.

It is thereby important to note that the Paris law is a satisfactory model for the Virkler data within Phase II of crack propagation (after crack initiation and before the onset of unstable fracture). As it can be seen in Fig. 6.2, the domain of the crack growth physics into which the Virkler data fall is indeed the linear domain.

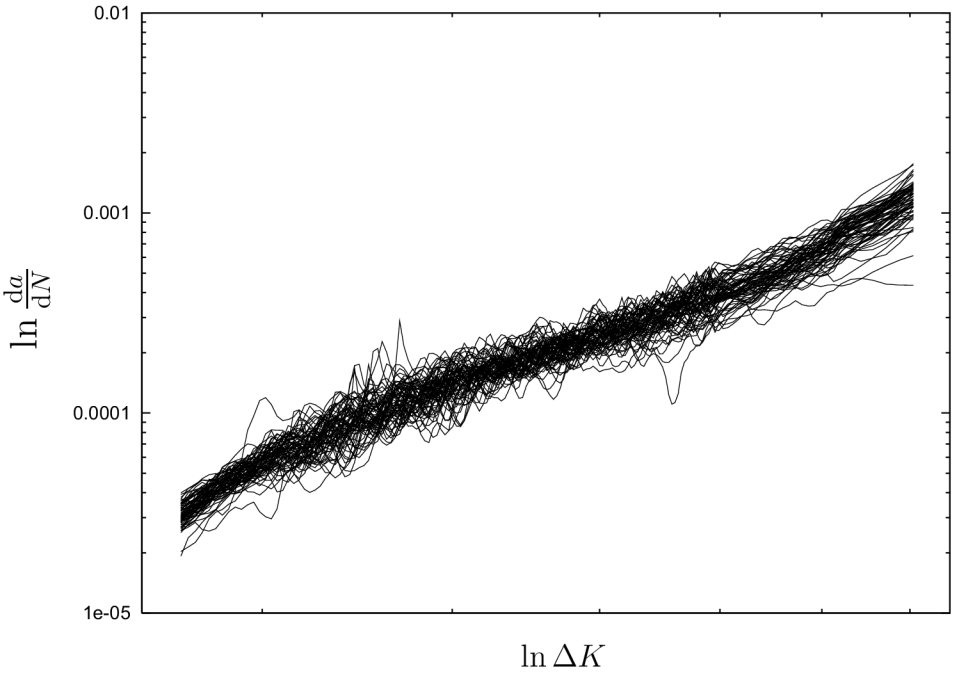

Figure 6.2: *A log-log plot of* $\frac{\mathrm{d}a}{\mathrm{d}N}(\Delta K)$ *based on the Virkler data* [89]

Taking a logarithm of an exponential function, we get a linear relation.

Plotting the same $\frac{\mathrm{d}a}{\mathrm{d}N}(\Delta K)$ data in log-log scales, one gets the picture as in Fig. 6.2. The data points for just a single specimen are shown in Fig. 6.4. The straight line in the latter Figure is the line $\ln \frac{\mathrm{d}a}{\mathrm{d}N} = \ln C + m \ln(\Delta K)$.

Randomisation of the Paris Law

We can now proceed to estimate the parameters C and m of the Paris law, Eq. (6.1). This implies that we consider the parameters to behave as random, a property evidenced by the crack propagation test results.

We will perform the statistical estimation on data obtained by a linear regression on the Paris law using *all points* of the $\frac{\mathrm{d}a}{\mathrm{d}N}(\Delta K)$ curve for the given specimen, determined as described above (averaging over 5 points, use of anlytical formula to calculate K). This will give us a single value of C and a single value of m for the specimen. The Paris law curve $C(\Delta K)^m$ is plotted in Fig. 6.3 using the two values C and m for the respective specimen. The Figure shows also the data points from which the two values were estimated.

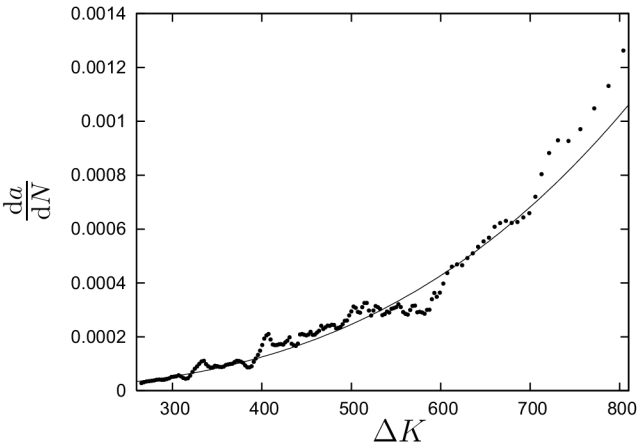

Figure 6.3: *A plot of the* $\frac{\mathrm{d}a}{\mathrm{d}N}(\Delta K)$ *data points and the fitting curve for a single CCT specimen.* [89]

Note that we are thus considering only the average crack growth velocity on the given specimen. The variability of crack growth rate thus determined will therefore account only for variability of the average crack growth rates on the individual specimens. In this approach, we are loosing some of the information contained in the Virkler data, in particular the information on the variability *within* the specimen.

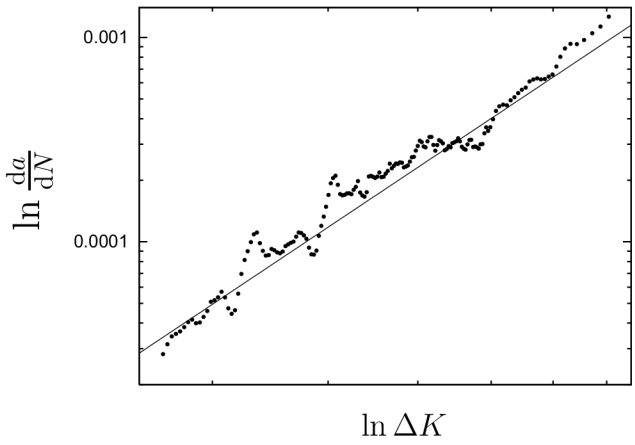

Figure 6.4: *A log-log plot of the* $\frac{\mathrm{d}a}{\mathrm{d}N}(\Delta K)$ *data points and fitting curve for a single CCT specimen.* [89]

To be able to model and estimate this intra-specimen variability, the crack growth within the specimen would need to be viewed as a random process. However, it is a question whether the extra effort in carrying along this richer information pays off in terms of any increased precision of the estimation of the total lifetime of a specimen under propagation of cracks.

Here, we are in fact questioning the accuracy of the Paris crack growth law model. While the exponential model appears feasible, one can see e.g. on the example of the crack growth rate in a single specimen shown in Fig. 6.3 and Fig. 6.4 that the experimental data deviates from the fitted curve. What we are witnessing here is a model error.

A plausible approach to address this model error issue is to explicitely introduce the model error into the model by means of a random variable, like it has been done in Reference [14]. In the context of the overall crack propagation analysis, this additional random variable may capture well enough the discrepancy between the Paris model and the reality, without the necessity to make recourse to random process. Indeed, the results in [14] show that this approach can provide accurate probablility of failure.

6.2.1 Parameter Estimation

Linear Regression

We see that the points in Fig. 6.2 lie roughly on a line. This leads us to estimate the parameters C and m of the Paris law by making a straight line

pass through the points in the log-log scale, see Fig. 6.4. This approach, making possible the use of linear regression, is the natural way any analyst would take to tackle the task, and is thus the common method to estimate C and m of the given specimen.

Before we proceed to the regression analysis, let us make one important comment. Regression coefficients are always correlated. In particular, linear regression consists in solving a linear problem, so a high correlation of the determined coefficients must be expected, no matter what the form of the fitted curve is. The correlation is also bound to increase with the number of regression coefficients decreasing. In the present case, the coefficients to fit are merely two, since we are fitting a straight line $y = ax + b$. Imagine a cloud of points we want to fit the line through. If we change the intercept b, the slope a cannot change independently of b – the line still needs to pass through the cloud of points. The correlation is negative. More concretely, if $\ln C$ increases, m will decease, and vice versa.

The linear regression on $\ln C$ and m to fit the straight line

$$\ln \frac{\mathrm{d}a}{\mathrm{d}N} = \ln C + m \ln (\Delta K) \tag{6.2}$$

through all the points of each single specimen separately gives us 68 pairs of C and m values. The estimators of the sample mean, standard deviation and correlation are listed in Table. 6.1.

	$\ln C$	m
mean	-26.0564	2.8553
standard deviation	0.9302	0.1658
correlation	-0.99795	

Table 6.1: *Estimates of the* $\ln C$*–*m *sample statistics.*

We were prepared to expect a high correlation between $\ln C$ and m, but the correlation coefficient $\rho_{\ln C\, m} = -0.99795$ differs from minus unity by about 2‰ only. Notwithstanding the fact that this correlation is due to the regression method used to estimate $\ln C$ and m, this high correlation motivates us to reduce the number of random variables by one and consider $\ln C$ as a function of m or vice-versa. However, as we will see later, this solution does not yield satisfactory results.

Non-linear Regression

Before we test any such models, let us renounce for a while on the use of the log-log scale in the regression to see what comes out if we perform

a non-linear regression on the equation $\frac{\mathrm{d}a}{\mathrm{d}N} = C\Delta K^m$ to estimate C and m directly, using a numerical minimisation of the least-square error. The

	C	m	$\ln C$ calculated
mean	$9.0401{\cdot}10^{-12}$	2.8560	-26.0329
standard deviation	$1.6657{\cdot}10^{-11}$	0.1672	0.9451
$\rho_{C\,m}$ from non-linear regression	-0.75313		
$\rho_{\ln C\,m}$ calculated		-0.99770	

Table 6.2: *Estimates of the C–m sample statistics.*

estimators of the sample mean, standard deviation and correlation of C and m are listed in Table. 6.2. In addition, the Table gives the estimates for $\ln C$, where $\ln C$ was computed by simply taking the logarithm of the C obtained from the non-linear regression. While the correlation between C and m is only moderate, we can see that the coefficient of correlation between $\ln C$ and m thus estimated does not differ much from the one coming from the linear regression.

Suppressing the Dimensional Dependence

To expore another possible reason for the correlation, we examine also the dimensional dependence between C and m, since, by the Paris law, the units of C depend on those of m. For this purpose, we modify the Paris law as follows

$$\frac{\mathrm{d}a}{\mathrm{d}N} = C'\left(\frac{\Delta K}{(1-R)K_0} - 1\right)^{m'} \quad , \Delta K > (1-R)K_0\,. \tag{6.3}$$

In the above equation, K_0 is a normalising stress intensity factor. It may be for example the threshold value below which there is no crack propagation, which is ensured by subtracting a unity from the ratio $\Delta K/(1-R)K_0$. Note that since ΔK and K_0 have the same dimension, the term $\frac{\Delta K}{(1-R)K_0}$ is a *dimensionless* normalised magnitude of the stress intensity factor. Therefore, the dimension of C' does not change when m' changes. The primes are used on C' and m' to mark their difference from the Paris law constants.

Table. 6.3 shows the estimators of the sample mean, standard deviation and correlation of these primed variables C' and m'. It can be seen that the suppression of the dimensional dependence between $\ln C'$ and m' leads to no significant reduction in the magnitude of the correlation coefficient.

	$\ln C'$	m'
mean	-14.6404	2.5945
standard deviation	0.0959	0.1503
correlation	-0.97993	

Table 6.3: *Estimates of the* $\ln C'$–m' *sample statistics with the dimensional dependence between* $\ln C'$ *and* m' *suppressed.*

It can thus be said that while having parameters with unclear and changing physical dimensions is generally undesirable, the *dimensional dependence* of C and m was shown *not to be the source of the correlation.*

6.2.2 Statistical Models

Distribution Types of C and m

Without presenting detailed hypothesis testing results, it can be said that the parameter m is appropriately modelled as a normal random variable and the parameter C as a lognormal random variable. This holds also for the statistical models of the variables $\ln C'$ and m', the dimensional dependence of which has been suppressed – see above. Figure 6.5 is presented as an

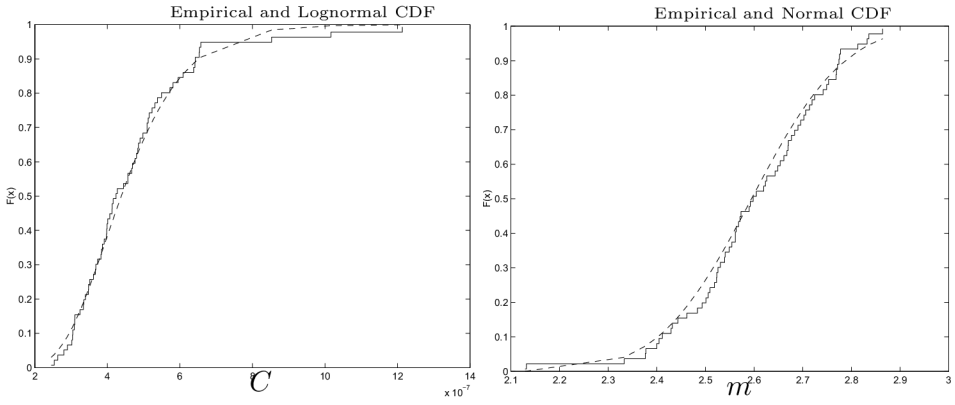

Figure 6.5: *Goodness of fit illustration for lognormal* C *(left) and normal* m *(right).*

illustration of the goodness of fit of lognormal C and normal m.

Thus, in the following, we will consider only statistical models randomising the Paris law that will involve lognormal C and normal m.

Goodness of a Model

Having tried various meaningful approaches to estimate C and m, we can now propose and test various statistic models of the random variables C and m. As the testing criterion, we will take the mean and the scatter of the final fatigue life observed in the original Virkler's tests, listed in Table 6.4.

	mean	standard deviation
total fatigue life	$2.5716{\cdot}10^5$	$1.8447{\cdot}10^4$

Table 6.4: *The sample statistics of fatigue life of the original Virkler tests.*

These reference values will be compared with the statistics of simulated fatigue lives. Each simulated life is obtained by generating a pair of C and m realisations from the underlying statistical model considered and integrating the Paris law from the initial to the final crack length using ΔK values given by an analytical model for the centre crack tension (CCT) specimen. Note that such result involves any error as a discrepancy between the analystical formula and the reality.

Bivariate Normal $\ln C$ and m

First, let's consider a statistical model of a bivariate normal distribution of $\ln C$ and m with the sample statistics and correlation coefficient as indicated in Table 6.1 above.

	mean	standard deviation
total fatigue life	$2.5030{\cdot}10^5$	$1.6101{\cdot}10^4$
error	-2.5%	-12.7%

Table 6.5: *The statistics of fatigue life simulation using a joint normal model for* $\ln C$ *and* m.

Table 6.5 gives the statistics of the simulated lifetime. It can be seen that the model reproduces the observed fatigue lives fairly good in terms of both mean and scatter. A discussion in Section 6.2.3, elaborating on the results of [14], sheds more light on the agreement between the expriment and the reality, showing that it is not quite satisfactory. As a matter of fact, the scatter is underestimated by some 13%. This suggests that by neglecting the intraspecimen error and modelling all of the complex physics of crack propagation within the specimen through the rigour of the Paris formula

allowing only two random parameters, one may perhaps be oversimplifying the reality.

Correlated Lognormal C and Normal m

The next model evaluated here is a statistical model involving a lognormal distribution of C and a normal distribution of m, with the two random variables being correlated. The parameters of these distributions have been estimated in Table 6.2. In particular, the correlation coefficient was -0.75313.

Note that the correlation coefficient of -0.75313 has been estimated from data fitting using a minimisation procedure. It may thus bear some imprecision. In addition, this magnitude of correlation is on the verge of what is numerically attainable when the realisations of the variables are generated as described in Section 4.2.2. As a consequence, the generated realisations of the correlated variables may not be fully correct.

	mean	standard deviation
total fatigue life	$3.0103 \cdot 10^5$	$9.6144 \cdot 10^4$
error	+17.0%	+521.2%

Table 6.6: *The statistics of fatigue life simulation using correlated lognormal C and normal m.*

The statistics of the total fatigue life simulated using the statistical model considered here are shown in Table 6.6. It can be seen that the scatter has dramatically increased. Perhaps, this gross error in the dispersion of the fatigue life is attributable to the inaccuracies in the estimation of sample statistics and in the generation of variables from the correlated distributions. As we will see later, the dispersion of the total fatigue life is extremely sensitive to the correlation coefficient.

m a Function of Normally Distributed $\ln C$

Let us now consider a model that one is tempted to use seeing the extremely high correlation of $\ln C$ and m. Consistently with the bivariate normal model above, a normal distribution is used for $\ln C$, but m is now a linear function of $\ln C$. The mean and standard variation of $\ln C$ are again those listed in Table 6.1.

As it can be seen in Table 6.7, the standard deviation in the total fatigue life simulated using the above statistical model is markedly reduced. Taking

	mean	standard deviation
total fatigue life	$2.4985{\cdot}10^5$	$2.9115{\cdot}10^3$
error	-2.8%	-84.2%

Table 6.7: *The statistics of fatigue life simulation using normal* $\ln C$ *and* m *a linear function of* $\ln C$*.*

a linear function instead of a correlation of -0.99795, the dispersion drops by 85%. This shows an extreme sensitivity to the correlation coefficient.

$\ln C$ a Function of Normally Distributed m

Let us examine the same approach changed-round, with m being the random variable and $\ln C$ the dependent variable. The statistics of the total fatigue life simulated based on this statistical model are given in Table 6.8. The underestimation of the standard deviation is as serious as before.

	mean	standard deviation
total fatigue life	$2.4986{\cdot}10^5$	$3.9139{\cdot}10^3$
error	-2.8%	-78.8%

Table 6.8: *The statistics of fatigue life simulation using normal* m *and* $\ln C$ *a linear function of* m*.*

6.2.3 The Correlation of C and m

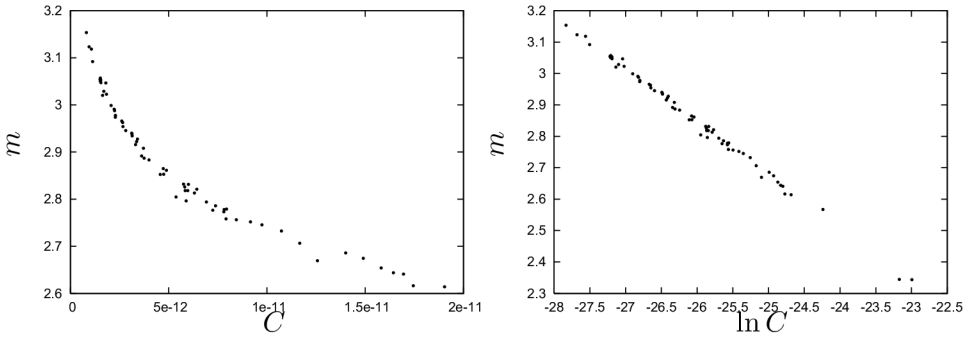

Figure 6.6: *A plot of the* C*–*m *data and the* $\ln C$*–*m *data.*

We have seen that whether we use a linear or a non-linear regression, we observe an extremely high correlation of the estimated $\ln C$ and m. We

have also proven that this is not due to the dimensional dependence. At the same time, the correlation of C and m is only moderate - indeed, the values in the left-hand chart of Fig. 6.6 do not lie on a line.

We were trying to estimate the parameters of a mathematical model that had been put forward as one that can represent well the dependence of the crack growth rate on the range of the stress intensity factor. Empirical data verify the correctness on the model to a certain extent. Note, however, that the two parameters of the model do not have a clear physical interpretation. This make also the interpretation of their correlation difficult.

Most of the correlation is probably attributable to the fact that C and m are obtained by regression as the parameters of the exponential model. C and m are bound together by the virtue of being two parameters of a single exponential curve. However, we have seen that replacing the strong correlation by an explicite linear dependence of m on $\ln C$ leads to a great underestimation of the standard deviation in the simulated fatigue life.

So it appears that the effect of C and m deviating from the relation tying them together is extremely important. As a matter of fact, generating m as a random variable correlated to $\ln C$ results in just a slightly higher standard deviation in m as compared to m tied to a random $\ln C$ by a function. But the crack growth rate given by the Paris law should be expected to be highly sensitive to m, the exponent on the stress intensity factor range. In addition, the effect of this slightly more dispersed m builds up through the integration of the fatigue life over the crack length. This can be a physical interpretation of how the sensitivity of the fatigue life to the correlation of $\ln C$ and m arises – the dispersion is magnified by being in the exponent and through integration.

Model Error and Decorrelation

Bourinet and Lemaire [14] have carried out a detailed study of the Virkler [89] data, proposing an accurate method to calculate sensitivity to correlation and investigating the accuracy of fatigue life prediction with respect to the real experiment.

From their analysis, it appeared that a simulation employing the model, which involved a statistical model of bivariate normal m and $\ln C$ and a use of the Paris carck growth law together with an anlytical formula for the stress intensity factor to calculate fatigue life, misclassified seven of the specimens that actually survived as specimens failing, and misclassified one actually surviving specimen as failed. The line between the safe and the failure domain was thereby drawn between the experimental specimens

having the 7^{th} and 8^{th} shortest life, respectively.

The authors turned their interest to the difference between the fatigue life prediction through the simulation model and the actual fatigue life in the experiment. This difference was then explicitely introduced into the simulation model as a random variable. With this, the previously misclassified experiments were already correcly placed within the safe and the failure domain, and the probability of failure corresponded very well to the experimental data. Although it can be argued that the bias of the model is perhaps more systematic than random, the correct classification of all of the experimental specimens as failed or surviving by the simulation proves the feasibility of this apprach.

We have seen above that a statistical model having only one random variable and the other one functinally related results in a gross underestimation of the scatter. To overcome this problem and to avoid the extreme sensitivity to the correlation at the same time, the authors took the following approach. Instead of considering $\ln C$ as a random variable, they chose a model which considers only the difference between the value of $\ln C$ and the expectation $E[\ln C|m]$ on $\ln C$ coming from regresion analysis. This difference, denoted $\varepsilon_{\ln C}$, thus became uncorrelated to m. The sensitivity to the correlation of $\varepsilon_{\ln C}$ and m was close to zero.

6.3 Crack Initiation

The physical mechanisms behind the initiation and the propagation of cracks were described in Section 2.2.1. Crack initiation could thus be defined as the occurrence of a crack that grows already by the mechanisms present in the crack propagation phase.

For the purposes of our crack propagation simulation, we will assume that crack initiation has already taken place at known or supposed locations and the existing cracks have such sizes that they already follow the Paris law. The size of the crack at a given instant or the time at which a crack will attain a given size is uncertain.

We will therefore not engage into any phenomenological or damage accumulation based modelling of crack initiation. We will instead treat crack initiation statistically.

There are basically two approaches to statistical modelling of crack initiation. Either, one can consider a random number of load cycles to the initiation of a crack of a given size. Or the crack length at a given time is taken as random.

The latter approach is retained in this thesis. The reason is that it finds application in Bayesian updating of the crack length based on inspection results.

In this thesis, no such relation to actual inspection data is made. The parameters of the statistical distribution of the initial crack length are simply assumed. This is undoubtedly a shortcoming when one attempts to present a complex crack propagation modelling approach. However, the focus of the thesis is on the propagation phase. Bayesian updating of the crack length has been described abundantly in the literature, in particular in the context of inspection planning [55], [56], [43].

Random initial crack lengths are often modelled by exponential or log-normal distributions.

6.4 Failure Model

In Section 2.4, we have defined for the purposes of this thesis the physical failure as the state when the value of the stress intensity factor characterising the stress field around the tip of the crack reaches the fracture toughness.

Ductile structures may also fail by plastic collapse. The ligament to which the grown cracks have reduced the material resisting the load may plastify completely and fail. When the two failure modes, i.e. fracture and plastic failure, compete, the so called R6 criterion [44] may be used.

However, empirical computational experience has shown that for the type of problems considered here, the fracture failure mode almost always prevails. Therefore, we will simply compare the stress intensity factor to the fracture toughness to see whether *structural failure* has yet occurred:

$$\text{structural failure if} \quad K_{eq} \geq K_{Ic}\,. \tag{6.4}$$

In the above equation, K_{Ic} is the Mode I fracture toughness of the material and K_{eq} is the Mode I-equivalent stress intensity factor that will be defined in Chapter 7.

Eq. (6.4) defines the event of structural failure. In our crack propagation problem, *failure for the purposes of reliability analysis* will be defined to occur if Eq. (6.4) becomes satisfied at a sustained crack propagation life N_R that is less than the required life under crack propagation N_S:

$$\text{reliability failure if} \quad N_R \leq N_S\,. \tag{6.5}$$

The life will be measured in load cycles. Other units could be used, including duty-cycles or number of aircraft flights. This thesis relies on the use of

characteristic load sequences specified for structures or machines of a given type to capture the complexity of loading. These are essentially sequences of peak and valleys, i.e. of load cycles with varying amplitude. Moreover, in reliability analysis with approximation methods, it is desirable that the response be a continuous variable rather than a discrete one. Therefore, we will measure life under crack propagation in cycles within the given load sequence rather than in multiples of the load sequences.

The reliability analysis works with the failure criterion rewritten as the performance function. Based on equation (6.5), we will define the performance function as follows:

$$G(\mathbf{x}) = \log \frac{N_R}{N_S}\,, \tag{6.6}$$

where $\mathbf{x}$ is the vector of random variables. The logarithmic form of the performance function was chosen for its advantages in optimisation numerics. It is preferable that the value of the performance function is a small rather than large number.

6.5 Reliability Methods Used

Load carrying engineering structures are required to have very low probabilities of failure. We thus need a reliability method that is capable of dealing with low-probability events.

In Chapter 4, we have seen that we can essentially choose between two major reliability analysis approaches: approximation methods or Monte Carlo simulation (MCS). To analyse low-probability failure events, MCS requires a large number of simulations. With growing number of simulations, there will be more samples of the random variables taken from the tails of their respective distributions. In Section 5.1.7, we have raised the issue of low-probability structural configurations. These require a particularly robust mechanical model, capable of calculating the response of configurations that are far from the usual features of the problem.

For these reasons, the approximations methods are used in this thesis. By applying the First Order Reliability Method (FORM), we will also take advantage of the straightforward computation of sensitivities of the reliability index within the method, see Section 4.3.

FORM appears appropriate for the present problem of crack propagation life. We will see that the solution algorithm converges. It also appears that we are dealing with a single design point only.

To evaluate some of the derivatives of the response needed at each step of the design point search, we will apply the sensitivity equations derived by direct differentiation in Sections 7.4.1 through 7.4.4. The remaining derivatives will be computed by the forward finite difference method.

6.6 Conclusions

The statistical analysis of the crack propagation data in Section 6.2 exposed the importance of correct statistical modelling of the random variables. Unjustified assumptions introduced in the statistical model may lead to a gross error in the response of the model.

It was shown that for the parameters of the Paris law, the bivariate normal model of $\ln C$ and m allows for a reproduction of the crack propagation data based on which the statistics of the parameters were estimated. The extremely high correlation of the two variables is mostly due to obtaining the $\ln C$–m couples as the parameters of the exponential Paris model by regression on the $\frac{da}{dN}(\Delta K)$ data. In addition, the life under fatigue crack propagation is extremely sensitive to the value of the correlation coefficient. This is due to a magnification of the amount of dispersion of the parameters by m being in the *exponent* of the Paris law and by integration.

In contrast to the careful statistical analysis of the crack propagation data, the crack initiation model was only assumed, using an exponential model for the initial crack size, which is a common approach. This model allows for Bayesian updating based on actual inspection results, but this procedure is not carried out within the scope of this thesis.

A simple failure model is used. The "resistance" is the total life under crack propagation N_R, which ends when the stress intensity factor attains fracture toughness. The "load" is then the required life N_S.

Approximation methods will be used in reliability analysis because they do not require the mechanical model to provide response for low-probability structural configurations and allow for a straightforward computation of sensitivities of the reliability index.

Chapter 7

Crack Propagation Procedure

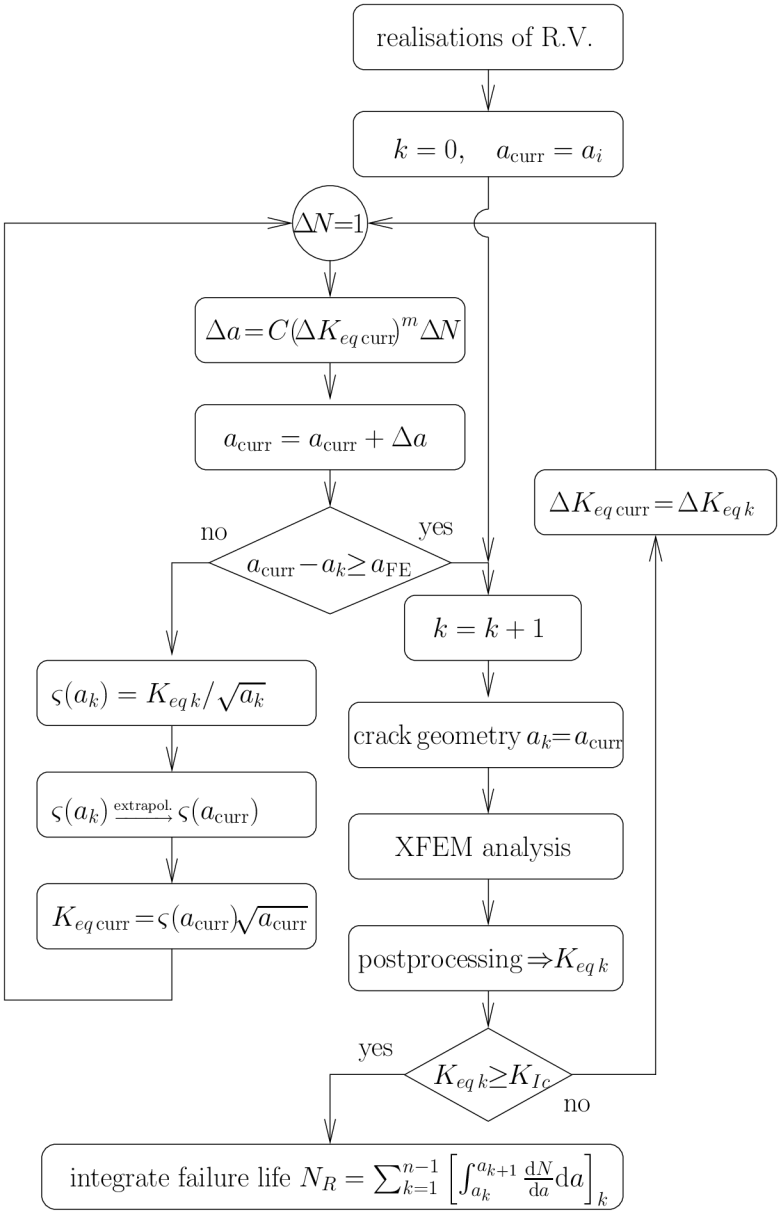

Figure 7.1: *The crack propagation simulation procedure*

7.1 Introduction

This Chapter describes the crack propagation procedure developed based on the strategies put forward in Chapter 5. This procedure is used to calculate the total life N_R under fatigue crack propagation. The value of N_R enters the performance function (6.6) in the reliability analysis.

The crack propagation procedure consists of three phases:

1. Load sequence preprocessing by PREFFAS.
2. Simulation of crack propagation as the multiple cracks follow their paths. The propagation velocity is governed by the Paris law, the direction by the maximal hoop stress criterion, Eq. (2.31). The stress intensity factors are regularly updated by solving the numerical mechanical model with the current geometry.
3. Fatigue propagation life integration.

The PREFFAS method has been described in Section 2.6. The crack propagation simulation and fatigue life integration procedures are described below.

7.2 Simulation of Propagation of Multiple Cracks

The lifetime under fatigue crack propagation N_R entering the performance function (Eq. (6.6)) is obtained by a numerical simulation of crack propagation involving structural analyses by the Extended Finite Element Method (XFEM) to compute the stress intensity factors (SIF).

The following assumptions are made. The cracks, which can be several, propagate in a linear elastic, isotropic, homogeneous body idealised as a two-dimensional plate. The propagation takes place in the plane of the plate under mixed mode conditions, and may thus be curvilinear. In the modelling, the curvilinear crack trajectory is replaced by a piece-wise linear shape. The plate may have an arbitrary geometry, including various openings in it.

All sequence and overload effects are assumed to have been accounted for through the PREFFAS method. Thus, it suffices to use a linear-elastic mechanical model describing a quasi-static crack propagation under constant-amplitude loading.

Given that the crack growth rate is modelled by the Paris law, N_R is obtained as:

$$N_R = \int_{a_i}^{a_f} \frac{1}{C\left[(1-R)K_{eq}\right]^m} \mathrm{d}a\,. \tag{7.1}$$

C and m are the parameters of the Paris law and R the stress ratio. The term $1/C\left[(1-R)K_{eq}\right]^m$ will be denoted $\frac{\mathrm{d}N}{\mathrm{d}a}$ in the following.

The lower integration limit a_i is of course the initial crack size, an important variable in terms of reliability analysis. The final crack length a_f is defined as the crack length at which the equivalent Mode I stress intensity factor K_{eq} [15] attains the fracture toughness K_{Ic}:

$$K_{Ic} = K_{eq} \equiv K_I \cos^3\frac{\theta}{2} - 3K_{II}\cos^2\frac{\theta}{2}\sin\frac{\theta}{2}, \tag{7.2}$$

where K_I and K_{II} are the Mode I and Mode II stress intensity factors, respectively, and θ is the crack propagation angle determined based on the maximal circumferential stress criterion, see Eq. (2.31).

If multiple cracks are present, N_R corresponds to the lifetime when the criterion 6.5 is first fulfilled at the tip of any of the cracks.

7.2.1 The Simulation Procedure

As there may be multiple mutually interfering cracks, each of which propagates with a different rate governed by the intensity of the stress field around its tip, it is not *a priori known* at which crack the critical stress intensity K_{Ic} will be attained first and at which crack length a_f this will happen.

This precludes a prior discretisation of the integration domain between a_i and a_f and requires that **the actual evolution of the cracks and the stress intensity factors at their tips be tracked along the loading history**.

Using the random variable approach (see Section 2.8.1), the crack propagation smulation procedure starts from a set of current realisation of the random variables, cf. Fig. 7.1 on page 108. With these variable values, including those determining the crack lengths, a first numerical mechanical analysis by XFEM is carried out to establish the stress field and the correspoding crack tip stress intensities and crack propagation directions at the beginning of the crack propagation history.

The cracks are then assumed to propagate obeying to the Paris law. The Paris equation is the central node of the crack propagation procedure (Fig. 7.1) and determines the crack length increment:

$$\Delta a = C\left(\Delta K_{eq}\right)^m \Delta N = C\left[(1-R)K_{eq}\right]^m \Delta N \tag{7.3}$$

The load cycle increment ΔN is taken equal to a single cycle: $\Delta N = 1$. Where the crack increment per cycle is negligeble, the load cycle increment

can be taken as different number given by a convenient function of the current inverse crack propagation rate $\frac{\mathrm{d}N}{\mathrm{d}a}$.

The length of each crack i has now grown by an increment of Δa_i. We could go back to the numerical mechanical model and update the stress filed. However, it would be inefficient and could lead to numerical problems in XFEM to calculate K_{eq} by a numerical analysis at very similar crack lengths after each load cycle (increment). Therefore, SIF are obtained by XFEM post-processing only every time an increment of the length of any of the cracks exceeds a predetermined user-defined value of Δa_{FE}. This is chosen with due consideration of the mesh size. For numerical stability in XFEM, the crack tip should advance beyond the area of a single finite element.

At intermediate crack lengths, K_{eq} is extrapolated from previous values, cf. Figure 7.1. The extrapolation is carried out as follows. It is assumed that the equivalent stress intensity factor for each crack can be as a linear function of the square root of the crack length a:

$$K_{eq} = \varsigma\sqrt{a} \tag{7.4}$$

The linear factor ς here accounts for all load and geometry effects, safe for the crack length itself. Separating out ς from (7.4), we can calculate it for two previous XFEM update points a_k and a_{k-1}, and extrapolate it based on the crack lenthts a_k and a_{k-1} to the current crack length a_{curr}. K_{eq} at the current crack length a_{curr} is obtained by simply inserting the extrapolated ς and the current a_{curr} into equation (7.4).

Linear extrapolation usually suffices. In case that numerical noise would occur and one of the last update points would be lying somewhat off the $K_{eq}(a)$ curve, higher order extrapolation could amplify the extrapolation error. It is important to note that the extrapolation is used only to determine the discretisation and approximate trajectory of the crack between a_i and a_f for integration purposes. K_{eq} entering Eq. (7.3) is obtained from XFEM analysis.

At the XFEM update point, the crack direction may change, being determined from Eq. (2.31).

The criterion (7.2) is checked at every load cycle of the above procedure. When it becomes fulfilled, the procedure is continued until Δa is attained by the increment of any of the cracks, and then stopped. Thus, we have available additional numerical analysis results for a point beyond the failure point. We will see in Section 7.3 how this will be useful.

The simulation procedure is thus very simple. We increment the length of each crack by Δa_i based on the Paris law and the load cycle incrememt

ΔN. Then we update the stress intensity factors by either XFEM or exptrapolation, and recycle to increment the crack lengths. When updating by XFEM, new crack propagation direction is determined. This is repeated until the toughness value is attained by the stress intensity factor ant any of the crack tips.

7.2.2 Simulation Output

As an output of the simulation, we have for each crack a set of n pairs of equivalent stress intensity factors K_{eq} and crack lengths a, at which the K_{eq} were calculated by XFEM.

The final point of crack propagation is determined for the leading crack (at which the failure actually occurred) by interpolating between the last few points of the $K_{eq}(a)$ history to obtain a_f at which the value K_{Ic} was actually attained. For the trailing cracks, K_{eq} is not yet equal to K_{Ic} at the instant of failure at the leading crack. Therefore, for each crack, say the j-th crack, a quadratic least-square fit of the curve $a_j\,(a_{cr})$ is constructed, expressing the relation between the length of the j-th crack a_j and the leading crack length a_{cr}. a_f for the j-th crack can then be calculated by interpolation using the value of a_f obtained for the leading crack.

By the Paris law, K_{eq} are easily converted to $\frac{\mathrm{d}N}{\mathrm{d}a}$. We thus obtain the discrete points of the $\frac{\mathrm{d}N}{\mathrm{d}a}(a)$ curve. Integrating this curve, we can calculate the life under crack propagation.

7.2.3 Numerical Aspects

While crack propagation has been successfully modelled using XFEM, an application of this numerical model in a probabilistic analysis is a novel approach. XFEM has effectively eliminated tedious remeshing to update the crack length as well as some numerical noise due to changing mesh. However, certain recommendations specific to XFEM need to be kept in mind.

In particular, the time stepping in the calculation of SIF should be such that the crack tip in the next step along the crack line polygon should lie within another element, otherwise numerical issues arise. Considering the algorithm described above, special care needs to be taken in this respect in problems with multiple crack where some cracks may propagate faster than others.

A second remark concerns the interaction between the crack line and the mesh. Remember that in XFEM, cracks can pass arbitrarily across the

elements. If the angle between the crack and an element edge is very acute, extremely pointed integration triangles are created, which leads to numerical problems that may affect the accuracy of calculation of the SIF.

This issue may be circumvented by choosing the integration zone for SIF computation (cf. Section 3.7.4) further away from the crack tip. Experience has shown that the SIF values calculated by integrating in a band made up from the third row of elements around the crack tip were less than 2% lower than the SIF integrated over the second row of elements. This is considered a fully acceptable trade-off in the interest of better stability of the results.

Elimination of Noisy Values

Any possible outlying points on the $\frac{\mathrm{d}N}{\mathrm{d}a}(a)$ curve can result in a grossly incorrect integration result. In XFEM, such outlier points were observed only in cases of the acute angles of element edge–crack trajectory intersections mentioned above. With wider SIF integration bands, the $\frac{\mathrm{d}N}{\mathrm{d}a}(a)$ curve was quite smooth.

In general, if such outlier points occur due to numerical problems arising in any numerical methods used to calculate the structural response, it might be a good idea to use the integration based on curve fitting as proposed in Section 7.3 below, instead of a classical quadrature rule. In addition, the following procedure was tested and proved efficient in eliminating the outlier points.

Outliers are first considered with respect to the curve $K_{eq}(a)$. In the first step, the monotonous increase of K_{eq} with growing a is checked. In general, K_{eq} may also drop with increasing a, but in many problems, K_{eq} can be assumed monotonously rising as the crack propagates. If this is the case, all points at which K_{eq} is lower than at the previous crack length should be removed.

Next, it is checked whether the first and last of the discrete $\frac{\mathrm{d}N}{\mathrm{d}a}$ values are outliers. The reference value is taken as the value of life time under fatigue crack propagation evaluated numerically using the formula (7.5) with the actual initial and final crack size as the integration bounds, but considering only the internal discrete points of the $\frac{\mathrm{d}N}{\mathrm{d}a}$ history. If, after evaluating the formula (7.5) considering also the first and the last point of the $\frac{\mathrm{d}N}{\mathrm{d}a}$ history, respectively, the value of the integrated life time changes by more than 1% with respect to the reference value, the respective extreme point is rejected as an outlier.

Finally, the internal points are checked for outlying. As a reference value, the life time is integrated using all of the $\frac{\mathrm{d}N}{\mathrm{d}a}$ points not removed so far, using

a quadrature whereby a second order Lagrange interpolation polynomial is passed through three consecutive points. The integration with Lagrange interpolation is then repeated with one of the internal points removed at a time. If the resulting life time differs by more than 1% from the above reference value, the respective extreme point is rejected as an outlier.

Note that "jackknife" resampling statistics of the integral in (7.5) appeared to be powerless in removing the outliers in this application.

7.3 Fatigue Propagation Life Integration

For each crack, we have n discrete points of the $\frac{\mathrm{d}N}{\mathrm{d}a}(a)$ curve available from the simulation described above. An accurate integration of this curve is needed to obtain accurate values of the limit state function and the gradients. A failure to integrate accurately may hamper the convergence to the design point in the reliability approximation methods.

Note that the intervals of discretisation of each crack are in general not of uniform length. This is because the discretisation points (at which K_{eq} was calculated) are set at times when the length increment of the leading crack reaches Δa_{FE}, while different cracks may be leading at different times.

The integration of (7.1) is carried out interval by interval, i.e.:

$$N_R = \sum_{k=1}^{n} \left[\int_{a_k}^{a_{k+1}} \frac{\mathrm{d}N}{\mathrm{d}a} \right]_k \tag{7.5}$$

where a_k and a_{k+1} are the lower and upper limit of the k-th interval, respectively. In the last interval, the upper limit $a_n = a_f$, where a_f is obtained for the loading and trailing cracks, respectively, as described above.

To integrate the fatigue life from the discrete, non-equidistant $\frac{\mathrm{d}N}{\mathrm{d}a}$ points, we need an accurate integration procedure. We could use an integration quadrature or fit a curve to the discrete points.

A quadrature rule can be constructed as follows. A second-order Lagrange polynomial is passed through the three points of two neighbouring intervals between x_{i-1} and x_{i+1}. The integral over the two intervals reads:

$$I = \sum_{j=i-1}^{i+1} y_j \int_{x_{i-1}}^{x_{i+1}} L_j \, \mathrm{d}a \,, \tag{7.6}$$

where L_j is the second-order Lagrange polynomial for x_j:

$$L_{j=i-1} = \frac{(x - x_j)\,(x - x_{j+1})}{(x_{j-1} - x_j)\,(x_{j-1} - x_{j+1})}\,,$$
$$L_{j=i} = \frac{(x - x_{j-1})\,(x - x_{j+1})}{(x_j - x_{j-1})\,(x_j - x_{j+1})}\,,$$
$$L_{j=i+1} = \frac{(x - x_{j-1})\,(x - x_j)}{(x_{j+1} - x_j)\,(x_{j+1} - x_{j-1})}\,. \tag{7.7}$$

The integral of $L(j)$ is easily found. Note that this integration scheme for non-equidistant intervals corresponds to the Simpson formula for equidistant intervals.

If one of the point y_j deviates from the general trend due to numerical error, the above quadrature scheme will yield an erroneous value of the integral over the intervals in question. It appears judicious to take into account the information also from the neighbouring interval.

Rather than making a Lagrange polynomial pass through the points, we shall fit a curve of a suitable form through all of the points considered. The equation of this curve can be integrated analytically.

In the current application, we deal with the $\frac{\mathrm{d}N}{\mathrm{d}a}$ curve. Considering its relation to the underlying variables, we will fit the integrand of (7.5) using the following form:

$$\frac{\mathrm{d}N}{\mathrm{d}a} = \alpha_1 a^{-2/m} + \alpha_2 a^2 + \alpha_3 a + \alpha_4\,. \tag{7.8}$$

The coefficients α_1 to α_4 are fit in the least square sense to the discrete points of the curve. Using four points of the discrete $\frac{\mathrm{d}N}{\mathrm{d}a}(a)$ history that lie the closest to the k-th interval lead to an integration scheme that was both accurate and stable.

7.4 Calculation of Sensitivities

We have seen in Section 7.3 that the total life under fatigue crack propagation, entering the performance function of the reliability analysis, is calculated by integrating the inverse crack propagation rate $\frac{\mathrm{d}N}{\mathrm{d}a}$ from the initial to the final crack length. While the $\frac{\mathrm{d}N}{\mathrm{d}a}$ values are derived from finite element results, the integration is a procedure independent of the numerical solution method.

The classical Direct Differentiation Method [39] deals with the calculation of derivatives of finite element responses. But in the crack propagation

context, the fact that the fatigue life is calculated by integration over the finite element results makes the computational procedure particularly suitable for an easy application of direct differentiation.

In Sections 7.4.1 through 7.4.4, the integral equation (7.1) giving the life under fatigue crack propagation is differentiated with respect to various variables entering the equation to provide explicite formulæ for the calculation of sensitivities of the fatigue life. In some cases, the derived sensitivity equations are very simple.

In the stochastic crack propagation analysis procedure developed in this thesis, these sensitivity equations are advantageously used to improve the speed, accuracy and stability in the reliability approximation method. Where the fatigue life integral cannot be directly differentiated with respect to a particular variable, or where the variable is a function of the numerical model response, the respective sensitivity is calculated by the forward finite difference method.

We are thus mixing two approaches to calculate sensitivities: direct differentiation and finite differences. However, it is probably better to be accurate where possible, rather than to be consistently inaccurate. To this point, it can be noted that one is inevitably inconsistent also when calculating the derivatives purely by finite differences. This is because the step forward, taken to calculate the difference, can hardly be chosen consistently for all variables given the varying units and statistics of the variables in the physical space. As a matter of fact, the calculation of derivatives through direct differentiation is consistent with the way the response itself is calculated.

By using the direct differentiation formulæ, the reliability approximation method becomes faster and more stable.

7.4.1 Sensitivities in the Paris Equation

Assuming that the fatigue crack propagation obeys the Paris law, see equation (2.13), the number of cycles at failure N_R is evaluated from the Eq. (7.1), which is shown also here for convenience:

$$N_R = \int_{a_0}^{a_f} \frac{1}{C\left[(1-R)K_{eq}\right]^m} da \tag{7.9}$$

In the above equation, C and m are the Paris law parameters for the given material, a_0 is the initial crack length from which the propagation is considered to start, a_f is the crack length at failure, R is the minimal to maximal stress ratio and K_{eq} is the Mode I-equivalent stress intensity factor (SIF).

In general, K_{eq} could be the effective SIF, considering the plasticity at the crack tip to account for retardation (see Sec. 2.6). However, we will assume in the following that K_{eq} is a function of nothing else but the crack length, the remote applied stress and geometry.

In this Chapter, we will consider the sensitivities of N_R which can be obtained by differentiating the above Eq. 7.9 with respect to the parameter of interest. These parameters include, with the notation introduced above, a_0 (Sec. 7.4.2), C, m, R and the remotely applied stress σ_{app} (Sec. 7.4.3).

7.4.2 Sensitivity to Initial Crack Length

The initial crack length a_0 appears to be one of the most critical factors influencing N_R. In practical problems, a_0 may be uncertain, given that it comes from measurements with uncertain accuracy and that some of the existing cracks may be overlooked in the inspection. This leads us to consider a_0 as random. Consequently, the sensitivity with respect to the initial crack length $\frac{\partial N_R}{\partial a_0}$ is of major interest for reliability analysis.

In line with the procedure described in Section 7.2, the number of load cycles at failure N_R is obtained by summing up the cycles numerically integrated on each of the intervals $1 \dots k \dots n$ along the crack length:

$$N_R = \sum_{k=1}^{n} \left[\int_{a_{k-1}}^{a_k} \frac{1}{C(\Delta K)^m} \, \mathrm{d}a \right]_k \quad \text{or } N_k = N_{k-1} + \int_{a_{k-1}}^{a_k} \frac{1}{C(\Delta K)^m} \, \mathrm{d}a \tag{7.10}$$

where the shorthand notation $\Delta K = (1 - R)K_{eq}$ has been used. Note that $a_{k-1} = a_0$ on the first interval and $a_k = a_f$ on the last interval.

In the same spirit, the derivative $\frac{\partial N_R}{\partial a_0}$ can be expanded it by the chain rule:

$$\frac{\partial N_R}{\partial a_0} = \frac{\partial N_R}{\partial N_{n-1}} \cdots \frac{\partial N_{n-k}}{\partial N_{n-k-1}} \cdots \frac{\partial N_1}{\partial a_0} \tag{7.11}$$

Since the fatigue life over a single interval $I_k = (N_k - N_{k-1})$ is an integral quantity, $\frac{\partial I_k}{\partial a_{k-1}}$ is a derivative of an integral functional with respect to the lower integration limit. Consider a general case of an integral with respect to t that is a function of another variable x and has variable integration limits $a(x)$ and $b(x)$:

$$y(x) = \int_{a(x)}^{b(x)} f(x, t) \, \mathrm{d}t \, . \tag{7.12}$$

A derivative of such integral with respect to x is given by [6]:

$$\frac{\partial y(x)}{\partial x} = \frac{\partial b(x)}{\partial x} f(x, b(x)) - \frac{\partial a(x)}{\partial x} f(x, a(x)) + \int_{a(x)}^{b(x)} \frac{\partial f(x,t)}{\partial x} \, \mathrm{d}t \,. \quad (7.13)$$

Applying this result to the integral of N_i, we have:

$$\begin{aligned} \frac{\partial I_k}{\partial a_{k-1}} &= \frac{\partial}{\partial a_{k-1}} \left[\int_{a_{k-1}}^{a_k} \frac{1}{C(\Delta K)^m} \, \mathrm{d}a \right] \\ &= \frac{\partial a_k}{\partial a_{k-1}} \frac{1}{C\left(\Delta K(a_k)\right)^m} - \frac{\partial a_{k-1}}{\partial a_{k-1}} \frac{1}{C\left(\Delta K(a_{k-1})\right)^m} \\ &+ \int_{a_{k-1}}^{a_k} \frac{\partial}{\partial a_{k-1}} \left(\frac{1}{C(\Delta K)^m} \right) \mathrm{d}a \end{aligned} \quad (7.14)$$

At this point, we make an important assumption. This assumption is that neither the path of the crack nor the final crack length a_f depend on the initial crack length a_0. In a structure with a single crack, this is rather obvious. With multiple cracks, the interaction of other cracks could compromise the assumption. However, since we are concerned in differentiation with an infinitesimal change in a_0, the assumption remains valid. It also corresponds to studying the sensitivity to the initial crack length, with everything else unchanged.

Then, we can consider the interval-end crack lengths $a_1 \ldots a_k \ldots a_f$ fixed when differentiating Eq. (7.10), with only a_0 varying (infinitesimally). This has several useful consequences that simplify the calculation.

First, the quantities $I_2 \ldots I_k \ldots I_n$ will not change and thus the derivatives $\frac{\partial N_{n-k}}{\partial N_{n-k-1}}$ in Eq. (7.11) will be equal to one.

Second, the derivative of ΔK in Eq. (7.14) with respect to a_{k-1} is zero. Thus, the last term in Eq. (7.14) vanishes.

And by the same token, $\frac{\partial a_k}{\partial a_{k-1}} = 0$. Thus, all that is left of Eq. (7.14) is the second term:

$$\frac{\partial I_k}{\partial a_{k-1}} = -\frac{1}{C\left(\Delta K(a_{k-1})\right)^m} \,. \quad (7.15)$$

Summarising the above, we obtain the result:

$$\frac{\partial N_R}{\partial a_0} = -\frac{1}{C\left(\Delta K(a_0)\right)^m} \,. \quad (7.16)$$

As a matter of fact, Eq. (7.16) allows to enumerate the sensitivity of N_R to the initial crack as a function of the Paris law parameters and the stress

intensity factor at a_0, even before the crack propagation simulation has started.

The surprisingly simple formula of Eq. (7.16) is due to the above assumption of invariability of crack path and final length. This assumption is equivalent to counting the propagation cycles along the same crack path, but starting a bit later – at the infinitesimally increased initial length.

Verification of the Sensitivity Equation for Initial Crack Length

The sensitivity equation (7.16) is verified here by comparing the results with sensitivities obtained by the forward finite differences (FFD) method. The FFD as a numerical differentiation technique consists in evaluating the response quantity V, in perturbing one input variable x_k at a time by a small step size h_k, in evaluating V at the perturbed point in the space of the input variables $\mathbf{x}_{(k)}$ and obtaining the sensitivity as:

$$\frac{\mathrm{d}V}{\mathrm{d}x_k} = \frac{V(\mathbf{x}_{,k}) - V(\mathbf{x})}{h_k}\,, \quad \mathbf{x}_{(k)} = x_1, \ldots, x_k + h_k, \ldots, x_n \tag{7.17}$$

This numerical evaluation of the sensitivities will inevitably show some dependence on the step size h_k.

The performance of the simple analytical formula in Eq. (7.16) in evaluating the sensitivity w.r.t. the initial crack length was tested on two examples. First, a centre crack tension (CCT) specimen was considered, which has a single crack.

Analytical Mechanical Model For a CCT, an analytical expression providing the stress intensity factor for a given crack length is known. We can thus directly use Eq. (7.9) to calculate the fatigue life, with K_{eq} supplied by the analytical equation. The integral in Eq. (7.9) is evaluated numerically using n integration intervals.

The perturbation of the initial crack length was introduced in one numerical study only to the initial crack length itself, with all other integration interval ends being unchanged w.r.t. the reference configuration. In another study, the positions of all interval ends were augmented by the perturbation, except for the final crack length.

Figure 7.2 shows the calculated FFD sensitivities to the initial crack length as a function of the chosen initial crack length perturbation size. The horizontal line indicates the value calculated by direct differentiation (DDM), while the two sloping lines are the FFD values calculated considering the two integration interval end perturbation approaches described

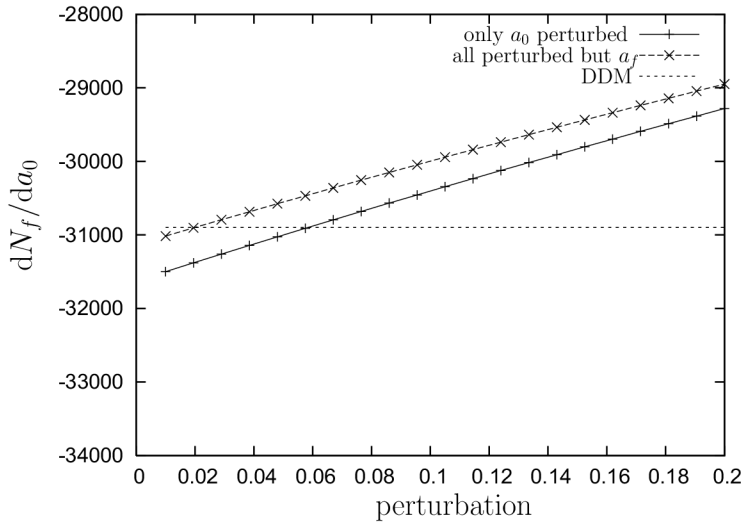

Figure 7.2: *FFD results for sensitivity to initial crack length as a function of the perturbation size.*

above. It can be seen that for small perturbations, the values obtained by FFD and by DDM are similar.

Figure 7.3 illustrates the dependence of the calculated sensitivity on the number of integration intervals, into which the crack length is divided. With the number of intervals increasing, the discrepancy between the direct differentiation value and the finite difference results becomes small. The DDM value thereby appears as the limiting value that the FFD results seem to approach.

Numerical Mechanical Model The above results could encourage us to use Eq. (7.16) indiscriminately for the prediction of sensitivity of fatigue propagation life to the initial crack length. Let us, however, consider a somewhat more complex example, in particular a specimen containing two cracks. Here, the equivalent stress intensity factor K_{eq} entering Eq. (7.9) will be calculated by a numerical mechanical model – the full fatigue propagation life calculation procedure as described in Chapter 7 will be used.

Figure 7.4 shows the evolution of the sensitivities calculated by FFD with the perturbation size for the *leading* crack, i.e. for the crack at the tip of which the stress intensity factor first reached the fracture toughness. This is how failure has been defined.

In the Figure, the FFD values seem to approach the DDM value for

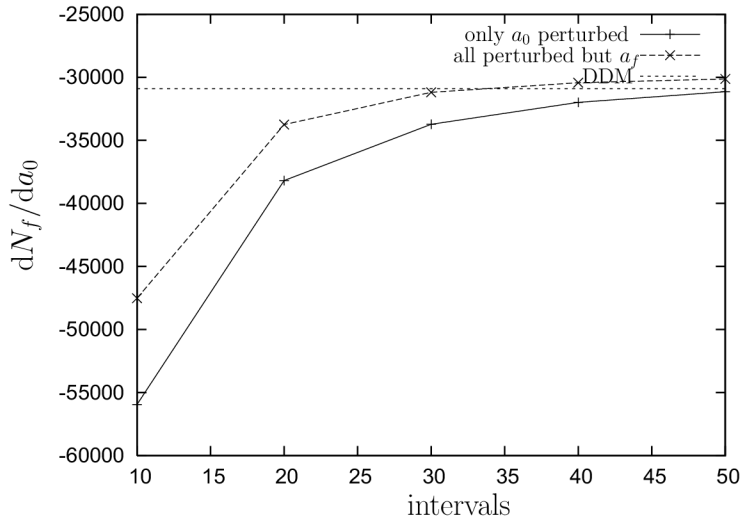

Figure 7.3: *FFD results for sensitivity to initial crack length as a function of the number of integration intervals.*

reasonable sizes of the initial crack length perturbation. The asymptotic line seems to correspond to a weaker sensitivity than the one obtained by direct differentiation. This might suggest that the computation of the sensitivity to the initial crack length by FFD is influenced by and sensitive to the domain discretisation and the errors building up in the integration of the stress intensity factors.

Yet, a discrepancy of about 20% should not incite us to reject the sensitivity equation (7.16) as invalid. It can be seen in the figures referred to previously that the choice of perturbation size and integration step size leads to even higher differences in the sensitivities predicted by FFD.

The picture changes dramatically when the same results are plotted for the *trailing* crack, i.e. the other crack than the one at the tip of which the failure event occurred. The comparison of sensitivity to initial crack length calculated by FFD and by DDM is presented in Figure 7.5.

It can be seen in the Figure that this time the DDM prediction is completely off the range of the FFD results. The reason is clear. We are studying the sensitivity of failure life to the initial length of the trailing crack, but the fatigue propagation lifetime is controlled by the leading crack.

Remember that we made the assumption in deriving the DDM formula for the sensitivity to the initial crack length that neither the path nor the final crack length change. However, the stress intensity factor at tip of the

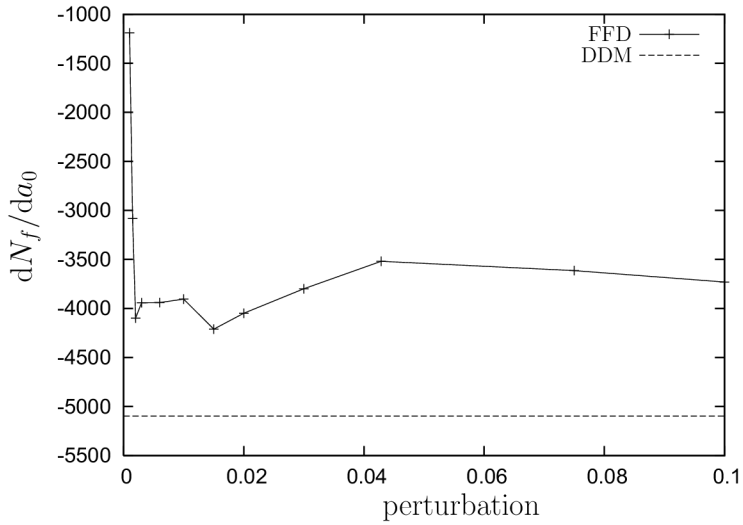

Figure 7.4: *FFD results for sensitivity to initial crack length for the leading crack.*

trailing crack does not reach toughness. Over the propagation lifetime of the leading crack, the trailing crack will thus grow beyond the final length a_f of the reference configuration when the initial length is increased. Thus, the assumption made above is violated.

We observe in Figure 7.5 that the sensitivities calculated by FFD are much weaker than the sensitivity predicted by DDM. In fact, we are studying here an influence of the initial length of a crack on a failure event that occurred somewhere else in the structure. The sensitivity of this failure event to the initial length of the trailing crack considered must as a matter of fact be expected to be much lower than in a case where failure would actually occur at this crack.

Limited Applicability of the Sensitivity Equation It can be concluded that the applicability of Eq. (7.16) to compute the sensitivity to the initial crack length is limited to the leading crack. In complex structural configurations, it is difficult to predict which crack will in fact be leading. But once the crack propagation simulation has been carried through, it is known which crack is the leading one. Sensitivity of fatigue propagation lifetime to the initial length of this crack can be computed using Eq. (7.16), while the sensitivities to the initial lengths of all remaining cracks need to be evaluated by a finite difference calculation.

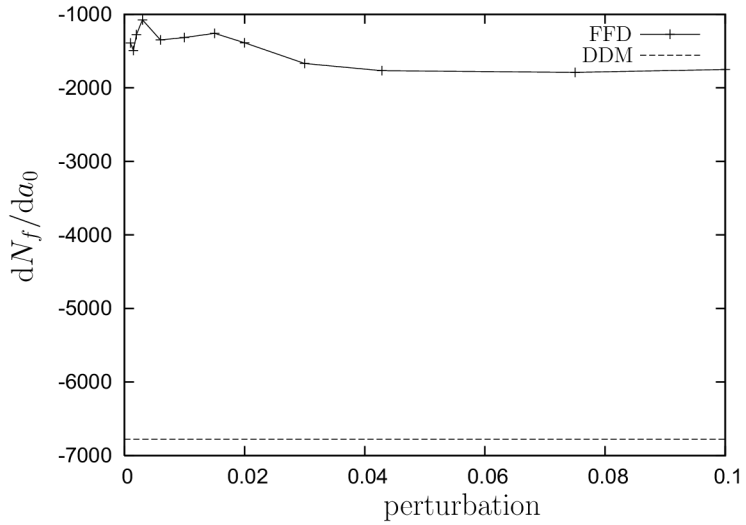

Figure 7.5: *FFD results for sensitivity to initial crack length for the trailing crack.*

7.4.3 Sensitivity to Paris Law Parameters, the Applied Stress and the Stress Ratio

Eq. (7.9) can also be differentiated w.r.t. the Paris law parameters C and m, the remote applied stress σ_{app} and the stress ratio R. Recall that the calculated fatigue propagation life N_R is composed of contributions from individual intervals over the crack length, evaluated from Eq. (7.10). The propagation life on a single interval k is:

$$I_k = \int_{a_{k-1}}^{a_k} \frac{1}{C\left[(1-R)K_{eq}\right]^m}\,\mathrm{d}a \tag{7.18}$$

Consistently with the propagation simulation procedure described in Section 7.2, the term $1/C\left[(1-R)K_{eq}\right]^m$ is considered to be given by a formula, which is a suitable function of the crack length a, the coefficients of which are fit by the least squares method to finite element results for K_{eq}. Recall that the curve fitting formula Eq. (7.8) used to integrate Eq. (7.18) is:

$$\frac{1}{C\left[(1-R)K_{eq}\right]^m} = \frac{\mathrm{d}N}{\mathrm{d}a} \approx \alpha_1 a^{-2/m} + \alpha_2 a^2 + \alpha_3 a + \alpha_4\,, \tag{7.19}$$

Invoking the rule of differentiation under the integral sign when the limits

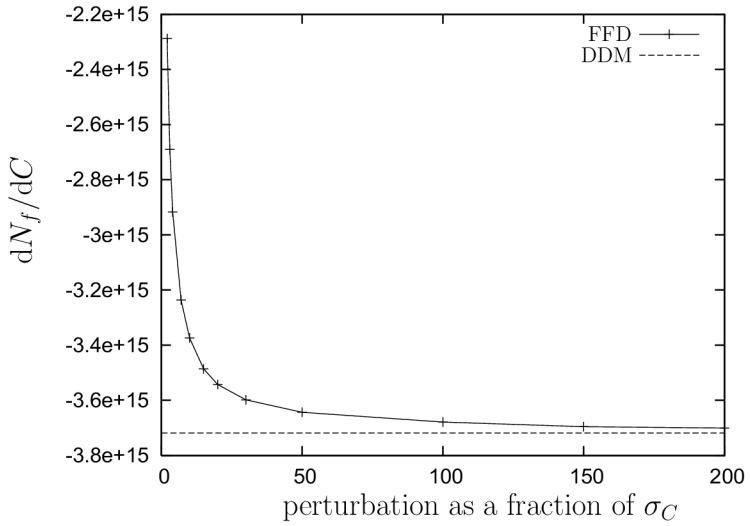

Figure 7.6: *FFD results for sensitivity to the Paris law multiplier C.*

are not functions of x:

$$\frac{\partial}{\partial x}\int_a^b f(x)\,\mathrm{d}x = \int_a^b \frac{\partial f(x)}{\partial x}\,\mathrm{d}x\,, \tag{7.20}$$

we see that the derivatives of N_R (Eq. (7.10)) will also be composed of contributions from individual intervals. When we use Eq. (7.20) to differentiate Eq. (7.18), we obtain for the sensitivity to C:

$$\frac{\partial I_k}{\partial C} = \int_{a_{k-1}}^{a_k} = -\frac{1}{C^2\left[(1-R)K_{eq}\right]^m}\,\mathrm{d}a = -\frac{1}{C}\,I_k \tag{7.21}$$

Thus, once the fatigue life has been integrated, the its sensitivity with respect to C is obtained very simply using the above Eq. (7.21) without any additional integration being necessary.

Differentiating Eq. (7.18) with respect to m, the resulting sensitivity formula reads:

$$\frac{\partial I_k}{\partial m} = \int_{a_{k-1}}^{a_k} -\frac{\ln\left[(1-R)K_{eq}\right]}{\left[(1-R)K_{eq}\right]^m}\,\mathrm{d}a \tag{7.22}$$

Here, an additional logarithm appears and the following equation is used to approximate the integrand, with its coefficients fit also here by the least squares method to finite element results for K_{eq}:

$$-\frac{\ln\left[(1-R)K_{eq}\right]}{\left[(1-R)K_{eq}\right]^m} = \frac{\mathrm{d}N}{\mathrm{d}a} \approx \alpha_1 \ln a + \alpha_2 a^2 + \alpha_3 a + \alpha_4\,. \tag{7.23}$$

For completeness, the integral of Eq. (7.23) is:

$$\int \frac{\mathrm{d}N}{\mathrm{d}a}\,\mathrm{d}a \approx \alpha_1 a \ln a - \alpha_1 a + \frac{\alpha_2}{3}a^3 + \frac{\alpha_3}{2}a + \alpha_4 a + \text{const.} \tag{7.24}$$

The sensitivity of the propagation life over an interval I_k to the stress ratio R is obtained as:

$$\begin{aligned}\frac{\partial I_k}{\partial R} &= \int_{a_{k-1}}^{a_k} \frac{mK_{eq}}{C\left[(1-R)K_{eq}\right]^{m+1}}\,\mathrm{d}a \\ &= \frac{m}{1-R}\int_{a_{k-1}}^{a_k} \frac{1}{C\left[(1-R)K_{eq}\right]^{m}}\,\mathrm{d}a = \frac{m}{1-R}\,I_k\end{aligned} \tag{7.25}$$

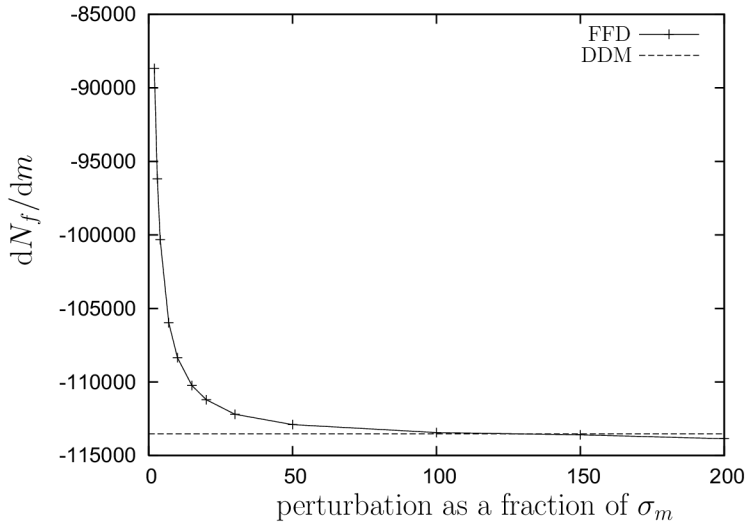

Figure 7.7: *FFD results for sensitivity to the Paris law exponent m.*

To be able to consider in the overall analysis the effect of varying applied stress σ_{app}, we will also need the sensitivity of the propagation life N_R to σ_{app}. When the equivalent stress intensity factor is expressed as a product of the stress by a function of a crack length, i.e. $K_{eq} = \sigma_{\text{app}}\gamma(a)$, the contribution to this sensitivity over an interval I_k can be calculated as:

$$\begin{aligned}\frac{\partial I_k}{\partial \sigma_{\text{app}}} &= \int_{a_{k-1}}^{a_k} \frac{-m(1-R)\gamma(a)}{C\left[(1-R)\sigma_{\text{app}}\gamma(a)\right]^{m+1}}\,\mathrm{d}a \\ &= -\frac{m}{C\sigma_{\text{app}}}\int_{a_{k-1}}^{a_k} \frac{1}{C\left[(1-R)K_{eq}\right]^{m}}\,\mathrm{d}a = -\frac{m}{C\sigma_{\text{app}}}\,I_k\end{aligned} \tag{7.26}$$

Similarly as in the case of sensitivity with respect to C, the sensitivities of fatigue life to the stress ratio R and the applied stress σ_{app} are directly obtained once the fatigue life itself is known.

Verification of the Sensitivity Equations

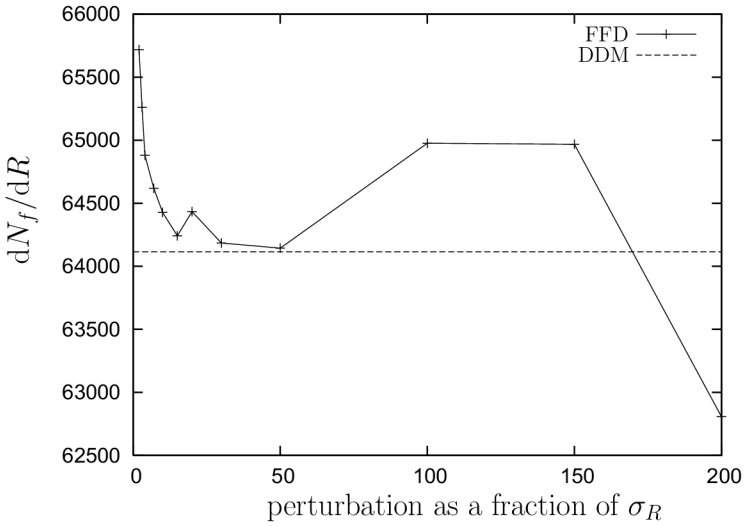

Figure 7.8: *FFD results for sensitivity to the stress ratio R.*

Unlike with the sensitivity to the initial crack length, the sensitivity to the Paris law multiplier C calculated by finite differences corresponds well to the value predicted by direct differentiation of the Paris law and approaches the DDM prediction in an asymptotic-like fashion as the FFD perturbation becomes finer. The same is true for the sensitivity to the Paris law exponent m.

Figures 7.6 and 7.7 show the sensitivities w.r.t. C and m, respectively, calculated with various finite difference perturbations. The perturbations are indicated as fractions of the standard deviation of the respective variables. The standard deviation considered for C was 0.97165 and the standard deviation used for m was 0.16584. For justification of these values, see Section 6.2.

The horizontal lines which the finite difference results approach mark the values computed by the direct differentiation Eqs. (7.21) and (7.22).

Note that here as well as in the case of the stress ratio, we are examining the sensitivity to a parameter that influences the lifetime under fatigue

propagation of all cracks and hence also at the leading crack.

It can be seen in Figure 7.8 that also for the stress ratio R, the sensitivity calculated by FFD quickly approaches in an asymptotic manner the DDM value coming from Eq. (7.25) as the perturbation is refined. In the Figure, the perturbation size is again indicated as a fraction of the standard deviation of R, which was in this case $\sigma_R = 0.2$.

Figure 7.8 also shows that precision is lost once the perturbation becomes too small. But perturbations within the range of $\sigma_R/20$ to $\sigma_R/50$ yield valid results.

7.4.4 Sensitivity to Toughness

The final crack length a_f is defined as the length at which K_{eq} attains the Mode I fracture toughness K_{Ic}. Its determination involves interpolation on the numerically obtained points of the $K_{eq}(a)$ curve (see Sec. 7.2) to find the length at which $K_{eq} = K_{Ic}$. Thus, the sensitivity to K_{Ic} (involving the derivative $\partial N_R/\partial a_f$) cannot be obtained by differentiating Eq. 7.9 and must be calculated by finite differences. However, since this does not require performing an additional complete crack propagation simulation, the description of the approach to calculate the sensitivity to K_{Ic} is included in this Chapter.

We consider a certain perturbation δK_{Ic} for the finite difference calculation at the perturbed point $K_{Ic} + \delta K_{Ic}$. We interpolate the same numerical data of the $K_{eq}(a)$ curve as we used in the current computation of fatigue propagation life to find the crack length $a_f + \delta a_f$ at which $K_{eq} = K_{Ic} + \delta K_{Ic}$. Then we integrate the $\mathrm{d}N/\mathrm{d}a(a)$ curve fitted to the finite element results for K_{eq} from a_0 up to the upper limit of $a_f + \delta a_f$, the result being the perturbed fatigue propagation life:

$$N_R + \delta N_R = \int_{a_0}^{a_f + \delta a_f} \frac{\mathrm{d}N}{\mathrm{d}a}\,\mathrm{d}a \tag{7.27}$$

The sensitivity of N_R to the toughness is then simply:

$$\frac{\partial N_R}{\partial K_{Ic}} = \frac{(N_R + \delta N_R) - N_R}{(K_{Ic} + \delta K_{Ic}) - K_{Ic}} \tag{7.28}$$

7.4.5 Concluding Remarks

Driven by the effort to improve the accuracy, stability and computational effectiveness in the evaluation of response sensitivities, researchers have developed techniques that avoid the use of finite difference method. The direct

differentiation method [3], [39] has been elaborated as a method of direct computation of sensitivities within the finite element context.

One of the concerns of this thesis was similar: to improve the computational efficiency, accuracy and stability in the calculation of the sensitivities of the life under fatigue crack propagation governed by an empirical crack growth law.

This section constitutes an important part of this thesis. The formulæfor the computation of the sensitivities of the fatigue propagation life derived herein represent a key concept in the stochastic crack propagation procedure proposed in this thesis. On the one hand, their application provides for the necessary accuracy that is required for the reliability approximation methods to converge. And on the other hand, the use of these sensitivity equations reduces the computational time as compared to sensitivity calculation by the finite difference method by a significant amount. This, in some applications, will be decisive for the sheer feasibility of analysing the crack propagation problem stochastically.

From the verification examples, it appears that in case of the Paris law parameters and the stress ratio, the equations for the sensitivity of the life under fatigue crack propagation derived in this section yield results that are only attainable with an optimal perturbation in the finite difference computation of sensitivities.

The values predicted by the direct differentiation based formula for sensitivity to the initial crack length indicate a stronger sensitivity than obtained by the finite difference method. However, the differences in FFD predictions for various perturbation sizes are higher than the discrepancy between FFD and DDM.

In conclusion, two important observations can be made based on the verification examples:

- In a differentiation by the finite difference method, the size of the perturbation taken to compute the differential responses has a great effect on the obtained value of the derivative. It is therefore advisable in a FFD calculation of derivatives to perform a convergence study to choose the correct perturbation size. In the example presented in Chapter 9, the perturbation sizes will be chosen based on the FFD convergence results plotted in the charts presented in this section.

- It is believed that all of the sensitivity equations derived by direct differentiation in this section can be trusted to provide reliable sensitivity results for use in reliability analysis.

7.5 Conclusions

This Chapter described the essentials of the implementation of the crack propagation model for the purposes of stochastic analysis. This computationally efficient and stable procedure is based on load history preprocessing by the PREFFAS method, simulation of crack growth with an update of the stress intensity factors by a structural analysis using the Extended Finite Element Method, and on an accurate and robust integration of the life under fatigue crack propagation.

Chapter 8

Distributed Computing

8.1 Introduction

In the calculation of response derivatives by the finite difference method, in the search for an optimal size of the step to take in the minimisation algorithm of reliability approximation methods and in Monte Carlo simulation, it is necessary to obtain several structural responses at a time.

If one has multiple networked computers available, distributed computing can be put in place so that the individual structural responses needed at a time can be computed in parallel. In such application, we deal with distributed computing, where a full but not extraordinarily large analysis is executed on a machine, as opposed to parallel computing. The latter computational method is used for the analysis of large systems, e.g. a parallel solution of a particularly large matrix, and requires parallel solution routines to be implemented within the analysis code.

On the other hand, all that is required for distributed computing is the possibility of remote execution of code in the networked system and the analysis software installed on each of the nodes (machines) in the system, with sufficient licenses available for the number of jobs to be executed. With commercial finite element packages, the latter condition can turn out to be prohibitively expensive.

The distribution of the computational tasks can advantageously be managed by a job distribution software. Alternatively, scripts written in Perl or other scripting language can also be used to control the remote job execution.

8.2 Computational Resources Available

The author had the opportunity to use for the purposes of this thesis the computational cluster, available at the Institut Français de Mécanique Avancée (IFMA) in Clermont-Ferrand. The cluster is built of IBM personal computers installed in a single rack. It consists of one master and 27 slave nodes running under Linux, each of which has two hyper-threaded XEON bi-processors. All in all, 108 virtual processors are available, which makes it possible to run 108 computations at the same time. The OpenPBS platform was used for job submission and control. The implementation of distributed computing was further facilitated by mirroring of the user directories to each and all of the slave nodes.

8.3 Implementation

The jobs actually submitted to the individual nodes for execution were UNIX scripts, which involved changing to the appropriate directory, calling the analysis, moving the files with the necessary results to the target directory and deleting the results not needed. These local execution scripts were in turn created by a master script written in Perl and launched from within the crack propagation simulation run in Matlab. The control of execution of the individual analyses was based on directory names involving a unique numerical identifier of the job.

The overall computation was steered by a Matlab code, cf. Fig. 8.1. The crack growth prediction with the stress intensity factor (SIF) being extrapolated from previous finite element (XFEM) results (see Section 7.2) takes place in a single Matlab run for all of the required response calculations. Once that all of the crack growth simulations require an update of the SIF by an XFEM analysis (crack increment exceeds Δa_{FE}), Matlab invokes the master script mentioned above that takes care of the execution of the XFEM analysis for all jobs in which failure has not yet occurred. Finally, when all of the crack growth simulations have reached failure, the fatigue life is integrated within the Matlab run.

At this point, we note a very significant advantage of the Extended Finite Element Method in distributed computation. The geometry of all discontinuities is defined in an ASCII file. This file is read by the XFEM code, while the same mesh file is used for all of the computations.

Note also that the same master script is called also when reliability analysis is carried out by means of Monte Carlo simulation. The Matlab script

allows for dividing the simulations into batches of the maximum number of jobs that can be taken by the system simultaneously. However, when using OpenPBS, splitting into batches is not necessary. The jobs are simply waiting in a queue for the slave nodes to complete the execution of pending jobs.

8.4 Conclusions

Distributed computing can make affordable many reliability analyses involving high computational effort. As in the current application, the individual machines do not need to have any particularly high performance. Connecting multiple PC workstations commonly available in many laboratories and firms into a network can be sufficient, provided that enough licenses are available for the structural analysis code. Under Unix and Linux operating systems, tools such as job distribution management, directory mirroring and scripting languages are available, which greatly simplify the implementation of distributed computing.

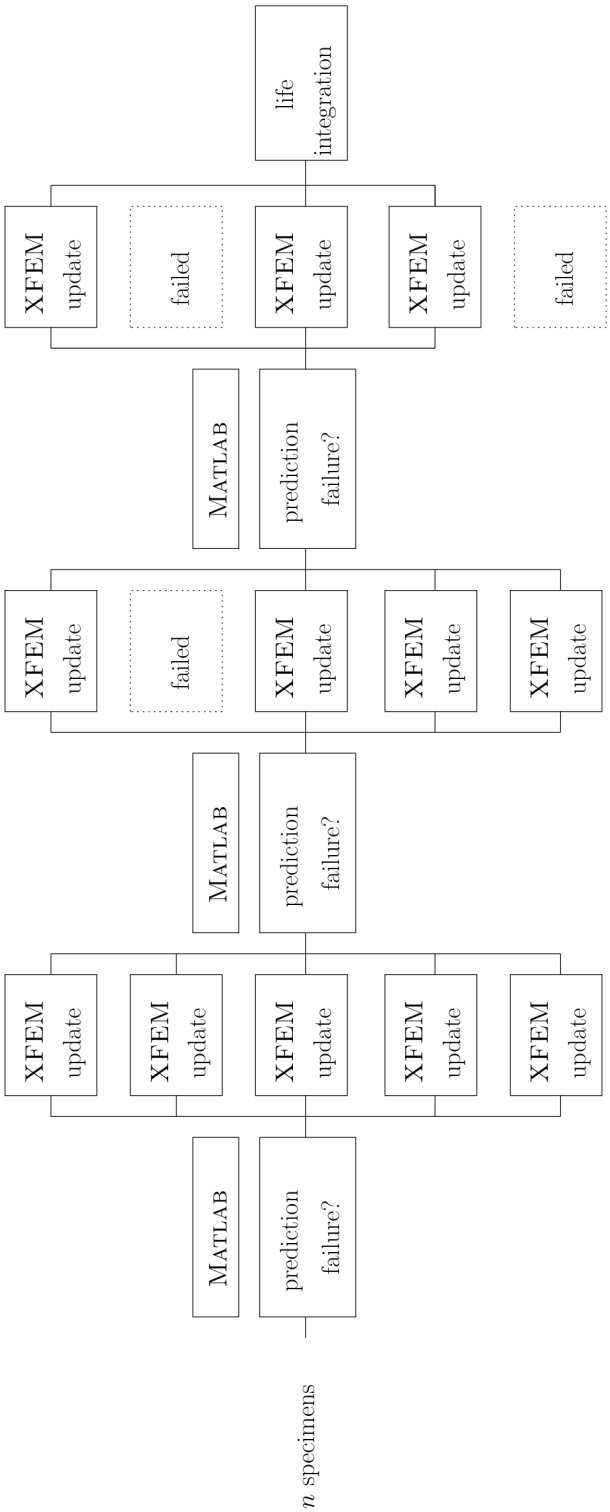

Figure 8.1: *The architecture of distributed computing*

Chapter 9

Application Examples

9.1 Introduction

In this Chapter, we finally put to work the techniques, procedures and analysis approaches proposed and developed in this thesis. Two stochastic crack propagation examples are presented in this chapter. They both consider a problem of a crack plate subjected to variable amplitude fatigue loading. These examples are a demonstration of a full implementation of the approach proposed earlier in this thesis, including distributed computing.

In the first example, the conversion of the variable amplitude loading to constant amplitude loading through PREFFAS and the crack propagation simulation are separated. This allows us to study the randomness in the material parameter b_U entering into the PREFFAS conversion algorithm. In the crack propagation simulation, the loading is considered deterministic. By running the two examples, we will have an opportunity to compare the reliability results obtained when loading is considered deterministic and when the procedure is applied in full scope, integrating also the PREFFAS load transformation and the random variables entering into it.

Within the first example, we will also compare the reliability results obtained when forward finite difference (FFD) method and direct differentiation method (DDM) are combined to calculate the response derivatives with results coming from a purely FFD calculation.

The two examples also have a different geometry. The first considers a problem with two cracks, the second with four cracks. For convenience, a procedure was developed to set the geometry of a plate with holes and cracks just by changing the control parameters. This of course does not preclude applying the crack propagation algorithm to other 2D geometries.

9.2 First Example

9.2.1 Problem Description

In the first example, we will consider a two-dimensional problem of propagation of cracks in a plate containing two holes, from which two cracks depart, facing each other, see Figure 9.1.

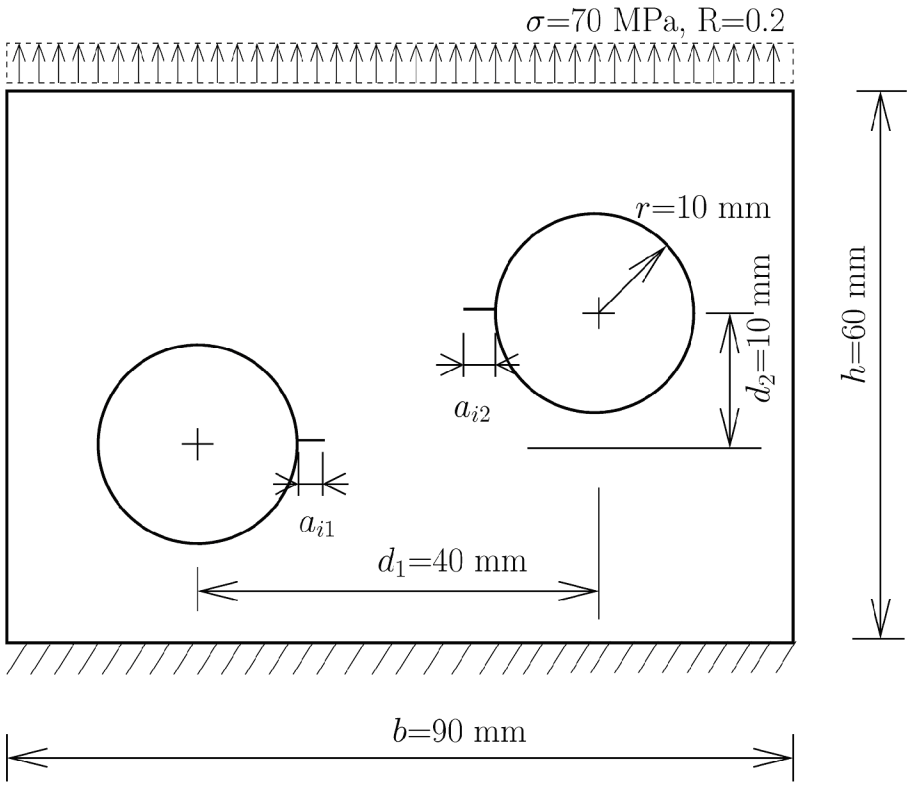

Figure 9.1: *Geometry of the problem – example 1*

The plate is constrained for both rotational and translational degrees of freedom along its bottom edge and a uniformly distributed traction loading is applied along the top edge.

9.2.2 Statistical Scatter in b_U

In a first step, we will study the randomness in PREFFAS, focussing on the statistical scatter of the material parameter b_U of Elber's crack closure model, cf. Eq. 2.23.

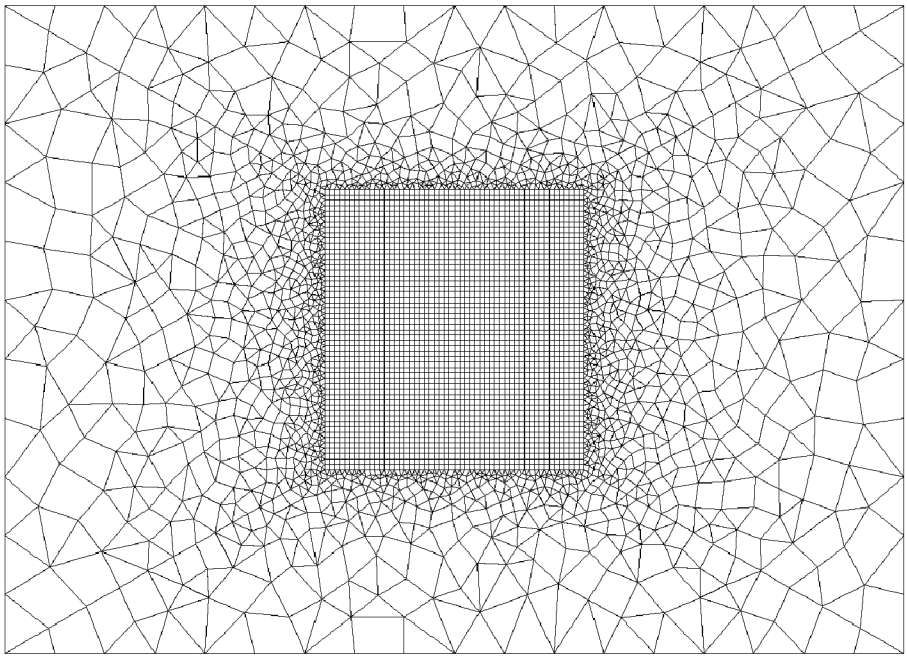

Figure 9.2: *Finite element mesh – example 1*

The parameter b_U can be determined as decribed in Section 2.6.4 when the crack grow retardation rate T_R and the Paris law exponent m are known. The statistics of m were estimated from the Virkler's experiments. Due to a lack of experimental data on T_R, we will assume a uniform distribution over the range of values indicated by Davy [21] on the basis of a scatter within a single set of crack propagation experiments (with and without overload). The statistics of T_R and m are shown in Table 9.1. The correlation coefficient of T_R and m is 0.427 and can thus be neglected as weak.

variable	type	parameter 1	parameter 2
T_R	uniform	min. 6.5	max. 16.0
m	normal	mean 2.8553	st.dev. 0.1658

Table 9.1: *Statistics of the Paris law exponent m and the crack length retardation rate T_R*

A simulation using the statistics in Table 9.1 yields a sample of b_U values. Its estimated statistics are shown in Table 9.2. A Chi squared test showed that the distribution of b_U can be considered normal.

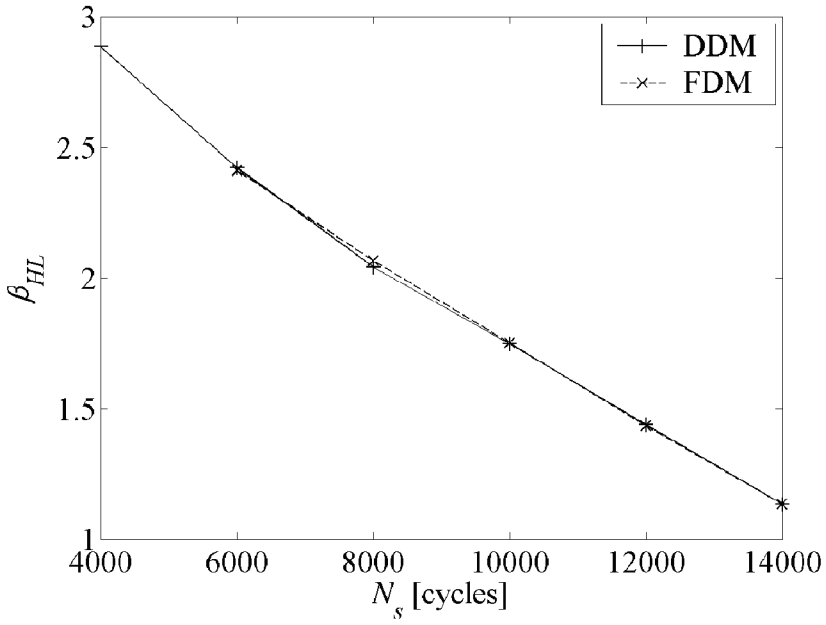

Figure 9.3: *Reliability index β_{HL}*

variable	type	mean	st. deviation
b_U	normal	0.5562	0.0215

Table 9.2: *Estimators of the statistics of the parameter b_U*

Together with the scatter in m, the statistics in Table 9.2 result in a coefficient of variation of the equivalent load stress σ_{eq} of only about 8% when simulations are performed using PREFFAS.

9.2.3 Fatigue Crack Growth Simulation

The only variables considered random in this example were the two initial crack lengths a_{i1} and a_{i2}, and the Paris law parameters C and m. Their statistics are given in Table 9.3.

A deterministic constant amplitude sinusoidal loading between a minimum of 14 MPa and a maximum of 70 MPa was applied to the structure (Fig. 9.1) and fatigue crack propagation was simulated using the procedure described in Chapter 7. The value of the fracture toughness entering into the fhysical failure criterion, cf. Eq. 6.4, was 1100 MPa$\sqrt{\text{mm}}$.

The finite element mesh used is shown in Figure 9.2. Discontinuities

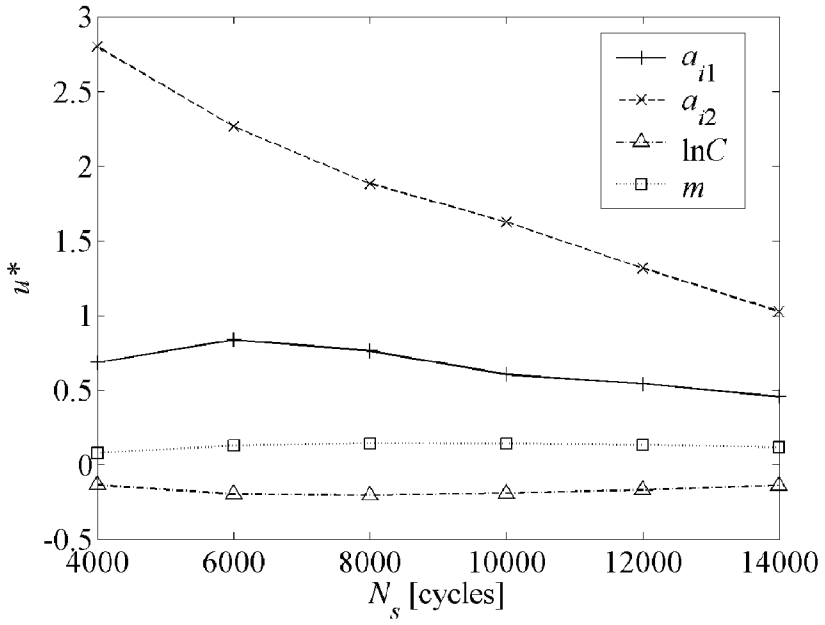

Figure 9.4: *Design point u^* (DDM)*

variable	distribution type	mean	std. dev.	correlation
a_i1, a_i2	i.i.d. exponential	1.5	1.5	–
$\log C$	normal	-26.056	0.972	-0.99759
m	normal	2.855	0.166	-0.99759

Table 9.3: *Statistics of the random variables of the crack propagation model*

(both the holes and the cracks) were introduced in the model through the Extended Finite Element Method techniques (see Section 3.4) implemented in the software ELFE_3D [46]. The size of the elements in the central zone where the cracks propagate (see Figure 9.1), was 0.4 mm.

The improved HL-RF algorithm was used for the search of the design point [101].

The convergence of the design point search in FORM is tested against two criteria. The first one is a criterion on the limit state function value:

$$e_1 = \left\| \frac{G}{G_0} \right\| \tag{9.1}$$

where G_0 is the limit state function value in the first iteration step.

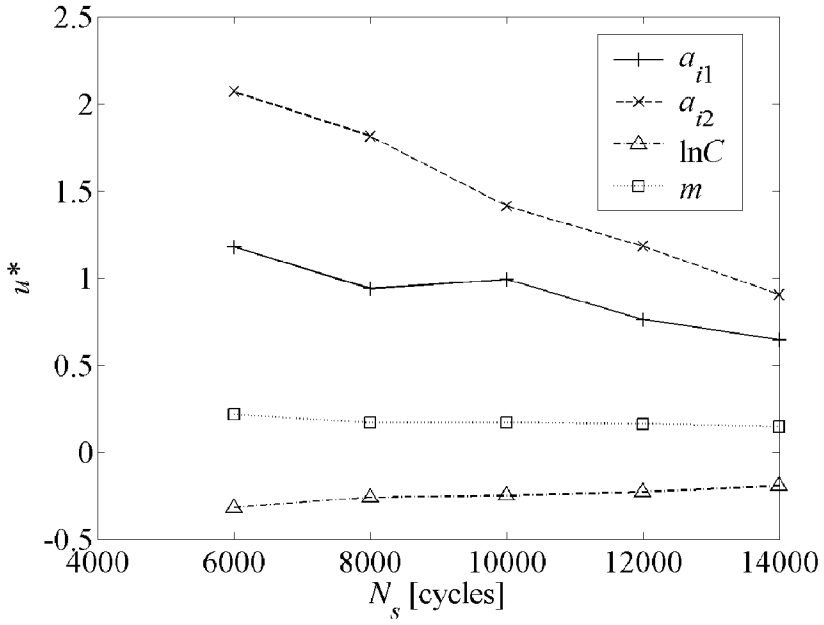

Figure 9.5: *Design point u^* (FDM)*

The second criterion tests whether $\mathbf{u}$ is parallel to the normalised gradient of G, whose components are the sensitivities at the design point, denoted α. Involving a dot product of vectors, the expression

$$\bar{e}_2 = \left\| \mathbf{u} - \alpha^T \mathbf{u} \alpha \right\| \tag{9.2}$$

will tend to zero as $\mathbf{u}$ and α are becoming parallel. The value returned by Eq. (9.2) depends on the size of $\mathbf{u}$. In fact, one computes a dot product of a unit vector with a vector of the size of $\|\mathbf{u}\|$. By normalising the resulting value of Eq. (9.2) by the size of $\|\mathbf{u}\|$, the criterion becomes independent of the probability of failure:

$$e_2 = \frac{\left\| \mathbf{u} - \alpha^T \mathbf{u} \alpha \right\|}{\|\mathbf{u}\|} \,. \tag{9.3}$$

Setting the convergence criteria to $e_1 = 0.05$ and $e_2 = 0.1$, convergence was achieved after only 3 to 4 iterations. These rather relaxed convergence criteria lead to some inaccuracy in the design point coordinates u^* in the standard normal space, as documented by the differences between u^* found with FDM and DDM estimation of gradients, respectively – cf. Figures 9.4

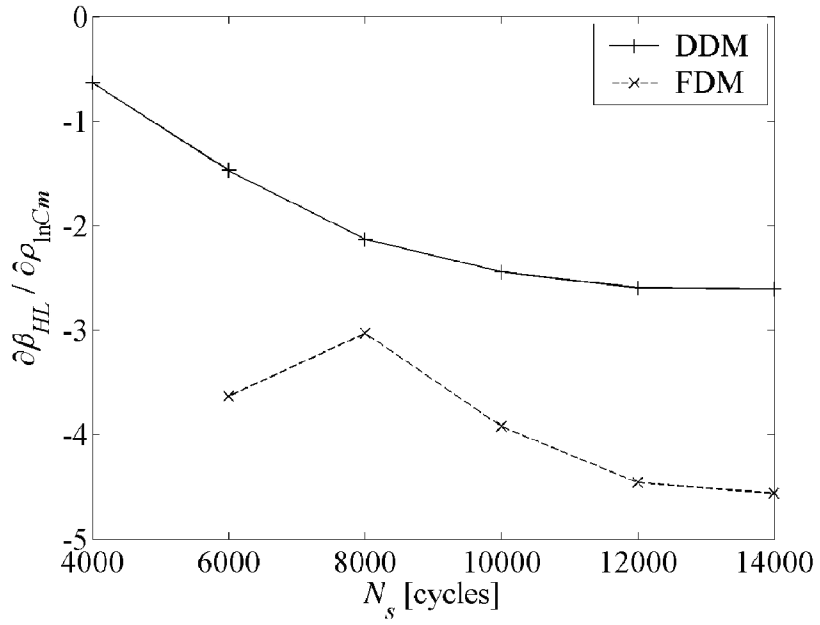

Figure 9.6: *Sensitivity of β_{HL} to the correlation of C and m*

and 9.5. But as it can be seen in Figure 9.3, the values of the reliability index β_{HL} obtained by the two methods are almost identical.

Figure 9.9 shows the reliability weights of the individual random variables expressed in terms of the importance factors γ, applicable in the case of correlated random variables. The γ factors have been defined in Section 4.5.2.

It can be seen in Figure 9.9 that with increasing required service life N_S and hence with increasing probability of failure, the weight of the initial crack sizes falls off while the Paris parameters C and m rise in importance.

A further observation regarding Figures 9.4, 9.5 and 9.9 is that at low N_S and hence low probability of failure, the effect of the initial crack size is predominant. Note that in all configurations considered, a_2 was the leading crack at the tip of which the failure actually occurred.

An important result is documented in Figure 9.6. It shows the sensitivities of the reliability index β_{H_L} to the correlation between the Paris parameters $\ln C$ and m. Comparing the sensitivity values in Figure 9.6 with sensitivities to the means and standard deviations plotted in Figures 9.7 and 9.8, one can see that the correlation coefficient has a significant effect on the reliability. This also explains why it was observed in Section 6.2 that

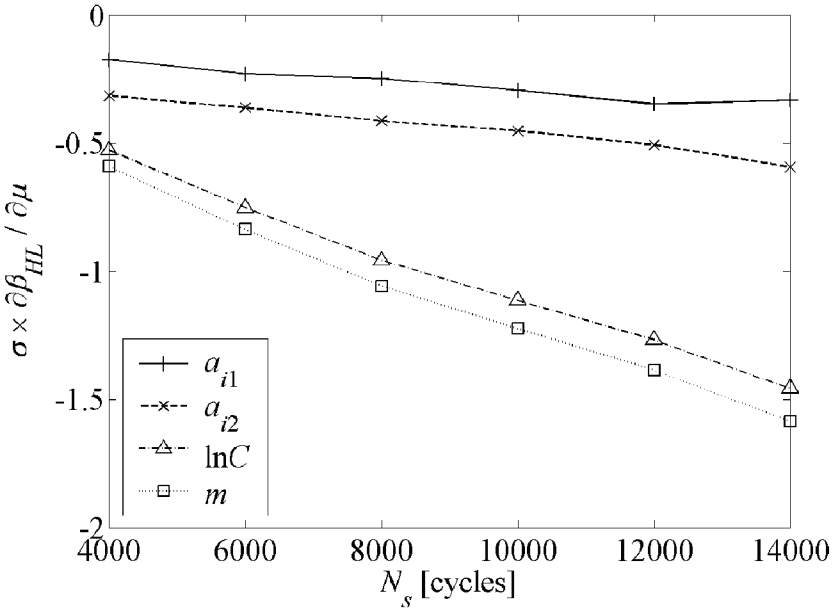

Figure 9.7: *Sensitivity of β_{HL} to the means of the variables*

the scatter in the fatigue propagation life could not be reproduced with a statistical model considering only one of the parameters C and m random and the other functionally related. Note that in the study presented in Section 6.2, the effect of $\rho_{\ln Cm}$ was even greater since C and m were the only random variables.

The differences between the sensitivities calculated from the reliability analysis results obtained with FDM and DDM estimation of gradients, respectively, are due to inaccuracies in the design point coordinates, which are in turn caused by the rather relaxed convergence criteria.

Figures 9.7 and 9.8 show the normalised sensitivities with respect to the the means and standard deviations of each random variable. It can be seen that the effects of the individual variables, in particular of the length of the leading crack, evolve with the required service life N_S. It appears that at low N_S, the reliability index is highly sensitive to the standard deviation of the length of the leading crack. On the other hand, at high N_S, it is the mean value of the Paris law parameters that are predominant.

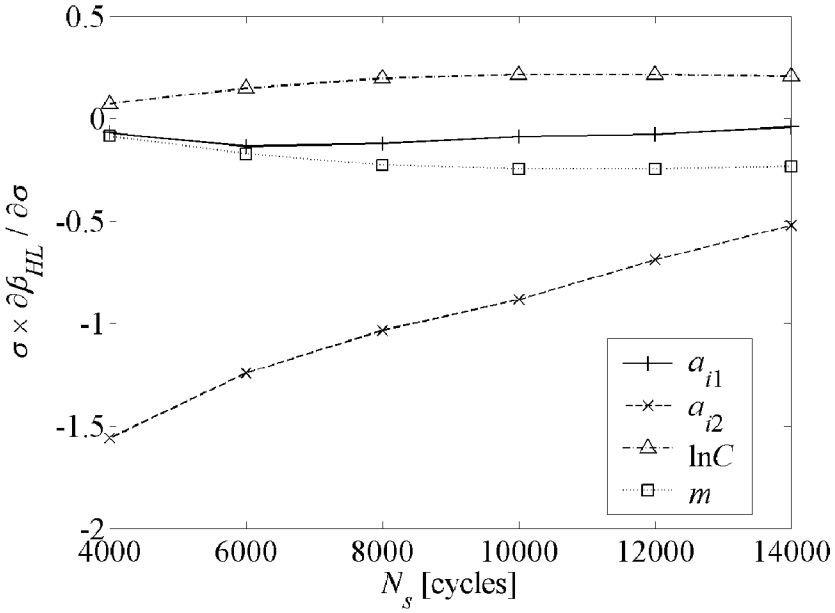

Figure 9.8: *Sensitivity of β_{HL} to the standard deviations*

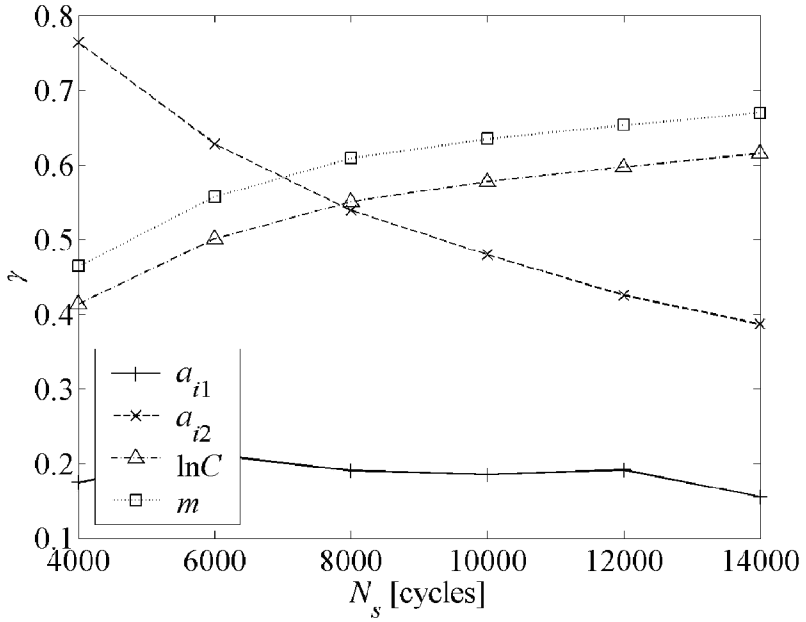

Figure 9.9: *Importance factors γ – example 1*

9.3 Second Example

The second example presents a full implementation of the proposed algorithm integrating the load transformation by the PREFFAS method into the overall crack propagation simulation algorithm. The purpose is to demonstrate the use of the algorithm on an example that shows the complexity of a real crack propagation problems in the aerospace industry.

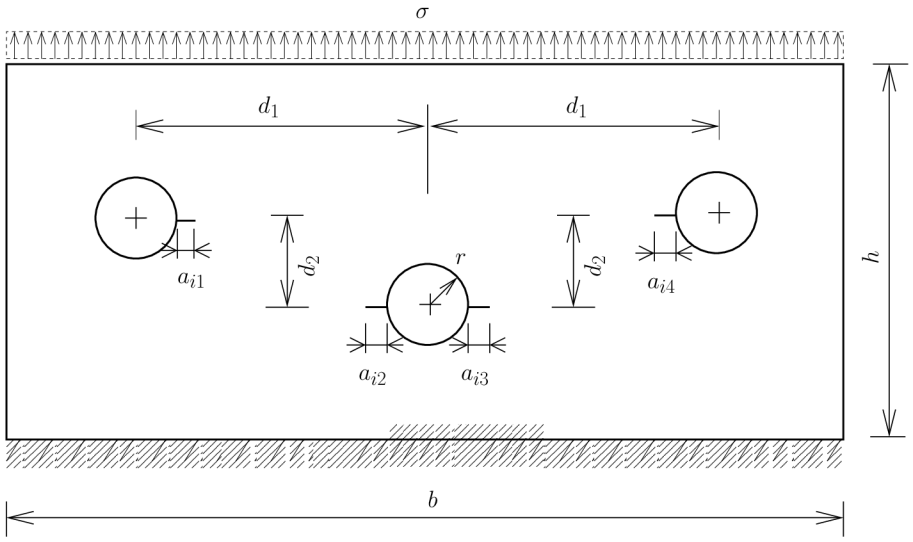

Figure 9.10: *Geometry of the problem – example 2*

9.3.1 Problem Description

In this example, we will consider a two-dimensional problem of propagation of cracks in a plate containing three holes, from which four cracks depart, facing each other, see Figure 9.10.

The plate is constrained for both rotational and translational degrees of freedom along its bottom edge and a uniformly distributed traction loading is applied along the top edge. The load history is input as a sequence of peaks and troughs. This may be a standard loading sequence applicable to the structure in question. For example the aerospace industry standards prescribe specific load histories for particular components and structures of the aircraft.

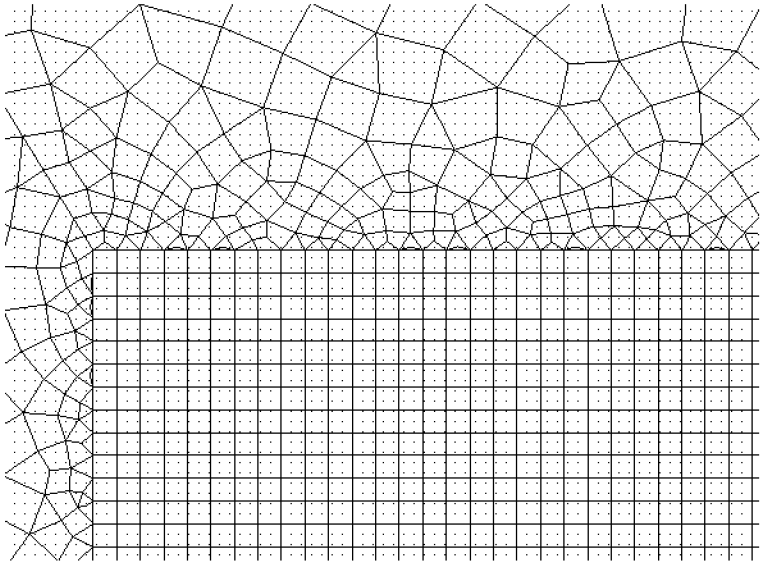

Figure 9.11: *A detail of the finite element mesh*

9.3.2 Input Parameters and Variables

As regards the geometrical parameters, only the initial crack sizes a_{i1} to a_{i4} are considered to be random variables. In line with common practice, a lognormal probability law is used. a_{i1} to a_{i4} are identically distributed, but independent. In a real application, their statistics would be derived from experiments, using Bayesian updating where information is limited. Here, no such data collection and evaluation was carried out and the statistics are just some reasonable values, not grounded by actual data.

In other calculations not documented in this thesis, the cracks were modelled as starting from a point on the circular hole given by a line running from the hole centre at an angle from the horizontal line. The cracks were initially oriented in the same angle. These angles were considered as independent random variables for each crack, with zero mean. However, the crack propagation life appeared to be rather insensitive to this angle. In fact, the cracks immediately regained the direction of propagation governed by the surrounding stress field.

Other geometrical parameters, including the horizontal and vertical spacing of the holes d_1 and d_2, respectively, the dimensions b and h of the plate, its thickness, as well as the radius of the holes r were treated as deterministic

parameters.

None of the material properties has as much effect on the crack propagation life and at the same time as much dispersion as the parameters of the Paris law. On the basis of the investigations carried out in Section 6.2, a statistical model of joint normally distributed m and $\ln C$ (for the two Paris parameters C and m) was employed.

The amplitude characteristic of the applied stress σ_L and the toughness K_{cr}, whose derivatives can be obtained without recourse to finite differences, were also considered as random variables. σ_L is actually the multiplier applied onto a standard peak-valley sequence as may be applicable by a standard for the given component and environment. σ_L was represented by normal distribution and K_{cr} was modelled as log-normally distributed.

The last random variable considered in the statistical modelling for this example problem was the material parameter b_U, which enters together with the Paris exponent m the load sequence transformation algorithm of the PREFFAS method. Its statistic distribution parameters have been determnined in the example above (Section 9.2) and will be reused here.

In summary, the variables considered random are the initial crack lengths a_i, logarithm of the Paris law factor $\ln C$, the Paris exponent m, the applied stress σ_L, the toughness K_{cr}, and the material parameter b_U of the PREFFAS method. Their statistics are listed in Table 9.4.

For discusion on the high and precisely given negative correlation coefficient between $\ln C$ and m, see the discussion in Section 6.2.

variable	distribution type	mean	std. dev.	correl.
a_i	lognormal	1.5	0.3	–
$\ln C$	normal	-26.056	0.97165	-0.99759
m	normal	2.8553	0.16584	-0.99759
K_{cr}	lognormal	1100	110	–
σ_L	normal	50	7	–
b_U	normal	0.56	0.02	–

Table 9.4: *Statistics of the random variables of the crack propagation model*

9.3.3 Solution Methods

This example demonstrates the computational procedure for probabilistic analysis of crack propagation problems put forward in the preceding chapters.

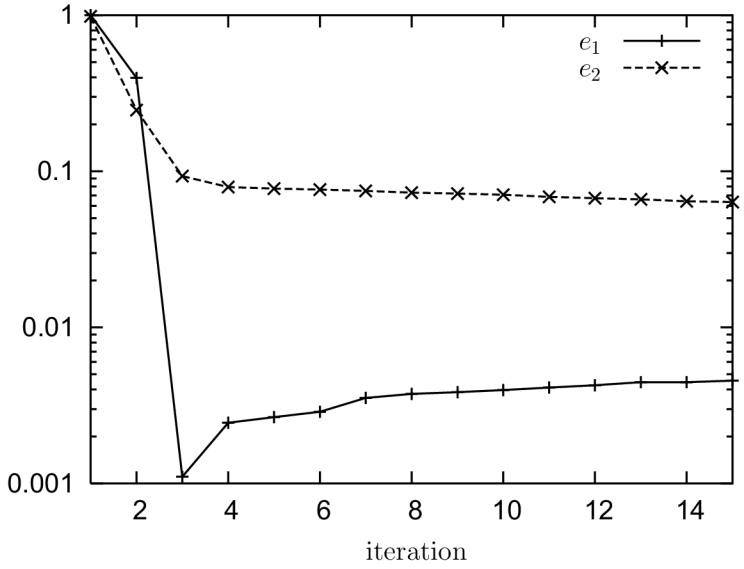

Figure 9.12: *Convergence criteria.*

The reliability problem with the limit state function defined by equation (6.6) is solved by the First Order Reliability Method (FORM). Whenever FORM requires a calculation of the response, the loading sequence is transformed by the PREFFAS method (Sec. 2.6.3) to the equivalent constant amplitude loading using the variable values passed by FORM.

The crack propagation simulation procedure is then executed as described in Chapter 7, with distribution of computational jobs outlined in Chapter 8 and with the mechanical response computed by the Extended Finite Element Method (Sec. 3.4), using the software ELFE_3D [46]. The crack propagation area is meshed with a rectangular mesh with an element size of 0.3 mm. Figure 9.3 shows a detail of the finite element mesh. Sensitivities of the life under fatigue crack propagation are computed by direct differentiation (see Section 4.4.1) where possible, and otherwise by the forward finite difference method. The convergence criteria used are the same as those introduced above in Eq. (9.1) and Eq. (9.3).

9.3.4 Results

The analysis was run first with a mesh size of 0.5 mm in the crack propagation zone. Because of slow convergence on the criterion e_2, the mesh was

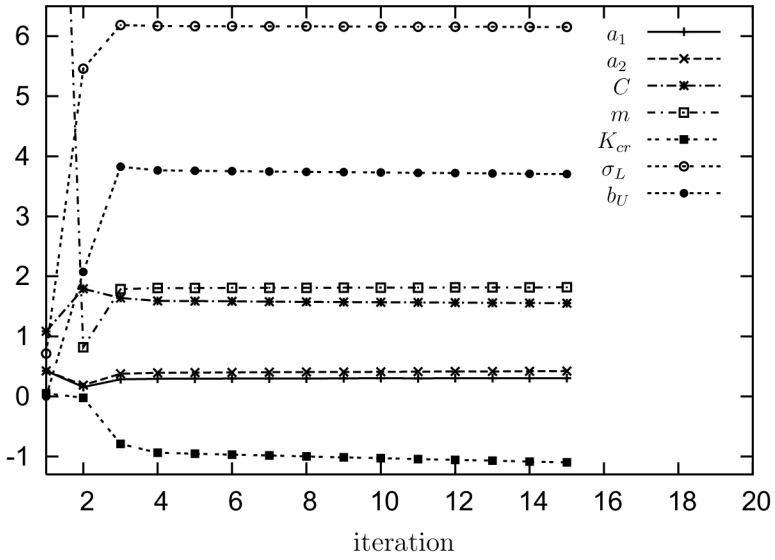

Figure 9.13: *Variable values in standard normal space through the iterations.*

refined with a hope that convergence will be faster. However, the difference was not very important and the little increase in the speed of convergence was paid for quite expensively by extra computational time. The history of the convergence criteria through the iterations of the FORM design point search is shown in Fig. 9.12 for the mesh size of 0.3 mm.

The values of the individual random variables in the standard normal space, i.e. the coordinates of the design point in the iterations of the design point search, are plotted in Fig. 9.13. In both Fig. 9.12 and Fig. 9.13, it can be seen that from the fourth iteration on, the values are quite stabilised and only a slow improvement in the e_2 criterion is achieved at the expense of deterioration in the e_1 criterion.

The Hasofer-Lind reliability index, see Section 4.3, was $\beta_{HL} = 7.55$, which corresponds to a FORM probability of failure of $2.25 \cdot 10^{-14}$. This is a very low probability and the fact that the design point search converged demonstrates the robustness and stability of the developed procedure.

However, we have relied on FORM only and it would be judicious to use the importance sampling simulation procedure in order to confirm the probability of failure and the inexistence of another design point.

Fig. 9.3.4 plots the importance factors γ. It can be seen that the material

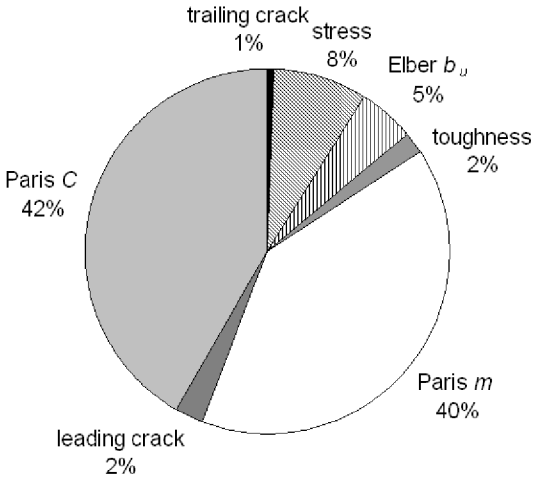

Figure 9.14: *Importance factors γ – example 2*

parameters C and m of the Paris crack propagation law have by far the highest potential to contribute to failure or survival of the structure. About four times lower is the effect of the third most important variable – the amplitude characteristic of the loading σ_L – followed by another material parameter – the b_U parameter of Elber's model used to convert the variable amplitude loading to an equivalent constant amplitude load.

The dominating importance of the material parameters governing the crack propagation rate suggests that only minor improvements in reliability can be achieved if one does not play on the material. But this may not be a feasible option, especially not in the case of a study of crack propagation in an existing structure. The third most important variable is the amplitude of the applied stress. It could therefore make sense to implement measures such as diverting the stresses from the cracked site by adding stiffness elsewhere.

It must be noted that the importance weights of the variables as shown in Fig. 9.3.4 are calculated for the current problem with given statistical model. The importance weights of each variable could look different if also other parameters were a part of the model. An example are the hole distances. Also, if real statistics of the initial crack lengths were used, their importance could also change. The same could be true also for the Elber's material parameter b_U if more statistical information on this parameter were available. On the same token, the importances of the variables would be also different if the minimum required service fatigue life N_S was different.

9.3.5 Discussion

Because of the novelty of the stochastic crack propagation analysis approach proposed in this thesis, the successful implementation and good functioning of the analysis procedure is probably more important to discuss than the specific values of the results.

Once the building blocks of the stochastic analysis procedures had been set out, the implementation of the entire procedure was a process in which various algorithmic challenges, interfacing problems and numerical difficulties had to be overcome. The results listed above were produced without encountering any errors that would interrupt the execution of the procedure or have an effect on the correctness of the results. And they were obtained in a quite reasonable time. The procedure was run also on a single processor PC and the computation was completed in about 10 days.

The above reliability analysis example has demonstrated the accuracy, efficiency and robustness of the proposed approach to stochastic analysis of complex two-dimensional crack propagation problems. After a relatively minor adaptation to other definitions of cracks than those departing from a hole, the procedure is ready for analysis of wide range of practical 2D crack propagation problems.

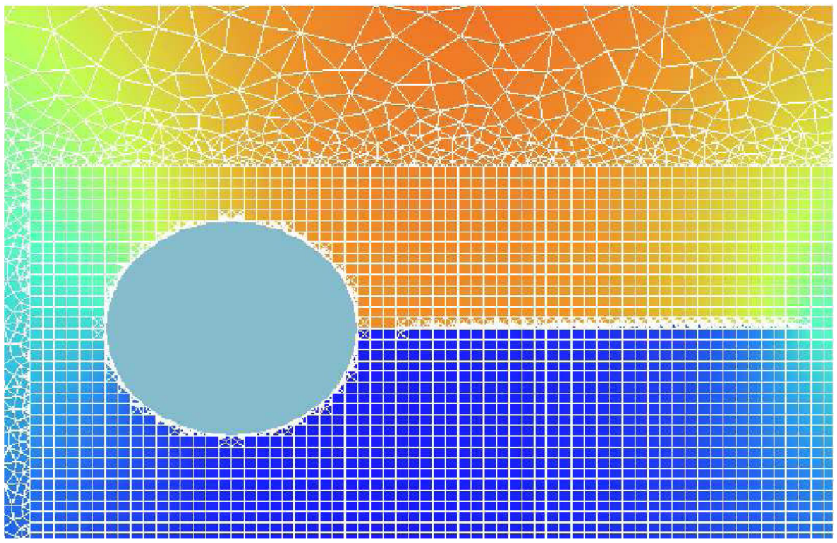

Figure 9.15: *Mesh with integration sub-elements and displacement results.*

9.4 Concluding Remarks on the Examples

Unlike in the first example, loading was studied in the second example as an integral part of the analysis procedure, which allowed us to model the load amplitude parameter σ_L and the material parameter b_U of PREFFAS load transformation algorithm as random variables.

Comparing the importance factors in Fig. 9.9 and Fig. 9.3.4 makes it apparent that by including the loading in the analysis, a different picture about the significance of the variables for reliability is drawn. As a matter of fact, the loading amplitude comes out as the third most important variable for the probability of failure. This illustrates how reliability results depend on appropriate modelling of the problem. In practical analysis, the uncertainty about any variable should not be disregarded until a sensitivity analysis has been carried out.

The Paris law exponent m enters also into the load transformation by PREFFAS. One could therefore attribute a part of the sensitivity to the Paris law parameters to the fact that they influence the reliability also through the loading. However, such intermediated influence is probably not high. Remember that in the first example, we have found only a small coefficient of variation for the transformed loading when only m and the the crack grow retardation rate T_R were considered as the random variables in the load transformation algorithm.

Note also that $\ln C$ and m are highly correlated, so any one of them cannot have a high significance for reliability without the other one being about the same important as well.

The first example focussed on specific aspects: (1) studying the randomness in the load tansformation through the PREFFAS method, (2) assessing the performance of and comparing the results obtained when using the finite difference method (FDM) and direct differentiation method (DDM) in the calculation of the gradients of the limit state function, (3) studying the evolution of the importance of the variables with the required fatigue service life and the probability of failure.

The purpose of the second example, on the other hand, was to demonstrate a full implementation of the proposed algorithm on an example of an industrial-level complexity.

The first example was calculated on the computational cluster described in Section 8.2 using distributed computing. The stochastic crack propagation analysis was complete in about 40 hours. The second example was calculated on a single PC with a 1.4 MHz processor and 1GB of RAM. 15 interations of the design point search algorithm were complete in about 10

days. This shows the versatility of the procedure that is capable of using the distributed computing technology, but can be run on a single PC as well.

The examples show that the proposed procedure to analyse stochastic fatigue crack propagation is solid and effcient and that it can be useful for industrial applications.

Chapter 10

Conclusions

This thesis had a double objective, corresponding to a differing research focus of the two research groups within which the author conducted his doctoral research under joint direction of his two tutors. In this closing chapter, we will not only discuss the results and contributions of the thesis, but it will also become apparent that lessons learnt in one part of the research came useful in the other, and vice-versa.

The Czech part of the research focused on investigation of through cracks in very thin foils with the objective to verify the hypothesis that the observed anomalous behaviour of such cracks can be explained by the stress conditions around the crack front determined based on continuum mechanics. The author reviewed the theoretical bases of the concepts commonly used in fracture mechanics to understand their applicability to problems with special geometries, such as the one of thin foils. A detailed numerical investigation of the stress conditions along and around the crack front was then carried out. This carefully elaborated 3D finite element models of through cracks in thin foils revealed some trends in the evolution of the stress field as the sheet metal becomes thinner. But none of the kind that would offer any explanation for the anomalous behaviour observed in fatigue tests on cracked thin foils.

Despite the fact that the above hypothesis appeared ungrounded, this research was also useful *per se* in that it help the author to fully appreciate the assumptions behind two-dimensional fracture mechanics models as well as behind two-dimensional crack propagation models.

The larger part of the thesis, which also brings an original contribution, deals with numerical modelling and stochastic analysis of complex-geometry crack propagation problems. This computational task requires a huge com-

putational effort together with a good accuracy in the numerical mechanical model.

At the same time, the life under fatigue crack propagation is known to show an extraordinary amount of scatter. The computational requirements arising when a numerical mechanical model needs to be used have long prevented engineers from taking the advantage of reliability analysis to gain a better understanding of problems such as inspection scheduling and crack repair design evaluation.

By employing several computational and analysis techniques, a stochastic crack propagation analysis procedure was developed in this thesis which makes it possible to conduct a reliability analysis of the problem with reasonable computational resources, while retaining the necessary robustness of the procedure.

Let us summarise the reasons that lead to the choice of the specific analysis methods that make up the important building blocks of the reliability analysis procedure and highlight the contribution of each.

The First Order Reliability Method (FORM) was chosen as the reliability analysis tool. It appeared that the problem analysed showed no important non-linearity. A first-order approximation of the limit state function was thus sufficient. FORM directly provides information on sensitivities. In comparison to Monte Carlo simulation, FORM is more demanding as regards the accuracy of the structural response computed. But is does not require the mechanical model to compute responses with very low-probability realisations of the random variables. These may lead to a different type of failure than the one actually analysed. FORM thus helps to contain the problem within the actual problem of interest.

For the class of problems of interest in this thesis, i.e. two-dimensional crack propagation problems involving crack-crack and crack-structure interactions, a solution of the underlying fracture mechanics problem by a numerical method becomes necessary. A classical finite element formulation requires updating the finite element mesh as the crack is growing. This requires highly performing meshing algorithms. But more importantly, remeshing introduces numerical noise which can easily hamper the convergence of the FORM reliability algorithm. The accuracy achievable with the finite elements that is quite satisfactory for deterministic purposes may at the same time be simply insufficient for the reliability approximation methods, such as FORM.

It was then natural to look for a numerical method that would be better performing for the purposes of reliability analysis of crack propagation problems. The Extended Finite Element Method (XFEM) avoids remeshing

and offers a good numerical stability. As compared to meshless methods, which were also explored, XFEM is faster. Also, it builds on the finite element method, so the computational technology developed for finite elements remains available also for XFEM.

The FORM algorithm requires the computation of the derivatives of the response. Obtaining them by numerical differentiation is time consuming and introduces numerical errors. This thesis therefore explored possibilities to calculate the response sensitivities by directly differentiating the response equation. Several useful formulæ were thus derived and used in the analysis algorithm. However, the response derivatives with respect to some variables can only be obtained by employing numerical differentiation by the finite difference method.

The author also had the opportunity to use a cluster of personal computers. This network of relatively inexpensive machines running Linux operating system with the OpenPBS distributed computing utility appeared to be perfectly suited and easy-to-use for reliability analysis purposes. The distribution of the computations of the structural response brought a further acceleration of the whole reliability analysis procedure.

The implemented procedure appeared capable to analyse a stochastic crack propagation problem, with a complexity at the level of an industrial application, with robustness, accuracy and reasonable requirements on computational hardware and time. After minor modifications to accommodate other definition of crack departure than from a hole, the procedure is ready to be applied on a wide range of complex-geometry two-dimensional crack propagation problems.

The extensibility of the method is limited mainly by the use of the stress intensity factor (SIF) as both the crack growth driver (trough the Paris law) and the failure criterion. As the fracture mechanics theory review in the first part of the thesis exposed, SIF is defined for two-dimensional problems. This fact would require a substantial re-formulation of the procedure, should it be extended to three-dimensional problems. On the other hand, XFEM has been successfully employed also in 3D crack propagation applications.

The part of the thesis dealing with stochastic crack propagation modelling also shed a different light on the problem of crack propagation in thin foils, investigated earlier in the thesis. It appeared that this phenomenon has much to do with the microstructure of the material. Correlating the average crack advance to the general level of stress around the crack, as in the Paris law, and stochastic modelling can perhaps be more successful in capturing the random effects of the material structure.

Appendix A

Fracture Mechanics Complements

A.1 Relation between the Energy Release Rate and the Stress Intensity Factor

Consider a crack with a length a in state 1, which grows to length $a + \Delta a$ in state 2 along the straight line of a. The states will be denoted by left superscripts. The two crack lips of the crack extension Δa will be denoted $\Gamma_{\Delta a}$ and will have their outward normals $\mathbf{n}^+$ and $\mathbf{n}^-$ coinciding with the unit vectors $\mathbf{e}_1$ and $\mathbf{e}_2$, respectively. Considering that the tractions in state 1 effectively close the crack over Δa, the geometries of state 1 and state 2 are the same and Betti's theorem can be invoked, subject to assuming linear elasticity [48]:

$$\int_{\partial\Omega} {}^1T_i \, {}^2u_i \, ds + \int_{\Gamma_{\Delta a}} {}^1T_i \, {}^2u_i \, ds = \int_{\partial\Omega} {}^2T_i \, {}^1u_i \, ds \,. \tag{A.1}$$

Note that ${}^2T_i$ is zero on $\Gamma_{\Delta a}$. The integrals over $\partial\Omega$ and $\Gamma_{\Delta a}$, respectively, are separated:

$$\int_{\Gamma_{\Delta a}} {}^1T_i \, {}^2u_i \, ds = \int_{\partial\Omega} \left({}^2T_i \, {}^1u_i - {}^1T_i \, {}^2u_i \right) ds = \int_{\partial\Omega} \left[\left({}^2T_i - {}^1T_i \right) {}^1u_i - {}^1T_i \left({}^2u_i - {}^1u_i \right) \right] ds \,. \tag{A.2}$$

Under constant loading, ${}^2T_i - {}^1T_i = \frac{\partial T_i}{\partial a}\Delta a$, and ${}^2u_i - {}^1u_i = \frac{\partial u_i}{\partial a}\Delta a$. Substituting this into (A.2), we have:

$$\int_{\Gamma_{\Delta a}} {}^1T_i \, {}^2u_i \, ds = \int_{\partial\Omega} \left(\frac{\partial T_i}{\partial a} u_i - T_i \frac{\partial u_i}{\partial a} \right) \Delta a \, ds \,, \tag{A.3}$$

where we recognise the form of equation (2.5) in the right hand side. Therefore:

$$G \, \Delta a = -\frac{1}{2} \int_{\Gamma_{\Delta a}} {}^1T_i \, {}^2u_i \, ds \,. \tag{A.4}$$

Let us now write the traction T_i and displacements u_i on the upper (+) and lower (–) crack face over $\Gamma_{\Delta a}$ with the polar coordinate system used for the in-plane stresses. For the upper face:

$$\begin{aligned} {}^1T_i^+ = {}^1\sigma_{ij}\mathbf{n}^+ &= \left(-{}^1\sigma_{\theta r}\mathbf{e}_1 - {}^1\sigma_{\theta\theta}\mathbf{e}_2 - {}^1\sigma_{23}\mathbf{e}_3\right) \;\; (r = x,\, \theta = 0) \\ {}^2u_i &= \left({}^2u_1\mathbf{e}_1 + {}^2u_2\mathbf{e}_2 + {}^2u_3\mathbf{e}_3\right) \;\; (r = \Delta a - x,\, \theta = \pi) \,. \end{aligned} \tag{A.5}$$

For the lower face:

$$\begin{aligned} {}^1T_i^- = {}^1\sigma_{ij}\mathbf{n}^- &= \left({}^1\sigma_{\theta r}\mathbf{e}_1 + {}^1\sigma_{\theta\theta}\mathbf{e}_2 + {}^1\sigma_{23}\mathbf{e}_3\right) \;\; (r = x,\, \theta = 0) \\ {}^2u_i &= \left({}^2u_1\mathbf{e}_1 + {}^2u_2\mathbf{e}_2 + {}^2u_3\mathbf{e}_3\right) \;\; (r = \Delta a - x,\, \theta = \pi) \,. \end{aligned} \tag{A.6}$$

When the expressions for stresses and displacements given in Subsection A.2.2 are inserted in (A.4) using (A.5) and (A.6) – see [48] for details – we obtain the Irwin's formula:

$$G = -\frac{1}{2\Delta a} \int_{\Gamma_{\Delta a}} {}^1T_i \, {}^2u_i \, ds = \frac{1-\nu^2}{E}(K_I^2 + K_{II}^2) + \frac{1+\nu}{E} K_{III}^2 \,. \tag{A.7}$$

A.2 Crack Tip Stress Field Expansion

A.2.1 Airy's Stress Function

Equilibrium and Compatibility Equations

Consider an element subjected to stresses as in Figure A.1. Assuming zero body forces, the following equations must hold for the stresses to be in equilibrium:

$$\begin{aligned} \frac{\partial \sigma_{xx}}{\partial x} + \frac{\partial \sigma_{xy}}{\partial y} &= 0 \\ \frac{\partial \sigma_{yy}}{\partial y} + \frac{\partial \sigma_{xy}}{\partial x} &= 0 \,. \end{aligned} \tag{A.8}$$

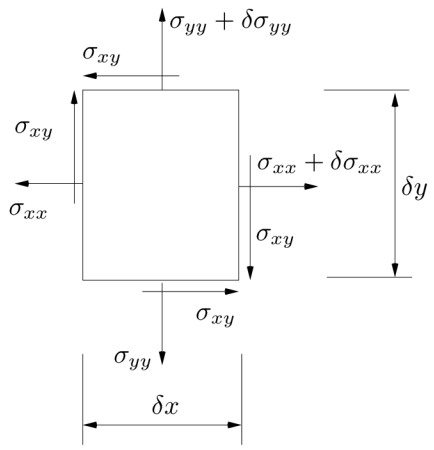

Figure A.1: *Stress equilibrium*

Equations (A.8) are fulfilled identically, if the components of the stress tensor are expressed using Airy's stress function Φ:

$$\begin{aligned} \sigma_{xx} &= \frac{\partial^2 \Phi}{\partial y^2}\,, \\ \sigma_{xy} &= -\frac{\partial^2 \Phi}{\partial x \partial y}\,, \\ \sigma_{yy} &= \frac{\partial^2 \Phi}{\partial x^2}\,. \end{aligned} \tag{A.9}$$

The identities are easy to see, e.g.:

$$\frac{\partial \sigma_{xx}}{\partial x} + \frac{\partial \sigma_{xy}}{\partial y} = \frac{\partial^3 \Phi}{\partial y^2 \partial x} - \frac{\partial^3 \Phi}{\partial y^2 \partial x} = 0\,. \tag{A.10}$$

Continuity of deformations is ensured by requiring the compatibility equations to be fulfilled. Again, assuming zero body forces, and writing the compatibility equations in stresses, they read:

$$\left(\frac{\partial^2}{\partial x^2} + \frac{\partial^2}{\partial y^2} \right) (\sigma_{xx} + \sigma_{yy}) = 0\,. \tag{A.11}$$

If the function Φ is bi-harmonic, i.e. if:

$$\nabla^2 \nabla^2 \Phi = 0\,, \tag{A.12}$$

then both equation (A.8) and equation (A.11) are satisfied.

The Laplacian ∇^2 in equation (A.12) in Cartesian coordinates is:

$$\nabla^2 = \left(\frac{\partial^2}{\partial x^2} + \frac{\partial^2}{\partial y^2} \right) . \tag{A.13}$$

After transformation to polar coordinates by substituting $x = r\cos\theta$ and $y = r\sin\theta$, it reads:

$$\nabla^2 = \left(\frac{1}{r^2}\frac{\partial^2}{\partial \theta^2} + \frac{1}{r}\frac{\partial^2}{\partial r} + \frac{\partial^2}{\partial r^2} \right) . \tag{A.14}$$

A.2.2 Williams's Expansion

Williams [97] presented a solution to equation (A.12) using an asymptotic expansion of the stress field with separation of the variables r and θ. Williams' solution is presented in the following.

Solution to Differential Equation of the Problem

A solution is to be found that satisfies equation (A.12) and the boundary conditions (see below). The solution is sought in a factorised form (with r and θ separated). Considering the form of equation A.14, a solution of the form

$$\Phi = K_\Phi \, r^{2-s} f(\theta) \tag{A.15}$$

will yield a convenient form of the results after the differentiation. K_Φ in equation A.15 is a proportionality factor applied to the stress distribution.

Let us now insert equation A.15 into equation A.12. First, let us apply the Laplacian ∇^2 on Φ the first time:

$$\begin{aligned} \left[\frac{1}{r^2} r^{2-s} f'' + \frac{1}{r}(2-s) r^{1-s} f + (1-s)(2-s) r^{-s} f \right] &= 0 \\ \left[r^{-s} f'' + \left((2-s) + (1-s)(2-s) \right) r^{-s} f \right] &= 0 \\ \left[r^{-s} f'' + \left(4 - 4s + s^2 \right) r^{-s} f \right] &= 0 \, . \end{aligned} \tag{A.16}$$

Applying the Laplacian ∇^2 a second time on equation A.16, we arrive at:

$$\begin{aligned} r^{-2-s} f'''' + r^{-2-s} \left(4 - 4s + s^2 \right) f'' \\ + (-s) r^{-2-s} f'' + \left(4 - 4s + s^2 \right) f (-s) r^{-2-s} \\ + (s + s^2) f'' + \left(4 - 4s + s^2 \right) (s + s^2) f r^{-2-s} = 0 \, . \end{aligned} \tag{A.17}$$

After arranging, we obtain:

$$f'''' + 2 \left(s^2 - 2s + 2 \right) f'' + s^2 (2-s)^2 f = 0 \, . \tag{A.18}$$

Unlike equation (A.12), which was a partial differential equation, equation (A.18) is a homogeneous ordinary differential equation, depending only on θ . Moreover, it is linear and has constant coefficients. Such equations can be solved by an exponential function, looking for a solution in the form $e^{k\theta}$.

However, when we consider the symmetry of the problem, solutions in the form of trigonometric functions can be used advantageously. In particular, symmetry of Mode I allows to use only cosines, looking for solutions in the form $\cos(k\theta)$. Antisymmetry of Mode II is represented by sines, with the solution sought in the form $\sin(k\theta)$.

Let us now limit our attention to the symmetric problem of Mode I. Inserting $\cos(k\theta)$ into equation (A.18), we obtain the characteristic equation:

$$\begin{aligned} k^4\cos(k\theta) - 2k^2\left(s^2-2s+2\right)\cos(k\theta) + s^2(2-s)^2\cos(k\theta) = 0\,, \\ k^4 - 2k^2\left(s^2-2s+2\right) + s^2(2-s)^2 = 0\,. \end{aligned} \tag{A.19}$$

Let us now explore separately two cases: where $s \neq 2$ and where $s = 2$.

Characteristic Equation with $s \neq 2$

First, let us consider the case where $s \neq 2$ when and the characteristic equation remains as in equation (A.19). It can be shown that $k = s$ and $k = 2 - s$ are solutions of equation (A.19). First, substituting s for k:

$$\begin{aligned} s^4 - 2s^2\left(s^2-2s+2\right) + s^2(2-s)^2 = 0\,, \\ s^4 - 2s^4 + 4s^3 - 4s^2 + 4s^2 - 4s^3 + s^4 = 0\,, \\ 0 = 0\,. \end{aligned} \tag{A.20}$$

For the other solution $k = 2 - s$:

$$\begin{aligned} (2-s)^4 - 2(2-s)^2\left(s^2-2s+2\right) + s^2(2-s)^2 = 0\,, \\ (2-s)^2 - 2\left(s^2-2s+2\right) + s^2 = 0\,, \\ 4 - 4s + s^2 - 2s^2 + 4s - 4 + s^2 = 0\,, \\ 0 = 0\,. \end{aligned} \tag{A.21}$$

Thus, the function $f(\theta)$ in the factorised Airy's stress function Φ in equation (A.15) has the form:

$$f(\theta) = c_1\cos(s\theta) + c_2\cos\left[(2-s)\theta\right]\,. \tag{A.22}$$

To find the constants c_1 and c_2 and the exponent in equation (A.15), we

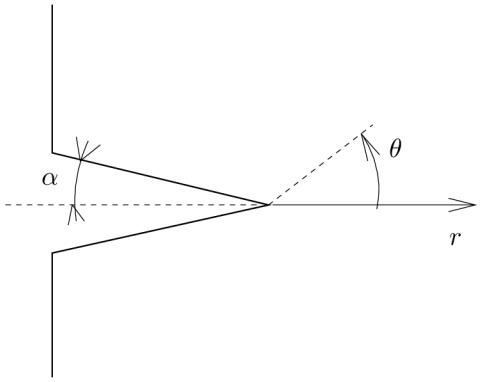

Figure A.2: *Crack tip field solution geometry.*

use the boundary conditions on the faces of the notch. The stresses perpendicular to the notch face and the shear stresses on the notch face must be equal to zero:

$$\begin{aligned} \sigma_{\theta\theta} &= 0\,, \\ \sigma_{r\theta} &= 0\,. \end{aligned} \tag{A.23}$$

Transforming the equations (A.9) into polar coordinates, we can express the stresses in terms of the equation (A.15):

$$\begin{aligned} \sigma_{\theta\theta} &= \frac{\partial^2\Phi}{\partial r^2} = K_\Phi \frac{1}{r^s}(2-s)(1-s)f(\theta)\,, \\ \sigma_{r\theta} &= -\frac{1}{r}\frac{\partial^2\Phi}{\partial r\partial\theta} = -K_\Phi \frac{1}{r^s}(1-s)f'(\theta)\,. \end{aligned} \tag{A.24}$$

If the boundary conditions (A.23) are to be fulfilled, it is apparent that at the notch face, i.e. at the angle $\theta = \pi - \alpha$, the value of $f(\theta)$ and its derivative $f'(\theta)$ must be equal to zero (for a non-trivial solution). That is:

$$\begin{aligned} c_1 \cos\left[s(\pi-\alpha)\right] + c_2 \cos\left[(2-s)(\pi-\alpha)\right] &= 0\,, \\ -c_1 s \sin\left[s(\pi-\alpha)\right] - c_2(2-s)\sin\left[(2-s)(\pi-\alpha)\right] &= 0\,. \end{aligned} \tag{A.25}$$

In matrix notation, the same equation (A.25) reads:

$$[\mathrm{T}]\,\{c\} = \{0\}\,,$$

$$\begin{bmatrix} \cos\left[s(\pi-\alpha)\right] & \cos\left[(2-s)(\pi-\alpha)\right] \\ -s\sin\left[s(\pi-\alpha)\right] & -(2-s)\sin\left[(2-s)(\pi-\alpha)\right] \end{bmatrix} \begin{bmatrix} c_1 \\ c_2 \end{bmatrix} = \begin{bmatrix} 0 \\ 0 \end{bmatrix} \tag{A.26}$$

For non-trivial solution of equation (A.25), it must hold that the determinant of the matrix [T] is equal to zero. Putting $|\mathrm{T}| = 0$, we obtain:

$$\begin{aligned} &-\cos\left[s(\pi-\alpha)\right](2-s)\sin\left[(2-s)(\pi-\alpha)\right] \\ &+s\sin\left[s(\pi-\alpha)\right]\cos\left[(2-s)(\pi-\alpha)\right] = 0\,. \end{aligned} \tag{A.27}$$

The roots of equation (A.27) are now the eigenvalues of the problem, which will yield the exponent in equation (A.15). They can be found by numerical methods, such as the interval bisection method. Based on physical considerations, we look for values within the interval $(0;1)$ only. The eigenvalues

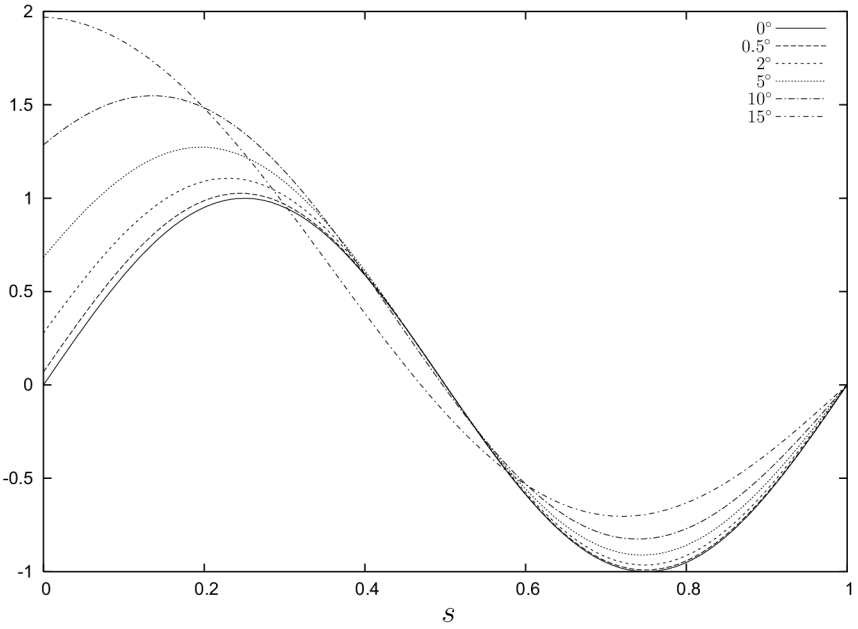

Figure A.3: *Plot of characteristic function for eigenvalues s and various notch angles α*

are listed in Table A.1 for selected angles α.

α	30°	45°	60°
s	0.488	0.456	0.384

Table A.1: Eigenvalues of equation (A.27).

Plotting the function on the left side of equation (A.27) for several chosen notch angles α, one can see the locations of the roots of (A.27) in the interval $(0;1)$ – see Fig. A.3.

For a crack, which is here the special case of a notch when $\alpha = 0$, $s = 0$ is also a root. The constant stress term of Williams eigen-series expansion corresponding to $s = 0$ is known as the T-stress.

It can be seen in Fig. A.3 that for notch angles $\alpha \neq 0$, $s = 0$ is not a root of equation (A.27) and hence also not an eigenvalue of the matrix [T] in equation (A.26). Therefore, it appears that in case of a notch, the T-stress term does not exist.

Characteristic Equation with $s = 2$

In this case, the characteristic equation (cf. A.19) will be:

$$k^4 - 4k^2 = 0\,. \tag{A.28}$$

The four roots of this equation (A.28) are $k_{1,2} = 0$, $k_{3,4} = \pm 2i$. Thus, the function $f(\theta)$ has the form:

$$f(\theta) = c_1 + c_2\theta + c_3 \sin(2\theta) + c_4 \cos(2\theta)\,. \tag{A.29}$$

Considering Mode I, the function $f(\theta)$ must be even, which leads to a reduction of equation (A.29) to

$$f(\theta) = c_1 + c_2 \cos(2\theta)\,. \tag{A.30}$$

From boundary conditions (A.23), $f(\theta)$ and its derivative $f'(\theta)$ must be equal to zero, i.e.:

$$\begin{aligned} c_1 + c_2 \cos[2(\pi - \alpha)] &= 0\,, \\ c_2 \sin[2(\pi - \alpha)] &= 0\,. \end{aligned} \tag{A.31}$$

Rearranging the equations (A.31) and replacing c_2 with the T-stress value T:

$$\begin{aligned} T\left\{\frac{c_1}{c_2} + \cos[2(\pi - \alpha)]\right\} &= 0\,, \\ T\,\{\sin[2(\pi - \alpha)]\} &= 0 \end{aligned} \tag{A.32}$$

If these equations (A.32) are to be fulfilled for any notch angle α, then the T-stress T must be equal to zero.

Thus, from a rigorous mathematical analysis of the problem as posed, it appears that the T-stress exists but in the case of a crack with zero initial opening angle.

A.3 Stress Behaviour along the Crack Front

This section of the appendix presents the results of numerical investigations of the behaviour of the stress field along the crack front, i.e. from one face of the cracked body through its thickness to the other face. This study was motivated by observations made on cracks in thin metallic foils, which have an application e.g. in micro-devices, operating as switches at frequencies ranging from 1 Hz to as much as 1 MHz. The research was induced by the hypothesis that it is possible to explain some of the crack growth behaviour of cracks in thin metallic foils by classical linear elastic fracture mechanics (LEFM) methods. The relevant effects in terms of LEFM include in particular the variation of the fracture parameter along the crack front as a result of the influence of stress singularity at the crack front corner. For obvious simplicity reasons, these initial analytical investigations are limited to the case including an edge singularity and one corner singularity. To keep the discussion even simpler, only Mode I fracture is considered; mixed mode considerations, the problem is becoming much more complex.

Before discussing the LEFM solutions, a note is made on the relevance of the present results for thin metallic sheets. Evidently, for LEFM to be applicable, it must be possible to reasonably assume that the body under investigation behaves as a continuum. In the literature (see e.g. Hadrboletz *et al.* [37]), a marked effect of microstructure on the crack propagation path and behaviour has been reported in thin sheets. Hadrboletz *et al.* [37] characterise the nature of the behaviour by the dependence on the ratio of material grain size to the foil thickness. The grain size in rolled material is in the order of a few dozens μm, while electro-deposited materials are very fine grained with grain sizes of just several μm. Grain boundaries give rise to strain gradients. The results herein are thus relevant only for thin sheets where a continuum behaviour can be reasonably assumed with regard to the grain size to sheet thickness ratio.

A.3.1 State of Stress in the Inner and Sheet Surface Regions

It is tempting to discuss the state of stress in the sheet subjected to Mode I loading in terms of plane stress or plane strain domination. This may be correct in regions sufficiently distant from the crack corner point. However, due to the presence of the corner-type singularity, the stress and displacement fields in the vicinity of the corner point are truly three-dimensional. This must be kept in mind when interpreting any numerical results.

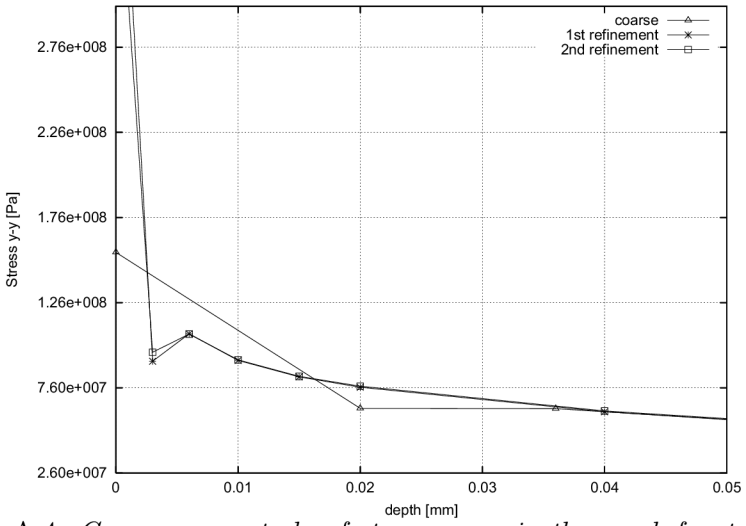

Figure A.4: *Convergence study of stresses σ_{yy} in the crack front vicinity*

A.3.2 Finite Element Modelling

In the finite element computations, the *ANSYS* [86] finite element code was used. A thin centre-cracked tension (CCT) specimen was considered with breadth $2W = 10$ mm, width $2H = 65$ mm, crack half length $a = 2.5$ mm. The model was loaded with a uniform tension of 10 MPa along the edge $y = W/2$. Three thicknesses 50 μm, 150 μm and 250 μm were considered. Due to symmetry, only 1/8 of the specimen needed to be modelled.

20-noded iso-parametric brick elements were used. In the planes perpendicular to the crack front, the finite element model had a typical fan arrangement of quarter-point elements around the crack tip, and the same geometry persisted throughout the thickness. The size of the first element at the crack front in the direction of the crack face was 3 μm. The individual layers of elements along the crack front had varying thicknesses, with the first five element layers being 3 μm thick and the next two layers 5 μm thick. The number of elements was 7462 in case of the 250 μm thick model. In addition, a smaller portion of the 50 μm model was discretised with a finer mesh to allow for better capturing of the stress distribution in the direction of the thickness. Here, the thickness of the first three element layers was only 1 μm. This reduced-size model (with a total of 13320 elements) was loaded with displacements obtained from the coarser-mesh model and applied at the respective nodes.

Fig. A.4 shows the results of a study of solution convergence with mesh

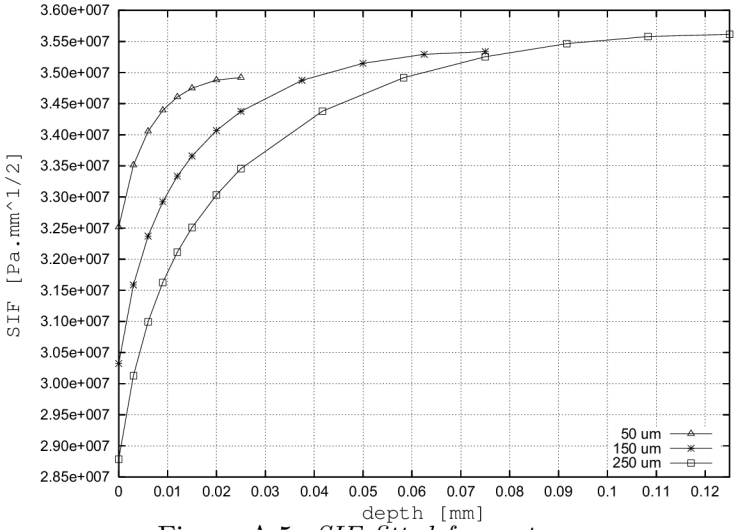

Figure A.5: *SIF fitted from stresses*

refinement on the 50 μm thick specimen. The size of the first element at the crack front in the direction normal to the crack front was 3 μm in case of the mesh denoted "coarse" in Fig. A.4 and 1 μm in the other two cases, which differ from each other by the element size in the crack front direction. This was 3 μm in case of the mesh denoted as "1$^{\text{st}}$ refinement" and 3 μm in case of the "2$^{\text{nd}}$ refinement". The plot still shows some convergence problems at the crack face even with the "2$^{\text{nd}}$ refinement", so even a finer mesh may still be needed to achieve trustable results.

Using quarter-point elements at the crack tip, a $1/\sqrt{\rho}$-type stress singularity is imposed [5]. In terms of the corner – edge singularity concept, no incorrect singularity is imposed as the order of singularity along the edge remains 1/2. The corner singularity is not explicitly modelled.

A.3.3 Computational Results

The global energy method (see paragraph 3.7.2) is used to obtain an asymptotic value of the SIF as a reference for other results. The SIF values computed are given in Table A.2. As expected, the values of SIF in Table A.2 are nearly the same for all thicknesses considered.

Figures A.5, A.6 and A.7 show the distributions of SIF obtained by fitting from stresses perpendicular to the crack face using least squares and fitting from crack opening displacements (see paragraph 3.7.1). In Fig. A.8, the SIF values obtained by the various methods are compared on the example

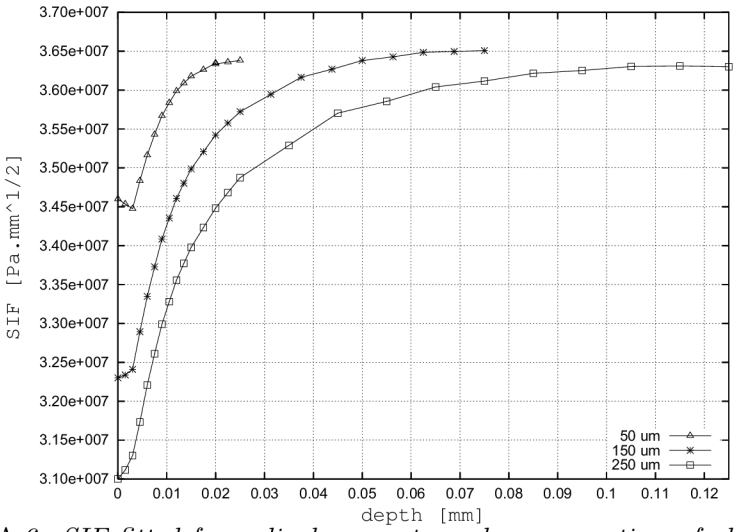

Figure A.6: *SIF fitted from displacements under assumption of plane strain*

Thickness	50 μm	150 μm	250 μm
SIF [Pa$\sqrt{\text{mm}}$]	$3.34 \cdot 10^7$	$3.23 \cdot 10^7$	$3.33 \cdot 10^7$

Table A.2: *Global SIF values*

of the 50 μm thick specimen.

Table A.3 lists the averages (weigthed by element length) along the crack front of the values of SIF computed using the various methods considered and plotted in Figs. A.5, A.6 and A.7.

Thickness	50 μm	150 μm	250 μm
Ingraffea & Manu [41], pl. strain, Fig. A.6	$3.54 \cdot 10^7$	$3.56 \cdot 10^7$	$3.57 \cdot 10^7$
Ingraffea & Manu [41], pl. stress, Fig. A.7	$3.11 \cdot 10^7$	$3.13 \cdot 10^7$	$3.14 \cdot 10^7$
Stress fitting, Fig. A.5	$3.44 \cdot 10^7$	$3.44 \cdot 10^7$	$3.46 \cdot 10^7$

Table A.3: *Averaged SIF values in* [Pa$\sqrt{\text{mm}}$] *for results plotted in Figs. A.5, A.6 and A.7*

In Fig. A.9, the stresses perpendicular to the crack face in the vicinity of the crack front are plotted using the FEM results obtained with the finest mesh considered.

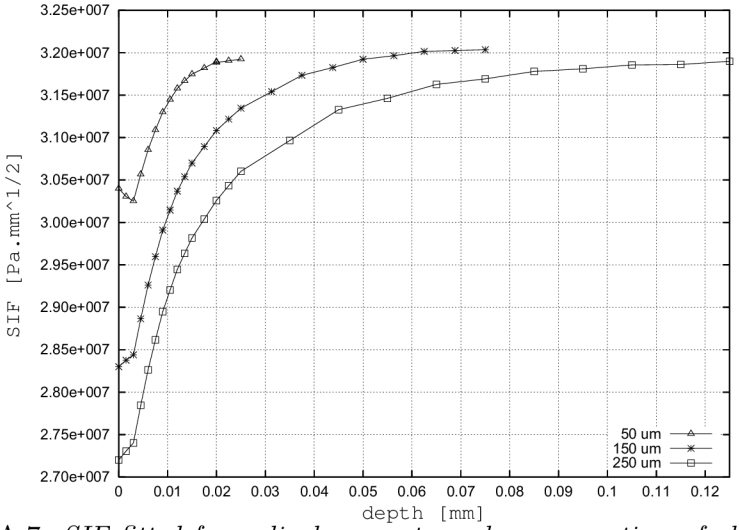

Figure A.7: *SIF fitted from displacements under assumption of plane stress*

A.3.4 Discussion of the Results

It can be seen in Fig. A.8 that throughout the specimen thickness, SIF values fitted from stresses lie between the values of the displacement fit obtained under the assumption of plane strain and plane stress, respectively. This could suggest that the actual behaviour is somewhere between plane strain and plane stress.

In Figs. A.5, A.6 and A.7, the SIF values converge to about the the same value as the specimen mid-thickness is approached (these asymptotic values somewhat differ optically in Fig. A.5, but the actual difference is within a 2 % tolerance). All of these asymptotic values are within about a 10 % deviation range from the "global" SIF values in Table A.2, obtained by the method described in paragraph 3.7.2.

The results in Figs. A.5, A.6 and A.7 seem to suggest that the surface corner point does not effect some region of a more or less constant absolute size for a given geometrical configuration with only the specimen thickness being different. Rather, there seems to be some relation between the thickness and the size of the corner influenced domain. However, it appears that these parameters are not linearly proportional – in the thinner specimen, a relatively larger portion of the specimen thickness appears to be significantly effected by the corner than in the thicker specimens. At the same time, the surface to mid-thickness SIF variation span increases with the thickness.

As can be seen in Table A.3, the crack front length average of the SIF

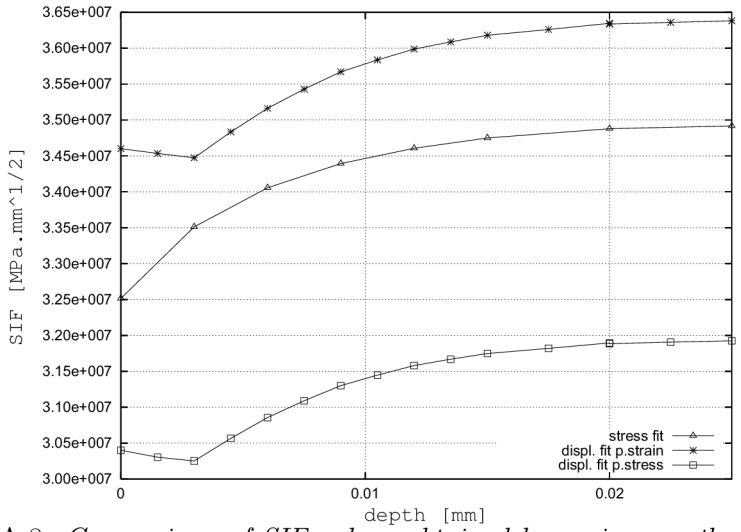

Figure A.8: *Comparison of SIF values obtained by various methods, 50 μm thick specimen*

values for a given method is the same for all thicknesses. The stress intensity is thus only differently distributed. The averages of the SIF values obtained by fitting to the stresses differ from the "global" SIF values in Table A.2 by no more than 3 to 5 %.

The stresses in the crack front vicinity (see the 3D plot in Fig. A.9) appear to be influenced by the surface corner effect in a significant way only within a small distance from the corner, about 3 to 5 μm, which is less than 10 % of the thickness (50 μm). However, as noted above, the effect observed on the SIF appears to reach deeper into the thickness.

From Fig. A.4 it appears that even with the very finely meshed model used, there are still numerical errors on the first one or two elements at the crack front. This suggests that a further refinement may be necessary.

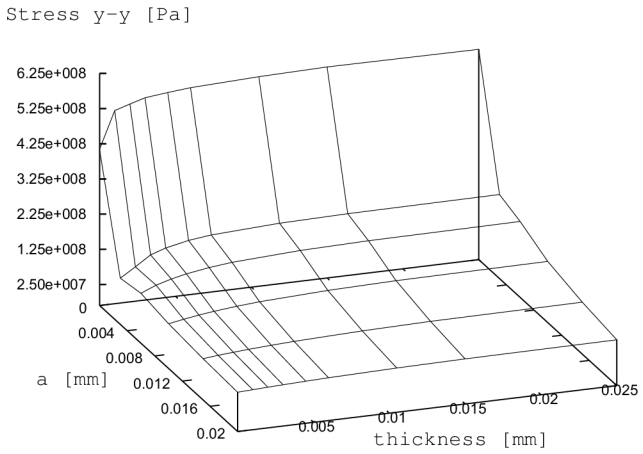

Figure A.9: *Variation of stresses σ_{yy} in the vicinity of the crack front*

A.4 The PREFFAS Method

In Section 2.6, the principles of the PREFFAS method were outlined. According to Eq. (2.27), the crack length increment can be calclated as

$$\Delta a = CF^m(a) \sum_{i=1}^{N} \left(\sigma_{\max,i} - \sigma_{0,i}\right)^m \ , \tag{A.33}$$

where C and m are the coefficients of the Pris crack growth law, $F(a)$ is the geometry factor, the index i runs through the N cycles in the load sequence considered, $\sigma_{\max,i}$ is the peak of the given stress cycle and $\sigma_{0,i}$ is the applicable crack opening stress.

This appendix provides details of the calculation of the load sequence $E_s = \sum_{i=1}^{N} \left(\sigma_{\max,i} - \sigma_{0,i}\right)^m$.

In the calculation, we process the sequence of stress peaks and troughs cycle by cycle, while constructing and storing stress cycles that will be significant for determining the opening stress level in the following cycles. Each of these significant history stress cycles consists of its maximum $H_{\max,j}$, opening stress $H_{o,j}$ and minimum $H_{\min,j}$.

Throughout the load sequence, a minimal crack opening stress $H_{o,1}$ applies, determined by the overall load maximum $H_{\max,1}$ and minimum $H_{\min,1}$ of the stress sequence using Eq. (2.23). These are the values stored as the initial history values and the PREFFAS algorithm is started.

A peak larger than $H_{\max,j}$

If the currently processed stress cycle i features a peak $\sigma_{\max,i}$ that is higher than any of the maxima stored in the history, the following procedure is carried out.

First, we find j such that $\sigma_{\max,i} > H_{\max,j}$ and $\sigma_{\max,i} < H_{\max,j-1}$. In a RainFlow-like manner, we update the sequence effect given by the history values:

$$\begin{aligned} E_s &= E_s + (\sigma_{\max,i} - H_{o,j-1})^m + \sum_{k=j}^{n} (H_{\max,k} - H_{o,k})^m \\ &- \sum_{k=j}^{n} (H_{\max,k} - H_{o,k-1})^m) \,. \end{aligned} \tag{A.34}$$

UNDERLOAD. Next, we check whether the current stress cycle presents also an underload w.r.t. $H_{\min,j-1}$, which is the minimum corresponding to $H_{\max,j}$. If so, we again find l such that $\sigma_{\min,i} < H_{\min,l}$ and $\sigma_{\min,i} > H_{\min,l-1}$, and take the corresponding maximum $H_{\max,l}$ to recalculate the crack opening stress for the history cycle l:

$$R_l = \frac{\sigma_{\min,i}}{H_{\max,l}} \,, \quad U_l = a_U R_l + b_U \,, \quad H_{o,l} = H_{\max,l} - U_l \,(H_{\max,l} - \sigma_{\min,i}) \,. \tag{A.35}$$

Due to the underload, we effectively scrap the history values from l onwards and reduce the applicable opening stress to $H_{o,l}$. If $H_{o,l} < H_{o,l-1}$, we erase the history cycle l as well and keep only the cycles up to $l-1$. The number of history values that are discarded here is determined by the underload w.r.t. l.

NO UNDERLOAD. If, on the other hand, the minimum of the current stress cycle is above all of the stored history minima, we check whether this stress cycle should be stored in the history, or whether we shall keep the history stress cycle having the maximum $H_{\max,j}$. For this purpose, we compare $H_{o,j-1}$ with $\sigma_{o,i}$, determined from Eq. (2.23).

If $\sigma_{o,i} > H_{o,j-1}$, we assign to the position j in the history the maximum, minimum and opening stress values of the cycle i, and discard all values from j onwards. Otherwise, we erase the position $j-1$ as well and retain just the history up to $j-1$.

A peak lower than the last history maximum

If the currently processed stress cycle i features a peak $\sigma_{\max,i}$ that is less than any of the history maxima, we just add a contribution to the sequence effect E_s:

$$E_s = E_s + (\sigma_{\max,i} - H_{o,m})^m \,, \tag{A.36}$$

where $H_{o,m}$ is the last opening stress stored in the history.

UNDERLOAD. In case that the cycle i presents an underload w.r.t. any of the history minima $H_{\min,m}$, we will again reduce the level of the crack opening stress and discard some of the history values. We proceed analogically to the case of a stress cycle with a new maximum and with an underload described above.

NO UNDERLOAD. This is the only case when we may add stress cycles to the recorded history. We will only do so if its opening stress level $\sigma_{o,i}$ is higher than the last of the history values $H_{o,m}$.

History values

Most of the time, a contribution to the sequence effect E_s will be calculated using Eq. (A.36) and the last crack opening stress $H_{o,m}$ stored in the history. The history will consist of stress cycles where each cycle will have a lower maximum, higher minimum and higher crack opening stress than the previous one. The history will usually not be very long, since we will occasionally add a cycle to it, but also remove cycles every time we encounter an underload.

Equivalent stress

One we have processed the entire load sequence, we obtain the cumulated stress effect E_s. This can be used to calculate an equivalent stress level σ_{eq} for any chosen number of load cycles N_{eq} and stress ratio R_{eq}:

$$\sigma_{\text{eq}} = \frac{\left(\frac{E_s}{N_{\text{eq}}}\right)^{\frac{1}{m}}}{(1 - R_{\text{eq}})\,(a_U R_{\text{eq}} + b_U)} \,. \tag{A.37}$$

Appendix B

Solution Methods Complements

B.1 Minimum Energy Principle and the Galerkin Method

In this appendix, the variational methods and in particular the Galerkin Method presented in Section 3.2 are illustrated in a greater detail by means of a simple one-dimensional example that will expose the general approach in a concise form.

An Illustration Example. Consider a linear-elastic bar in traction and compression with section $A(x)$, Young's modulus $E(x)$, of length l, statically loaded by a continuous loading $f(x)$. As regards the boundary conditions, consider both ends of the bar to be fixed for now, i.e. $u(0) = u(l) = 0$.

The governing equation of the problem is:

$$-(AE\,u')' = f \tag{B.1}$$

where the short hand notation $u' \equiv \frac{\mathrm{d}u}{\mathrm{d}x}$ was introduced and E, A and f continue to be considered as known functions of x, although the function notation was dropped for brevity.

The problem to solve reads:

$$\text{find}\, u \in V_0 \,\text{such that}\, Lu = f \tag{B.2}$$

where

$$Lu = -(AE\,u')'\,.$$

Eq. (B.2) is called the *strong form* of the problem.

B.1.1 Variational Methods

Let us first show that the variationsl solution u minimizes the potential energy Π. The potential energy of the system is:

$$\Pi(u) = \frac{1}{2}\int_0^l AE\left(u'\right)^2 \,\mathrm{d}x - \int_0^l fu\,\mathrm{d}x, u \in V_0\,, \tag{B.3}$$

where V_0 is a space of functions continuous on $\langle 0, l\rangle$ up to their second derivatives such that $u(0) = u(l) = 0$. Consider a variation of u as $w = u+\epsilon v$ such that $v \in V_0$. Then

$$\Pi(u+\epsilon v) = \epsilon\int_0^l AEu'v' - fv\,\mathrm{d}x + \frac{1}{2}\epsilon^2\int_0^l AE\left(v'\right)^2 + v^2\,\mathrm{d}x\,. \tag{B.4}$$

We take the limit

$$\lim_{\epsilon\to 0}\frac{\Pi(u+\epsilon v)-\Pi(u)}{\epsilon} \equiv \delta\Pi = \int_0^l AEu'v' - fv\,\mathrm{d}x\,. \tag{B.5}$$

$\delta\Pi$ is called the first variation of Eq. (B.2). The first term in the integral of $\delta\Pi$ is manipulated as follows:

$$\int_0^l AEu'v'\,\mathrm{d}x = \int_0^l \left(AEu'v\right)' - \left(AEu'\right)'v\,\mathrm{d}x = \int_0^l -\left(AEu'\right)'v\,\mathrm{d}x + (AEu'v)|_0^l.$$

But $v \in V_0$ vanishes at both ends, so, from Eq. (B.5):

$$\delta\Pi = \int_0^l \left(AEu'\right)'v - fv\,\mathrm{d}x = \int_0^l (Lu-f)v\,\mathrm{d}x = 0 \tag{B.6}$$

because u safisfies $Lu = f$ and $v \in V_0$. Therefore, Π has is stationary with the displacement u.

Introducing the notation

$$a(u,v) = \int_0^l AEu'v'\,\mathrm{d}x, \quad (f,v) = \int_0^l fv\,\mathrm{d}x\,, \tag{B.7}$$

$\delta\Pi = 0$ can be rewritten as $a(u,v) = (f,v)$ and we formulate the problem in its *weak form*:

$$\text{find}\, u \in V_0 \,\text{such that}\, a(u,v) = (f,v)\,\text{for all}\, v \in V_0\,. \tag{B.8}$$

It follows from Eq. (B.5) and (B.6) that the u found in this way is the solution of $Lu = f$.

B.1.2 Natural Boundary Conditions

Let us now consider the present example with different boundary conditions. Instead of fixing both ends, we prescribe a displacement at the left end: $u(0) = d_0$ and a force F_l acting on the right end $x = l$. The boundary condition on the basic variable u is called an *essential* or *Dirichlet* condition. The prescribed boundary force is termed a *natural* or *Neumann* boundary condition. Note that the latter boundary condition can be written as:

$$E(l)A(l)u'(l) = F_l \tag{B.9}$$

to match the prescribed force with the internal force.

B.1.3 The Galerkin Method

We define a space V_0 as a space of functions continuous up to the first derivative on the interval $\langle 0, l\rangle$ and vanishing at points where an essential boundary condition is prescribed, i.e. $V_0 = \{v \in C^1\langle 0, l\rangle : v(0) = 0\}$, and call a function $v \in V_0$ a *test function*.

Multiply Eq. (B.1) with a test function v, integrate over $\langle 0, l\rangle$ by parts and use the boundary condition (B.9):

$$\begin{aligned}\int_0^l f v \,\mathrm{d}x = \int_0^l \left[-\left(AEu'\right)'\right] v \,\mathrm{d}x = \\ -AEu'v|_0^l + \int_0^l \left(AEu'v'\right)\,\mathrm{d}x = \\ -F_l v(l) + \int_0^l \left(AEu'v'\right)\,\mathrm{d}x\,.\end{aligned} \tag{B.10}$$

We will seek the solution u from the space of *trial functions* $W = \{w \in C^2\langle 0, l\rangle : w(0) = d_0\}$ satisfying the Dirichlet boundary condition. We now have the following *weak form*:

$$\text{find } u \in W \text{ such that } a(u, v) = (f, v) + F_l v(l) \text{ for all } v \in V_0\,. \tag{B.11}$$

Note that the natural boundary condition has become a part of the integral equation (B.11) and is therefore automatically satisfied.

B.1.4 The Finite Element Method

When the test function v is assumed to be a series of the form $v_n(x) = \sum_i^n a_i\varphi_i(x)$, the variation of $v_n(x)$ is:

$$\delta v_n(x) = \sum_{i=1}^{n} \frac{\partial v_n(x)}{\partial a_i}\delta a_i = \varphi_1(x)\delta a_1 + \varphi_2(x)\delta a_2 + \dots . \tag{B.12}$$

Substituting such $v_n(x)$ into Eq. (B.10):

$$-F_l \sum_{i=1}^{n} a_i\varphi_i(l) + \int_0^l AEu' \sum_{i=1}^{n} \delta a_i\varphi_i(x)\,\mathrm{d}x = \int_0^l f \sum_{i=1}^{n} a_i\varphi_i(x)\,\mathrm{d}x \tag{B.13}$$

This, in general terms, is the mathematical basis of the finite element method, where both the trial functions u and test functions v are constructed using the finite element shape functions, the test functions satisfying the essential boundary conditions. Eq. (B.13) leads directly to the set of finite element equations, see Appendix B.2.

□

B.2 FEM Equations for Plane Problems

In this Appendix, it is shown how the finite element equations for a plane strain/plane stress problem can be derived based on the Galerkin weak form as outlined in Appendix B.1.

In the plane strain/plane stress problem, the solution consists of two functions, namely the displacement functions $v_1(x, y)$ and $v_2(x, y)$ in the directions of the two coordinate axes. We will use a tensor notation and the new introduced matrices will also be exposed in full.

B.2.1 Plane Strain/Plane Stress – Governing Equations

The problem unknowns and the body forces are collected in vectors:

$$\begin{aligned}
\text{displacements}: \quad & \mathbf{u} = [u_x \; u_y]^T \,, \\
\text{strains}: \quad & \boldsymbol{\epsilon} = [\epsilon_{xx} \; \epsilon_{yy} \; 2\epsilon_{xy}]^T = \left[\frac{\partial v_1}{\partial x}, \frac{\partial v_2}{\partial y}, \frac{\partial v_1}{\partial y} + \frac{\partial v_2}{\partial x}\right]^T \,, \\
\text{stresses}: \quad & \boldsymbol{\sigma} = [\sigma_{xx} \; \sigma_{yy} \; \sigma_{xy}]^T \,, \\
\text{body forces}: \quad & \boldsymbol{f} = [f_1, f_2]^T \,.
\end{aligned}$$

We have the following governing equations:

$$\begin{aligned} \text{equilibrium} \quad &: \quad \mathbf{D}^T\boldsymbol{\sigma} + \boldsymbol{f} = \mathbf{0}\,, && \text{(B.14)}\\ \text{kinematic} \quad &: \quad \boldsymbol{\epsilon} = \mathbf{D}\mathbf{u}\,, && \text{(B.15)}\\ \text{constitutive} \quad &: \quad \boldsymbol{\sigma} = \mathbf{E}\boldsymbol{\epsilon}\,. && \text{(B.16)} \end{aligned}$$

The gradient operator matrix $\mathbf{D}$ reads:

$$\mathbf{D} = \begin{bmatrix} \frac{\partial}{\partial x} & 0 \\ 0 & \frac{\partial}{\partial y} \\ \frac{\partial}{\partial y} & \frac{\partial}{\partial x} \end{bmatrix}\,. \tag{B.17}$$

For isotropic materials with Young's modulus E and Poisson's ratio ν the stress-strain matrix is for plane stress:

$$\mathbf{E} = \frac{E}{1-\nu^2}\begin{bmatrix} 1 & \nu & 0 \\ \nu & 1 & 0 \\ 0 & 0 & \frac{(1-\nu)}{2} \end{bmatrix}\,, \tag{B.18}$$

and for plane strain:

$$\mathbf{E} = \frac{E}{(1+\nu)(1-2\nu)}\begin{bmatrix} 1-\nu & \nu & 0 \\ \nu & 1-\nu & 0 \\ 0 & 0 & \frac{(1-2\nu)}{2} \end{bmatrix}\,. \tag{B.19}$$

Alternatively, introducing the Lamé constants

$$\begin{gathered} \mu = \tfrac{E}{2(1+\nu)}\,, \\ \lambda = \tfrac{\nu E}{1-\nu^2}\ \text{(plane stress)}\,, \quad \lambda = \tfrac{\nu E}{(1+\nu)(1-2\nu)}\ \text{(plane strain)}\,, \end{gathered} \tag{B.20}$$

the stress-strain matrix can be written as:

$$\mathbf{E} = \begin{bmatrix} \lambda+2\mu & \lambda & 0 \\ \lambda & \lambda+2\mu & 0 \\ 0 & 0 & \mu \end{bmatrix}\,. \tag{B.21}$$

B.2.2 Boundary Conditions

On the Dirichlet boundary Γ_u, displacements are prescribed:

$$u_1 = d_1, \quad u_2 = d_2 \quad \text{on}\,\Gamma_u\,. \tag{B.22}$$

On the Neumann boundary Γ_t, the static boundary conditions are:

$$\sigma_{xx}n_x + \sigma_{xy}n_y = T_1, \quad \sigma_{yy}n_y + \sigma_{xy}n_x = T_2 \quad \text{on}\,\Gamma_t\,, \tag{B.23}$$

in which $\mathbf{n} = (n_x, n_y)^T$ is the unit vector of the outward normal to the boundary Γ. We note that for the total boundary Γ, the following holds: $\Gamma = \Gamma_u \cup \Gamma_t$, whereby $\Gamma_u \cap \Gamma_t = \emptyset$.

B.2.3 Weak Form

Let us define a space X of function couples $\mathbf{v}(x,y) = (v_1(x,y), v_2(x,y))^T$ as $X = \left\{\mathbf{v} | v_1(x,y) \in H^1(\Omega),\, v_2(x,y) \in H^1(\Omega)\right\}$, where Ω is the domain of the two-dimensional body in consideration and H^1 is a normed space of square-integrable functions continuous up to the first derivative.

Test functions will be chosen from the space $V = \{\mathbf{v} \in X | \mathbf{v} = 0 \,\text{on}\,\Gamma_u\}$. Solution is sought in the trial functions space $W = \{\mathbf{u} \in X | \mathbf{u} = \mathbf{d} \,\text{on}\,\Gamma_u\}$, in which $\mathbf{d} = \{d_1, d_2\}^T$ is the prescribed displacement.

The static equilibrium equations (B.14) written out in full read:

$$\frac{\partial \sigma_{xx}}{\partial x} + \frac{\partial \sigma_{xy}}{\partial y} + f_1 = 0, \quad \frac{\partial \sigma_{yy}}{\partial y} + \frac{\partial \sigma_{xy}}{\partial x} + f_2 = 0\,. \tag{B.24}$$

In a manner analogous to the procedure used in the Galerkin method, multiply the first of the above equations (B.24) by v_1 and the second one by v_2, add up the two equations and integrate over Ω. Then, using the Green's theorem, the Neumann boundary conditions (B.23), the kinematic equations (B.15) and the Hooke's law (B.16), we find:

$$\begin{aligned}
&\int_\Omega \left[\left(\frac{\partial \sigma_{xx}}{\partial x} + \frac{\partial \sigma_{xy}}{\partial y} + f_1 \right) v_1 + \left(\frac{\partial \sigma_{yy}}{\partial y} + \frac{\partial \sigma_{xy}}{\partial x} + f_2 \right) v_2 \right] \mathrm{d}x\mathrm{d}y = \\
&= \int_\Gamma \left[\left(\sigma_{xx}n_x + \sigma_{xy}n_y \right) v_1 + \left(\sigma_{yy}n_y + \sigma_{xy}n_x \right) v_1 \right] \mathrm{d}S - \\
&- \int_\Omega \left(\sigma_{xx}\frac{\partial v_1}{\partial x} + \sigma_{xy}\frac{\partial v_1}{\partial y} + \sigma_{xy}\frac{\partial v_2}{\partial x} + \sigma_{yy}\frac{\partial v_2}{\partial y} \right) \mathrm{d}x\mathrm{d}y + \\
&+ \int_\Omega \left(f_1 v_1 + f_2 v_2 \right) \mathrm{d}x\mathrm{d}y = \\
&= \int_{\Gamma_t} \left(T_1 v_1 + T_2 v_2 \right) \mathrm{d}S - \int_\Omega \boldsymbol{\epsilon}(\mathbf{v}) \cdot \boldsymbol{\sigma}\, \mathrm{d}x\mathrm{d}y + \int_\Omega \mathbf{v} \cdot \mathbf{f} \mathrm{d}x\mathrm{d}y = \\
&= \int_{\Gamma_t} \mathbf{v} \cdot \mathbf{T}\, \mathrm{d}S - \int_\Omega \boldsymbol{\epsilon}(\mathbf{v}) \cdot \mathbf{E}\boldsymbol{\epsilon}(\mathbf{u})\, \mathrm{d}x\mathrm{d}y + \int_\Omega \mathbf{v} \cdot \mathbf{f}\, \mathrm{d}x\mathrm{d}y\,.
\end{aligned}$$

Therefore, we may write the weak form of the plane strain/stress problem as follows:

$$\text{find}\,\mathbf{u} \in W \,\text{such that}\, a(\mathbf{u},\mathbf{v}) = L(\mathbf{v}) \,\text{for all}\, \mathbf{v} \in V\,, \tag{B.25}$$

where

$$a(\mathbf{u},\mathbf{v}) = \int_\Omega \boldsymbol{\epsilon}(\mathbf{v}) \cdot \mathbf{E}\boldsymbol{\epsilon}(\mathbf{u})\,\mathrm{d}x\mathrm{d}y\,, \tag{B.26}$$

$$L(\mathbf{v}) = \int_\Omega \mathbf{v}\cdot\mathbf{f}\,\mathrm{d}x\mathrm{d}y + \int_{\Gamma_t} \mathbf{v}\cdot\mathbf{T}\,\mathrm{d}S\,. \tag{B.27}$$

B.2.4 Discrete Weak Form

We discretise the domain Ω into elements. We may for example use some triangulation to get triangular elements. The elements have a total of NN nodes, including BN nodes on the Dirichlet boundary (in which displacements are prescribed) and $IN = NN - BN$ interior nodes.

We can then define a space X_h of functions that are piecewise (or rather element-wise) continous up to the first derivative. The test functions space is defined as:

$$V_h = \{\mathbf{v} | v_1 \in X_h, v_2 \in X_h \,\wedge\, \mathbf{v}(P_j) = \mathbf{0}\,\forall\, P_j \in \Gamma_u\}\,, \tag{B.28}$$

where $P_j \in \Gamma_u$ are the nodes on the essential (Dirichlet) boundary. The trial functions belong to the space:

$$W_h = \{\mathbf{U}_h | v_1 \in X_h, v_2 \in X_h \,\wedge\, \mathbf{U}_h(P_j) = \mathbf{d}\,\forall\, P_j \in \Gamma_u\}\,, \tag{B.29}$$

in which $\mathbf{d}$ stands for the prescribed displacements. The test and trial functions can then be represented as follows:

$$\mathbf{v}(x,y) = \sum_{j=1}^{IN} [v_1(x_j,y_j)N_j(x,y) + v_2(x_j,y_j)N_j(x,y)] \tag{B.30}$$

$$\begin{aligned}\mathbf{U}_h(x,y) &= \sum_{j=1}^{IN} [v_1(x_j,y_j)N_j(x,y) + v_2(x_j,y_j)N_j(x,y)] + \\ &+ \sum_{j=IN+1}^{NN} [d_1(x_j,y_j)N_j(x,y) + d_2(x_j,y_j)N_j(x,y)]\,,\end{aligned} \tag{B.31}$$

where N_j are base functions chosen from the space X_h such that $N_j = 1$ at the node P_j and $N_j = 0$ at all other nodes. Note that this corresponds to the *partition of unity* concept discussed in Section 3.3.

We then write the discrete weak form of the plane strain/stress problem as:

$$\text{find}\,\mathbf{U}_h \in W_h \,\text{such that}\, a(\mathbf{U}_h, \mathbf{v}) = L(\mathbf{v})\,\forall\,\mathbf{v} \in V_h\,, \tag{B.32}$$

where

$$a_h(\mathbf{U}_h, \mathbf{v}) = \sum_{e\in\Omega} \int_{\Omega_e} \boldsymbol{\epsilon}(\mathbf{v}) \cdot \mathbf{E}\,\boldsymbol{\epsilon}(\mathbf{U}_h)\,\mathrm{d}\Omega_e\,, \tag{B.33}$$

$$L_h(\mathbf{v}) = \sum_{e\in\Omega} \int_{\Omega_e} \mathbf{v}\cdot\mathbf{f}\,\mathrm{d}\Omega_e + \sum_{\Gamma_e\in\Gamma_t} \int_{\Gamma_e} \mathbf{v}\cdot\mathbf{T}\,\mathrm{d}\Gamma_e\,. \tag{B.34}$$

The integral over an element Ω_e or over a boundary element edge Γ_e is evaluated using Gauss quadrature. Denoting the value of the components U_1 and U_2 of the discretised solution $\mathbf{U}_h$ at node P_j as U_{j1} and U_{j2}, respectively, and denoting the components v_1 and v_2 of the test function $\mathbf{v}$ at node P_i as Θ_{i1} and Θ_{i2}, respectively, we may rewrite Eq. (B.30) and (B.31) as:

$$\mathbf{v}(x,y) = \sum_{i=1}^{IN} [\Theta_{i1}N_i(x,y) + \Theta_{i2}N_i(x,y)] \tag{B.35}$$

$$\begin{aligned}\mathbf{U}_h(x,y) &= \sum_{j=1}^{IN} [U_{j1}N_j(x,y) + U_{j2}N_j(x,y)] + \\ &+ \sum_{j=IN+1}^{NN} [d_1(x_j,y_j)N_j(x,y) + d_2(x_j,y_j)N_j(x,y)]\,.\end{aligned} \tag{B.36}$$

B.2.5 Element Matrices and Vectors

To formulate the finite element equations based on the weak form (B.32), we further proceed as follows. The base functions defined on an element with n nodes are arranged in the matrix

$$\mathbf{N}^e = \begin{bmatrix} N_1^e & 0 & N_2^e & 0 & \dots & N_n^e & 0 \\ 0 & N_1^e & 0 & N_2^e & \dots & 0 & N_n^e \end{bmatrix}, \tag{B.37}$$

the values of the element nodal displacements in the vector

$$\mathbf{U}^e = \begin{bmatrix} U_{11}^e & U_{12}^e & U_{21}^e & U_{22}^e & \dots & U_{n1}^e & U_{n2}^e \end{bmatrix}, \tag{B.38}$$

and the element nodal values of the test function in the vector

$$\boldsymbol{\Theta}^e = \begin{bmatrix} \Theta_{11}^e & \Theta_{12}^e & \Theta_{21}^e & \Theta_{22}^e & \dots & \Theta_{n1}^e & \Theta_{n2}^e \end{bmatrix}. \tag{B.39}$$

We further define the strain-displacement matrix $\mathbf{B}$ of the size $3 \times 2n$ (n is the number of element nodes)

$$\mathbf{B}^e = \mathbf{D}\,\mathbf{N}^e = \begin{bmatrix} \frac{\partial N_1^e}{\partial x} & 0 & \frac{\partial N_2^e}{\partial x} & 0 & \dots & \frac{\partial N_n^e}{\partial x} & 0 \\ 0 & \frac{\partial N_1^e}{\partial y} & 0 & \frac{\partial N_2^e}{\partial y} & \dots & 0 & \frac{\partial N_n^e}{\partial y} \\ \frac{\partial N_1^e}{\partial y} & \frac{\partial N_1^e}{\partial x} & \frac{\partial N_2^e}{\partial y} & \frac{\partial N_2^e}{\partial x} & \dots & \frac{\partial N_n^e}{\partial y} & \frac{\partial N_n^e}{\partial x} \end{bmatrix}, \tag{B.40}$$

allowing us to write the kinematic relation (B.15) in the discretised form $\boldsymbol{\epsilon}$=$\mathbf{Bu}$, and assume that the elasticity matrix $\mathbf{E}$ is constant over the element. We are then able to write the integrals in Eq. (B.33) and (B.34) as follows:

$$\begin{aligned} \int_{\Omega_e} \boldsymbol{\epsilon}^e(\mathbf{v}) \cdot \mathbf{E}^e \boldsymbol{\epsilon}^e(\mathbf{U}_h)\,\mathrm{d}\Omega_e &= [\boldsymbol{\Theta}^e]^T \int_{\Omega_e} [\mathbf{B}^e]^T\,\mathbf{E}^e\mathbf{B}^e\,\mathrm{d}\Omega_e\,\mathbf{U}^e = \\ &= [\boldsymbol{\Theta}^e]^T\mathbf{K}^e\mathbf{U}^e, \qquad \text{(B.41)} \\ \int_{\Omega_e} \mathbf{v}\cdot\mathbf{f}\,\mathrm{d}\Omega_e &= [\boldsymbol{\Theta}^e]^T \int_{\Omega_e} [\mathbf{N}^e]^T\,\mathbf{f}\,\mathrm{d}\Omega_e = [\boldsymbol{\Theta}^e]^T\mathbf{F}^e, \qquad \text{(B.42)} \\ \int_{\Gamma_e} \mathbf{v}\cdot\mathbf{T}\,\mathrm{d}\Gamma_e &= [\boldsymbol{\Theta}^s]^T \int_{\Gamma_e} [\mathbf{N}^e]^T\mathbf{T}\,\mathrm{d}\Gamma_e = [\boldsymbol{\Theta}^s]^T\mathbf{F}^s. \qquad \text{(B.43)} \end{aligned}$$

Substituting into Eq. (B.32), we find

$$0 = a_h(\mathbf{U}_h, \mathbf{v}) - L_h(\mathbf{v}) = \sum_{e\in\Omega} [\boldsymbol{\Theta}^s]^T(\mathbf{K}^e\mathbf{U}^e - \mathbf{F}^e) - \sum_{S\in\Gamma_t} [\boldsymbol{\Theta}^s]^T\mathbf{F}^s \tag{B.44}$$

and invoking the arbitrariness of the variations and thus the arbitrariness of the vectors $\boldsymbol{\Theta}^e$ and $\boldsymbol{\Theta}^s$, we finally obtain the familiar finite element equation at the element level:

$$\mathbf{K}^e\mathbf{U}^e = \mathbf{F}^e + \mathbf{F}^s\,. \tag{B.45}$$

$\mathbf{K}^e$ is called the element stiffness matrix and $\mathbf{F}^e + \mathbf{F}^s$ is called the element load vector.

Isoparametric Elements

On isoparametric elements, the shape functions are defined in terms of local geometrical coordinates on the element. E.g. for quadrilaterals, these coordinates vary between -1 and 1. The global geometric position of a point on the element is established by interpolating the nodal global coordinate to that point using the shape functions in the same way as the displacements are interpolated (therefore the term isoparametric):

$$x = \sum_{i=1}^{n} x_i N_i^e\,, \quad y = \sum_{i=1}^{n} y_i N_i^e\,. \tag{B.46}$$

When strains are calculated using Eq. (B.40), the partial derivatives of the shape functions with respect to the local coordinates ξ, η are easily found. These derivatives need to be transformed to partial derivatives with respect to the global coordinates x, y using the Jacobian matrix:

$$\begin{bmatrix} \frac{\partial N_i^e}{\partial x} \\ \frac{\partial N_i^e}{\partial y} \end{bmatrix} = \begin{bmatrix} \frac{\partial \xi}{\partial x} & \frac{\partial \eta}{\partial x} \\ \frac{\partial \xi}{\partial y} & \frac{\partial \eta}{\partial y} \end{bmatrix} \begin{bmatrix} \frac{\partial N_i^e}{\partial \xi} \\ \frac{\partial N_i^e}{\partial \eta} \end{bmatrix} = \mathbf{J}^{-1} \begin{bmatrix} \frac{\partial N_i^e}{\partial \xi} \\ \frac{\partial N_i^e}{\partial \eta} \end{bmatrix} \tag{B.47}$$

Let us now calculate the elements $\frac{\partial x}{\partial \xi}, \ldots$ of the Jacobian matrix. Substituting for the global coordinates from Eq. (B.46) and differentiating with respect to the local coordinates, we have:

$$\begin{aligned} \frac{\partial x}{\partial \xi} &= \sum_{i=1}^{n} x_i \frac{\partial N_i^e}{\partial \xi}\,, \quad \frac{\partial y}{\partial \xi} = \sum_{i=1}^{n} y_i \frac{\partial N_i^e}{\partial \xi}\,, \\ \frac{\partial x}{\partial \eta} &= \sum_{i=1}^{n} x_i \frac{\partial N_i^e}{\partial \eta}\,, \quad \frac{\partial y}{\partial \eta} = \sum_{i=1}^{n} y_i \frac{\partial N_i^e}{\partial \eta}\,. \end{aligned}$$

Because the nodal coordinates x_i, y_i do not depend on ξ, η, the Jacobian can be written as:

$$\mathbf{J} = \mathbf{P}\mathbf{X} = \begin{bmatrix} \frac{\partial N_1^e}{\partial \xi} & \frac{\partial N_2^e}{\partial \xi} & \cdots & \frac{\partial N_n^e}{\partial \xi} \\ \frac{\partial N_1^e}{\partial \eta} & \frac{\partial N_2^e}{\partial \eta} & \cdots & \frac{\partial N_n^e}{\partial \eta} \end{bmatrix} \begin{bmatrix} x_1 & y_1 \\ x_2 & y_2 \\ \vdots & \vdots \\ x_n & y_n \end{bmatrix}. \tag{B.48}$$

The inverse Jacobian $\mathbf{J}^{-1}$ is obtained by numerical inversion.

B.2.6 Numerical Integration and Assembly

The stiffness matrix and the load vector appearing in equation Eq. (B.45) are calculated using a Gauss quadrature. In the computer implementation, the contributions from the individual quadrature points are usually directly added to the respective positions in the global stiffness matrix. To this end, a mapping between the local and global numbers of the element degrees of freedom (DOF) is necessary. If $r = k \ldots l$ is the sequence of the global DOF of the element nodes, w_j is the weight of the quadrature point q_j of the m quadrature points on the element e, then the elements at the positions (r, r) of global stiffness matrix $\mathbf{K}$ are computed as follows:

$$\mathbf{K}(r,r) = \mathbf{K}(r,r) + \sum_{e} \sum_{j}^{m} \mathbf{B}^T \mathbf{E} \mathbf{B}\, w_j \left|\mathbf{J}\right|\,. \tag{B.49}$$

The global load vector $\mathbf{F}$ is computed likewise by numerical integration. It is a sum of the surface forces and the body forces. For example, the contribution of the body forces acting on the element to the positions (r) of the global load vector $\mathbf{F}$ are, c.f. Eq. (B.42):

$$\mathbf{F}(r) = \mathbf{F}(r) + \sum_{e} \sum_{j}^{m} \mathbf{N}(q_j)\, f(q_j)\, w_j\, |\mathbf{J}| \;, \tag{B.50}$$

where $\mathbf{N}(q_j)$ is the value of the shape function at the quadrature point q_j and $f(q_j)$ is the value of the body force at the quadrature point.

B.3 Moving Least Squares Approximation

In the moving least squares (MLS) approximation, the displacement field approximation is constructed separately for each integration point. The function basis of the approximation is usually polynomial, but an enriched basis can be used to account e.g. for cracks in the domain of interest [28]. The idea is to minimise for the given point of interest the sum of squares of the differences between the approximation and the nodal value at the nodes of influence. Each node is thereby given a certain weight in the minimisation depending on its distance from the point of interest.

In the case of a polynomial base, the value of the approximating function $u^h(\mathbf{x})$ at any point $\mathbf{x}$ in the domain Ω is given for an approximating polynomial constructed for the point of interest $\boldsymbol{\xi}$ by:

$$u^h(\mathbf{x}) = \sum_{i=1}^{m} p_i(\mathbf{x}) a_i(\boldsymbol{\xi}) = \mathbf{p}^T(\mathbf{x})\mathbf{a}(\boldsymbol{\xi}) \tag{B.51}$$

where m is the number of terms in the polynomial, $\mathbf{a}(\boldsymbol{\xi})$ are the coefficients of the approximation polynomial, and $\mathbf{p}^T(\mathbf{x})$ is a base of monomes, which may consist in a 2D case of

$$\mathbf{p}^T(\mathbf{x}) = \{p_1(\mathbf{x}), \ldots, p_m(\mathbf{x})\} = \left\{1, x, y, xy, x^2, y^2, \ldots\right\} \;. \tag{B.52}$$

Note that the number n of nodes whose support domains contain the point $\boldsymbol{\xi}$ must satisfy $n > m$ so that $\mathbf{a}(\boldsymbol{\xi})$ can be determined.

At the location $\mathbf{x}_I$ of a node I, u_h will amount to

$$u^h(\mathbf{x}_I) = \mathbf{p}^T(\mathbf{x}_I)\mathbf{a}(\boldsymbol{\xi}) \tag{B.53}$$

and we want to minimise the squares of the differences $u^h(\mathbf{x}_I) - \mathbf{u}_I$, with $\mathbf{u}_I$ being the known values at nodes. Note that this is a least squares technique,

so after $\mathbf{a}(\boldsymbol{\xi})$ have been found, the approximation $u^h(\mathbf{x})$ will not pass through the nodal values.

The weight of each node in the minimisation is determined by a weighting function $w_I(\boldsymbol{\xi}\text{-}\mathbf{x}_I)$ such that $w(0) = 1$ (i.e. for $\boldsymbol{\xi} = \mathbf{x}_I$) and $w = 0$ for all $\boldsymbol{\xi}$ outside the support domain of node I. In summary, we seek to minimise

$$R(\boldsymbol{\xi}) = \sum_{j=1}^{n} w_I(\boldsymbol{\xi} - \mathbf{x}_I) \left[\mathbf{p}^T(\mathbf{x})\mathbf{a}(\boldsymbol{\xi}) - \mathbf{u}_I\right]^2 . \tag{B.54}$$

Upon expanding the squared term, the minimum condition $\frac{\partial R}{\partial \mathbf{a}} = 0$ gives the following set of equations:

$$\mathbf{A}(\boldsymbol{\xi})\mathbf{a}(\boldsymbol{\xi}) - \mathbf{B}(\boldsymbol{\xi})\mathbf{u}_I = \mathbf{0} \tag{B.55}$$

with

$$\mathbf{A}(\boldsymbol{\xi}) = \left[w_I(\boldsymbol{\xi} - \mathbf{x}_I)\mathbf{p}(\mathbf{x}_I)\mathbf{p}^T(\mathbf{x}_I)\right] , \quad \mathbf{B}(\boldsymbol{\xi}) = \left[w_I(\boldsymbol{\xi} - \mathbf{x}_I)\mathbf{p}(\mathbf{x}_I)\right] . \tag{B.56}$$

Remembering that $u^h(\mathbf{x}) = \mathbf{p}^T(\mathbf{x})\mathbf{a}(\boldsymbol{\xi})$, the approximation can be finally expressed as:

$$u^h(\mathbf{x}) = \mathbf{p}^T(\mathbf{x})\mathbf{A}^{-1}(\boldsymbol{\xi})\mathbf{B}(\boldsymbol{\xi})\mathbf{u}_I \quad \text{or} \quad u^h(\mathbf{x}) = \boldsymbol{\Phi}_I(\boldsymbol{\xi}, \mathbf{x})\mathbf{u}_I , \tag{B.57}$$

where

$$\boldsymbol{\Phi}_I(\boldsymbol{\xi}, \mathbf{x}) = \mathbf{p}^T(\mathbf{x})\mathbf{A}^{-1}(\boldsymbol{\xi})\mathbf{B}(\boldsymbol{\xi}) \tag{B.58}$$

is the MLS shape function.

For completeness, we note that the derivative of the MLS shape function can be computed as:

$$\boldsymbol{\Phi}_{I,x} = \mathbf{p}_{,x}^T\mathbf{A}^{-1}\mathbf{B} + \mathbf{p}^T\left(-\mathbf{A}^{-1}\mathbf{A}_{,x}\mathbf{A}^{-1}\right)\mathbf{B} + \mathbf{p}^T\mathbf{A}^{-1}\mathbf{B}_{,x} , \tag{B.59}$$

where the functional notation has been dropped and indicial notation for derivatives used to reduce clutter. Note that the derivative of $\mathbf{A}^{-1}$ is not necessary.

Finally, a note should be made about the enforcement of essential boundary conditions in an element free Galerkin method (EFGM) using MLS approximation. This is not as straightforward as in the finite element method, where it suffices to prescribe the respective nodal displacements. As it has been said above, the MLS approximation does not pass through the nodal values it approximates. Various approaches have been proposed to remedy this problem. From among the common ones, let us mention Lagrange multipliers and a coupling with a finite element domain, where a transition by weighting is effectuated between the approximations in the FEM and the EFGM domains.

Appendix C

The Direct Differentiation Method

The presentation in this Section consists merely in a simplification of the developments in [39] to the static, linear elastic case.

When the finite element equation (B.45) is written at the global level and with the definitons introduced in equations (B.41) to (B.43), we have:

$$\int_\Omega \mathbf{B}^T\mathbf{E}\mathbf{B}\,\mathrm{d}\Omega\,\mathbf{U} = \int_\Omega \mathbf{N}^T\mathbf{f}\,\mathrm{d}\Omega + \int_\Gamma \mathbf{N}^T\mathbf{T}\,\mathrm{d}\Gamma\,. \tag{C.1}$$

Note that $\mathbf{EBU}$ is the internal stress $\boldsymbol{\sigma}$. This notation will be introduced now for brevity. We can thus write:

$$\underbrace{\int_\Omega \boldsymbol{\sigma}\mathbf{B}\,\mathrm{d}\Omega}_{\mathbf{P}_{\mathrm{int}}} = \underbrace{\int_\Omega \mathbf{f}\mathbf{N}\,\mathrm{d}\Omega + \int_\Gamma \mathbf{T}\mathbf{N}\,\mathrm{d}\Gamma}_{\mathbf{P}_{\mathrm{ext}}}\,, \tag{C.2}$$

which expresses the balance of the internal forces $\mathbf{P}_{\mathrm{int}}$ and the external forces $\mathbf{P}_{\mathrm{ext}}$. Differentiating Eq. (C.2) with respect to a parmeter h, the sensitivity in respect of which is of interest, we get:

$$\frac{\partial \mathbf{P}_{\mathrm{int}}}{\partial \mathbf{u}}\frac{\partial \mathbf{u}}{\partial h} + \left.\frac{\partial \mathbf{P}_{\mathrm{int}}}{\partial h}\right|_{\mathbf{u}\,\mathrm{fixed}} = \frac{\partial \mathbf{P}_{\mathrm{ext}}}{\partial h}\,. \tag{C.3}$$

We introduce the tangent stiffness matrix

$$\overline{\mathbf{K}} = \frac{\partial \mathbf{P}_{\mathrm{int}}}{\partial \mathbf{u}} = \int_\Omega \frac{\partial \boldsymbol{\sigma}}{\partial \mathbf{u}}\mathbf{B}\,\mathrm{d}\Omega = \int_\Omega \frac{\partial \boldsymbol{\sigma}}{\partial \boldsymbol{\epsilon}}\frac{\partial \boldsymbol{\epsilon}}{\partial \mathbf{u}}\mathbf{B}\,\mathrm{d}\Omega = \int_\Omega \mathbf{B}^T\frac{\partial \boldsymbol{\sigma}}{\partial \boldsymbol{\epsilon}}\mathbf{B}\,\mathrm{d}\Omega\,. \tag{C.4}$$

In the *linear* elastic case, the tangent stiffness matrix is equivalent to the stiffness matrix itself since the Hooke's law remains valid: $\frac{\partial \boldsymbol{\sigma}}{\partial \boldsymbol{\epsilon}} = \mathbf{E}$. Denoting the displacement sensitivity as $\frac{\partial \mathbf{u}}{\partial h}$ as $\mathbf{a}$, we may rewrite Eq. (C.3) as:

$$\overline{\mathbf{K}}\mathbf{a} = \frac{\partial \mathbf{P}_{\text{ext}}}{\partial h} - \left.\frac{\partial \mathbf{P}_{\text{int}}}{\partial h}\right|_{\mathbf{u}\,\text{fixed}} . \tag{C.5}$$

This is the key equation, from which the displacement sensitivities $\mathbf{a}$ can be directly obtained in our static, linear elastic analysis. Then, one may calculate from $\mathbf{a}$ the sensitivities of the derived response quantities, such as the stresses. This is done in the same way as the derived response quantities themselves are calculated using the displacement vector $\mathbf{u}$.

In line with the presentation in [39], the equations to calculate $\frac{\partial \mathbf{P}_{\text{int}}}{\partial h}$ and $\frac{\partial \mathbf{P}_{\text{ext}}}{\partial h}$ will be given next.

C.1 Sensitivity with Respect to a Material Parameter

When the parameter h of interest is a material parameter, the derivative of the external force vector $\frac{\partial \mathbf{P}_{\text{ext}}}{\partial h}$ vanishes, since it does not depend on the material parameters.

From Eq. (C.2), where the internal force vector is

$$\mathbf{P}_{\text{int}} = \int_{\Omega} \boldsymbol{\sigma}\mathbf{B}\,\mathrm{d}\Omega\,, \tag{C.6}$$

and differentiate Eq. (C.6) with respect to h, which is now a material parameter:

$$\frac{\partial \mathbf{P}_{\text{int}}}{\partial \mathbf{u}}\frac{\partial \mathbf{u}}{\partial h} + \left.\frac{\partial \mathbf{P}_{\text{int}}}{\partial h}\right|_{\mathbf{u}\,\text{fixed}} = \int_{\Omega} \frac{\partial \boldsymbol{\sigma}}{\partial h}\mathbf{B}\,\mathrm{d}\Omega \tag{C.7}$$

We introduce the notation $\overline{\mathbf{K}} = \frac{\partial \mathbf{P}_{\text{int}}}{\partial \mathbf{u}}$ defined above and expand the derivatives by the chain rule:

$$\overline{\mathbf{K}}\frac{\partial \mathbf{u}}{\partial h} + \left.\frac{\partial \mathbf{P}_{\text{int}}}{\partial h}\right|_{\mathbf{u}\,\text{fixed}} = \int_{\Omega} \left[\frac{\partial \boldsymbol{\sigma}}{\partial \boldsymbol{\epsilon}}\frac{\partial \boldsymbol{\epsilon}}{\partial h} + \left.\frac{\partial \boldsymbol{\sigma}}{\partial h}\right|_{\boldsymbol{\epsilon}\,\text{fixed}}\right]\mathbf{B}\,\mathrm{d}\Omega\,. \tag{C.8}$$

Also the strain derivative is expaned by the chain rule:

$$\frac{\partial \boldsymbol{\epsilon}}{\partial h} = \frac{\partial \boldsymbol{\epsilon}}{\partial \mathbf{u}}\frac{\partial \mathbf{u}}{\partial h} + \left.\frac{\partial \boldsymbol{\epsilon}}{\partial h}\right|_{\mathbf{u}\,\text{fixed}} . \tag{C.9}$$

Introducing the material tangent stiffness $\mathbf{k} = \frac{\partial \boldsymbol{\sigma}}{\partial \boldsymbol{\epsilon}}$ and the relation $\frac{\partial \boldsymbol{\epsilon}}{\partial \mathbf{u}} = \mathbf{B}$, Eq. (C.8) can be rewritten as:

$$\overline{\mathbf{K}} \frac{\partial \mathbf{u}}{\partial h} + \left.\frac{\partial \mathbf{P}_{\text{int}}}{\partial h}\right|_{\mathbf{u}\,\text{fixed}} = \int_\Omega \left[\mathbf{B}^T \mathbf{k} \mathbf{B} \frac{\partial \mathbf{u}}{\partial h} + \mathbf{k}\mathbf{B} \left.\frac{\partial \boldsymbol{\epsilon}}{\partial h}\right|_{\mathbf{u}\,\text{fixed}} + \mathbf{B}^T \left.\frac{\partial \boldsymbol{\sigma}}{\partial h}\right|_{\boldsymbol{\epsilon}\,\text{fixed}} \right] \mathrm{d}\Omega. \tag{C.10}$$

From Eq. (C.4), we see that the terms $\overline{\mathbf{K}} \frac{\partial \mathbf{u}}{\partial h}$ and $\int_\Omega \mathbf{B}^T \mathbf{k} \mathbf{B} \frac{\partial \mathbf{u}}{\partial h} \mathrm{d}\Omega$ mutually cancel out. In addition, the material paramaters do not enter the kinematic equations, so for a parameter h being a material one, it holds:

$$\left.\frac{\partial \boldsymbol{\epsilon}}{\partial h}\right|_{\mathbf{u}\,\text{fixed}} = 0\,.$$

Eq. (C.10) thus further simplifies to the following relation for the conditional derivative of the internal force vector in the static case:

$$\left.\frac{\partial \mathbf{P}_{\text{int}}}{\partial h}\right|_{\mathbf{u}\,\text{fixed}} = \int_\Omega \mathbf{B}^T \left.\frac{\partial \boldsymbol{\sigma}}{\partial h}\right|_{\boldsymbol{\epsilon}\,\text{fixed}} \mathrm{d}\Omega\,. \tag{C.11}$$

In the case of linear elasticity, where $\boldsymbol{\sigma} = \mathbf{EBU}$, one can write Eq. (C.11) more explicitely as:

$$\left.\frac{\partial \mathbf{P}_{\text{int}}}{\partial h}\right|_{\mathbf{u}\,\text{fixed}} = \int_\Omega \mathbf{B}^T \frac{\partial \mathbf{E}}{\partial h} \mathbf{B}\, \mathrm{d}\Omega\, \mathbf{U}\,. \tag{C.12}$$

C.2 Sensitivity with Respect to Nodal Coordinates

The terms that need to be evaluated in the top-level sensitivity equation (C.5) are both the derivative of the internal force vector $\frac{\partial \mathbf{P}_{\text{int}}}{\partial h}$ and of the external force vector $\frac{\partial \mathbf{P}_{\text{ext}}}{\partial h}$. In the latter case, the surface and body forces are integrated over the elements, cf. Eq. (B.42) and (B.43) and the change of a nodal coordinate affects the element integral.

Consistently with Section B.2.6, the elemment integrals are assumed to be evaluated using a Gauss quadrature – for a general integrand, the quadrature with m quadrature points resumes to (in 2D):

$$\int_{\Omega_e} f(x,y)\, \mathrm{d}\Omega_e \approx \sum_{j=1}^{m} \omega_j f(\xi,\eta)\, |\mathbf{J}|\,, \tag{C.13}$$

where $\mathbf{J}$ is the Jacobian of transformation from the global to the isoparametric coordinates, see Eq. (B.48). It is implicitely understood that (ξ, η)

are the isoparametric coordinates of the integration point with the weight ω_j. The derivative of the integral is then:

$$\frac{\partial}{\partial h}\left(\int_{\Omega_e} f(x,y)\,\mathrm{d}\Omega_e\right) \approx \sum_{j=1}^{m} \omega_j \left[\frac{\partial f(\xi,\eta)}{\partial h}\,|\mathbf{J}| + f(\xi,\eta)\frac{\partial\,|\mathbf{J}|}{\partial h}\right]. \tag{C.14}$$

The Jacobian derivative provides for the mapping between the element with the actual geometry in the space of physical cocordinates $x_i = \{x, y\}$ and the parent element with an invariable geometry in the space of the isoparametric coordinates $\xi_j = \{\xi, \eta\}$. Thus, a sensitivity to a change in the physical geometry translates to the sensitivity of the Jacobian derivative $\frac{\partial|\mathbf{J}|}{\partial h}$. To find what this derivative equals, we expand it by the chain rule and use the equality $\frac{\partial|\mathbf{J}|}{\partial \mathbf{J}} = |\mathbf{J}|\,\mathbf{J}^{-T}$, with the superscript $-T$ signifying the inverse transpose. We get:

$$\frac{\partial\,|\mathbf{J}|}{\partial h} = \frac{\partial\,|\mathbf{J}|}{\partial \mathbf{J}}\frac{\partial \mathbf{J}}{\partial h} = |\mathbf{J}|\,\mathbf{J}^{-T}\frac{\partial \mathbf{J}}{\partial h}. \tag{C.15}$$

Eq. (B.48) tells us that $\mathbf{J} = \mathbf{P}\mathbf{X}$, where $\mathbf{P}$ is the matrix of shape function derivatives. Thus, if h is the i-th coordinate of the p-th node, the derivative $\frac{\partial \mathbf{J}}{\partial h}$ reads:

$$\frac{\partial J_{x_i,\xi_j}}{\partial h} = \frac{\partial N_{ip}}{\partial \xi_j} \quad \text{or} \quad \frac{\partial \mathbf{J}}{\partial h} = \mathbf{P}\frac{\partial \mathbf{X}}{\partial h}. \tag{C.16}$$

Having found the derivative of the Jacobian determinant, we are ready to look at the derivatives of the internal and external force vector.

C.2.1 Derivative of the Internal Force vector

As a point of departure for finding the derivative, the internal force vector evaluated by numerical integration

$$\mathbf{P}_{\text{int}} \approx \sum_{j=1}^{m} \omega_j \boldsymbol{\sigma}\mathbf{B}\,|\mathbf{J}| \tag{C.17}$$

is differentiated with respect to the nodal coordinate parameter h:

$$\frac{\partial \mathbf{P}_{\text{int}}}{\partial \mathbf{u}}\frac{\partial \mathbf{u}}{\partial h} + \left.\frac{\partial \mathbf{P}_{\text{int}}}{\partial h}\right|_{\mathbf{u}\,\text{fixed}} \approx \sum_{j=1}^{m} \omega_j \left(\frac{\partial \boldsymbol{\sigma}}{\partial h}\mathbf{B}\,|\mathbf{J}| + \boldsymbol{\sigma}\frac{\partial \mathbf{B}}{\partial h}\,|\mathbf{J}| + \boldsymbol{\sigma}\mathbf{B}\frac{\partial\,|\mathbf{J}|}{\partial h}\right), \tag{C.18}$$

whereby the derivative $\frac{\partial|\mathbf{J}|}{\partial h}$ is evaluated from Eq. (C.15) and (C.16). The terms $\frac{\partial\boldsymbol{\sigma}}{\partial h}$ and $\frac{\partial\mathbf{B}}{\partial h}$ are expanded by the chain rule and Eq. (C.9) is further used. We thus obtain:

$$\begin{aligned}\overline{\mathbf{K}}\frac{\partial\mathbf{u}}{\partial h}+\left.\frac{\partial\mathbf{P}_{\text{int}}}{\partial h}\right|_{\mathbf{u}\text{ fixed}} &\approx \sum_{j=1}^{m}\omega_j\,|\mathbf{J}|\left(\mathbf{B}^T\mathbf{k}\mathbf{B}\frac{\partial u}{\partial h}+\mathbf{B}^T\mathbf{k}\left.\frac{\partial\boldsymbol{\epsilon}}{\partial h}\right|_{\mathbf{u}\text{ fixed}}\right.\\ &+ \mathbf{B}^T\left.\frac{\partial\boldsymbol{\sigma}}{\partial h}\right|_{\boldsymbol{\epsilon}\text{ fixed}}+\boldsymbol{\sigma}\frac{\partial\mathbf{B}}{\partial h}+\boldsymbol{\sigma}\mathbf{B}\mathbf{J}^{-T}\frac{\partial\mathbf{J}}{\partial h}\Bigg),\end{aligned} \tag{C.19}$$

where use has been made of Eq. (C.16) and of the notation $\mathbf{k}=\frac{\partial\boldsymbol{\sigma}}{\partial\boldsymbol{\epsilon}}$. From Eq. (C.4), we see that the terms $\overline{\mathbf{K}}\frac{\partial\mathbf{u}}{\partial h}$ and $\sum_{j=1}^{m}\omega_j\,|\mathbf{J}|\,\mathbf{B}^T\mathbf{k}\mathbf{B}\frac{\partial\mathbf{u}}{\partial h}$ mutually cancel out. The above Eq. (C.19) thus simplifies to:

$$\begin{aligned}\left.\frac{\partial\mathbf{P}_{\text{int}}}{\partial h}\right|_{\mathbf{u}\text{ fixed}} &\approx \sum_{j=1}^{m}\omega_j\,|\mathbf{J}|\left(\mathbf{B}^T\mathbf{k}\left.\frac{\partial\boldsymbol{\epsilon}}{\partial h}\right|_{\mathbf{u}\text{ fixed}}+\mathbf{B}^T\left.\frac{\partial\boldsymbol{\sigma}}{\partial h}\right|_{\boldsymbol{\epsilon}\text{ fixed}}\right.\\ &+ \boldsymbol{\sigma}\frac{\partial\mathbf{B}}{\partial h}+\boldsymbol{\sigma}\mathbf{B}\mathbf{J}^{-T}\frac{\partial\mathbf{J}}{\partial h}\Bigg).\end{aligned} \tag{C.20}$$

In linear elasticity, $\boldsymbol{\sigma}$=$\mathbf{E}\boldsymbol{\epsilon}$ and $\boldsymbol{\epsilon}$=$\mathbf{B}\mathbf{U}$. We can thus express

$$\begin{aligned}\left.\frac{\partial\boldsymbol{\epsilon}}{\partial h}\right|_{\mathbf{u}\text{ fixed}} &= \frac{\partial\mathbf{B}}{\partial h}\mathbf{U}\,,\\ \left.\frac{\partial\boldsymbol{\sigma}}{\partial h}\right|_{\boldsymbol{\epsilon}\text{ fixed}} &= \mathbf{E}\frac{\partial\mathbf{B}}{\partial h}\mathbf{U}\,.\end{aligned}$$

Using these results and noting that for linear elastic materials, $\mathbf{k}=\mathbf{E}$, Eq. (C.20) may be rewritten to its final form in linear elasticity:

$$\begin{aligned}\left.\frac{\partial\mathbf{P}_{\text{int}}}{\partial h}\right|_{\mathbf{u}\text{ fixed}} &\approx \sum_{j=1}^{m}\omega_j\,|\mathbf{J}|\left(\mathbf{B}^T\mathbf{E}\frac{\partial\mathbf{B}}{\partial h}\mathbf{U}+\mathbf{B}^T\mathbf{E}\frac{\partial\mathbf{B}}{\partial h}\mathbf{U}\right.\\ &+ \boldsymbol{\sigma}\frac{\partial\mathbf{B}}{\partial h}+\boldsymbol{\sigma}\mathbf{B}\mathbf{J}^{-T}\frac{\partial\mathbf{J}}{\partial h}\Bigg)\\ &= \sum_{j=1}^{m}\omega_j\,|\mathbf{J}|\left(2\mathbf{B}^T\mathbf{E}\frac{\partial\mathbf{B}}{\partial h}\mathbf{U}+\left[\frac{\partial\mathbf{B}}{\partial h}\right]^T\mathbf{E}\mathbf{B}\mathbf{U}\right.\\ &+ \mathbf{B}^T\mathbf{E}\mathbf{B}\mathbf{U}\,\mathbf{J}^{-T}\frac{\partial\mathbf{J}}{\partial h}\Bigg)\end{aligned} \tag{C.21}$$

It remains to find the derivative of strain-displacement matrix $\frac{\partial\mathbf{B}}{\partial h}$. The elements of $\mathbf{B}$ are calculated by multiplying the shape function derivatives

with respect to the isoparametric coordinates by the inverse Jacobian, see Eq. (B.47). Thus, their derivative with respect to the k-th component of the nodal coordinate $h = X_{rk}$ of node r is:

$$\frac{\partial \mathbf{B}}{\partial X_{rk}} = \frac{\partial}{\partial X_{rk}} \frac{\partial N_{ip}}{\partial x_j} = \frac{\partial N_{ip}}{\partial \xi_l} \frac{\partial}{\partial X_{rk}} \frac{\partial \xi_l}{\partial x_j} = \mathbf{P} \frac{\partial \mathbf{J}^{-1}}{\partial h} \,. \tag{C.22}$$

While $\frac{\partial N_{ip}}{\partial \xi_l}$ is easlily obtained, the term $\frac{\partial}{\partial X_{rk}} \frac{\partial \xi_l}{\partial x_j}$ is the derivative of the inverse jacobian. It is shown in [39] that it can be obtained as follows:

$$\frac{\partial}{\partial h} \left[\frac{\partial x_j}{\partial \xi_k} \right]^{-1} = - \left[\frac{\partial x_i}{\partial \xi_j} \right]^{-T} \frac{\partial}{\partial h} \frac{\partial x_i}{\partial \xi_l} \left[\frac{\partial x_l}{\partial \xi_k} \right]^{-1} = \mathbf{J}^{-T} \frac{\partial \mathbf{J}}{\partial X_{rk}} \mathbf{J}^{-1} \,. \tag{C.23}$$

The derivative of the Jacobian is given in Eq. (C.16) and the inverses of the Jasobian itself are obtained numerically.

C.2.2 Derivative of the External Force vector

When the loads are prescribed in terms of nodal forces and the problem is geometrically linear, then the derivative $\frac{\partial \mathbf{P}_{\text{ext}}}{\partial h}$ vanishes. However, in the case of distributed loads, the nodal coordinate enters the calculation of the Jacobian in the numerical integration of the global load vector (c.f. Eq. (B.50)). The integration formula is differentiated using Eq. (C.15) and Eq. (C.16) to obtain e.g. for the integral of the body forces:

$$\frac{\partial \mathbf{P}_{\text{ext}}}{\partial h} \approx \sum_{j=1}^{m} \omega_j \mathbf{N}(q_j) \, f(q_j) \, |\mathbf{J}| \, \mathbf{J}^{-T} \frac{\partial \mathbf{J}}{\partial h} \,. \tag{C.24}$$

Bibliography

[1] H. Alizadeh, S. Simandjuntak, D. Smitd, and M. Pavier. Prediction of fatigue crack growth rates using crack closure finite element analysis. *International Journal of Fatigue*, 29:1711–1715, 2007.

[2] T.L. Anderson. *Fracture Mechanics: Fundamentals and Applications*. CRC Press, Boston, 1995.

[3] J.S. Arora and E.J. Huang. Methods of design sensitivity analysis in structural optimisation. *AIAA Journal*, 17:970–974, 1979.

[4] I. Babuška and J.M. Melenk. The partition of unity finite element method: Basic theory and applications. *Computer Methods in Applied Mechanics and Engineering*, 39:289–314, 1996.

[5] R.S. Barsoum. On the use of isoparametric finite elements in linear fracture mechanics. *International Journal for Numerical Methods in Engineering*, 10:25–37, 1976.

[6] J. Bass. *Cours de mathématiques*, volume 1. Masson, Paris, 1977.

[7] Z.P. Bažant and L.F. Estenssoro. Surface singularity and crack propagation. *International Journal of Solids and Structures*, 15:405–426, 1979.

[8] T. Belytschko, Y. Krongauz, D. Organ, M. Fleming, and P. Krysl. Meshless methods: An overview and recent developments. *Computer Methods in Applied Mechanics and Engineering*, 139:3–47, 1996.

[9] T. Belytschko, Y.Y. Lu, and L. Gu. Element-free Galerkin methods. *International Journal for Numerical Methods in Engineering*, 37:229–256, 1994.

[10] J.P. Benthem. State of stress at a vertex of a quarter-infinite crack in a half-space. *International Journal of Solids and Structures*, 13:479–492, 1977.

[11] T.N. Bittencourt, P.A. Wawrzynek, A.R. Ingraffea, and Sousa J.L.A. Quasi-automatic simulation of crack propagation for 2D LEFM problems. *Engineering Fracture Mechanics*, 55:321–334, 1996.

[12] J.L. Bogdanoff, W. Krieger, and F. Kozin. A new cumulative damage model, Part I-Part III. *Journal of Applied Mechanics*, 45:245–257,733–739, 1978.

[13] U. Bourgund and C.G. Bucher. Importance sampling procedure using design points (ISPUD) – a user's manual. Technical Report 8-86, Institut für Mechanik, Universität Innsbruck, Innsbruck, Austria, 1986.

[14] J.-M. Bourinet and M. Lemaire. Form sensitivities to correlation: Application to fatigue crack propagation basd on Virkler data. In *4th International ASRANet Colloquium*, Athens, Greece, June 2008. ASRANet Ltd., Glasgow, UK.

[15] D. Broek. *Elementary Engineering Fracture Mechanics*. Martinus Nijhoff Publishers, Dordrecht, The Netherlands, fourth edition, 1986.

[16] H.D. Bui. *Mécanique de la rupture fragile*. Masson, Paris, 1978.

[17] R.A. Chaudhuri and Xie. M. A novel eigenfunction expansion for three-dimensional crack problems. *Composite Science and Technology*, 60:2565–2580, 2000.

[18] R. Courant. Variational methods for the solution of problems of equilibrium and vibrations. *Bulletin of American Mathematics Society*, 49:1–23, 1943.

[19] M. Dauge. Singularities of corner problems and problems of corner singularities. In *Actes du 30ème Congrès d'Analyse Numérique: CANUM'98*, Arles, France, 1998. Société de Mathématiques Appliquées et Industrielles, ESAIM.

[20] M. Dauge. "Simple" corner-edge asymptotics. Internet publication, http://perso.univ–rennes1.fr/monique.dauge/publis/corneredge.pdf, 2000.

[21] A. Davy. *Modélisation de la fissuration en fatigue sous chargements d'amplitude variable : Application aux spectres d'avions civils.* PhD thesis, Université de Technologie de Compiègne, Compiègne, France, 1985.

[22] A. Der Kiureghian. Alternative derivation of importance vectors α and γ. Course notes of the Structural Reliability course taught at UC Berkeley, 2006.

[23] A. Der Kiureghian and P.L. Liu. Structural reliability under incomplete probability information. *ASCE Journal of Engineering Mechanics*, 112(1):85–104, 1986.

[24] W. Elber. Fatigue crack closure under cyclic tension. *Engineering Fracture Mechanics*, 2:37–45, 1970.

[25] W. Elber. The significance of fatigue crack closure. *ASTM STP*, 486:230–242, 1971.

[26] T. Elguedj, A. Gravouil, and A. Combescure. X-FEM method for elastic-plastic fatigue crack growth simulations. In *International Conference on Fatigue Design*, Senlis, France, November 2005. CETIM.

[27] F. Erdogan and G.C. Sih. On the crack extension in plates under plane loading and transverse shear. *Journal of Basic Engineering*, 85:519–527, 1963.

[28] M. Fleming, Y.A. Chu, B. Moran, and T. Belytschko. Enriched element-free Galerkin methods for crack tip fields. *International Journal for Numerical Methods in Engineering*, 40:1483–1504, 1997.

[29] E.S. Folias. On the tree-dimensional theory of cracked plates. *ASME Journal of Applied Mechanics*, 42:663–674, 1975.

[30] R.G. Forman, V.E. Kearney, and R.M. Engle. Numerical analysis of crack propagation in cyclic-loaded structures. *Journal of Basic Engineering, Transactions of the American Society of Mechanical Engineers*, 89:459–464, 1967.

[31] P.J.E. Forsyth. Fatigue damage and crack growth in aluminium alloys. *Acta Metallurgica*, 11:703–715, 1963.

[32] D. François. *Endommagements et rupture de matériaux.* EDP Sciences, France, 2004.

[33] B.G. Galerkin. Series solutions of some problems of elastic equilibrium of rods and plates. *Vestnik Inzhenerov*, 1:897–908, 1915.

[34] H. Ghonem and S. Dore. Experimental study of constant probability crack growth curves under constant amplitude loading. *Engineering Fracture Mechanics*, 27(1):1–25, 1987.

[35] R. Gingold and J. Monaghan. Smoothed particle hydrodynamics: theory and application to non-spherical stars. *Monthly Notices of the Royal Astronomical Society*, 181:375–389, 1977.

[36] A.A. Griffith. The phenomena of rupture and flow in solids. *Philosophical Transactions of the Royal Society of London, A*, pages 163–197, 1921.

[37] A. Hadrboletz, B. Weiss, and G. Khatibi. Fatigue and fracture properties of thin metallic foils. *International Journal of Fracture*, 109:69–89, 2001.

[38] A.M. Hasofer and N.C. Lind. Exact and invariant second-moment code format. *Journal of Engineering Mechanics Division, ASCE*, 100(1):111–121, 1974.

[39] T. Haukaas. *Finite Element Reliability and Sensitivity Methods for Performance-Based Engineering.* PhD thesis, University of California, Berkeley, 2003.

[40] M.A. Hussain, S.U. Pu, and J. Underwood. Strain energy release rate for a crack under combined mode I and II. *ASTM STP*, 560:2–28, 1974.

[41] A.R. Ingraffea and C. Manu. Stress-intensity factor computation in three dimensions with quarter-point elements. *International Journal for Numerical Methods in Engineering*, 15:1427–1445, 1980.

[42] G.R. Irwin. Analysis of stresses and strains near the end of a crack traversing a plate. *Journal of Applied Mechanics*, 24:361–364, 1957.

[43] G. Jiao and T. Moan. Methods of reliability model updating through additional events. *Structural Safety*, 9:139–153, 1990.

[44] F. Kaninen and B. Popelar. *Advanced Fracture Mechanics.* Oxford University Press, New York, USA, 1985.

[45] Z. Knésl, S. Seitl, and P. Hutař. Accounting for effects of constraint on propagation of a fatigue crack. In C.A Brebbia and S.-I. Nishida, editors, *Damage and Fracture Mechanics VII (Computer Aided Assessment and Control)*, page 245, Southampton, 2002. WIT Press.

[46] LaMCoS. Software ELFE_3D developed at the LaMCoS laboratory of INSA de Lyon (MSE team).

[47] P. Lancaster and K. Salkauskas. Surfaces generated by moving least squares methods. *Mathematics of Computation*, 37:141–158, 1981.

[48] J.-B. Leblond. *Mécanique de la rupture fragile et ductile.* Hermès Science, Lavoisier, Paris, France, 2003.

[49] M. Lemaire. *Fiabilité des structures. Couplage mécano-fiabiliste statique. En collaboration avec A. Chateauneuf et J.-C. Mitteau.* Lavoisier, Paris, 2005.

[50] M. Lemaire, J. Goyet, J.C. Mitteau, and A. Mohamed. *Fiabilité des structures mécaniques – Couplage mécano-fiabiliste statique.* Cours de l'Institut Français de Mécanique Avancée, 2000.

[51] Y.K. Lin and J.N. Yang. On statistical moments of fatigue crack propagation. *Engineering Fracture Mechanics*, 18(2):243–256, 1983.

[52] G.-R. Liu. *Mesh free methods: moving beyond the finite element method.* CRC Press LLC, Boca Raton, USA, 2003.

[53] P.-L. Liu and A. Der Kiureghian. Finite element reliability of geometrically nonlinear uncertain structures. *Journal of Engineering Mechanics*, 17:1806–1825, 1991.

[54] W.K. Liu, Y. Chen, T. Belytschko, and Y.J. Lua. Three reliability methods for fatigue crack growth. *Engineering Fracture Mechanics*, 53(5):733–752, 1996.

[55] H.O. Madsen. *Probabilistic Methods for Structural Design*, chapter Stochastic Modelling of Fatigue Crack Growth and Inspection, pages 59–83. Kluwer Academic Publishers, The Netherlands, 1997.

[56] H.O. Madsen and J.D. Sorensen. Probability-based optimisation of fatigue design inspection and maintenance. In *International Symposium on Offshore Structures*, University of Glasgow, 1990.

[57] M. Matsuiski and T. Endo. Fatigue of metals subjected to varying stress. Paper presented at the Kyushu district meeting of the Japan Society of Mechanical Engineers, March 1968.

[58] M.D. McKay, W.J. Conover, and R.J. Beckmann. A comparison of three methods for selecting values of input variables in the analysis of output from a computer code. *Technometrics*, 116(1):189–203, 1979.

[59] P. Mialon. Calcul de la dérivée d'une grandeur par rapport à un fond de fissure par la méthode thêta. *E.D.F. Bulletin de la Direction des Etudes et Recherches*, 3:1–28, 1988.

[60] M. A. Miner. Cumulative damage in fatigue. *Journal of Applied Mechanics*, 12:159–164, 1945.

[61] N. Möes, J. Dolbow, and T. Belytschko. A finite element method for crack growth without remeshing. *International Journal for Numerical Methods in Engineering*, 46:131–150, 1990.

[62] N. I. Muskhelishvili. *Some basic problems of the mathematical theory of elasticity*. Noordhoff International Publishing, Leyden, The Netherlands, 1975.

[63] K.B. Narayana, S. George, B. Dattaguru, and K. Vijayakumar T.S. Ramamurthy. Modified crack closure integral (MCCI) for 3-d problems using 20-noded brick elements. *Fatigue and Fracture of Engineering Materials and Structures*, 17:145–157, 1994.

[64] A. Nataf. Détermination des distributions dont les marges sont données. *Comptes Rendus de l'Académie des Sciences*, 225:42–43, 1962.

[65] B. Nayroles, G. Touzot, and P. Villon. Generalising the finite element method: diffuse approximation and diffuse elements. *Computational Mechanics*, 10:307–318, 1992.

[66] L. Nespurek, C. Proppe, and G.I. Schuëller. Reliability analysis of an aircraft fuselage component with multi-site damage subjected to fatigue loading. In G.I. Schuëller and P.D. Spanos, editors, *Proceeding of the International Conference on Monte Carlo Simulation MCS_2000*, pages 357–364, Monaco, 18.-21.6. 2000. Swets and Zeitlinger BV, The Netherlands.

[67] J.C. Newman. A crack-closure stress model for predicting fatigue crack growth under aircraft spectrum loading. In *Methods and models for predicting fatigue crack growth under random loading.* ASTM STP 748, 1981.

[68] J.C. Newman. A crack-opening stress equation for fatigue crack growth. *International Journal of Fatigue*, 24, 1984.

[69] G.P. Nikishkov and S.N. Atluri. Calculation of fracture mechanics parameters for an arbitrary three-dimensional crack by equivalent domain integration method. *International Journal for Numerical Methods in Engineering*, 24:1801–1821, 1987.

[70] T. Nishioka and S. N. Atluri. Analytical solution for embedded elliptical cracks and finite element-alternating method for elliptical surface cracks, subjected to arbitrary loadings. *Engineering Fracture Mechanics*, 17:247–268, 1983.

[71] Oden. *Finite elements for nonlinear continua.* McGraw-Hill, New York, 1972.

[72] P.C. Paris. Fracture mechanics and fatigue: A historical perspective. *Fatigue and Fracture of Engineering Materials and Structures*, 21(5):535–540, 1998.

[73] P.C. Paris and F. Erdogan. A critical analysis of crack propagation laws. *Journal of Basic Engineering, Transactions of the American Society of Mechanical Engineers*, 85:528–534, 1963.

[74] P.C. Paris, M.P. Gomez, and W.E. Anderson. A rational analytic theory of fatigue. *The Trend in Engineering at the University of Washington*, 13(1):9–14, 1961.

[75] L.P. Pook. Some implications of corner point singularities. *Engineering Fracture Mechanics*, 48:367–378, 1994.

[76] T.S. Ramamurthy, T. Krishnamurthy, K.B. Narayana, B. Dattaguru, and K. Vijayakumar. Modified crack closure integral method with quarter-point elements. *Mechanics Research Communications*, 13:179–186, 1986.

[77] N. Recho. *Rupture par fissuration des structures.* Hermès, Paris, France, 1995.

[78] W. Ritz. Über eine Methode zur Lösung Gewissen Variations-Probleme der Mathematischen Physik. *Journal für reine und angewandte Mathematik*, 135:1–61, 1908.

[79] E.F. Rybicki and M.F. Kanninen. A finite element calculation of stress intensity factors by a modified crack closure integral. *Engineering Fracture Mechanics*, 9:931–938, 1977.

[80] G.C Sih. Strain energy density factor applied to mixed mode crack problems. *International Journal of Fracture*, 10:305–321, 1974.

[81] R. Singh. Universal crack closure integral for SIF estimation. *Engineering Fracture Mechanics*, 60:133–146, 1988.

[82] K. Sobczyk and B.F. Spencer Jr. *Random fatigue: from data to theory.* Academic Press, San Diego, California, USA, 1992.

[83] K. Sobczyk and J. Trebicki. Modelling of random fatigue by cumulative jump processes. *Engineering Fracture Mechanics*, 34(2):477–493, 1989.

[84] K. Sobczyk, J. Trebicki, and B.F. Spencer Jr. Modelling of curvilinear random fatigue crack growth. *Engineering Fracture Mechanics*, 52(4):703–715, 1995.

[85] I.S. Sokolnikoff. *Mathematical Theory of Elasticity.* McGraw-Hill, New York, USA, 1956.

[86] Swansons Analysis Systems, Houston, PA, USA. *ANSYS User's Manual for Rev. 5.6.*, 1999.

[87] H.J. Ten Hoeve and A.U. de Koning. Implementation of the improved strip yield model into nasgro software - architecture and detailed design document. Technical Report NLR CR 95312L, National Aerospace Laboratory (NLR), The Netherlands, 1995.

[88] M.J. Turner, R.W. Clough, H.C. Martin, and L.J. Topp. Stiffness and deflection analysis of complex structures. *Journal of Aeronautical Sciences*, 23:805–824, 1956.

[89] D.A. Virkler, B.M. Hillbery, and P.K. Goel. The statistical nature of fatigue crack propagation. *Journal of Engineering Materials and Technology, ASME*, 101:148–153, 1979.

[90] M. Vořechovský and D. Novák. Statistical correlation in stratified sampling. In *9-th International Conference on Applications of Statistics and Probability in Civil Engineering*, pages 119–124, San Francisco, USA, July 2003. Millpress, Rotterdam.

[91] C.-T. Wang. *Applied Elasticity.* McGraw-Hill, New York, USA, 1953.

[92] L. Wang, F. W. Brust, and S. N. Atluri. The elastic-plastic finite element alternating method (EPFEAM) and the prediction of fracture under WFD conditions in aircraft structures. *Computational Mechanics*, 19:275–277, 1997.

[93] P.H. Wen, M.H. Aliabadi, and D.P. Rooke. A contour integral for three-dimensional crack elastostatic analysis. *Engineering Analysis with Boundary Elements*, 20:101–111, 1997.

[94] O.E. Wheeler. Spectrum loading and crack growth. ASTM paper No. 71-Met-X, 1971.

[95] J.R. Whiteman. *A bibliography for finite elements.* Academic Press, London, 1975.

[96] J. Willenborg, R.M Engle, and H.A. Wood. A crack growth retardation model using an effective stress concept. Technical Report TM 71-1-FBR, Air Force Flight Dynamics Laboratory, Wright Patterson Air Force Base, 1971.

[97] M.L. Williams. On the stress distribution at the base of a stationary crack. *Journal of Applied Mechanics*, 24:109–114, 1957.

[98] A. Wöhler. Versuche zur Ermittlung der auf die Eisenbahnwagen-Achsen einwirkenden Kräfte und der Widerstandsfähigkeit der Wagen-Achsen. *Zeitschrift für Bauwesen*, 10:583–616, 1860.

[99] W.A. Wood. Recent observations on fatigue and fracture in metals. *ASTM Special Technical Publications*, 237:110–121, 1958.

[100] J. Yau, S. Wang, and H. Corten. A mixed-mode crack analysis of isotropic solids using conservation laws of elasticity. *Journal of Applied Mechanics*, 47:335–341, 1980.

[101] Y. Zhang and A. Der Kiureghian. Two improved algorithms for reliability analysis. In R. Rackwitz, G. Augusti, and A. Borri, editors, *Reliability and Optimization of Structural Systems, Proceedings of the*

6th IFIP WG 7.5 Working Conference on Reliability and Optimisation of Structural Systems, pages 297–304, Assisi, Italy, 1995. Chapman & Hall, London, UK.

[102] O. C. Zienkiewicz and Y. K. Cheung. Finite elements in the solution of field problems. *The Engineer*, 220(507-510), 1965.